Diversity and systematics of *Trichomycterus* Valenciennes 1832 (Siluriformes: Trichomycteridae) in the Rio Doce Basin: iterating DNA, phylogeny and classical taxonomy

VINÍCIUS REIS[1,2,*] and MÁRIO DE PINNA[1]

[1]*Museu de Zoologia da Universidade de São Paulo, 481 Avenida Nazaré, São Paulo, São Paulo, 04263-000, Brazil*
[2]*Institut de Systématique, Evolution, Biodiversité, Muséum national d'Histoire naturelle, CNRS, Sorbonne Université, EPHE, Université des Antilles, CP 30, Paris, France*

The catfish genus *Trichomycterus* is a recognized taxonomic bottleneck in Neotropical ichthyology. The hitherto poorly-known diversity of *Trichomycterus* in the Rio Doce Basin, Brazil, is here investigated using an iterative approach based on morphology and cytochrome oxidase subunit I (*COI*) sequence data. Specimens from the entire Rio Doce Drainage and adjacent basins are analysed, including from type localities. Iteration of different sources of data, dense sampling and taxonomic representation, plus information on relevant type specimens allows a clear view of the diversity, relationships and nomenclature of *Trichomycterus* in the Rio Doce Basin. Results indicate the presence of at least 14 species in the basin, seven of which are new. A lectotype is designated for *Trichomycterus immaculatus* and the type locality is accordingly restricted to the Rio São Mateus, a satellite basin north of the Rio Doce. Geographic distributions are mapped for all recognized species. The wide distributions of some species (e.g. *Trichomycterus alternatus*, *T. immaculatus*) are explained against information on geomorphological processes and comparative information on their biology. A Bayesian phylogenetic analysis shows that a large portion of the assemblage of *Trichomycterus* in the Rio Doce forms a clade, a pattern relevant to understanding the evolution of the genus in eastern South America.

ADDITIONAL KEYWORDS: biogeographic dispersal – DNA barcoding – integrative taxonomy – Neotropical catfish – north-eastern Atlantic Forest ecoregion – species delimitation.

INTRODUCTION

Trichomycteridae is one of the most diverse families in the order Siluriformes (Fricke *et al.*, 2021). It constitutes a monophyletic group currently subdivided into nine subfamilies: Copionodontinae, Glanapteryginae, Microcambevinae, Sarcoglanidinae, Stegophilinae, Trichogeninae, Trichomycterinae, Tridentinae and Vandellinae. Fishes from this family are characterized, among other particularities, by a highly modified opercular apparatus, adapted for attachment or locomotion on hard substrates and, in the case of parasitic forms (mostly Stegophilinae and Vandellinae) to attach onto the host fish or into its gill cavity (de Pinna, 1998; Adriaens *et al.*, 2010). Due to the ability to climb waterfalls in some lineages, many species are found at high elevations. This leads to the colonization of extreme reaches of headwaters, which in turn results in pronounced endemism (Eigenmann, 1918; Santos, 2012).

Of the currently recognized trichomycterid subfamilies, Trichomycterinae is the most species rich (Fricke *et al.*, 2021). Nine genera are allocated therein: *Bullockia* Arratia, Chang, Menu-Marque & Rojas, 1978, *Cambeva* Katz, Barbosa, Mattos & Costa, 2018, *Eremophilus* Humboldt, 1805, *Hatcheria* Eigenmann, 1909, *Ituglanis* Costa & Bockmann, 1993, *Rhizosomichthys* Miles, 1943, *Scleronema* Eigenmann, 1917, *Silvinichthys* Arratia, 1998 and *Trichomycterus* Valenciennes, 1832 (Datovo & Bockmann, 2010;

*Corresponding author. E-mail: carvalhvinicius@gmail.com

344

Katz *et al.*, 2018; Ochoa *et al.*, 2020). Of these, *Trichomycterus* has the largest number of nominal species, more than 200 (Fricke *et al.*, 2021), and it is currently the most complex taxon in the family due to its geographical distribution, non-monophyletic status and confusing taxonomy (de Pinna, 1989, 1998; Ochoa *et al.*, 2020; Lima *et al.*, 2021).

The type species of *Trichomycterus* is *Trichomycterus nigricans* Valenciennes, 1832, from Rio de Janeiro, Brazil (Costa *et al.*, 2020a). Many other species have been described since and today the genus is one of the most diverse in the Neotropics. Species of the genus have historically been described mostly on the basis of external traits, such as number of fin rays, body proportions and pigmentation. Standards used in descriptions of *Trichomycterus* species have been highly heterogeneous, resulting in difficulties in comparing data among different species. Starting with Tchernavin (1944), traditional distinguishing characteristics have been gradually shown not to always constitute reliable taxonomic proxies for species differentiation, mostly due to intraspecific and ontogenetic variation and allometric effects.

Despite some recent efforts (e.g. Reis & de Pinna, 2019), the situation is still far from satisfactory. Standards are not yet uniformly rigorous and the taxonomy of the genus is still inordinately complex. From the middle of the 20th century until now, the number of nominal *Trichomycterus* species from south-eastern Brazil has increased more than six-fold, from nine to 65 species (Fricke *et al.*, 2021). Although the diversity of *Trichomycterus* is gradually being revealed, diagnosing species of the genus continues to be a problem, especially when allied with their morphological plasticity (e.g in colour pattern and morphometrics), as has been demonstrated in *Cambeva davisi* (Haseman, 1911), *Trichomycterus brasiliensis* Lütken, 1874 (Bockmann & Sazima, 2004; Barbosa & Costa, 2010; Nascimento *et al.*, 2017) and many other species from Colombia (DoNascimiento & Prada-Pedreros, 2020).

The Rio Doce Basin spans the Brazilian states of Minas Gerais and Espírito Santo. It contains one of the most diverse fish faunas among eastern Brazilian drainages, including a significant proportion of endemics (Barros *et al.*, 2012; Dergam *et al.*, 2017; Sales *et al.*, 2018). Unfortunately, the Rio Doce is severely degraded by anthropic impacts such as damming, and sewage and industrial discharge. The 2015 bursting of the Samarco SA ore tailing dam was a major catastrophe that critically endangered nearly all aquatic biodiversity in the basin.

There are currently nine *Trichomycterus* species reported for the Rio Doce: *Trichomycterus alternatus* (Eigenmann, 1917); *Trichomycterus argos* Lezama, Triques & Santos, 2012; *Trichomycterus astromycterus* Reis *et al.*, 2019; *Trichomycterus auroguttatus* Costa, 1992; *Trichomycterus brasiliensis* Lutken, 1874; *Trichomycterus immaculatus* (Eigenmann & Eigenmann, 1889); *Trichomycterus melanopygius* Reis *et al.*, 2020; *Trichomycterus pradensis* Sarmento-Soares, 2005 and *Trichomycterus reinhardti* (Eigenmann, 1917) (Sato *et al.*, 2004; Vieira, 2010; Lezama *et al.*, 2012; Da Silva *et al.*, 2013; Sales *et al.*, 2018; Reis *et al.*, 2019, 2020; Costa & Katz, 2021). Of these, *T. alternatus*, *T. argos*, *T. astromycterus* and *T. melanopygius* were originally described from the basin, with the first also reported from other river basins of eastern Brazil (Lima *et al.*, 2021). Examination of material available in museum collections has revealed significant unreported diversity of *Trichomycterus* in the waters of the Rio Doce, with several forms that clearly do not fit currently known taxa. It has also shown that the applicability of most available names is largely arbitrary and poorly supported by data. Resolution of this issue requires both a systematic investigation into the biological reality of the specific entities assignable to *Trichomycterus* in the Rio Doce and a taxonomic investigation on the applicability of available taxon names.

Molecular analyses using mitochondrial DNA have often been employed alongside morphological data in order to investigate taxonomic groups of fishes and to assess phylogenetic relationships (Avise *et al.*, 1998; Avise & Walker, 1999; Martin & Bermingham, 2000; Chiachio *et al.*, 2008; Cardoso & Montoya-Burgos, 2009; Carvalho *et al.*, 2015, Costa-Silva *et al.*, 2015; Sales *et al.*, 2018; Reis *et al.*, 2020). DNA barcoding in particular has been applied to help discriminate species of Trichomycteridae in south-eastern Brazil, as a test of the efficiency of alpha-taxonomic studies (Pereira *et al.*, 2010, 2013; Ochoa *et al.*, 2017; Sales *et al.*, 2018; Reis *et al.*, 2020). Mitochondrial genes, such as cytochrome *b (Cytb)* and cytochrome oxidase subunit I (*COI*), have been widely used in this sort of study, because of their advantages relative to nuclear markers in species-level applications, such as absence of introns, haploid mode of inheritance and limited recombination (Saccone *et al.*, 1999).

Among multiple mitochondrial markers, *COI* has been the most widely employed to distinguish species. This gene stands out because of its fast evolutionary rate, and its low conspecific variation relative to its congeneric variation (Hebert *et al.*, 2003). Of course, despite such advantages the use of *COI* in systematic studies has its caveats, as expected from any single source of data. These include the occasional inability to segregate morphologically well-differentiated species and the possibility of mitochondrial introgression (Rubinoff *et al.*, 2006). A reasonable assessment of

taxonomic entities requires evidence from different sources of data. The resolution of nomenclatural problems that require data on type specimens, and previous applications of available names, unavoidably requires that phenotypic information be included as part of any thorough effort at taxonomic progress.

This study investigates the diversity of the genus *Trichomycterus* in the Rio Doce Basin using both *COI* data and phenotypic characteristics. Our aim is to employ multiple lines of evidence to handle real-life taxonomic situations and constraints, such as incomplete comparative data, cases of *COI* divergence without corresponding phenotypic differentiation (and the reverse), highly variable widespread species, species known from few specimens and incompletely-known or heterogeneous type material. We make a special effort to disentangle nomenclatural conundrums, to provide information on intraspecific and ontogenetic variation and detailed assessments of geographical distribution, objectives that require taxonomic and sampling density. Our results demonstrate that *Trichomycterus* species in the Rio Doce were poorly known from all aspects, including cases of previously entirely unknown species, cryptic species, vaguely-defined species and species described multiple times (i.e. synonyms). We combine our molecular and morphological dense representation of samples from the Rio Doce with those from other areas, forming a view of the evolution of *Trichomycterus* species in the basin and their relationships to congeners elsewhere. We also offer insights into the biogeographic history of some taxa and possible explanations why some species are widespread in the basin while others are narrowly restricted.

MATERIAL AND METHODS

FIELDWORK AND SPECIMEN SOURCE

A total of 1921 specimens were used in this study, including both old and newly collected material. The new specimens were obtained during fieldwork conducted by the authors and concentrated on poorly-sampled locations and some type localities. Examined material is listed under each species account.

The care and use of experimental animals complied with animal welfare laws, guidelines and policies as approved by Conselho Nacional de Controle e Experimentação Animal (CONCEA, 2013) under a collecting permit from the Instituto Brasileiro do Meio Ambiente e dos Recursos Naturais Renováveis (SISBIO #61727). As recommended by the CONCEA (2013), specimens sampled in this study were euthanized by immersion in a solution of eugenol. Tissue samples for molecular studies were taken from the right side

in the posterior region of the flanks and immediately preserved in absolute ethanol. Fishes were then fixed in 10% formalin for 1 week and subsequently transferred to 70% ethanol for permanent storage. Specimens collected directly for this study are deposited in the ichthyological collection of the Museum of Zoology of the University of São Paulo, others are deposited as per information in the 'Material examined'.

Institutional acronyms: Field Museum of Natural History, Chicago, Illinois, USA (FMNH); Ichthyological Collection, Universidade Estadual Paulista, Botucatu, São Paulo, Brazil (LBP); Museu de História Natural and Laboratório de Genética Comparada, Pontifícia Universidade Católica de Minas Gerais, Belo Horizonte, Minas Gerais, Brazil (LGC); Museu de Biologia Melo Leitão, Instituto Nacional da Mata Atlântica, Santa Teresa, Rio de Janeiro, Brazil (MBML); Museum of Comparative Zoology, Harvard University, Cambridge, Massachusetts, USA (MCZ); Ichthyological Collection, Universidade Federal de Viçosa, Viçosa, Minas Gerais, Brazil (MZUFV); Museu Nacional do Rio de Janeiro, Rio de Janeiro, Brazil (MNRJ); Museu de Zoologia da Universidade de São Paulo, São Paulo, Brazil (MZUSP); and National Museum of Natural History, Smithsonian Institution, Washington DC, USA (NMNH).

MORPHOLOGY

Meristics and morphometrics

Morphometric data were taken with digital callipers (0.1 mm). Morphometric and meristic data were obtained following de Pinna (1992b) and Bockmann & Sazima (2004). Following the latter, fin-ray counts discriminated rays into three groups (unsegmented and unbranched represented by lower-case Roman numerals; segmented and unbranched represented by upper-case Roman numerals; segmented and branched represented by Arabic numerals), the posterior closely-set two rays in dorsal and anal fins were counted separately as branched rays. Principal caudal-fin ray counts included all branched rays plus one unbranched ray in each lobe; counts given for each lobe (upper first) were separated by a plus sign. Vertebrae numbers did not include those involved in the Weberian complex, and the compound caudal centrum was counted as one element. Vertebrae counts were taken from cleared and stained or radiographed material. Meristic and morphometric data were taken on the left side of specimens whenever possible.

Osteology

Osteological data were obtained from cleared and stained preparations, radiographs and computerized tomography in a few cases. Clearing and double-staining

procedures followed Taylor & Van Dyke (1985), with some previously-prepared specimens stained for bone only. Radiographs were taken with a digital X-ray Faxitron system at the Departamento de Biologia, Faculdade de Filosofia, Ciências e Letras de Ribeirão Preto, Universidade de São Paulo. Dissection of cleared and stained specimens followed Weitzman (1974) with small changes to fit the anatomical peculiarities of Siluriformes. Osteological nomenclature followed de Pinna (1989), Lundberg (1982) and Johnson & Patterson (1993). Nomenclature of the laterosensory system followed Pastana *et al.* (2019).

Pigmentation analyses

Pigmentation on the entire body was examined by shape and distribution on regions of the body. Pigmented regions were described in the following order: dorsum, lateral surface of the body (divided into dorsal and ventral to lateral midline, when pertinent) ventral side of the body, head and fins. Pigmentation patterns may vary markedly in species of *Trichomycterus* and this variation is accounted for in descriptions. Ontogenetic variation can also be pronounced in species of the genus; in a few cases where such information was available, it was also included in colour descriptions of individual species.

Cartography and image records

Global Positioning System (GPS) data from specimens of *Trichomycterus* reported from the Rio Doce Basin were clustered into species groups and plotted into GoogleEarth Pro in order to create a Keyhole Markup Language (KML) file for each species. These files were then used in the free software QGIS 2.16 to create maps showing the geographical distribution of each species. Photographs of dorsal, lateral and ventral views of all species were taken with a Nikon P700 camera. Final illustrations were prepared using image-editing software.

MOLECULAR ANALYSES

DNA sampling, extraction and sequencing

Sequences of *COI* utilized in this study were either newly extracted or obtained from GenBank, and the BOLD website, the latter selected after evidence of correct identification either by direct examination of vouchers or other associated information allowing verification in published sources (Table 1; Supporting Information). Sampling density was a prime concern because of the specific challenges faced by taxonomic revisions (see Discussion). All sequences used in molecular analyses were deposited in GenBank. Total DNA was extracted from either muscle tissue and/or

gills using an Invitrogen PureLink Genomic DNA Kit (ThermoFisher Brazil) according to the manufacturer's protocol. Laboratory procedures were conducted in the Molecular Systematics Laboratory at Museu de Zoologia da Universidade de São Paulo (MZUSP) and in the Laboratory of Analytical Biology (LAB), National Museum of Natural History, Smithsonian Institution. Quantification used a Qubit 2.0 fluorometer (Thermo Fisher) and was done exclusively at LAB.

In both laboratories, the *COI* primers used were those described in Ward *et al.* (2005). Amplification at MZUSP followed the protocol of Reis *et al.* (2020). At LAB, amplification was performed in a total volume of 11 μL with 5 μL of 10 × Promega Go Taq G2 Hot Start Master Mix (M7833), 0.3 μL of each primer (0.01 mM), 0.1 μL BSA (New England Biolabs B9000S), 4.3 μL of nuclease-free water and 1 μL of template DNA. The thermal-cycler profile consisted of a first cycle at 95 °C for 5 min; 35 cycles of 95 °C for 30 s, 48 °C for 30 s and 72 °C for 45 s; and a final extension of 72 °C for 5 min. Each PCR reaction was checked by electrophoresis in agarose at 1.5%. Only those showing successful amplification were purified using ExoSAP-IT (Affymetrix) (0.5 μL ExoSap enzyme, 1.5 μL nuclease-free water per reaction). The thermal-cycler profile for PCR purification was 36 °C for 30 min followed by 80 °C for 20 min.

Sequencing reactions were performed using 1 μL of purified PCR product in a 10 μL reaction containing 0.5 μL primer, 1.75 μL Big Dye buffer and 0.5 μL Big Dye (Life Technologies). The thermal-cycler profile consisted of 35 cycles of denaturation (95 °C, 30 s), annealing (50 °C, 30 s) and extension (60 °C, 4 min). The BigDye products were purified with Sephadex G-50 (Sigma-Aldrich) on Millipore Sephadex plates (MAHVN-4550) to remove unincorporated ddNTPs, and dried at 95 °C for 15 min. The purified products were then loaded on an ABI 3730XL automatic sequencer at LAB. The successfully sequenced specimens are listed in Table 1.

Sequence analysis

Sequences from *COI* were used for both barcoding analysis and phylogenetic inference. Although the marker is widely used for the former application, its use in the latter is less common. Mitochondrial inheritance, fast evolutionary rate and potential for introgression are possible caveats of using *COI* for reconstructing phylogenies. Due to particularities of the present case, those factors were not impeditive. Much of the present analysis involved entities (potential species) whose boundaries are not firmly defined a priori, thus requiring detection of potential intraspecific structuring by a fast-evolving marker. Also, parameters of Bayesian analysis are optimized

Table 1. *Trichomycterus* specimens from which *COI* gene was sequenced and used in this work. Institutional abbreviations provided in text

#	Sample	Taxon	Drainage	Coordinates
1	MZUSP121709_MZICT288	*Trichomycterus alternatus*	Middle Rio Doce	19°25'0.42"S 42°43'20.68"W
2	MZUSP121709_MZICT286	*Trichomycterus alternatus*	Middle Rio Doce	19°25'0.42"S 42°43'20.68"W
3	MBML6822_AA80	*Trichomycterus alternatus*	Lower Rio Doce	19°50'20.7"S 40°34'04.3"W
4	MBML6822_AA81	*Trichomycterus alternatus*	Lower Rio Doce	19°50'20.7"S 40°34'04.3"W
5	MBML6822_AA86	*Trichomycterus alternatus*	Lower Rio Doce	19°50'20.7"S 40°34'04.3"W
6	MBML6841_AB14	*Trichomycterus alternatus*	Lower Rio Doce	19°53'20.3"S 40°34'32.8"W
7	MBML6207_AB16	*Trichomycterus alternatus*	Lower Rio Doce	19°50'26.0"S 40°37'47.3"W
8	MBML4438_AB32-3	*Trichomycterus alternatus*	Lower Rio Doce	19°47'02.1"S 40°38'52.0"W
9	MBML7641_AD18	*Trichomycterus alternatus*	Lower Rio Doce	20°11'42"S 41°03'43"W
10	MBML7641_AD19	*Trichomycterus alternatus*	Lower Rio Doce	20°11'42"S 41°03'43"W
11	MBML7641_AD20	*Trichomycterus alternatus*	Lower Rio Doce	20°11'42"S 41°03'43"W
12	MBML7642_AD21-1	*Trichomycterus alternatus*	Lower Rio Doce	20°10'59"S 41°04'46"W
13	MBML7642_AD22-2	*Trichomycterus alternatus*	Lower Rio Doce	20°10'59"S 41°04'46"W
14	MBML7642_AD23	*Trichomycterus alternatus*	Lower Rio Doce	20°10'59"S 41°04'46"W
15	MBML7665_AD24-1	*Trichomycterus alternatus*	Lower Rio Doce	19°13'00"S 40°52'01"W
16	MBML7665_AD25-2	*Trichomycterus alternatus*	Lower Rio Doce	19°13'00"S 40°52'01"W
17	MBML7665_AD26-3	*Trichomycterus alternatus*	Lower Rio Doce	19°13'00"S 40°52'01"W
18	MBML7672_AD27	*Trichomycterus alternatus*	Lower Rio Doce	19°13'46"S 40°48'52"W
19	MBML7672_AD29-3	*Trichomycterus alternatus*	Lower Rio Doce	19°13'46"S 40°48'52"W
20	MBML7681_AD30-1	*Trichomycterus alternatus*	Lower Rio Doce	19°52'57"S 40°41'24"W
21	MBML7681_AD31-2	*Trichomycterus alternatus*	Lower Rio Doce	19°52'57"S 40°41'24"W
22	MBML6207_AG16-A	*Trichomycterus alternatus*	Lower Rio Doce	19°50'26.0"S 40°37'47.3"W
23	MBML6207_AG17-B	*Trichomycterus alternatus*	Lower Rio Doce	19°50'26.0"S 40°37'47.3"W
24	MBML6210_AG20-A	*Trichomycterus alternatus*	Lower Rio Doce	19°52'41.6"S 40°36'48.5"W
25	MBML6210_AG21-B	*Trichomycterus alternatus*	Lower Rio Doce	19°52'41.6"S 40°36'48.5"W
26	MBML6210_AG22	*Trichomycterus alternatus*	Lower Rio Doce	19°52'41.6"S 40°36'48.5"W
27	MBML6210_AG23-A	*Trichomycterus alternatus*	Lower Rio Doce	19°52'41.6"S 40°36'48.5"W
28	MBML6211_AG24-B	*Trichomycterus alternatus*	Lower Rio Doce	19°53'49.2"S 40°36'10.9"W
29	MBML6211_AG25	*Trichomycterus alternatus*	Lower Rio Doce	19°53'49.2"S 40°36'10.9"W
30	MBML6833_AG80	*Trichomycterus alternatus*	Lower Rio Doce	19°53'04.4"S 40°34'30"W
31	MBML6833_AG81	*Trichomycterus alternatus*	Lower Rio Doce	19°53'04.4"S 40°34'30"W
32	MBML6833_AG82	*Trichomycterus alternatus*	Lower Rio Doce	19°53'04.4"S 40°34'30"W
33	MBML8191_AN76-2	*Trichomycterus alternatus*	Lower Rio Doce	20°22'10.4"S 41°51'28.4"W
34	MBML8191_AN77-3	*Trichomycterus alternatus*	Lower Rio Doce	20°22'10.4"S 41°51'28.4"W
35	MBML8191_AN78-4	*Trichomycterus alternatus*	Lower Rio Doce	20°22'10.4"S 41°51'28.4"W
36	MBML8426_AP79-2	*Trichomycterus alternatus*	Lower Rio Doce	19°57'52.5"S 40°44'20.4"W
37	MBML8426_AP80-3	*Trichomycterus alternatus*	Lower Rio Doce	19°57'52.5"S 40°44'20.4"W
38	MBML8426_AP81-5	*Trichomycterus alternatus*	Lower Rio Doce	19°57'52.5"S 40°44'20.4"W
39	MZUSP121709_MZICT287	*Trichomycterus alternatus*	Middle Rio Doce	19°25'0.42"S 42°43'20.68"W
40	LBP12259_52186	*Trichomycterus alternatus*	Upper Rio Doce	21°09'09.7"S 43°31'37.9"W
41	MBML6822_BC88	*Trichomycterus alternatus*	Lower Rio Doce	19°50'20.7"S 40°34'04.3"W
42	MBML6822_BC89	*Trichomycterus alternatus*	Lower Rio Doce	19°50'20.7"S 40°34'04.3"W
43	MBML6822_BD00	*Trichomycterus alternatus*	Lower Rio Doce	19°50'20.7"S 40°34'04.3"W
44	MBML6822_BD001	*Trichomycterus alternatus*	Lower Rio Doce	19°50'20.7"S 40°34'04.3"W
45	MZUSP121719_MZICT278	*Trichomycterus alternatus*	Middle Rio Doce	19°19'20.24"S 42°31'38.49"W
46	LBP8350_40416	*Trichomycterus alternatus*	Middle Rio Doce	19°40'53.8"S 43°00'50.1"W
47	MZUSP121719_MZICT277	*Trichomycterus alternatus*	Middle Rio Doce	19°19'20.24"S 42°31'38.49"W
48	LBP12259_52186	*Trichomycterus alternatus*	Upper Rio Doce	21°09'09.7"S 43°31'37.9"W
49	MZUSP121719_MZICT275	*Trichomycterus alternatus*	Middle Rio Doce	19°19'20.24"S 42°31'38.49"W
50	LBP8350_40415	*Trichomycterus alternatus*	Middle Rio Doce	19°40'53.8"S 43°00'50.1"W
51	MZUSP121719_MZICT279	*Trichomycterus alternatus*	Middle Rio Doce	19°19'20.24"S 42°31'38.49"W
52	LBP12259_52190	*Trichomycterus alternatus*	Upper Rio Doce	21°09'09.7"S 43°31'37.9"W

Table 1. Continued

#	Sample	Taxon	Drainage	Coordinates
53	LBP12259_52189	*Trichomycterus alternatus*	Upper Rio Doce	21°09'09.7"S 43°31'37.9"W
54	LGC3708	*Trichomycterus alternatus*	Middle Rio Doce	18°57'13"S 43°26'21"W
55	LGC5720	*Trichomycterus alternatus*	Middle Rio Doce	18°48'50"S 43°24'50"W
56	LGC5727	*Trichomycterus alternatus*	Middle Rio Doce	18°46'01"S 43°25'33"W
57	LGC5778	*Trichomycterus alternatus*	Middle Rio Doce	18°55'59"S 43°26'48"W
58	LGC5779	*Trichomycterus alternatus*	Middle Rio Doce	18°55'59"S 43°26'48"W
59	LGC5790	*Trichomycterus alternatus*	Middle Rio Doce	18° 55'29"S 43°27'57"W
60	LGC5798	*Trichomycterus alternatus*	Middle Rio Doce	18°59'22"S 43°22'58"W
61	LGC5799	*Trichomycterus alternatus*	Middle Rio Doce	18°59'22"S 43°22'58"W
62	MBML6841_AB15	*Trichomycterus alternatus*	Lower Rio Doce	19°53'20.3"S 40°34'32.8"W
63	MNRJ50893	*Trichomycterus alternatus*	Middle Rio Doce	18°21'20.00"S 43°10'12.00"W
64	MZUSP123357_MZICT3134	*Trichomycterus alternatus*	Middle Rio Doce	18°56'2.50"S 42°5'2.18"W
65	MZUSP123357_MZICT3164	*Trichomycterus alternatus*	Middle Rio Doce	18°56'2.50"S 42°5'2.18"W
66	MZUSP123397_MZICT3173	*Trichomycterus alternatus*	Middle Rio Doce	19°51'20.22"S, 42°8'24.63"W
67	MZUSP123397_MZICT3174	*Trichomycterus alternatus*	Middle Rio Doce	19°51'20.22"S, 42°8'24.63"W
68	MZUSP123761_MZICT6308	*Trichomycterus alternatus*	Upper Rio Doce	20°14'13.05"S 42°56'53.65"W
69	MZUSP123763_MZICT6313	*Trichomycterus alternatus*	Upper Rio Doce	20°12'21.63"S 42°52'56.24"W
70	MZUSP123764_MZICT6309	*Trichomycterus alternatus*	Upper Rio Doce	20°12'22.03"S 42°52'57.44"W
71	MZUSP123764_MZICT6310	*Trichomycterus alternatus*	Upper Rio Doce	20°12'22.03"S 42°52'57.44"W
72	MZUSP123764_MZICT6311	*Trichomycterus alternatus*	Upper Rio Doce	20°12'22.03"S 42°52'57.44"W
73	MZUSP123764_MZICT6312	*Trichomycterus alternatus*	Upper Rio Doce	20°12'22.03"S 42°52'57.44"W
74	LBP12259_52188	*Trichomycterus alternatus*	Upper Rio Doce	21°09'09.7"S 43°31'37.9"W
75	LGC5723	*Trichomycterus astromycterus*	Middle Rio Doce	18°46'33"S 43°24'34"W
76	LGC3017	*Trichomycterus astromycterus*	Middle Rio Doce	18°46'33"S 43°24'34"W
77	LGC3018	*Trichomycterus astromycterus*	Middle Rio Doce	18°46'33"S 43°24'34"W
78	MZUSP123361_MZICT3170	*Trichomycterus astromycterus*	Middle Rio Doce	19°14'0.76"S 42°19'26.52"W
79	MZUSP123361_MZICT3171	*Trichomycterus astromycterus*	Middle Rio Doce	19°14'0.76"S 42°19'26.52"W
80	MZUSP123361_MZICT3172	*Trichomycterus astromycterus*	Middle Rio Doce	19°14'0.76"S 42°19'26.52"W
81	MZUSP123760_MZICT6314	*Trichomycterus astromycterus*	Upper Rio Doce	20°11'40.32"S 42°51'8.47"W
82	MZUSP123760_MZICT6315	*Trichomycterus astromycterus*	Upper Rio Doce	20°11'40.32"S 42°51'8.47"W
83	MZUSP123760_MZICT6316	*Trichomycterus astromycterus*	Upper Rio Doce	20°11'40.32"S 42°51'8.47"W
84	MZUSP123760_MZICT6317	*Trichomycterus astromycterus*	Upper Rio Doce	20°11'40.32"S 42°51'8.47"W
85	MZUSP123365_IV	*Trichomycterus astromycterus*	Middle Rio Doce	19°14'0.76"S 42°19'26.52"W
86	MZUSP123365_V	*Trichomycterus astromycterus*	Middle Rio Doce	19°14'0.76"S 42°19'26.52"W
91	MZUFV 2565_JD1456	*Trichomycterus tantalus*	Upper Rio Doce	20°9'32.47"S 42°24'9.57"W
92	MZUSP 123369_MZICT3129	*Trichomycterus tantalus*	Middle Rio Doce	19°1'33.62"S 42°7'29.12"W
93	MZUSP 123369_MZICT3130	*Trichomycterus tantalus*	Middle Rio Doce	19°1'33.62"S 42°7'29.12"W
94	MZUSP 123369_MZICT3131	*Trichomycterus tantalus*	Middle Rio Doce	19°1'33.62"S 42°7'29.12"W
98	LGC3687	*Trichomycterus ipatinga*	Middle Rio Doce	18°58'34"S 43°22'21"W
99	LGC3719	*Trichomycterus ipatinga*	Middle Rio Doce	18°59'22"S 43°22'58"W
100	LGC3721	*Trichomycterus ipatinga*	Middle Rio Doce	18°58'47"S 43°23'02"W
101	LGC5721	*Trichomycterus ipatinga*	Middle Rio Doce	18°48'50"S 43°24'50"W
102	LGC5736	*Trichomycterus ipatinga*	Middle Rio Doce	18°58'27"S 43°22'19"W
103	LGC5740	*Trichomycterus ipatinga*	Middle Rio Doce	18°58'27"S 43°22'19"W
104	LGC5745	*Trichomycterus ipatinga*	Middle Rio Doce	18°58'34"S 43°22'21"W
105	LGC5753	*Trichomycterus ipatinga*	Middle Rio Doce	18°58'40"S 43°22'26"W
106	LGC5797	*Trichomycterus ipatinga*	Middle Rio Doce	18°59'22"S 43°22'58"W
107	LGC3686	*Trichomycterus ipatinga*	Middle Rio Doce	18°58'27"S 43°22'19"W
110	MZUSP123750_MZICT6303	*Trichomycterus vinnulus*	Upper Rio Doce	20°12'21.63"S 42°52'56.24"W
111	MZUSP123750_MZICT6302	*Trichomycterus vinnulus*	Upper Rio Doce	20°12'21.63"S 42°52'56.24"W
112	MZUSP123750_MZICT6304	*Trichomycterus vinnulus*	Upper Rio Doce	20°12'21.63"S 42°52'56.24"W
113	MZUSP123750_MZICT6305	*Trichomycterus vinnulus*	Upper Rio Doce	20°12'21.63"S 42°52'56.24"W
114	MZUSP123750_MZICT6306	*Trichomycterus vinnulus*	Upper Rio Doce	20°12'21.63"S 42°52'56.24"W

Table 1. Continued

#	Sample	Taxon	Drainage	Coordinates
115	MZUSP123757_MZICT6307	*Trichomycterus vinnulus*	Upper Rio Doce	20°11'40.32"S 42°51'8.47"W
147	LGC5732	*Trichomycterus* aff. *caipora*	Middle Rio Doce	18°45'42"S 43°25'44"W
148	MZUSP123393_MZICT3132	*Trichomycterus* sp. 1	Middle Rio Doce	19°1'3.06"S 42°7'16.31"W
149	MZUSP123176_MZICT2661	*Trichomycterus* sp. 2	Cubatão	23°54'3.04"S 46°28'7.51"W
150	MZUSP123176_MZICT2662	*Trichomycterus* sp. 2	Cubatão	23°54'3.04"S 46°28'7.51"W
151	MZUSP123176_MZICT2663	*Trichomycterus* sp. 2	Cubatão	23°54'3.04"S 46°28'7.51"W
152	MZUSP123176_MZICT2670	*Trichomycterus* sp. 2	Cubatão	23°54'3.04"S 46°28'7.51"W

for *COI* evolution, thus minimizing its potential pitfalls for phylogenetic reconstruction. Occurrence of substitution saturation was evaluated using the index of substitution saturation (*Iss*) test as described by Xia *et al.* (2003) and Xia & Lemey (2009) implemented in the software DAMBE 5.3.8 (Xia, 2013). Finally, sampling density is a prime factor in solving the kind of problems addressed here. For practical reasons, addition of other markers would inevitably result in a decrease of our aimed inter- and intraspecific density. Our results are not significantly divergent from those using multigene and genomic analyses in the overlapping parts of their coverage (Ochoa *et al.*, 2017, 2020; Katz *et al.*, 2018; Costa, 2021), suggesting that any phylogenetic distortion associated with *COI* use is not rampant.

Alignments and sequence editing were performed in a non-commercial license of GENEIOUS 11.1.7 software to obtain a consensus sequence. Alignments were generated using the MUSCLE algorithm (Edgar, 2004), under default parameters. The resulting matrix was visually inspected for any insertions and deletions. No gaps were found in the matrix analysed. Stop codons were checked using GENEIOUS. In order to analyse the genetic distance, a Kimura 2-parameter model (K2P; Kimura, 1980) was calculated with the help of MEGA-X software (Kumar *et al.*, 2018). Results were compared with those presented by Pereira *et al.* (2013) and Sales *et al.* (2018), which found genetic divergences below 2% among *Trichomycterus* species. Those analyses served as comparative parameters to evaluate the fit of models in the genus, as well as to test the efficiency of the method in intraspecific limit identification.

Phylogenetic relationships were inferred by Bayesian inference using an uncorrelated relaxed molecular clock (lognormal) using a MRBAYES 3.2.6 (Huelsenbeck & Ronquist, 2001) plug-in developed by Marc Suchard in GENEIOUS 11.1.7. The diversification rate was left as default. The substitution model used was GTR with Gamma rate variation at four gamma categories. Random seed was 29 520. The analysis was programmed to run for 2.1 million generations of Markov chain Monte Carlo (saving one best tree every 200 generations), under a birth-death tree prior as determined by default. The first 210 000 generations (10%) were discarded as burn-in, and remaining trees were used to summarize results of the Bayesian analysis in GENEIOUS. The analysis was rooted on *Eremophilus* following Ochoa *et al.* (2020).

SPECIES DELIMITATION

The species concept followed de Pinna (1999), Nelson & Platnick (1981) and Nixon & Wheeler (1990), where diagnosability by unique character states or unique combinations of character states is integrated with hierarchical information from an inferred scheme of relationships. Monophyly of species-level taxa is not a necessary precondition and a large proportion of natural species are indeed not monophyletic (Funk & Olmland, 2003; Mutanen, 2016). No fixed threshold value was defined as a standard limit for species differentiation in barcoding data. A value of 2% or higher has been applied as indicative of species-level differentiation in animal species, such as in bony fish species (Hebert *et al.*, 2003; Ward *et al.*, 2009; Pereira *et al.*, 2010, 2011, 2013; Carvalho *et al.*, 2011; Sales *et al.*, 2018). However, such fixed values have been repeatedly shown to violate species boundaries in actual situations (Vinas & Tudela, 2009; Carvalho *et al.*, 2011; Costa-Silva *et al.*, 2015; Shum *et al.*, 2017; de Queiroz *et al.*, 2020). Clearly, the application of a fixed threshold for all fish species is unrealistic (Krieger & Fuerst, 2002; de Queiroz *et al.*, 2020) and such protocols rely on assumptions parameters, which are variable. As a corollary, we did not adopt an automated procedure for delimiting species boundaries on the basis of barcoding data. Also, due to a lack of sequence data for some species from the Rio Doce, we use corrected distances only as a heuristic guide to observed divergence, rather than automatically mapping species limits with analyses such as general mixed yule-coalescent (GMYC) or Bayesian poisson tree processes model (bPTP). Those protocols are designed for evolutionarily meaningful unities and

may be unadvisable when that precondition is not met, such as in the present case.

Our use of *COI* data (and reciprocally morphological data) can be characterized as a discovery procedure that helps to locate species boundaries, rather than a species-delimitation protocol. Final taxonomic decisions were based on a combination of molecular, morphological and geographical variables (cf. Yang *et al.*, 2019). Such strategy is in tune with the multidimensional nature of taxonomic discovery procedure and yields a more realistic outlook on the complexity of natural situations, with problems such as incomplete taxonomic representation and species known from morphology only. While this certainly adds an element of heterogeneity in our approach, our proposals about species limits and composition are testable hypotheses (DeSalle *et al.*, 2005).

For morphological data, species-level differentiation was determined by the presence of unique combinations of character states verifiable in all specimens of an examined cluster, permitting diagnosability from all other similar clusters. Divergence based on statistical frequency alone was not considered sufficient to diagnose a species. Continuous characters (both morphometric and meristic) were taken as evidence of differentiation only when associated with well-defined gaps in their distribution values.

Geography was an important element in the process of determining species-level boundaries (DeSalle *et al.*, 2005). Sympatry among species-candidates was considered a test of their integrity as lineages and evidence of isolation even in face of close contact, which might otherwise cross reproductive barriers (this is an old concept called non-dimensional species; Mayr, 1969). On the other hand, differentiation in sympatry was a flag for potential cases of sexual dimorphism, polymorphism and, in presence of different body sizes, ontogenetic variation. Such cases were examined in more detail using molecular analyses. The strategy adopted here did not assume single-basin endemism, because some species of *Trichomycterus* are known to be distributed across more than one hydrographic system and basins in general are not necessarily proxies for historical cohesiveness (Dagosta & de Pinna, 2017). Therefore, although the scope of this paper is the Rio Doce Basin, resolution of the taxonomic and nomenclatural situation of the species therein relied on information extrapolating the boundaries of that basin. In fact, most decisions on species limits and names resorted to a comparative scope encompassing the entire genus.

The procedure for detecting taxonomic differentiation was based on a stepwise mutual-illuminating strategy for searching for discontinuities in intrinsic biological attributes, which were then subjected to various tests and cross-references in order to identify indicatives of lineage differentiation. The process started with a circumscription of phenotypic categories characterized by an overlap of diagnostic characteristics from various morphological systems (colour pattern, meristics, morphometrics, osteology, etc). The existence of overlapping gaps in one or more of those variables among phenotypes were considered as suggestive of species-level limits. The entities thus delimited were then tested for consistency and taxonomic integrity against supplemental information on possible sexual dimorphism, ontogenetic changes, polymorphism, sympatry, geographically intermediate populations and intermediate phenotypes. After such potential causative factors were properly considered and discarded, the entities still maintaining their integrity were considered as likely candidates for individual lineages representing species-level taxa. Genetic analyses utilized samples representing a broad range of the phenotypic variation detected, with multiple representatives of each potential lineage and geographical locations whenever possible. This ensured that species undetected phenotypically could be disclosed by genetic distances and then re-examined in more detail for subtle morphological divergence not noticed in previous examination.

RESULTS

Results from molecular data are presented upfront in order to provide a framework against which remaining parts of the paper are organized. Morphological data are included in the taxonomic accounts, which is also the section where all data are integrated with broader taxonomic and nomenclatural considerations into formal species accounts. The limits and applicability of species names used henceforth are those formalized in the taxonomy section, with potentially confusing situations highlighted when necessary.

DNA SEQUENCE DATA

Two hundred and twenty-seven specimens of Trichomycterinae from the Rio Doce and other South American basins, representing three genera and 53 species, are used as data sources for *COI*. Of those, 112 sequences are new (see Table 1) and remaining ones are from the GenBank and BOLD databases (see Supporting Information). The maximum length of amplified sequences ranged from 491 to 702 bp. No insertions, deletions or stop codons are observed. The nucleotide composition of the concatenated matrix is 28.7% thymine, 28.3% cytosine, 23.9% adenine and 19.2% guanine. The *Iss* index indicates no saturation, with an *Iss.c* value greater than *Iss* in all three codon

positions. Several species are represented by a single sequenced specimen, especially those from GenBank. However, potentially complex taxa of direct interest are densely represented, e.g. *T. alternatus* with 87 sequenced specimens followed by *T. immaculatus* with 33 from the entire Rio Doce Drainage and adjacent basins. DNA samples are not available for some species (*T. argos*, *Trichomycterus barrocus* sp. nov., *Trichomycterus brucutu* sp. nov., *Trichomycterus brunoi* Barbosa & Costa, 2010 and *Trichomycterus illuvies* sp. nov.) and their treatment is at this time based entirely on morphological data.

BARCODING RESULTS

For barcoding, a total of 152 *COI* sequences are used, 112 of which are new (see Table 1) and 40 from GenBank. This sequence sampling represents seven nominal species from the Rio Doce, plus two which remain unnamed: *T. alternatus*, *T. astromycterus*, *Trichomycterus* aff. *caipora*, *T. immaculatus*, *Trichomycterus ipatinga* sp. nov., *T. melanopygius*, *Trichomycterus tantalus* sp. nov., *Trichomycterus vinnulus* sp. nov., *Trichomycterus* sp. 1 (see Discussion for the delimitation of these taxa); and two others from separate south-eastern Brazilian basins, *T. brasiliensis* (from the type locality, Rio das Velhas, São Francisco Basin), representing a more distantly-related group (based on Ochoa *et al.*, 2020) and *Trichomycterus* sp. 2 (from Rio Cubatão), a close relative to taxa in the Rio Doce, based on the phylogenetic analysis herein. Most of these species are represented by numerous samples from distinct localities in order to assess their possible barcoding and geographic variability. The maximum length of amplified sequences in this subsample ranges from

684 to 702 bp, with no insertions, deletions or stop codons. Sampling representation reflects the apparent complexity of each potential species and availability of material. Phenotypes from the Rio Doce corresponding to *T. alternatus* are the most densely sampled, with 74 sequenced specimens, while at the other extreme *Trichomycterus* sp. 1 is represented by a single individual.

Nearly all species recognized (91.66%) show conspecific Kimura 2-Parameters (K2P) divergence under 1%, a threshold closely matching species boundaries defined by morphological diagnoses. The exception is *T. alternatus*, which has conspicuously high intraspecific genetic divergence (1.73%), and overlapping conspecific and congeneric K2P distances (0.8% to 7.86% congeneric species) (Table 2). The lowest congeneric species divergence is 0.8% between *T. melanopygius* and *T. ipatinga*, two morphologically well-differentiated species, while the highest is 7.86% between *T. brasiliensis* and *Trichomycterus* sp. 2. Despite DNA barcoding divergence below 2% between many species pairs such as *T. alternatus* and *T. astromycterus* (1.4%), *T. alternatus* and *T. vinnulus* (1.9%), *T. tantalus* and *T. ipatinga* (1.8%), *T. tantalus* and *T. melanopygius* (1.5%) and *T. melanopygius* and *T. ipatinga* (0.8%), the average congeneric divergence is 4.3% among the remaining species. Considering only specimens from the Rio Doce, this value drops to 3.7% (Table 2).

Two samples assignable (or previously assigned) to *T. alternatus* are highly divergent. The first one (at 3.06%) is *Trichomycterus* sp. 1 from the Middle Rio Doce at Baguari, in the district of Governador Valadares (represented by a single specimen, MZICT 3132). The second one (at 3.17%) is *Trichomycterus* sp. 2 from the

Table 2. Average barcoding divergence (%) among *Trichomycterus* species in the Rio Doce Basin, based on a Kimura-Two-Parameters model (K2P) using the *COI* data matrix. Values in diagonal (bold) refer to intraspecific distance within each species

#	Taxon	1	2	3	4	5	6	7	8	9	10	11	12
1	*T. immaculatus*	0.001											
2	*T. immaculatus* (ex-*T. pradensis*)	0.012	0.003										
3	*T. brasiliensis*	0.062	0.065	0.000									
4	*Trichomycterus* sp. 1	0.052	0.059	0.066	n/c								
5	*Trichomycterus* sp. 2	0.060	0.065	0.079	0.036	0.000							
6	*T. alternatus*	0.050	0.049	0.065	0.031	0.032	0.017						
7	*T. astromycterus*	0.048	0.048	0.062	0.027	0.032	0.014	0.001					
8	*T.* aff. *caipora*	0.050	0.053	0.067	0.060	0.063	0.048	0.046	n/c				
9	*T. tantalus*	0.038	0.040	0.061	0.052	0.056	0.043	0.045	0.029	0.002			
10	*T. ipatinga*	0.038	0.038	0.048	0.040	0.043	0.034	0.032	0.026	0.018	0.002		
11	*T. melanopygius*	0.038	0.032	0.055	0.046	0.046	0.033	0.033	0.023	0.015	0.008	0.003	
12	*T. vinnulus*	0.054	0.049	0.073	0.038	0.033	0.019	0.020	0.051	0.048	0.038	0.031	0.000

n/c, not computed, as it is represented by only one specimen.

Rio Cubatão, a population of historical interest because of its mention in a classical study (Eigenmann, 1918) as a representative of *Cambeva zonata* (Eigenmann, 1918) (formerly *Trichomycterus zonatus*). Those two cases cannot be resolved with barcoding distances alone and are further discussed in the next section. At the other extreme, two other species are unambiguously diagnosable as distinct species by morphological data (*T. astromycterus* and *T. vinnulus*), but show no significant *COI* divergence relative to remaining samples assignable to *T. alternatus*, with low K2P genetic interspecific divergence (Table 2; Fig. 1).

Trichomycterus immaculatus, as defined here (see Taxonomic accounts below), is the most homogenous species analysed in this paper, especially in view of its wide geographical range and number of representative specimens (33 *COI* sequences). This species is morphologically and molecularly well defined, with a low conspecific genetic divergence of 0.21% (Table 2). Moreover, *T. immaculatus* is distinguished from all analysed species by its high congeneric divergence, ranging from 3.77% to 6.21% (Table 2).

PHYLOGENETIC RELATIONSHIPS

A Bayesian phylogenetic analysis including dense representation of *Trichomycterus* taxa from the Rio Doce, in combination with equivalent data available for samples outside of the basin, yields key results for understanding the structure and evolution of the genus. Our results agree in major features with those from other recent studies (Ochoa *et al.*, 2017, 2020; Katz *et al.*, 2018; Fernandez *et al.*, 2021; Lima *et al.*, 2021): south-eastern Brazilian *Trichomycterus* is a monophyletic group and sister to a clade composed of *Cambeva* plus *Scleronema*. Perhaps the most surprising result regarding relationships of *Trichomycterus* in our analysis is the existence of a large monophyletic group corresponding almost entirely to the assemblage of species from the Rio Doce (called the 'Doce clade' henceforth). The Doce clade includes *T. alternatus*, *T. astromycterus*, *T.* aff. *caipora*, *Trichomycterus caudofasciatus* Alencar & Costa 2004, *T. immaculatus*, *T. ipatinga*, *T. melanopygius*, *T. tantalus* and *T. vinnulus*. The position of species not available as DNA samples (*T. argos*, *T. barrocus*, *T. brucutu*, *T. brunoi*, *T. illuvies*) cannot be determined at this time. The Doce clade is divided into three major branches: (1) *T. immaculatus*, (2) *T. alternatus*, *T. astromycterus*, *T. caudofasciatus* and *T. vinnulus* and (3) *T.* aff. *caipora*, *T. ipatinga*, *T. melanopygius* and *T. tantalus*. The sister group to the Doce clade is unresolved, but its potential closest relatives include taxa from the Rio Paraíba do Sul, São Francisco, Ribeira de Iguape and Rio Grande. The existence of the Doce clade is unexpected because no phenotypic similarities

were found to reflect such an assemblage. Also, previously published results did not foreshadow the clade, mostly due to a lack of sufficient representation from the Rio Doce Basin. Lima *et al.* (2021) found that *T. alternatus* from the Rio Doce forms a subclade in the species, itself the sister group to all other *T. alternatus*, a finding in agreement with the Doce clade, but of course limited to that single species.

As suggested by barcoding distances and morphological heterogeneity, *T. alternatus* forms a most complex situation. The species is structured in several subclusters in the Bayesian tree. Although extreme subclusters in this species may have high K2P divergence, they are bridged by other subclusters with intermediate values of molecular divergence. This fact, paralleled in equally continuous phenotypic differentiation (see next section), suggests that none of those cases (except perhaps the two mentioned below) warrant separate species status. Further complicating the issue, in the *T. alternatus* clade there are also cases of species with no genetic divergence, but decisive phenotypic differentiation. Those are *T. astromycterus*, *T. vinnulus* and *T. caudofasciatus* (discussed in the next section) and their existence implies that *T. alternatus* is a metaspecies (see Remarks under *T. alternatus*).

The situation of two problematic taxa mentioned above, *Trichomycterus* sp. 1 and *Trichomycterus* sp. 2, is better understood in light of phylogenetic results. *Trichomycterus* sp. 1 forms a long divergent branch inside the *T. alternatus* clade. Given its level of divergence, it may represent an additional case of within-lineage species divergence. More representative specimens of *Trichomycterus* sp. 1, both for morphology and sequence data, are needed to resolve the question. *Trichomycterus* sp. 2 from Rio Cubatão forms a well-delimited clade with other *T. alternatus*-like specimens from the Rio Paranaguá and Rio Ribeira de Iguape basins. All three basins are located far south of the Rio Doce, but this southern clade is not the sister group of all remaining *T. alternatus*. Instead, it is nested in the *T. alternatus* clade, composed mostly of Rio Doce forms. Again, this southern clade may have diverged enough to constitute a separate species, a case in which the metaspecific condition of *T. alternatus* is again corroborated. As yet no phenotypic divergence is detected for that clade. Resolution of the question depends on additional data from these and other intervening basins.

Geographical exceptions exist in the Doce clade as represented in our analysis. Most of them are within *T. alternatus*, a species with an unusually wide geographic distribution. As seen above, samples readily identifiable as *T. alternatus* from other major basins are inside the *T. alternatus* clade (and thus in the Doce clade as well), such as those previously mentioned from the Rio Cubatão and even as far south as the Rio Paranaguá and the Rio Ribeira de Iguape. There are also nominal
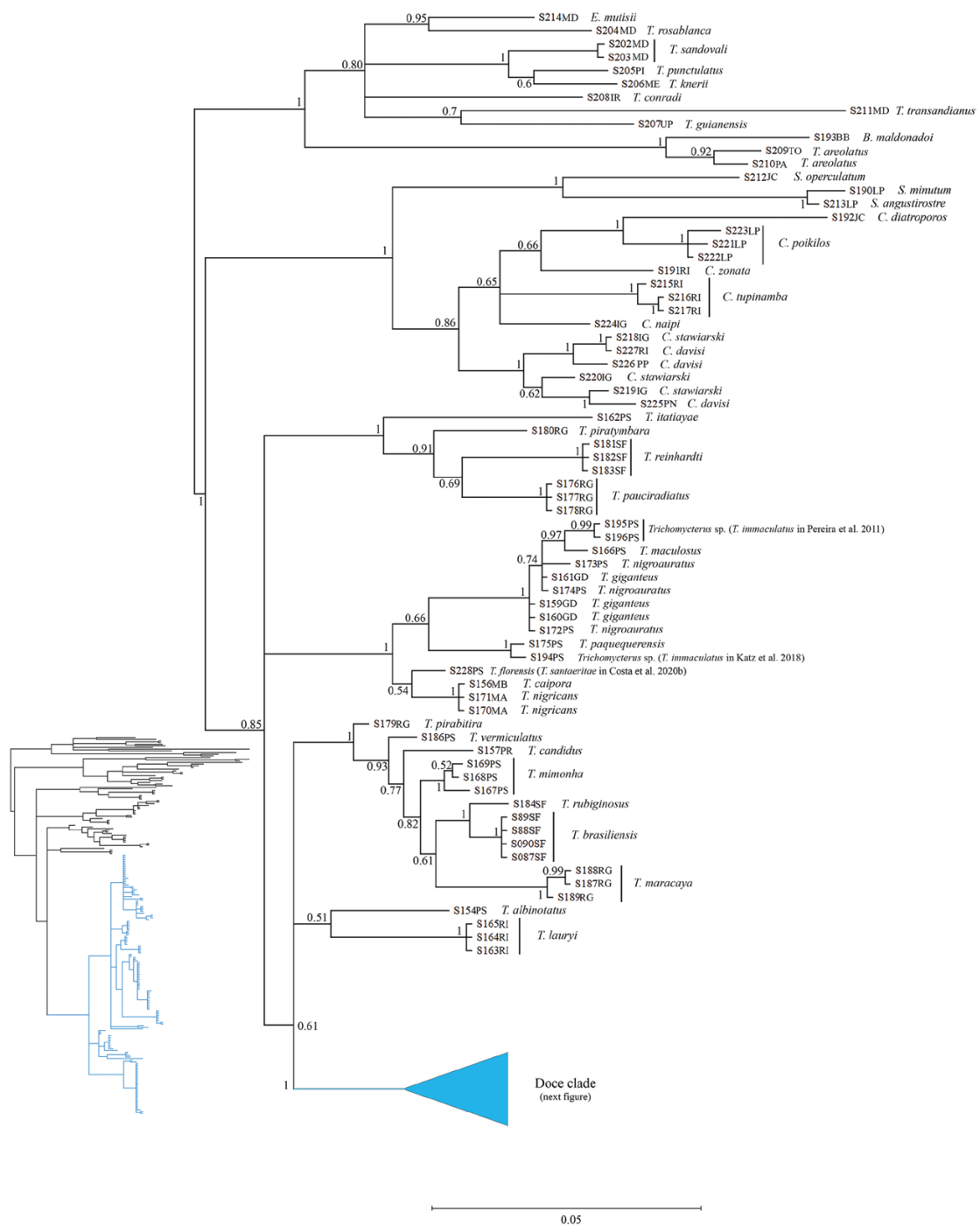
Figure 1. Phylogenetic relationships of *Trichomycterus* species from Rio Doce Basin and related lineages based on mitochondrial data (*COI*) using Bayesian inference. For clarity, phylogenetic tree divided into three parts over separate pages; position of each part indicated by black lines in complete tree on left. Node numbers correspond to Bayesian posterior probability. Abbreviations: in front of each sample number, BB, Biobio River; CT, Cubatão River; GD, Guandu River; IB, Itabapoana River; IG, Iguaçu River; IR, Ireng River; ITN, Itaúnas River; JC, Jacuí River; JU, Jucuruçu River; LP, Lagoa dos Patos; LRD, Lower Rio Doce; LU, Lower Uruguay River; MA, Macacu River; MB, Macabu River; MD, Magdalena River; MRD, Middle Rio Doce; ME, Meta River; NO, Nonguen River; PA, Paicavi River; PG, Paranaguá River; PI, Pisco River; PN, Paraná River; PP, Paranapanema River; PR, Rio Paranaíba; PS, Paraíba do Sul; RG, Rio Grande; RI, Ribeira de Iguape; SF, São Francisco; SM, São Mateus River; TO, Toltén River; URD, Upper Rio Doce; UP, Upper Potaro River.
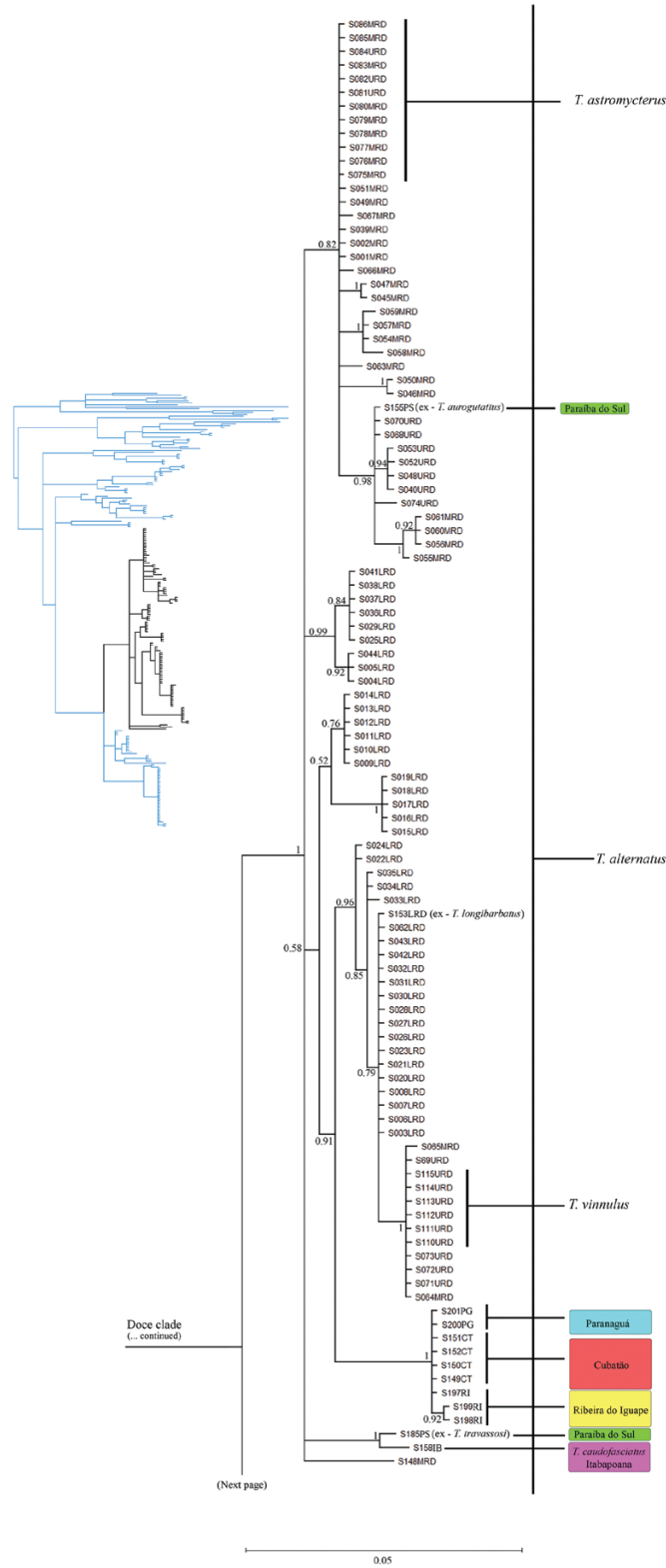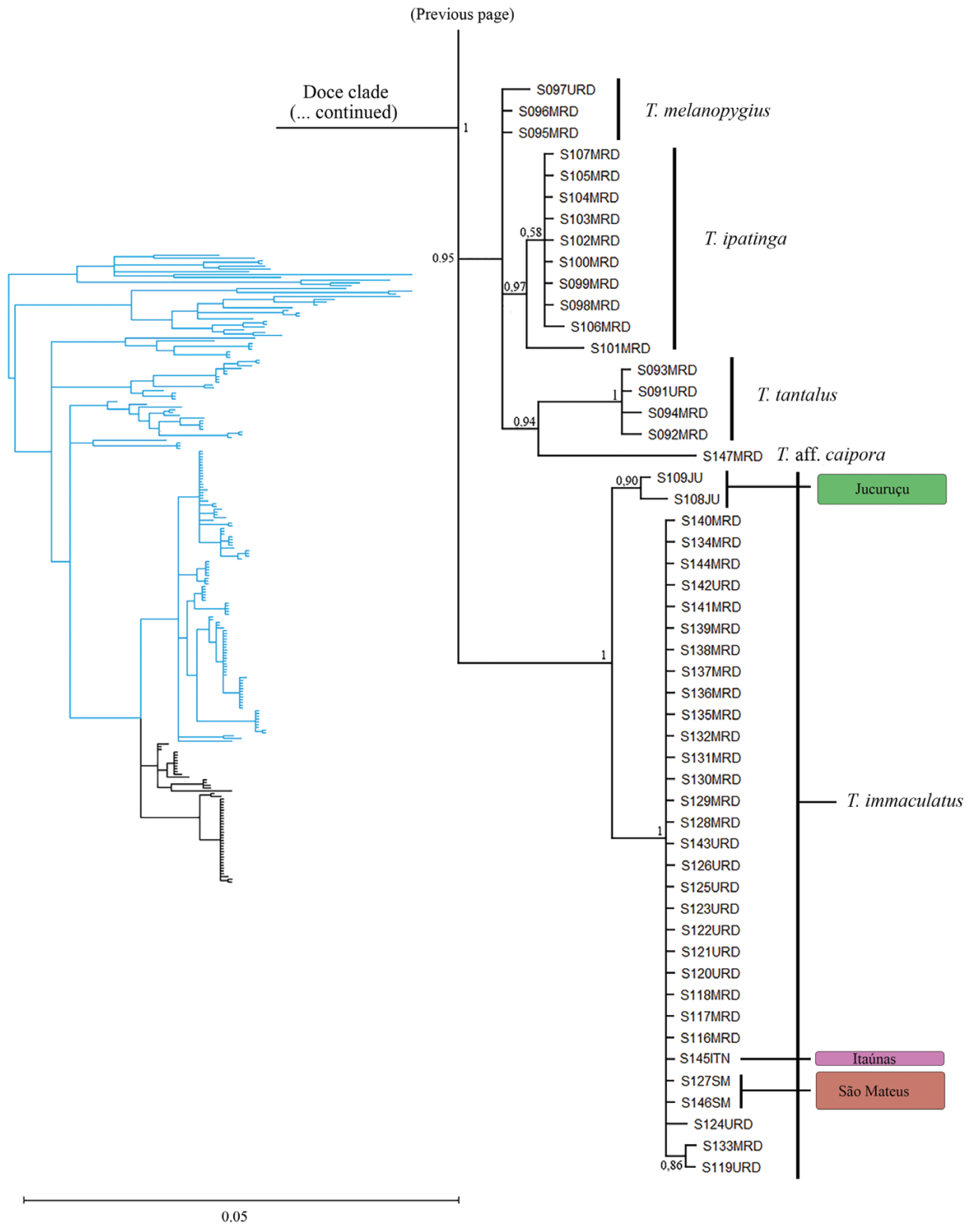
Figure 1. Continued.

Figure 1. Continued.

species in the *T. alternatus* clade which occur outside the Rio Doce, such as *T. caudofasciatus*, and those formerly known as *T. auroguttatus* and *T. longibarbatus* (here considered as junior synonyms of *T. alternatus*; see next section). These are all cases of species in the Doce clade which occur outside the Rio Doce Basin. The opposite kind of exception may also exist, i.e. taxa occurring in the Rio Doce but which do not belong to the Doce clade, although this cannot be positively demonstrated at this time because of the lack of sequence data of the relevant species. A possible case is *Trichomycterus reinhardti*, described from the Rio das Velhas, a tributary of the São Francisco Basin. Recently, Costa & Katz (2021) reported a *T. reinhardti* population from the Rio Doce, an identification we confirmed by examination of the same sample. Although there are no molecular samples from the Rio Doce population, a sample of *T. reinhardti* from the Rio San Francisco included in our phylogeny does not group with the Doce Clade. This species might have reached the Rio Doce by headwater capture. Two other such candidates are *T. argos* and *T. brunoi*, regarded as part of the *T. brasiliensis* clade, a group geographically predominant in basins other than the Rio Doce. The two species are not available for molecular study at this time, but if their affinity with the *T. brasiliensis* group is correct, then these species are members of the Rio Doce assemblage, which does not belong to the Doce clade. Of course, other species currently known only from morphology (*T. barrocus*, *T. brucutu* and *T. illuvies*) and unresolved as to their phylogenetic position, are also potential candidates.

Other species recognized in the Rio Doce constitute mostly cohesive monophyletic groups showing little or no internal structuring. Such is the case with *T. immaculatus*, *T. ipatinga* and *T. tantalus*. Samples of *T. melanopygius* do not cluster in a group together, but they are all joined to a single node without intervening non-conspecific taxa, thus in line with these being a single species (de Pinna, 1999). Our sample of *T.* aff. *caipora* from the Rio Doce comes as the sister group to *T. tantalus* and is separated from the latter by substantial divergence, corroborating its distinctiveness on the basis of morphological characters. However, the sample of *T.* aff. *caipora* from the Rio Doce is phylogenetically distant from the representative of the species from the type locality and the two forms are probably not conspecific (see Remarks under *T.* aff. *caipora* in next section).

TAXONOMIC ACCOUNTS

This section is presented as a synthesis resulting from the molecular analyses presented above in combination with morphological evidence discussed under each species account, along with other technical taxonomic considerations, such as nomenclatural changes, synonyms and new species. Recognized species are formally presented in alphabetical order, with a Remarks section for each of them containing arguments relevant for their delimitation, including reference to molecular results when pertinent.

Each recognized species is provided with a synonymy, diagnosis, description, etymology, remarks and geographic distribution, when pertinent. Diagnoses are comparative and begin with unique characteristics of the taxon (if any), followed by a list of characteristics that in combination permit its identification in *Trichomycterus*, and then by a similar list allowing identification among congeners in the Rio Doce Basin. Any additional information that may have practical value in identifying the species is added at the end (usually details that help differentiate it from phenotypically-close congeners). An identification key is provided at the end of the taxonomic section.

SPECIES ACCOUNTS

TRICHOMYCTERUS ALTERNATUS (EIGENMANN, 1917)

(FIGS 2–4)

Pygidium alternatum Eigenmann, 1917: 700 [type locality: Rio Doce, Brazil, holotype: FMNH 58082 (exCM 7079), paratypes: CAS 64575 (4), FMNH 58083 (62)]; Henn, 1928: 79 (type catalogue); Gosline, 1945: 60 (authorship mistakenly cited as Eigenmann, 1918); Ibarra & Stewart, 1987: 72 (type catalogue); Ferraris, 2007: 414 (checklist).

Trichomycterus alternatum; Burgess, 1989: 321 (list).
Trichomycterus alternatus; Costa, 1992: 104 (comparisons); Bizerril, 1994: 623 (list); Costa & Bockmann, 1994: 717 (comparative material); Miquelarena & Fernández, 2000: 44 (list); de Pinna & Wosiacki, 2003: 279 (checklist); Wosiacki & Garavello, 2004: 5 (list); Triques & Vono, 2004: 170 (comparisons); Bockmann & Sazima 2004: 71 (comparisons); Bockmann *et al.*, 2004: 227 (citation); Alencar & Costa, 2004: 3 (comparisons); Wosiacki, 2005: 51 (comparisons); Wosiacki & Oyakawa, 2005: 470 (comparisons); Ingenito & Buckup, 2007: 1177 (biogeography); Lima *et al.*, 2008: 315 (comparisons); Barbosa & Costa, 2010: 120 (comparisons); Sarmento-Soares *et al.*, 2011: 262 (comparisons); Roldi *et al.*, 2011: 2 (comparisons); Barbosa & Costa, 2011: 308 (comparisons); Barbosa & Costa, 2012: 155 (comparisons); Barbosa, 2013: 274 (comparisons); DoNascimiento *et al.*, 2014a: 709 (comparative material); García-Melo *et al.*, 2016: 238 (comparisons); Ochoa *et al.*, 2017: 75 (relationships, molecular data); Sales *et al.*, 2018: 4 (comparisons); Reis & de Pinna, 2019: 1 (type specimen description, disambiguation of type locality, comparisons); Reis *et al.*, 2019: 12 (comparisons); Donin *et al.*, 2020: 1 (discussion); Reis
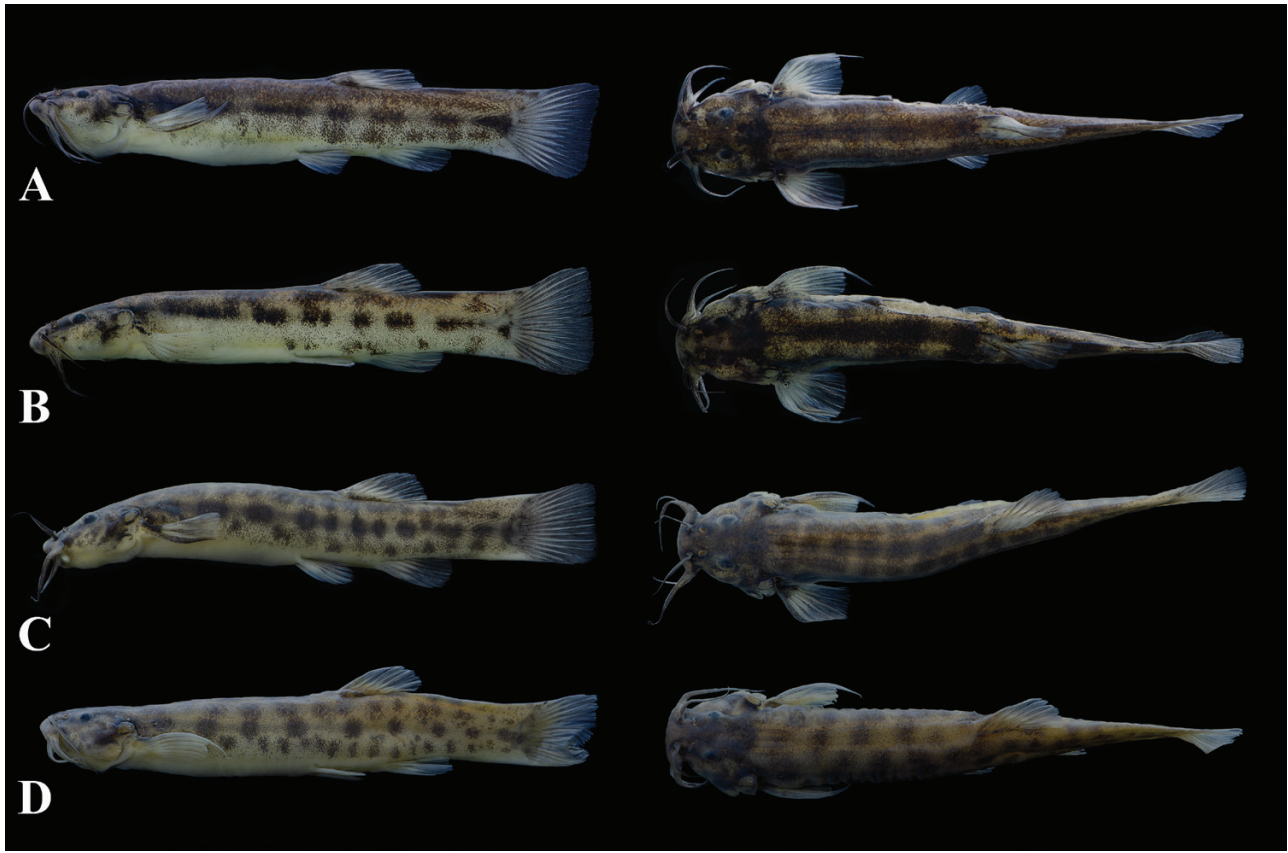
Figure 2. *Trichomycterus alternatus*, topotypes (left, lateral view; right, dorsal view): all from the state of Minas Gerais, Rio Doce Municipality, Rio Doce Basin. A-C, Córrego dos Borges Creek; D, Córrego da Laje Creek. A, MZUSP 123764_MZICT 6310, 43 mm SL; B, MZUSP 123764_MZICT 6309, 44.4 mm SL; C, MZUSP 123763, 45.4 mm SL; D, MZUSP 123761, 51 mm SL.

et al., 2020: 3 (comparisons); DoNascimiento & Prada-Pedreros, 2020: 978 (discussion); Costa *et al.*, 2020: 2924 (discussion); Fernandez *et al.*, 2021: 5 (citation); Ochoa *et al.*, 2020: 3 (discussion on relationship); Lima *et al.*, 2021: 1 (biogeography).

Pygidium travassosi Miranda Ribeiro, 1949: 145, fig. 2 (original description); Miranda Ribeiro, 1954: 12 (type catalogue); Ferraris, 2007: 414 (type catalogue).

Trichomycterus travassosi (Miranda Ribeiro, 1949); Bizerril, 1994: 623 (taxonomic change); de Pinna & Wosiacki, 2003: 279 (synonym of *T. alternatus*); Bockmann *et al.*, 2004: 227 (comparison); Barbosa & Costa, 2008: 184 (comparison); Lima *et al.*, 2008: 316 (citation); Barbosa & Costa, 2010: 121 (comparison); Barbosa & Costa, 2011: 308 (comparison); Barbosa & Costa, 2012: 79 (comparison); Reis & de Pinna, 2019: 100 (citation); Costa *et al.*, 2020: 2924 (discussion); DoNascimiento & Prada-Pedreros, 2020: 978 (discussion).

Trichomycterus longibarbatus Costa, 1992: 104 (original description); Ferraris 2007: 420 (type catalogue); Bizerril, 1994: 623 (citation); Burgess & Finley, 1996: 168 (atlas); de Pinna & Wosiacki, 2003: 282 (checklist); Bockmann *et al.*, 2004: 227 (comparison),

Alencar & Costa, 2004: 3 (comparison); Barbosa & Costa, 2010: 121 (comparison); Rizzato *et al.*, 2011: 485 (comparison); Barbosa & Costa, 2011: 308 (comparison); Barbosa & Costa, 2012: 156 (comparison); Bichuette & Rizzato, 2012: 52 (comparison), Barbosa, 2013: 274 (comparison); Reis & de Pinna, 2019: 100 (citation); Costa *et al.*, 2020: 2924 (discussion); DoNascimiento & Prada-Pedreros, 2020: 978 (discussion).

Trichomycterus auroguttatus Costa, 1992:105, fig. 6 (original description); Ferraris 2007: 420 (type catalogue); Bizerril, 1994: 623 (citation); Burgess & Finley, 1996: 168 (atlas); de Pinna & Wosiacki, 2003: 282 (checklist); Bockmann *et al.*, 2004: 227 (comparison); Alencar & Costa, 2004: 3 (comparison); Barbosa & Costa, 2010: 121 (comparison); Barbosa & Costa, 2011: 308 (comparison); Barbosa & Costa, 2012: 81 (comparison); Reis & de Pinna, 2019: 100 (citation); Costa *et al.*, 2020: 2924 (discussion); DoNascimiento & Prada-Pedreros, 2020: 978 (discussion).

Diagnosis: Trichomycterus alternatus is the most complex taxon to diagnose among those treated in this work. While clearly distinct from all other
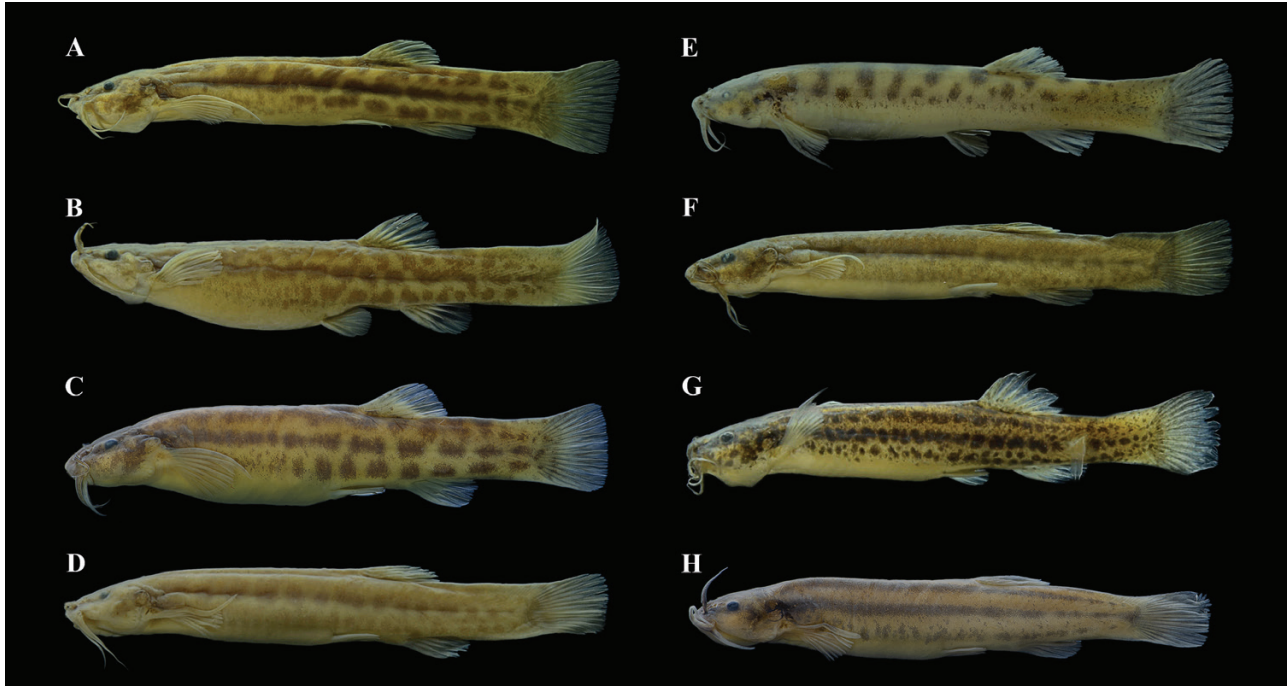
Figure 3. Pigmentation and external morphological variation in *T. alternatus*: All from Brazil, state of Minas Gerais, except (E), from state of Espírito Santo, A, MZUSP 110937, 65.2 mm SL, Mariana Municipality, Rio Piracicaba Drainage; B, MZUSP 87832, 58.2 mm SL, Santo Antonio de Itambé Municipality, Lageado Creek, Rio Mão D'Água, Rio Santo Antônio Drainage; C, MZUSP 94564, 58.5 mm SL, Desterro de Melo Municipality, Rio Xopotó, tributary of Rio Piranga Drainage; D, MZUSP 109311, 49.3 mm SL, Conceição do Mato Dentro Municipality, Rio Santo Antônio Drainage; E, MBML 6200, 47.0 mm SL, Santa Teresa Municipality, Rio Santa Maria do Rio Doce Drainage; F, MZUSP 109302, 53.6 mm SL, Conceição do Mato Dentro Municipality, Rio Santo Antônio Drainage; G, MZUSP 121719, 40.9 mm SL, Santana do Paraíso Municipality, Rio Piracicaba Drainage; H, MZUSP 123339, 35.3 mm SL, Santa Rita de Minas Municipality, Rio Caratinga Drainage.

valid congeners in the Rio Doce Basin, its reported presence outside the basin and the existence of numerous names of uncertain status applied to poorly-known similar forms in surrounding basins (e.g. *T. caudofasciatus*, *Trichomycterus gasparinii* Barbosa, 2013, *Trichomycterus jequitinhonhae* Triques & Vono, 2004, *Trichomycterus landinga* Triques & Vono, 2004, *Trichomycterus mimosensis* Barbosa, 2013, *Trichomycterus nigroauratus* Barbosa & Costa, 2008, *Trichomycterus pantherinus* Alencar & Costa, 2004, *Trichomycterus puriventris* Barbosa & Costa, 2012; see Discussion) make any diagnosis unavoidably dependent on additional data from those nominal species. Still, *T. alternatus* is the oldest available name in that assemblage and it has priority over these other names in case they are found to be synonyms. The combination of the following traits distinguishes *T. alternatus* from congeners (excepting probable junior synonyms mentioned above): (1) colour pattern of body consisting of four rows of large maculae on (one row mid-dorsal, other three rows on flanks and sides), often disguised by variable fusions and anastomoses, forming patterns ranging from spotted to nebulous, sometimes with a lateral stripe; (2) I + 7 pectoral-fin rays (vs.

I + 5, I + 6 or I + 8); (3) two lateral-line pores (vs. three); (4) subtruncate to truncate caudal fin (vs. round or concave); (5) dorsal-fin rays II + 7 (vs. II + 8 or more). Among congeners in south-eastern South America, character 1 distinguishes *T. alternatus* from *T. barrocus* and *Trichomycterus itatiayae* Miranda Ribeiro, 1906, from all taxa in the *T. brasiliensis* and *T. reinhardti* species complex (Barbosa & Costa, 2010; Costa, 2021; Costa & Katz, 2021), from the species that exhibit the *T. nigricans* colour pattern (Reis *et al.*, 2020), from *Trichomycterus caipora* Lima, Lazzarotto & Costa 2008, *T.* aff. *caipora*, *Trichomycterus giganteus* Lima & Costa, 2004, *T. illuvies*, *Trichomycterus itacambirussu* Triques & Vono, 2004 and *Trichomycterus lauryi* Donin, Ferrer & Carvalho, 2020; character 2 distinguishes *T. alternatus* from the *T. brasiliensis* and *T. reinhardti* species complex (Barbosa & Costa, 2010; Costa, 2021; Costa & Katz, 2021), plus *Trichomycterus trefauti* Wosiacki, 2004 (all preceding with I + 6 or fewer), *T. astromycterus*, *T. caipora*, *T. giganteus*, *T. immaculatus*, *T. lauryi*, *T. nigricans* and *T. tantalus* (with I + 8 or more); character 3 distinguishes *T. alternatus* from *T. astromycterus*, *T.* aff. *caipora*, *T. ipatinga*, *T. nigricans*, *T. tantalus* and *T. vinnulus* (all with three or more lateral-line

Figure 4. Pigmentation and external morphological variation in *T. alternatus*, MZUSP 123339, Brazil, state of Minas Gerais, Santa Rita de Minas Municipality, Rio Caratinga Drainage. A, 33.7 mm SL; B, 35.3 mm SL; C, 70 mm SL.

pores); character 4 distinguishes *T. alternatus* from *T. astromycterus* and *T. tantalus* (both with a concave caudal fin); and character 5 distinguishes *T. alternatus* from *T. astromycterus* (with II + 8 or II + 9 dorsal-fin rays). Among congeners in the Rio Doce Basin, *T. alternatus* is most similar to *T. barrocus* and *T. illuvies* (both described in this paper). It can be distinguished from those two species, in addition to characters mentioned above, by the presence of a large fenestra between the orbitosphenoid and the frontal (vs. absent), by having fewer odontodes in the opercle (12–16) and interopercle (25–34) (vs. 15–25 opercular and 30–49 interopercular in *T. barrocus* and *T. illuvies*) and by having more numerous dorsal procurrent rays in the caudal fin (18–25) (vs. 12–17 in *T. barrocus* and *T. illuvies*). *Trichomycterus alternatus* can be further distinguished from *T. barrocus* by the deeper body (13.80–18.31% vs. 9.0–13.9%) and the larger prepelvic length (52.8–70.9% vs. 41.9–52.5%).

Description: Morphometric data for specimens examined is presented in Table 3. Body long and

almost entirely straight, trunk roughly round in cross-section near head, then slightly deeper than wide and gently compressed towards caudal peduncle, tapering to caudal fin. Dorsal profile of body gently convex to dorsal-fin origin, then straight or slightly concave along caudal peduncle to caudal-fin origin. Ventral profile convex from gular region to vent, due partly to abdominal distension, then straight or slightly concave along anal-fin origin to caudal-fin base. Caudal peduncle almost as deep as body at beginning of anal-fin base.

Head approximately 1/5 of SL, pentagonal, slightly longer than wide and depressed. Mouth sub-terminal. Upper jaw slightly longer than lower one. Upper lip wider than lower lip, and laterally continuous with base of maxillary barbel. Lower lip small, approximately 2/3 width of upper one, partly divided into right and left portions by median concavity. Lower lip with uniform covering of tiny villi, not clustered into large papillae, resulting in velvet-like surface. Region between upper and lower lips with slender fleshy lobe.

Table 3. Morphometric data of *T. alternatus* based on type and comparative material. Abbreviations: (A) holotype and paratypes of *T. alternatus* (*N* = 11), FMNH 58082, 58083; (B) comparative material from the Rio Doce Basin (*N* = 27), MZUSP 94564, 109302, 121710, 121719, 87832, 110937, 109311, 123761, 123764, 123763, MBML 607, 6200, 2290; (C) holotype and paratypes of *T. longibarbatus* (*N* = 7), MZUSP 43339, 23812; (D) holotype and paratypes of *T. auroguttatus* (*N* = 4), MZUSP 43341, 43342

	A			B			C			D		
	Range	Mean	SD	Range	Mean	SD	Range	Mean	SD	Range	Mean	SD
Standard length (mm)	42.5–65	50.1	-	33.3–70.6	46.2	-	34.8–57.4	42.9	-	33.8–50.6	42.2	-
% of standard length												
Anal-fin base	7.1–9.6	8.3	0.6	6.7–9.7	8.4	0.8	7.0–8.9	8.1	0.6	5.8–9.9	7.8	1.5
Body depth	11.2–16.0	14.0	1.3	13.8–18.3	14.9	1.2	14.3–18.0	16.2	1.0	12.3–14.0	13.1	0.6
Caudal peduncle depth	9.1–13.3	12.4	0.7	9.6–14.1	12.1	0.9	11.9–13.8	12.6	0.7	9.4–11.3	10.1	0.7
Dorsal-fin base	9.3–11.6	10.5	0.7	8.2–13.0	10.8	1.2	9.3–10.8	10.2	0.5	9.7–10.9	10.2	0.5
First pectoral-fin length	12.3–16.0	20.8	1.4	12.4–18.7	14.3	1.3	13.7–18.2	16.2	1.5	14.9–19.2	17.0	1.6
Head length	17.7–20.6	18.9	0.9	16.1–20.7	18.8	1.1	19.1–21.3	20.2	0.8	18.7–20.7	19.5	0.8
Preanal length	71.8–76.6	74.0	1.4	63.8–82.9	71.2	3.2	70.6–75.6	72.2	1.5	66.3–70.9	69.1	1.7
Predorsal length	62.9–67.1	65.2	1.3	55.4–70.3	63.4	3.4	62.8–67.8	65.0	1.7	56.7–60.6	58.8	1.6
Prepelvic length	54.4–59.1	57.1	1.5	52.8–70.9	56.9	5.1	54.8–59.5	56.9	1.5	49.6–55.3	53.1	2.1
% of head length												
Eye diameter	16.7–22.5	19.3	1.7	15.8–22.3	19.4	1.6	14.6–18.4	16.3	1.3	15.2–17.9	16.6	1.0
Interorbital width	22.1–30.7	26.0	2.3	21.6–31.6	26.3	2.9	26.7–34.4	31.3	2.3	28.1–28.5	28.4	0.2
Snout length	41.8–50.7	45.1	2.6	30.1–57.9	44.4	5	36.5–52.8	44.1	4.5	47.4–51.6	49.1	1.5
Mouth width	35.4–50.8	39.8	4.3	27.0–50.8	35.8	4.6	35.6–47.1	40.5	3.8	28.4–40.6	34.2	4.7

Dentary and premaxillary teeth similar to each other in shape. Dentary teeth conical, arranged in two to four irregular rows, first row with 9–11 teeth, extending from base to slightly up of coronoid process, with size of individual teeth increasing markedly towards symphysis and from posterior to anterior rows. Premaxillary teeth conical, arranged irregularly in two to four rows over entire ventral surface of premaxilla, first row with 8–10 teeth. Total area of premaxillary teeth visually slightly smaller than that of dentary.

Eye medium sized, slightly protruding, positioned laterodorsally on head, without free orbital rim and covered with transparent skin. Eye located on anterior half of HL, closer to lateral border of head than to the midline in dorsal view. Anterior naris surrounded by tube of integument directed anterolaterally, continuous posterolaterally with nasal barbel. Posterior naris closer to anterior naris than to eyes, surrounded by tube of integument incomplete posteriorly. Maxillary barbel narrowing markedly towards fine tip, reaching anteromesial border of eyes or 1/4 of pectoral-fin base. Rictal barbel inserted immediately ventral to maxillary barbel, its tip reaching from anterior border of eyes to base of pectoral fin. Nasal barbel originating on posterolateral region of anterior naris, reaching anywhere from anterior border of posterior naris to posterior portion of opercle. Interopercular patch of odontodes medium to large compared to head length, oval in shape and with well-developed odontodes, prominent in ventral aspect of head. Interopercular patch of odontodes extending from vertical through ventroposterior border of eye to ventroanterior to opercle patch of odontodes. Odontodes arranged in three or four irregular series, with those on mesial series much longer than those on lateral one; odontodes gradually larger posteriorly in both series, with those posteriorly on mesial row largest. Interopercular odontodes 25–34. Opercular patch of odontodes on dorsolateral surface of posterior part of head, positioned anterodorsally to pectoral-fin base, roundish in shape and larger than eye in dorsal aspect of head. Opercular odontodes 12–16, sunk in individual slits of integument, progressively larger posteriorly, all with fine tips, with largest ones curved distally and claw-like. Entire patch surrounded by rim of integument.

Pectoral fin with its base immediately posterior and ventral to opercular patch of odontodes. Pectoral-fin rays I + 7. First pectoral-fin ray (unbranched) longest, prolonged as filament beyond fin margin, with variable length. Other rays progressively shorter, their tips following continuous line along fin margin. Pelvic fin with convex distal profile, just covering anal and urogenital openings in adults, its origin slightly posterior to middle of SL and anterior to vertical through dorsal-fin origin. Bases of pelvic fins separated by one eye diameter from each other. Pelvic-fin rays

I + 4. Anterior process of basipterygium long and thin. Dorsal fin long, its distal margin sinusoidal. Dorsal-fin origin closer to base of caudal fin than to tip of snout. Dorsal-fin rays (ii or iii) + II + 7. Anal fin slightly smaller than dorsal fin, its distal margin gently convex. Anal-fin origin posterior to vertical through end of dorsal-fin base. Anal-fin rays (i, ii or iii) + II + 5. Caudal fin ranging from round to truncate in shape, with 6 + 7 principal rays. Adipose fin absent or represented by low integument fold extending between end of dorsal fin and caudal-fin origin. Post-Weberian vertebrae 34 (1), 35 (10), 36 (9), 37 (1). First dorsal-fin pterygiophore immediately anterior to neural spine of 15th (5), 16th (15), 17th (2) vertebra, first anal-fin pterygiophore immediately anterior to neural spine of 19th (2), 20th (13), 21st (7) vertebra. Caudal-fin procurrent rays plus one segmented non-principal ray dorsally and ventrally. Procurrent caudal-fin rays, 18–25 dorsally and 11–15 ventrally, beginning anteriorly at 28th to 32nd vertebrae. Ribs 10 (1), 11 (10), 12(9), 13 (4). Branchiostegal rays 6 (2) to 7 (18), some specimens with six on one side and seven on the other. Dorsal-fin pterygiophores 8. Anal-fin pterygiophores 6.

Cephalic lateral-line canals with simple non-dendritic tubes ending in single pores. Supraorbital canal mostly in frontal bone. Supraorbital pores invariably present: s1 mesial to nasal-barbel base and autopalatine, s3 mesial to posterior nostril and anterior to frontal, and single or paired s6 posteromedial to eye and at midlength of frontal. Infraorbital latero-sensory canal incomplete with four pores, i1 and i3 anteriorly and i10 and i11 posteriorly. This canal extending from sphenotic posteriorly to terminal pore located ventroposteriorly to eye. Infraorbital pore i1 located ventrolateral to nasal-barbel base and autopalatine, i3 ventrolateral to posterior nostril and anterior to frontal, i10 and i11 posterior to eye. Otic canal without pores. Postotic pores po1, anteromedial to opercular patch of odontodes, and po2, mesial to opercular patch of odontodes. Lateral line of trunk anteriorly continuous with postotic canal and reduced to short tube. Lateral line pores ll1 and ll2 dorsomedial to pectoral-fin base.

Coloration in ethanol: Pigmentation pattern extremely variable both within and among populations (Figs 2–4). Basic colour of body consisting of large roundish maculae disposed in four irregular rows. One mid-dorsal row along entire dorsum, from occiput to dorsal edge of caudal peduncle. Second row ventrolateral to mid-dorsal one, extending from base of head, along upper part of flanks, entering dorsal half of caudal peduncle to base of caudal fin. Third row running along mid-lateral line, from end of opercle to base of caudal fin. Fourth row ventrolateral, less conspicuous and shorter than remaining three, extending along posterior part of abdomen, through posterior margin of pelvic fin to base of caudal fin. Four-row pattern partly or mostly disrupted by irregular fusions (mostly along anterior part of body) and misaligned maculae, resulting in various different configurations (Figs 2–3). At one extreme, maculae are well separated by extensive white areas (Fig. 3F). At other extreme, maculae are largely fused into nebulous pattern forming long stripes (Fig. 3H) or barely discernible (Fig. 3E). Intermediate patterns include partial or total fusion of mid-lateral row into mid-lateral stripe (Fig. 3A, G-H) or overall fragmentation of maculae into nearly uniform mottled covering (Fig. 3E, G). Middorsal row sometimes entirely fused into broad dark band (Fig. 3H). Ventral row of spots sometimes as well-defined and conspicuous as other rows (Fig. 3A-C), sometimes reduced in size to irregular speckles or nearly absent (Fig. 3D-G). Ventral row usually restricted to posterior part of abdomen and caudal peduncle, extending anteriorly as cloud of small spots. Ventral side of abdomen lacking dark pigment. Head darkest on region corresponding to neurocranium, outlined by brain pigment seen by transparency. Dark spot at base of opercular patch of odontodes, with additional dark markings on cheeks. Distal margin of integument fold of opercular patch of odontodes darkly pigmented. Interopercular patch of odontodes unpigmented. Light teardrop-shaped area extending from posterior margin of eye to base of opercular patch of odontodes, corresponding to position of levator operculi muscle. Base of nasal barbel surrounded with concentration of dark pigment, extending posteriorly as elongate dark field to anterior margin of eyes. Dark pigmentation of fins restricted to irregular spots at bases of dorsal, caudal and pectoral fins, with thin dark streaks along fin rays.

Remarks: Trichomycterus alternatus was described from the Upper Rio Doce Basin in the town of Rio Doce, state of Minas Gerais (Reis & de Pinna, 2019). Representatives of the species have historically been reported from numerous south-eastern Brazilian localities, both in the Rio Doce and other basins (Barbosa, 2004; Lima, 2008, 2021; Volpi, 2017; Lima *et al.*, 2021). Widespread uncertainty about the application of the name *T. alternatus* lingered for a long time after its description, mostly due to confusion with *C. zonata*, and lack of detailed information on relevant type specimens, a situation which has recently been ameliorated (Reis & de Pinna, 2019). Material examined during the present work, including type specimens and samples from the type-locality, shows that *T. alternatus* is widespread throughout the Rio Doce Basin and several other south-eastern and south Brazilian basins. Such conclusion is corroborated by both morphological and molecular data, which show

uniformity or continuity across the range of the species. Our comparative analysis included extensive representation of *T. alternatus* from the Lower, Middle and Upper Rio Doce, in addition to data from several other basins (Rio Paraíba do Sul, Rio Itabapoana, Rio Paranaguá, Rio Cubatão and Rio Ribeira de Iguape), covering a large portion of the south-eastern Brazilian region. Phylogenetic analysis (see Phylogenetic relationships above; Fig. 1) shows that samples of *T. alternatus* from across that range cluster in a clade. In combination with their phenotypic continuity, this strongly indicates the species is an evolutionarily cohesive unit (with some isolated diverging lineages, as discussed below). Interestingly, samples of *T. alternatus* from basins outside of the Rio Doce are mostly nested in populations of that basin. Such results have important consequences for inferences about the history of diversification and dispersion of *T. alternatus* (see Discussion).

Different populations of *T. alternatus* in the Rio Doce may show local morphological and colour pattern peculiarities which, if taken in isolation, seem to distinguish them from more typical specimens of *T. alternatus*. For example, some samples (e.g. MZUSP 110937, from Rio Piracicaba at Mariana, and MBML 6200 Santa Maria do Rio Doce, Santa Tereza) have long barbels relative to head length, resembling the phenotype described for *T. longibarbatus* (nasal barbel length: 78.4–102.6%; maxillary barbel length: 87.4–113.2%). At the other extreme, barbels are short in some other populations (nasal barbel length: 34.2–62.3%; maxillary barbel length: 38.1–64.9%) (e.g. MZUSP 52542, from Santo Antônio River, Braúnas, MBML 2290, from Rio Guandu Basin at Afonso Cláudio), matching those considered typical of *T. auroguttatus*. Similar patterns of apparent differentiation occur also in the first pectoral-fin ray, which can be prolongued into a filament varying widely in length. Pronounced variation is also observed in pigmentation and the degree to which the pelvic fin reaches or covers the urogenital opening. The pigmentation pattern of *T. alternatus* is extremely variable, ranging from rows of round maculae along the body to fused maculae forming longitudinal dark stripes or irregular isolated maculae (Fig. 3). The most morphologically divergent population examined of *T. alternatus* in the Rio Doce is from the Caratinga River in Minas Gerais State (MZUSP 123339) (Figs 3H, 4). Specimens from that locality diverge from typical *T. alternatus* in features such as smaller head (HL 6.5–8.4% SL), shorter snout (41.2–52.1% HL), abrupt depression on caudal peduncle (9.5–11.6% SL), smaller and shallower caudal fin (Figs 3H, 4) and a peculiar predominant colour pattern (Figs 3H, 4). However, examination of numerous *T. alternatus* populations in the Rio Doce shows that such variation grades into one another,

leaving no gaps or clear-cut distinctions that would indicate taxonomic differentiation at the species level, according to criteria adopted in this work. Colour pattern is in fact variable in that population, because one specimen in the lot has a typical *T. alternatus* pattern, and another has an intermediate condition (Fig. 4). Unfortunately, samples of that population suitable for DNA analysis are not available, but phenotypic data do not support recognition of a separate species.

Similar conclusions are supported also by the lack of significant divergence in *COI* sequences in instances where data is available. An example is a population of *T. alternatus* from the Piranga River (Upper Rio Doce Basin; MZUSP 94485) and another from Santa Maria do Rio Doce River (Lower Rio Doce Basin; MBML 4642), which differ markedly in characters such as barbel length, first pectoral-fin ray length and to a small degree, colour pattern. In combination, the differences are suggestive of separate species under superficial examination. However, as in the previous example, there are intervening populations with intermediate conditions which bridge the apparent morphological gap. That inference is corroborated by a low *COI* divergence among various populations of *T. alternatus* (1.7%), well within estimates of intra- and interspecific genetic differentiation (Sales *et al.*, 2018) (Table 2). A similar situation was reported by Nascimento *et al.* (2017) in *Cambeva davisi*, a species with wide variation in morphology and colour pattern. Although colour pattern has been shown to be conservative in some *Trichomycterus* species (Bockmann & Sazima, 2004), this is by no means the rule in species of the genus, where colour pattern may be subject to pronounced polymorphism (Arratia *et al.*, 1978; Triques & Vono, 2004; Castellanos-Morales, 2007; Lima *et al.*, 2008; Silva *et al.*, 2010; Ferrer & Malabarba, 2013; Buckup *et al.*, 2014). Marked degrees of intraspecific variation in colour pattern and other morphological traits exist in several *Trichomycterus* species in the Rio Doce, in addition to *T. alternatus*, such as *T. argos*, *T. tantalus*, *T. ipatinga*, *T. immaculatus* and *T. vinnulus* (Figs 3–10, respectively). *COI* sequences of samples of *T. tantalus*, *T. ipatinga*, *T. immaculatus* and *T. vinnulus* lack significant intraspecific divergence (below 0.3%; Table 2), whereas *T. alternatus* has 1.7% divergence. Divergence below 2% has been shown to indicate 95% probability in belonging to the same species (Ward *et al.*, 2009). Similar results were reported for several other groups of fishes (Hubert *et al.*, 2008; Ward, 2009; Pereira *et al.*, 2010, 2011; Carvalho *et al.*, 2011; Mabragaña *et al.*, 2011; Sales *et al.*, 2018). Of course, a 2% barcoding divergence, in isolation, cannot be taken as an absolute threshold and may even be unrealistic for species of *Trichomycterus* and other taxa (Pereira *et al.*, 2010, 2013; Donin *et al.*, 2020; de Queiroz *et al.*, 2020).

Figure 5. *Trichomycterus argos*, MZUSP 106274, paratype (A, lateral; B, dorsal; C, ventral view) 56.8 mm SL and (D, lateral; E, dorsal; F, ventral view) 90.8 mm SL. Brazil, state of Minas Gerais, Araponga Municipality, Parque Estadual da Serra do Brigadeiro, Córrego Serra Nova, tributary of Rio Casca Drainage.
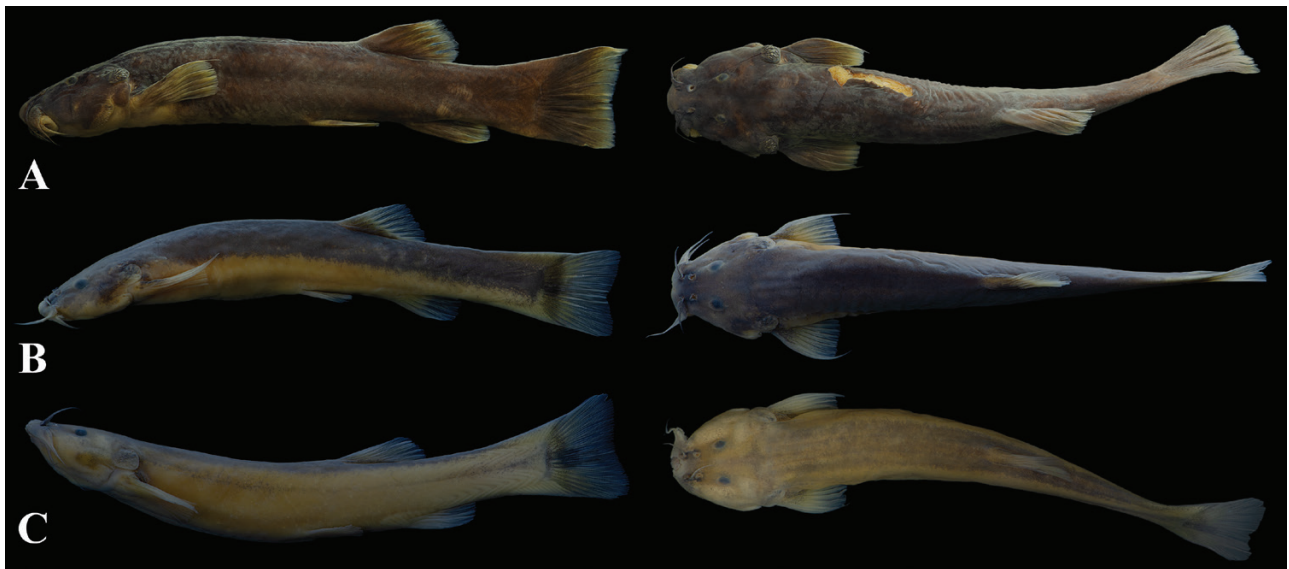
Figure 6. Pigmentation and external morphological variation in *Trichomycterus tantalus* sp. nov. (left, lateral views; right, dorsal views): all from Brazil, state of Minas Gerais, A, MZUFV 2565, paratype, 154 mm SL, Raul Soares Municipality, Rio Matipó; B, MZUSP 123369, holotype, 76 mm SL, Baguari Municipality, main channel of Rio Doce; C, same as preceding, 74.8 mm SL.

However, congruence of morphological and molecular data represents a strong signal that *T. alternatus* as recognized here is a single widespread species.

Considerations above led us to propose or confirm some nominal forms in our synonymic list of *T. alternatus*. Examination of type and non-type material referable
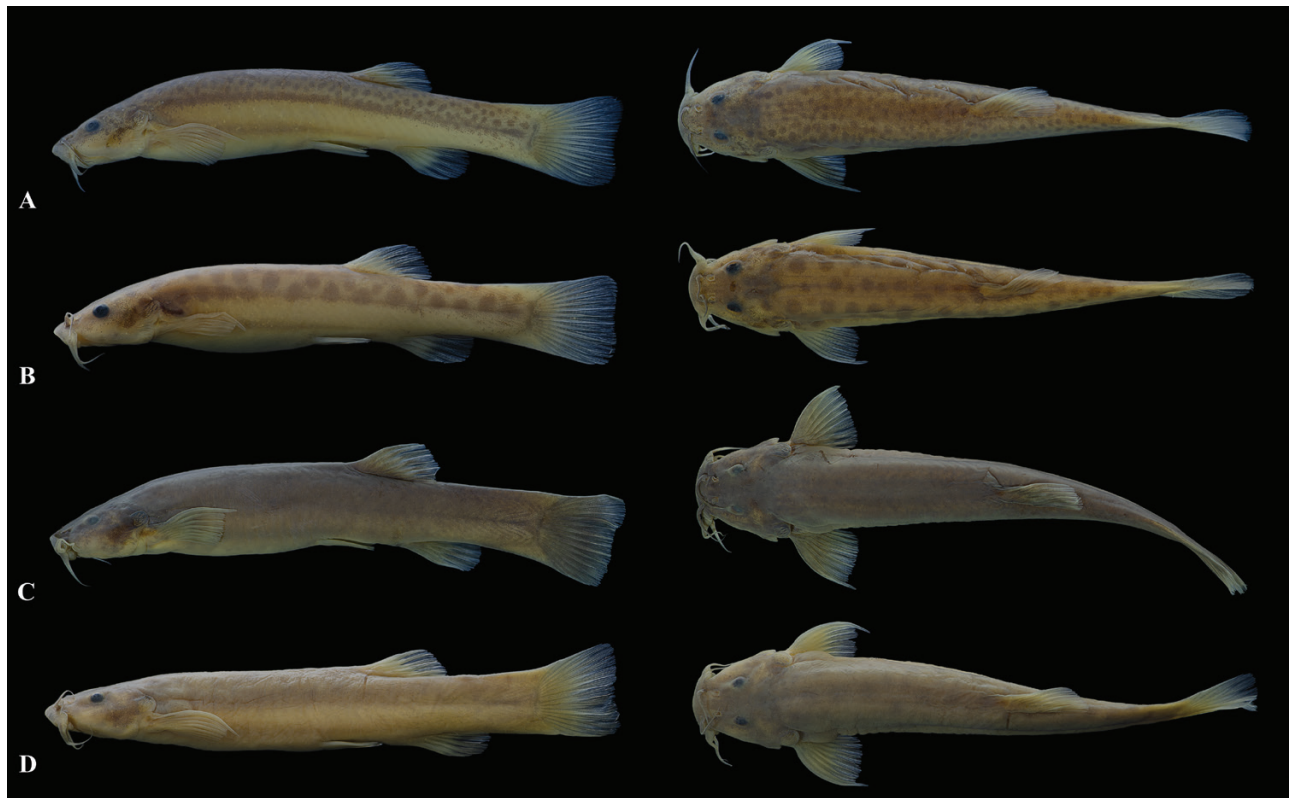
Figure 7. Pigmentation and external morphological variation in *Trichomycterus ipatinga* sp. nov. (lateral views). All from Brazil. (A) and (B) from state of Minas Gerais, (C) from state of Espírito Santo; A, MZUSP 104702, 67.6 mm SL, Conceição do Mato Dentro Municipality, Faia Creek, tributary of Rio São João Drainage; B, MZUSP 112277 94.7 mm SL, Conceição do Mato Dentro Municipality, Rio São João Drainage; C, MBML 6223, 68.7 mm SL, Afonso Cláudio Municipality, Rio Guandu Drainage.

to *T. auroguttatus*, *T. longibarbatus* and *T. travassosi* did not reveal evidence of differentiation beyond the clinal variation observed for *T. alternatus* in various phenotypic traits such as those described in species descriptions. Also, sequence data of samples putatively representing members of the three forms showed no significant differentiation from *T. alternatus*. With no evidence of species-level divergence from either morphology or DNA sequences, we consider these three forms are junior synonyms of *T. alternatus*, the oldest available name. Other previously described taxa, such as *T. caudofasciatus* (Rio Itabapoana) also fall in the *T. alternatus* clade according to *COI* data, but that taxon still needs a more detailed phenotypic assessment.

At the other end of the spectrum, there are taxa that differentiated to species-level in the *T. alternatus* lineage. Those species are subsets of *T. alternatus* which have diverged to separate species levels as evidenced by phenotypic data, such as *T. astromycterus* and

T. vinnulus, as well as probably those which diverged in *COI* sequences but not in morphology, such as *Trichomycterus* sp. 1 and *Trichomycterus* sp. 2 discussed above. This implies that *T. alternatus* is a metaspecies (Donoghue, 1985; de Queiroz & Donoghue, 1988; Archibald, 1994), with parts of it differentiated into full species, which we call exospecies. Unusually however, according to our analyses *T. alternatus* is polyphyletic, a relatively rare phenomenon also found in some species of *Gymnotus* (Mutanen *et al.*, 2016; Craig *et al.*, 2019), rather than paraphyletic as in most documented cases of metaspecies [*Anetia jaegeri* (Ménétriés, 1832) in Ackery & Vane-Wright 1984, *Characidium zebra* Eigenmann, 1909 in Buckup, 1992, *Lariosaurus balsami* Curioni, 1847 in Rieppel, 2000, *Mastiglanis asopos* Bockmann, 1994 in de Pinna & Keith, 2019] (see Discussion). Among a distantly related group of organisms, a case similar to that of *T. alternatus* happens with the distantly related macaque *Macaca mulatta* (Zimmermann, 1780), widely distributed from Afghanistan to the east coast of China

Figure 8. Pigmentation and external morphological variation in *T. immaculatus* in paratypes of *T. pradensis* (left, lateral views; right, dorsal views). All from Brazil, state of Bahia: A, MNRJ 28484, 48.4 mm SL, Jucuruçu Municipality, Rio Jucuruçu Drainage; B, MNRJ 28485, 39.8 mm SL, Rio Peruípe Drainage; C, MNRJ 28488, 67.4 mm SL, Palmópolis Municipality, Rio Dois de Abril, Rio Jucuruçu Drainage; D, MNRJ 28490, 67.4 mm SL, Itanhém Municipality, Água Fria Creek, Rio Itanhém Drainage.

(Fooden, 1980; Chu *et al.*, 2007; Evans *et al.*, 2020). That species forms a monophyletic group with *Macaca fuscata* Blyth, 1875 and *Macaca cyclopis* (Swinhoe, 1862), both endemic to Pacific islands off the East Asian coast (Japan and Taiwan, respectively). Considering their geographical range and mitochondrial DNA structure, their ancestor is inferred to have invaded those islands during periods of low sea level and then becoming isolated when the sea level rose. This event probably allowed populations of *M. mulatta* next to these islands to become molecularly closer to those two insular species, thus turning *M. mulatta* into a polyphyletic metaspecies (Hoelzer & Melnick, 1994; Chu *et al.*, 2007).

Finally, there are cases of taxa that are phenotypically similar, if not identical, to *T. alternatus* which nonetheless lie outside of the species clade as defined here and seem to be a different species on the basis of DNA sequence differences alone. Such is the case with *T. florensis* (Miranda Ribeiro, 1943), recently synonymized under *T. santaeritae* (Eigenmann, 1918) (Costa *et al.*, 2020b). The taxon reported as *T. santaeritae*

in Costa *et al.* (2020b) indeed matches *T. florensis*, but not *T. santaeritae*. Data from the holotype and original description of *T. santaeritae* unambiguously show a fish with a round caudal fin, short nasal barbels and 11 dorsal pterygiophores, different from the emarginated caudal fin, long nasal barbels and eight dorsal pterygiophores of *T. florensis* and the specimens reported in Costa *et al.* (2020b). That being the case, *T. santaeritae* remains an enigmatic taxon in the genus, to our knowledge still known from the holotype only. In any case, *T. florensis* is morphologically similar to *T. alternatus*, with a colour pattern also well within the range of variation known for the latter species. Based on that alone, there would be little doubt that it represents simply an additional occurrence of *T. alternatus*. However, genetic distance and phylogenetic position indicate that it is an entirely different taxon, altogether outside of both the *T. alternatus* and the Rio Doce clades. *Trichomycterus florensis*, is sister group to *T. caipora* plus *T. nigricans* (Fig. 1), both from the Paraíba do Sul Drainage. Based on such results plus information from Costa *et al.* (2020b), we found that

Figure 9. Pigmentation and external morphological variation in *T. immaculatus* from the Rio Doce Basin (left, lateral views; right, dorsal views). All from Brazil, state of Minas Gerais: A, MZUSP 123368, 56.3 mm SL, Baguari Municipality, main channel of Rio Doce Basin; B, MZUSP 123357, 69.4 mm SL, Baguari Municipality, Rio Suaçuí Pequeno Drainage, tributary of Rio Doce Basin; C, MZUSP 123353, 69.7 mm SL, Baguari Municipality, São Mateus Creek, tributary of Rio Corrente Grande Drainage; D, MZUSP 126408, 91 mm SL, Córrego dos Borges stream flowing into left bank of Risoleta Neves Reservoir.

T. florensis is a valid species, different from both *T. alternatus* and *T. santaeritae*.

Geographical distribution: Trichomycterus alternatus is distributed throughout the entire Rio Doce Basin (Fig. 11), in tributaries of its upper, middle and lower courses. Records of the species are all from tributaries, sometimes close to their mouth on the Rio Doce, but not on the main river channel. *Trichomycterus alternatus* occurs also in most other basins in southeastern Brazil, such as Cubatão, Itabapoana, Paraíba do Sul, Paranaguá and Ribeira do Iguape (Barbosa, 2004; Volpi, 2017; Donin *et al.*, 2020; Lima *et al.*, 2021). The current confirmed range is from the Rio Doce in the north to the Rio Paranaguá in the south, but its precise limits are still undetermined.

Type material examined: holotype FMNH 58082, 65.6 mm SL; Rio Doce, near the village of Rio Doce, Minas Gerais, Brazil, Rio Doce Basin; col. J. Haseman, 25 May 1908; paratypes FMNH 58083, 62, 30.4–57.9 mm SL;

same data as holotype. *Trichomycterus longibarbatus*, all from Brazil, Espirito Santo, Santa Tereza; holotype MZUSP 043339, 1, 57.32 mm SL; near the village of Santa Tereza, Reis Magos River; col. M. Gomes, O. Peixoto, S. Carvalho & E. Izecksohn, 10 October 1991. Paratype MZUSP 023812, 17, 23.81–47.33 mm SL; Leste Drainage, Lombardina Creek; col. Zoology Department, MZUSP expedition, 2 April 1969. *Trichomycterus auroguttatus*, all from Brazil, Rio de Janeiro State; holotype MZUSP 43341, 1, 50.6 mm SL, 1 km to west of the village of Mauá, Marimbondo River, tributary of Rio Preto, Paraíba do Sul Basin; col. W.J.E.M. Costa & U. Neira, 1 December 1991. Paratype MZUSP 43342, 4, 33.8–47.68 mm SL; same locality of the holotype; col. W.J.E.M. Costa & U. Neira, 1 December 1991.

Additional specimens studied: Topotypic material of *T. alternatus*: MZUSP 123761, 1, 50.9 mm SL; Rio Doce Municipality, Córrego da Laje Creek near town of Rio Doce, tributary of main channel of Rio Doce Basin (20°14'13.05"S 42°56'53.65"W); col. V.J.C. Reis,

Figure 10. Pigmentation and external morphological variation in *Trichomycterus vinnulus* sp. nov. (left, lateral views; right, dorsal views). All from Brazil, state of Minas Gerais: A, 38.9 mm SL and B, 47.1 mm SL, MZUSP 126760, same locality as holotype; C, MZUSP 123750, holotype, 54 mm SL, Rio Doce Municipality, Córrego dos Borges Creek running into the Risoleta Neves Hydroelectric Dam; D, MZUSP 123757, 60.6 mm SL, Rio Doce Municipality, Rio do Peixe, tributary of Rio Piranga Drainage.

M.C.C. de Pinna, G.F. de Pinna & G. Ballen, 23 June 2018. MZUSP 123763, 1, 46.3 mm SL; Rio Doce Municipality, Córrego dos Borges, stream flowing into left bank of Risoleta Neves Reservoir, Rio Doce Basin (20°12'21.63"S 42°52'56.24"W); col. V.J.C. Reis, M.C.C. de Pinna, G.F. de Pinna & G. Ballen, 24 June 2018. MZUSP 123764, 4, 42.7–47.3 mm SL; Rio Doce Municipality, Córrego dos Borges, stream flowing into left bank of Risoleta Neves Reservoir (20°12'22.03"S 42°52'57.44"W); col. V.J.C. Reis, M.C.C. de Pinna, G.F. de Pinna & G. Ballen, 24 June 2018. Brazil, state of Espírito Santo. MBML 607, 2, 39.2–56.1 mm SL; Itarana, Limoeiro Creek, tributary of Santa Joana Basin (19°52'26"S 40°52'31"W); col. R.L. Teixeira & P.S. Miller, 18 October 2000. MBML 646, 7, 21.1–50.67 mm SL; Itarana, Jatibocas Creek, Santa Joana Basin (19°52'26"S 40°52'31"W); col. R.L. Teixeira & P.S. Miller, 19 April 2001. MBML 690, 6, 25–62.3 mm SL; Itarana, Jatibocas Creek, Santa Joana Basin

(19°52'26"S 40°52'31"W); col. R.L. Teixeira & P.S. Miller, 10 August 2000. MBML 727, 1, 33.6 mm SL; Itarana, Santa Joana Basin (19°52'26"S 40°52'31"W); col. R.L. Teixeira & P.S. Miller, 18 October 2000. MBML 755, 9, 29–48 mm SL; Itarana, Jatibocas Creek, Santa Joana River (19°52'26"S 40°52'31"W); col. R.L. Teixeira & P.S. Miller, 18 October 2000. MBML 811, 1, 33 mm SL; Itarana, Jatibocas Creek, tributary of Santa Joana River (19°52'26"S 40°52'31"W); col. R.L. Teixeira & P.S. Miller, 8 February 2001. MBML 1051, 3, 55.4–76.3 mm SL; Santa Teresa, Vinte e Cinco de Julho Creek, at headwaters of Santo Antônio River, tributary of Santa Maria do Rio Doce Basin (19°56'08"S 40°36'01"W); col. R.L. Teixeira, 19 March 2005. MBML 1339, 2, 46.5–57.4 mm SL; Santa Teresa, Rio Cinco de Novembro River, Santa Maria do Rio Doce Basin (19°56'08"S 40°36'01"W); col. R.L. Teixeira, 11 May 2005. MBML 1361, 3, 26.8–37.7 mm SL; Itarana, Córrego Sossego Creek, tributary of Santa Joana River (19°52'26"S
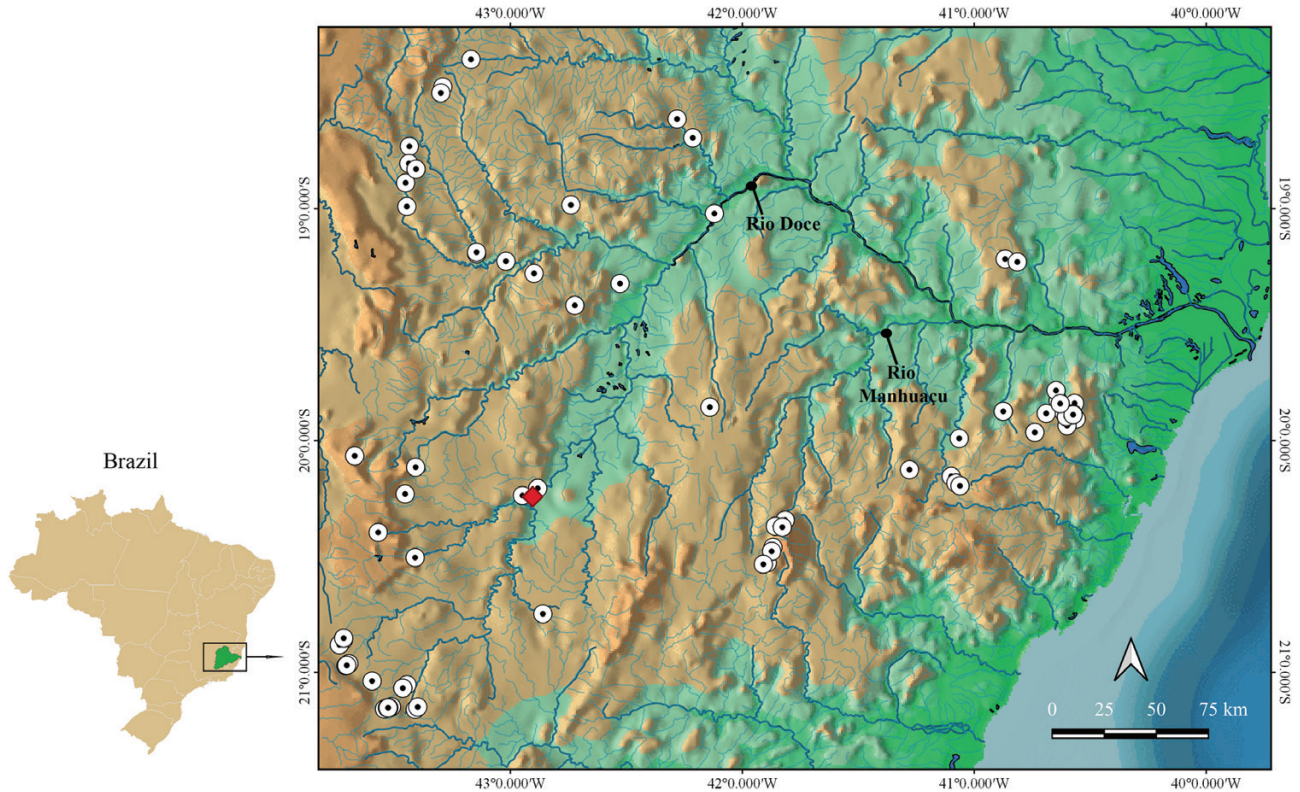
Figure 11. Geographical distribution of *T. alternatus* in the Rio Doce Basin. Red diamond = type locality; white dotted circles = additional Rio Doce localities.

40°52'31"W); col. R.L. Teixeira, 20 August 2000. MBML 2230, 11, 28.8–59.6 mm SL; Afonso Cláudio, Córrego do Cedro Creek, Guandu Basin (20°11'42"S 41°03'42"W); col. L.M. Sarmento-Soares, R.F. Martins-Pinheiro, A.T. Aranda, R.L. Teixeira, M.M.C. Roldi & M.M. Lopes, 12 June 2009. MBML 2234, 12, 26.8–84.1 mm SL; Afonso Cláudio, Guandu Basin (20°09'16"S 41°05'59"W); col. L.M. Sarmento-Soares, R.F. Martins-Pinheiro, A.T. Aranda, R.L. Teixeira, M.M.C. Roldi & M.M. Lopes, 12 June 2009. MBML 2237, 3, 26.4–39.6 mm SL; Laranja da Terra, Ribeirão Lagoa Stream, tributary of Guandu Basin (19°59'26"S 41°03'54"W); col. L.M. Sarmento-Soares, R.F. Martins-Pinheiro, A.T. Aranda, R.L. Teixeira, M.M.C. Roldi & M.M. Lopes, 12 June 2009. MBML 4306, 6, 20.9–56.8 mm SL; Iúna, Rio Claro River, tributary of Manhuaçu River (20°22'24.2"S 41°49'39.7"W); col. L.M. Sarmento-Soares, M.R. Britto, V.C. Espíndola, F.M.R.S. Pupo, R.F.M. Pinheiro & M.M.C. Roldi, 9 September 2011. MBML 4309, 2, 21.4–28.1 mm SL; Iúna, Ribeirão do Brás Creek, Manhuaçu Basin (20°20'33.9"S 41°48'55.6"W); col. L.M. Sarmento-Soares, M.R. Britto, V.C. Espindola, F.M.R.S. Pupo, R.F.M. Pinheiro & M.M.C. Roldi, 10 September 2011. MBML 4338, 7, 27–38.5 mm SL; Júna, José Pedro River, tributary of Manhuaçu Basin (20°22'09.5"S 41°51'27.5"W); col.

L.M. Sarmento-Soares, M.R. Britto, V.C. Espindola, F.M.R.S. Pupo, R.F.M. Pinheiro & M.M.C. Roldi, 10 September 2011. MBML 4438, 2, 26.3–40.0 mm SL; Santa Teresa, near Milanesi Municipality, Santa Maria do Rio Doce Basin (19°47'02.1"S 40°38'52.0"W); col. R.B. Soares, J. Gurtler & V.R. Bada, 24 September 2011. MBML 4642, 2, 38.2–47.5 mm SL; Santa Teresa, Santo Antônio Creek, Santa Maria do Rio Doce Basin (19°53'17.1"S 40°34'27.1"W); col. L.M. Sarmento-Soares, R.F.M. Pinheiro, M.M.C. Roldi & R.B. Soares, 12 February 2012. MBML 6160, 8, 27.1–56.2 mm SL; Santa Teresa, Espanhol Creek, Santa Maria do Rio Doce Basin (19°52'41.6"S 40°36'48.5"W); col. C.J. Cunha, J.P. Silva & R.B. Soares, 20 August 2012. MBML 6161, 13, 17.8–50.1 mm SL; Santa Teresa, Cinco de Novembro River, tributary of Santa Maria do Rio Doce Basin (19°53'49.2"S 40°36'10.9"W); col. C.J. Cunha, J.P. Silva & R.B. Soares, 20 August 2012. MBML 6200, 1, 47 mm SL; Cinco de Novembro River to the left of Es-080 road, straigth from Santo Antônio do Canaã to Santa Teresa municipalities, Santa Maria do Rio Doce River (19°49'42.9"S 40°38'18.4"W); col. C. J. Cunha, J. P. Silva e R. B. Soares, 20 August 2012. MBML 6207, 2, 32.1–36.5 mm SL; Santa Teresa, Cinco de Novembro River, at the left side of ES-080, straigth from Santo Antônio do Canaã to Santa Teresa, Rio

Santa Maria do Rio Doce (19°50'26.0"S 40°37'47.3"W); col. C.J. Cunha, J.P. Silva & R.B. Soares, 20 August 2012. MBML 6210, 2, 36.3–37.1 mm SL; Santa Teresa, Espanhol Creek near to the mouth of Cinco de Novembro River, tributary of Santa Maria do Rio Doce Basin (19°52'41.6"S 40°36'48.5"W); col. C.J. Cunha, J.P. Silva & R.B. Soares, 20 August 2012. MBML 6211, 1, 38.6 mm SL; Santa Teresa, Cinco de Novembro River, tributary of Santa Maria do Rio Doce Basin (19°53'49.2"S 40°36'10.9"W); col. C.J. Cunha, J.P. Silva & R.B. Soares, 20 August 2012. MBML 6228, 12, 36.2–76.7 mm SL, Brejatuba, Córrego da Passagem Creek, Guandu River (20°7'33.00"S 41°16'47.00"W); col. Biodiverses Project staff, 11 August 2012. MBML 6627, 2, 26.9–39.6 mm SL; Pancas, Cachoeira do Bassini Waterfall, Pancas Basin (19°50'26.0"S 40°37'47.3"W); col. C.J. Cunha, J.P. Silva & R.B. Soares, 20 August 2012. MBML 6822, 14, 33.3–55.3 mm SL; Santa Teresa, Vinte cinco de Julho River, tributary of Santa Maria do Rio Doce Basin (19°50'20.7"S 40°34'04.3"W); col. L.M. Sarmento-Soares, R.F. Martins Pinheiro, M.M.C. Roldi & R. Becalli, 5 May 13. MBML 6833, 4, 35.1–49.1 mm SL; Santa Teresa, Santo Antônio Creek, Santa Maria do Rio Doce Basin (19°53'04.4"S 40°34'30"W); col. L.M. Sarmento-Soares, R.F. Martins Pinheiro, M.M.C. Roldi & R. Becalli, 5 May 2013. MBML 6841, 5, 34.8–40.6 mm SL; Santa Teresa, Santo Antônio Creek, Santa Maria do Rio Doce Basin (19°53'20.3"S 40°34'32.8"W); col. L.M. Sarmento-Soares, R.F. Martins Pinheiro, M.M.C. Roldi & R. Becalli, 5 May 2013. MBML 6860, 6, 34.5–63.5 mm SL; Santa Teresa, Santo Antônio River, tributary of Santa Maria do Rio Doce Basin (19°53'20.3"S 40°34'32.8"W); col. L.M. Sarmento-Soares, R.F. Martins Pinheiro, M.M.C. Roldi & R. Becalli, 5 May 2013. MBML 7598, 4, 43.1–74.1 mm SL; Afonso Cláudio, Córrego do Cedro Creek, tributary of Guandu River (20°11'42"S 41°03'43"W); col. T.A. Volpi & M.M. Lopes, 9 December 2013. MBML 7641, 42, 23.8–57.9 mm SL; Afonso Cláudio, Córrego do Cedro Creek, Guandu Basin (20°11'42"S 41°03'43"W); col. T.A. Volpi & M.M. Lopes, 9 December 13. MBML 7642, 6, 35.6–68.5 mm SL; Afonso Cláudio, Boa Sorte River, tributary of Guandu Basin (20°10'59"S 41°04'46"W); col. T.A. Volpi & M.M. Lopes, 9 December 2013. MBML 7665, 7, 19.8–39.1 mm SL; Pancas, Panquinhas Stream, tributary of Pancas Basin (19°13'00"S 40°52'01"W); col. T.A. Volpi & M.M. Lopes, 10 December 2013. MBML 7672, 2, 30.9–36.1 mm SL; Pancas, São Luís Creek, Pancas Basin (19°13'46"S 40°48'52"W); col. T.A. Volpi & M.M. Lopes, 11 December 2013. MBML 7681, 10, 24.6–32.2 mm SL; Santa Teres, Tabocas River, tributary of Pancas Basin (19°52'57"S 40°41'24"W); col. T.A. Volpi & M.M. Lopes, 11 December 2013. MBML 8191, 1, 39.3 mm SL; Iúna, José Pedro Stream, Manhuaçu Basin (20°22'10.4"S 41°51'28.4"W); col. T.A. Volpi, K.B.S. de Paula & E.L. Muhl, 10 May

2014. MBML 8426, 7, 28.8–47.4 mm SL; Santa Teresa, Santa Maria do Rio Doce Basin, near to its spring (19°57'52.5"S 40°44'20.4"W); T.A. Volpi, M.M. Lopes, K.B.S. de Paula & E.L. Muhl, 18 May 2014. MBML 8502, 2, 53.6–54 mm SL; Santa Teresa, Santa Maria do Rio Doce Basin (19°57'52.5"S 40°44'20.4"W); col. T.A. Volpi, M.M. Lopes, K.B.S. de Paula & E.L. Muhl, 18 May 2014. MBML 9977, 2, 34.3–44.5 mm Sl; Santa Teresa, Tabocas River, tributary of Santa Maria do Rio Doce Basin (19°52'57"S 40°41'24"W); col. T.A. Volpi & M.M. Lopes, 11 December 2013. Brazil, state of Minas Gerais. MZUSP 52542, 1, 45 mm SL; Braúnas, Pitangas Creek, tributary of Santo Antônio River; col. P.M.C. Araujo & F.A. Bockmann, 7 October 1997. MZUSP 58474, 1, 46.1 mm SL; Braúnas, Córrego do Gaspar Creek, Santo Antônio Basin (18°58'60.00"S 42°44'21.00"W); col. P.M.C. Araujo & F.A. Bockmann, 4 October 1997. MZUSP 69366, 14, 31.8–51.7 mm SL; Coroaci, Suaçuí Basin (18°41'38.00"S 42°12'50.00"W); col. A.M. Zanata, 29 April 2001. MZUSP 72962, 81, 23.5–48.2 mm SL, 3 c&s 30.0–48.9 mm SL; Santa Teresa, Reserva de Nova Lombardia (19°54'23.91"S 40°33'38.66"W); col. J.L. Helmer, 8 January 1993. MZUSP 73148, 8, 19.9–31.9 mm SL; Conceição do Mato Dentro, Rio do Peixe River, Santo Antônio Basin (19°11'14.20"S 43° 8'45.31"W); col. F. Di Dario & S. Kakinami, 13 September 2001. MZUSP 73163, 7, 16.6–29.9 mm SL; Conceição do Mato Dentro, Rio do Peixe, Santo Antônio Basin (19°11'40.04"S 43° 8'43.99"W); col. F. Di Dario & S. Kakinami, 14 September 2001. MZUSP 75254, 3, 81.5–85.7 mm SL; Ouro Preto, Tripuí Creek, tributary of Piranga Basin (20°23'45.63"S 43°34'11.92"W); col. M.R. Silvério, D.C. Oliveira & A. Oliveira, 1 March 2001. MZUSP 82369, 5, 50.0–58.4 mm SL; Caranaíba, Papagaio River (20°51'12.00"S 43°43'12.00"W); col. J.C. Oliveira, A.L. Alves & L.R. Sato, 13 October 2001. MZUSP 82371, 1, 66.7 mm SL; Caranaíba, Piranga Basin (20°58'17.00"S 43°42'33.00"W); col. J.C. Oliveira, A.L. Alves & L.R. Sato, 12 October 2001. MZUSP 82370, 1, 42.9 mm SL; Desterro de Melo, Xopotó River, tributary of Piranga River (21°9'34.00"S 43°24'37.00"W); col. J.C. Oliveira, A.L. Alves, L.R. Sato, 12 October 2001. MZUSP 87825, 4, 48.0–61,6 mm SL; Santo Antônio do Itambé, Santo Antônio Basin (18°30'0.00"S 43°17'60.00"W); col. A. Carvalho Filho, 9 August 2004. MZUSP 87832, 5, 36.3–57.7 mm SL, 2 c&s, 52.3–52.6 mm SL; Santo Antonio de Itambé, Lageado Creek, Mão D'Água River, Santo Antônio Basin (18°28'27.12"S 43°17'29.27"W); col. A. Carvalho Filho, 30 August 2004. MZUSP 94485, 3, 34.5–42.3 mm SL; Alto Rio Doce, Xopotó River, tributary of Piranga River (21°4'4.00"S 43°27'50.00"W); col. O. Oyakawa, E. Baena & M. Loeb, 11 July 2007. MZUSP 94486, 1, 27.8 mm SL; Alto Rio Doce Rio, Xopotó River, tributary of Piranga River (21°4'4.00"S 43°27'50.00"W); col. O. Oyakawa, E. Baena & M. Loeb,

11 July 2007. MZUSP 94503, 3, 42.8–50.8 mm SL; Caranaiba, Piranga River (20°51'37.00"S 43°43'11.00"W); col. O. Oyakawa, E. Baena & M. Loeb, 9 July 2007. MZUSP 94512, 4, 34.3–39.0 mm SL; Alto Rio Doce, Xopotó River, Piranga River (21°3'11.00"S 43°26'46.00"W); col. O. Oyakawa, E. Baena & M. Loeb, 11 July 2007. MZUSP 94518, 2, 54.3–62.6 mm SL; Desterro de Melo; Xopotó River, tributary of Piranga River (21°9'29.00"S 43°32'34.00"W); col. O. Oyakawa, E. Baena & M. Loeb, 10 July 2007. MZUSP 94520, 2, 43.2–60.2 mm SL; Caranaiba, Piranga River (20°52'52.00"S 43°44'15.00"W); col. O. Oyakawa, E. Baena & M. Loeb, 9 July 2007. MZUSP 94522, 7, 43.0–62.1 mm SL; Caranaiba, Piranga Basin (20°52'52.00"S 43°44'15.00"W); col. O. Oyakawa, E. Baena & M. Loeb, 9 July 2007. MZUSP 94531, 3, 29.2–48.1 mm SL; Desterro de Melo, Xopotó River, tributary of Piranga Basin (21°9'10.00"S 43°31'49.00"W); col. O. Oyakawa, E. Baena & M. Loeb, 10 July 2007. MZUSP 94536, 2, 26.2–35.5 mm SL; Desterro de Melo, Xopotó River, Piranga Basin (21°9'10.00"S 43°31'28.00"W); col. O. Oyakawa, E. Baena & M. Loeb, 9 July 2007. MZUSP 94538, 3, 44–47.1 mm SL; Desterro de Melo, Xopotó River, tributary of Piranga Basin (21°9'10.00"S 43°31'28.00"W); col. O. Oyakawa, E. Baena & M. Loeb, 10 July 2007. MZUSP 94547, 14, 22.8–39.7 mm SL; Carandaí, Piranga Basin (20°57'45.00"S 43°41'48.00"W); col. O. Oyakawa, E. Baena & M. Loeb, 9 July 2007. MZUSP 94548, 6, 32.3–58.5 mm SL; Carandaí, Piranga River (20°57'45.00"S 43°41'48.00"W); col. O. Oyakawa, E. Baena & M. Loeb, 9 July 2007. MZUSP 94564, 75, 37.0–55.7 mm SL, 3 c&s 40.14–46.0 mm SL; Desterro de Melo, Xopotó River, tributary of Piranga River (21°8'53.00"S 43°30'46.00"W); col. O. Oyakawa, E. Baena & M. Loeb, 10 July 2007. MZUSP 109302, 5, 33.3–53.1 mm SL, 2 c&s, 39.7–40.9 mm SL; Conceição do Mato Dentro, Santo Antônio Basin (18°43'50.00"S 43°26'8.00"W); col. T.C. Pessali, December 2010. MZUSP 109304, 4, 21.3–40.6 mm SL; Conceição do Mato Dentro, Santo Antônio Basin (18°53'18.00"S 43°27'7.00"W); col. T.C. Pessali, December 2010. MZUSP 109311, 4, 33.8–49.0 mm SL, 1 c&s 41 mm SL; Conceição do Mato Dentro, Santo Antônio Basin (18°49'44.00"S 43°24'25.00"W); col. T.C. Pessali, December 2010. MZUSP 109313, 2, 49.2–49.7 mm SL; Conceição do Mato Dentro, Santo Antônio Basin (18°48'16.00"S 43°26'16.00"W); col. T.C. Pessali, December 2010. MZUSP 109319, 3, 31.0–33.3 mm SL; Conceição do Mato Dentro, Santo Antônio Basin (18°59'25.00"S 43°26'47.00"W); col. T.C. Pessali, December 2010. MZUSP 109352, 1, 39 mm SL; Catas Altas, Paracatu Creek, tributary of Piracicaba Basin (20° 6'53.00"S 43°24'31.00"W); col. B. Maia, 31 March 2010. MZUSP 109391, 3, 42.7–64.1 mm SL, 1 c&s 52 mm SL; Santa Bárbara, Ribeirão Preto Creek, tributary of Piracicaba Basin (20° 3'57.00"S 43°40'16.00"W); col. B. Maia, 31 July 2010. MZUSP 109392, 1, 59 mm SL; Santa Barbara, Ribeirão Preto, tributary of Piracicaba Basin (20°3'57.00"S 43°40'16.00"W); col. B. Maia, August 2010. MZUSP 110933, 1, 37.1 mm SL; Mariana, Gualaxo do Sul River (20°30'16.97"S 43°24'39.28"W); col. L.F. Salvador Jr. & L.A.C. Missiaggia, 5 July 2012. MZUSP 110937, 1, 66.6 mm SL; Mariana, Piracicaba Basin (20°13'48.93"S 43°27'14.34"W); col. L.F. Salvador Jr. & L.A.C. Missiaggia, 5 October 2012. MZUSP 112753, 4, 35.9–41.8 mm SL; Ferros, Santo Antônio Basin (19°13'34.50"S 43° 1'9.50"W); col. O.T. Oyakawa & T.F. Teixeira, 16 August 2012. MZUSP 121709, 1, 48.5 mm SL; Coronel Fabriciano, Cachoeira do Escorrega Waterfall, tributary of Piracicaba Basin (19°25'0.42"S 42°43'20.68"W); col. V.J.C. Reis, 22 March 2017. MZUSP 69333, 1, 63 mm SL; Coroací, Suaçuí Basin (18°36'45.93"S 42°16'52.91"W); col. A.M. Zanata, 28 April 2001. MZUSP 121710, 1, 48.9 mm SL; Coronel Fabriciano, Cachoeira do Escorrega Waterfall, Piracicaba Basin (19°25'0.42"S 42°43'20.68"W); col. V.J.C. Reis, 22 March 2017. MZUSP 121719, 4, 40.9–52.1 mm SL; Santana do Paraíso, Piracicaba Basin (19°19'20.24"S 42°31'38.49"W); col. V.J.C. Reis, 23 March 2017. MZUSP 123339, 15, 14, 30.8–68.6 mm SL, 3 c&s, 33.2–34.9 mm SL; Santa Rita de Minas, Caratinga River, tributary of Rio Doce Basin (19°51'20.22"S 42°8'24.63"W); col. T. Pessali, 8 September 2015. MZUSP 123393, 1, 43.5 mm SL; Baguarí, main stream of Rio Doce (19°1'14.00"S 42°7'14.40"W); col. V.J.C. Reis & T. Pessali, 12 November 2017. LBP 1013, 1, 62.1 mm SL; Caranaíba, Piranga River (21°8'56.82"S 43°23'58.38"W); col. J.C. Oliveira, A.L. Alves & L.R. Sato, 12 October 2001. LBP 1016, 3, 44.3–56.5 mm SL; Caranaíba, Piranga River (20°58'10.26"S 43°42'19.86"W); col. J.C. Oliveira, A.L. Alves & L.R. Sato, 13 October 2001. LBP 1020, 12, 36.2–51.1 mm SL; Caranaíba, Papagaio River (20°51'7.74"S 43°43'7.62"W); col. J.C. Oliveira, A.L. Alves & L.R. Sato, 13 October 2011. LBP 8350, 1, 39 mm SL; Ferros, Piçarrão River (19°16'43.87"S 42°53'53.40"W); col. C. Oliveira, G.J.C. Silva, F.F. Roxo & T.N.A. Pereira, 18 May 2009. LBP 12259, 15, 35.1–56.8 mm SL; Desterro de Melo, Xopotó River (21°9'9.70"S 43°31'37.90"W); col. A. Ferreira, F.F. Roxo & G.J. Costa e Silva, 19 June 2011. MNRJ 1152, 16, 31.6–66.2 mm SL; Viçosa, Piranga River (20°44'51.10"S 42°51'35.95"W); col. J. Moojen Oliveira, no date. MNRJ 22400, 6, 32.8–56.3 mm SL; Caparaó, Grumarim Creek, tributary of Capim Roxo River (20°31'38.69"S 41°53'33.83"W); col. A.T. Aranda, F.A.G. Melo & F.P. Silva, 7 August 2001. MNRJ 30980, 2, 62.8–76.0 mm SL; Senhora dos Remédios, Piranga River (21° 2'13.69"S 43°35'46.63"W); col. M. Britto, N. Tamaio & I. Tamaio, 30 December 2006. MNRJ 39468, 9,

25.2–40.1 mm SL; Alto Caparaó, Caparaó River, tributary of Manhuaçu Basin (20°27'38.26"S 41°52'5.40"W); col. L.M. Sarmento-Soares, M.R. Britto, 9 September 2011. MNRJ 42745, 1, 68.3 mm SL; Caparaó, Caparaó River, tributary of Manhuaçu River (20°32'0.17"S 41°54'34.70"W); col. P. Buckup, M. Britto & D.F. Moraes Jr., 14 April 2014. MNRJ 43174, 1, 60.6 mm SL; Alto Caparaó, Caparaó River, tributary of Manhuaçu Basin (20°28'39.58"S 41°52'25.50"W); col. E. Pauls, 8 May 1997. MNRJ 50893, 3, 43.5–43.8 mm SL; Serra Azul, main stream of Suaçuí Grande Basin; col. S.A. Santos & T.C. Pessali, 16 February 2018.

TRICHOMYCTERUS ARGOS LEZAMA ET AL., 2012
(FIG. 5)

Trichomycterus argos Lezama, Triques & Santos, 2012: 62, figs 2, 3a [type locality: Parque Estadual da Serra do Brigadeiro, Córrego Nova, headwaters of the Rio Casca, right bank tributary of Rio Doce at the limits of Rio Doce and Rio Paraíba do Sul basins, 20°43'19"S 42°28'43"W, Minas Gerais State, Brazil; holotype: AZUFMG 103, paratypes: DZUFMG 058 (1), 059 (14), 067 (1, c&s); MZUSP 106274 (3)]; DoNascimiento *et al.*, 2014b: 724 (comparison); García-Melo *et al.*, 2016: 237 (citation, relationships); Donin *et al.*, 2020: 3 (comparison); Reis *et al.*, 2020: 2 (diversity); DoNascimiento & Prada-Pedreros, 2020: 978 (comparison).

Diagnosis: The combination of the following traits distinguishes *T. argos* from congeners: (1) pectoral-fin rays I + 6, (vs. I + 5, I + 7 or I + 8); (2) colour pattern composed of irregular round, vermiculate or reticulate maculae randomly distributed over most of body; (3) suture line between parietosupraoccipital and frontal bones straight and oriented orthogonally to longitudinal body axis (vs. irregular and oblique) (Lezama *et al.*, 2012: fig. 3a); (4) large foramen for ramus lateralis accessorius facialis nerve on parietosupraoccipital, visible in dorsal view (Lezama *et al.*, 2012: fig. 3) (vs. foramen minute, hardly visible in dorsal view). Among congeners in south-eastern South America, character 1 distinguishes *T. argos* from all congeners except *Trichomycterus pirabitira* Barbosa & Azevedo 2012, *T. itatiayae*, *T. trefauti*, those in the *T. reinhardti* species complex (Costa & Katz, 2021), except from *Trichomycterus humboldti* Costa & Katz 2021, *Trichomycterus pauciradiatus* Alencar & Costa 2006, *Trichomycterus piratymbara* Katz, Barbosa & Costa, 2013 and *Trichomycterus sainthilairei* Katz & Costa, 2021 and those in the *T. brasiliensis* species complex (Barbosa & Costa, 2010); character 2 from all congeners except those in the *T. brasiliensis* species complex, plus *T. lauryi* and *T. pirabitira*; characters 3 and 4 each distinguishes *T. argos* from species in the *T. brasiliensis* species complex. Among congeners in the Rio Doce Basin, *T. argos* is most similar to *T. brunoi*. In addition to characters above, *T. argos* can be further distinguished from *T. brunoi* by the longer snout (41.9–45.9% vs. 28.0–41.2%), the longer prepelvic length (59.5–60.6% vs. 41.4–58.5%) and the more numerous interopercular odontodes (39–40 vs. 26–31).

Description: Morphometric data for specimens examined is presented in Table 4. Body long and almost totally straight, trunk roughly round in cross-section near head, then slightly deeper than wide and gently compressed to caudal peduncle, tapering to caudal fin. Dorsal profile of body gently convex to dorsal-fin origin, then straight or slightly concave along caudal peduncle to caudal-fin origin. Ventral profile convex from gular region to vent, due partly to abdominal distension, then straight or slightly concave along anal-fin origin to caudal-fin base. Caudal peduncle as deep as body from beginning of anal-fin base to slightly at the base of caudal-fin rays.

Head approximately 1/5 to 1/4 of SL, pentagonal, longer than wide and depressed, with a long snout. Mouth subterminal. Upper jaw slightly longer than lower. Upper lip wider than lower lip, and laterally continuous with base of maxillary barbel. Lower lip small, approximately 2/3 width of upper one, partly divided into right and left portions by median concavity. Lower lip with uniform covering of tiny villi, resulting in velvet-like surface and not clustered into large papillae. Region between upper and lower lips with slender fleshy lobe.

Dentary and premaxillary teeth similar to each other in shape. Dentary teeth conical, size of individual teeth increasing markedly towards symphysis and from posterior to anterior rows. Total area of premaxillary teeth slightly smaller than that of dentary, with teeth arranged irregularly in four rows over entire ventral surface of premaxilla. Premaxillary teeth conical.

Eye small, protruding, positioned dorsally on head, without free orbital rim and covered with transparent skin. Eye located on anterior half of HL, closer to lateral border of head than to midline in dorsal view. Anterior naris surrounded by tube of integument directed anterolaterally, continuous posterolaterally with nasal barbel. Posterior naris closer to anterior naris than to eyes, surrounded by tube of integument incomplete posteriorly. Maxillary barbel narrowing markedly towards fine tip, reaching base of pectoral fin. Rictal barbel inserted immediately ventral to maxillary barbel, its tip reaching lateroposterior border of interopercle. Nasal barbel originating on posterolateral region of anterior naris, reaching from slightly anterior to anterior border of opercle to touching, but not surpassing, anterior border of opercle.

Table 4. Morphometric data of *T. argos* based on part of paratype material (MZUSP 106274)

	Range (*N* = 3)	Mean	SD
Standard length (mm)	56.1–90.8	71.7	-
% of standard length			
Anal-fin base	7.8–8.8	8.2	0.6
Body depth	15.0–16.2	15.6	0.6
Caudal peduncle depth	14.8–15.3	15.1	0.3
Dorsal-fin base	9.6–10.5	10.0	0.4
First pectoral-fin length	11.3–12.5	11.9	0.6
Head length	20.7–20.9	20.8	0.1
Preanal length	71.3–72.3	71.8	0.5
Predorsal length	63.9–65.4	64.8	0.8
Prepelvic length	59.5–60.6	59.9	0.6
% of head length			
Eye diameter	8.9–10.8	10.2	1.1
Interorbital width	23.6–25.0	24.3	0.7
Snout length	41.9–45.9	44.0	2.0
Mouth width	40.7–46.0	42.5	3.0

Interopercular patch of odontodes, oval in shape and with well-developed odontodes, prominent in ventral aspect of head. Interopercular patch of odontodes extending from vertical through ventroposterior border of eye to ventroanterior to opercle patch of odontodes. Odontodes arranged in three irregular series, with those on mesial series much longer than those on lateral one; odontodes gradually larger posteriorly in both series, with those posteriorly on mesial row largest. Interopercular odontodes 39–40. Opercular patch of odontodes on dorsolateral surface of posterior part of head, positioned anterodorsally to pectoral-fin base, roundish in shape slightly smaller than eye in dorsal aspect of head. Opercular odontodes 14–18, sunk in individual slits of integument, progressively larger posteriorly, all with fine tips, with largest ones curved distally and claw-like. Entire opercular patch surrounded by rim of integument.

Pectoral fin inserted immediately posterior and ventral to opercular patch of odontodes. Pectoral-fin rays I + 6. First pectoral-fin ray (unbranched) longe, prolonged as filament beyond fin margin, with short filament. Other rays progressively shorter, their tips following continuous line along fin margin. Pelvic fin with convex distal profile, its origin slightly posterior to middle of SL and anterior to vertical through dorsal-fin origin, surpassing anal and urogenital openings in adults. Pelvic-fin rays I + 4, fin bases close to each other. Dorsal fin long, its distal margin sinusoidal. Dorsal-fin origin closer to base of caudal-fin than to tip of snout. Dorsal-fin rays II + 7. Anal fin slightly smaller than dorsal fin, its distal margin gently convex. Anal-fin origin posterior to vertical through end of dorsal-fin base. Anal-fin rays II + 5. Caudal fin rounded with 6 + 7 principal rays. Adipose fin absent or modified into low integumentary fold extending between end of dorsal fin and caudal-fin origin. Post-Weberian vertebrae 39 (1). First dorsal-fin pterygiophore immediately anterior to neural spine of 20th (1) vertebra, first anal-fin pterygiophore immediately anterior to neural spine 23rd (1) vertebra. Caudal-fin procurrent rays plus one segmented non-principal ray dorsally and ventrally. Procurrent caudal-fin rays, 20 dorsally and 15 ventrally, beginning anteriorly at 33rd to 35th vertebrae, respectively. Ribs 14 (1). Branchiostegal rays 8 (1). Dorsal-fin pterygiophores 8. Anal-fin pterygiophores 6. Cephalic lateral line canals with simple, non-dendritic tubes ending in single pores. Supraorbital canal mostly in frontal bone. Supraorbital pores invariably present: s1 mesial to nasal-barbel base and autopalatine, s3 mesial to posterior nostril and anterior to frontal, paired s6, posteromedial to eye and at midlength of frontal, as distant from the orbits as from the mesial line. Infraorbital laterosensory canal incomplete with four pores, i1 and i2 anteriorly and i10 and i11 posteriorly. This canal extending from sphenotic posteriorly to terminal pore located ventroposteriorly to eye. Canal lacking associated ossification. Infraorbital pore i1 located ventrolateral to nasal-barbel base and autopalatine, i3 ventrolateral to posterior nostril and anterior to frontal, i10 and i11 posterior to eye. Otic canal without pores. Postotic pores po1, anteromedial to opercular patch of odontodes and po2, mesial to opercular patch of odontodes. Lateral line of trunk anteriorly continuous with postotic canal and reduced to short tube. Lateral line pores ll1 and ll2 dorsomedial to pectoral-fin base.

Coloration in ethanol: Trichomycterus argos has two basic types of pigmentation patterns, probably associated with ontogeny. Contrary to original

description, a small paratype of this species (Fig. 5A-C) has chromatophores forming round dark maculae bigger than eye diameter disposed in a row along mid-lateral portion of body begining immediately posterior to opercle and extending to end of dorsal-fin base. Mid-lateral line maculae faint or entirely absent in large specimens (90.8 mm SL). In both small and large paratypes dorsally to mid-lateral line, several smaller, round to amoeboid dark blurred maculae, coalescent or not. Maculae or spots randomly distributed dorsally on trunk. Ventrally to mid-lateral line, round dark maculae randomly distributed, fewer and larger than dorsal maculae. Caudal peduncle with fewer chromatophores than rest of body. Few or no dark pigmentation ventrally on abdomen. Fins with few or no dark pigment, except for vertical dark bar at base of caudal fin. Mid-dorsum with dark chromatophores forming small round to amoeboid blurred and partly coalescent maculae. Concentration of chromatophores on entire body increasing with size of specimens. Head with numerous dark round, variably-sized, widely-spaced maculae laterally in small specimens. In the larger specimen vermiculate to amoeboid maculae lateral on head. Tip of snout, cheeks and region ventroposterior to eye with fewer chromatophores than remainder of head. Region surrounding opercular odontodes darkly pigmented, most concentrated on surrounding integument fold. Region surrounding interopercular odontodes without dark pigmentation.

Remarks: Trichomycterus argos clearly fits the so-called *Trichomycterus brasiliensis* complex (Bockmann & Sazima, 2004; Barbosa & Costa, 2010), sharing characters such as I + 6 pectoral-fin rays, a similar colour pattern and closely-set pelvic-fin bases. Its presumably close relative, *T. brunoi* Barbosa & Costa, 2010, is already in that complex and the two species are the only taxa resembling *T. brasiliensis* so far known to occur in the Rio Doce. *Trichomycterus brasiliensis* itself has never been recorded from the Rio Doce basin. A lot from Piranga basin (MNRJ 789) includes two specimens closely resembling *T. brasiliensis*. Due to entanglements in the taxonomy of that species complex (Barbosa & Costa, 2010), with 14 very similar nominal species, and because there are only two old specimens, additional material and analyses are needed in order to confirm their identity.

Lezama *et al.* (2012) reported that *T. argos* is distinguished from *T. brunoi* exclusively by its colour pattern (presence of stripes, vermiculations or reticulations in the former and their absence in the latter). However, within samples examined referable to the two species, the ranges of coloration variation clearly overlap, thus blurring the apparent limits between the two taxa (Figs 5, 12). Indeed, colour pattern

has been reported to vary considerably within species of the *T. brasiliensis* species complex (Barbosa & Costa, 2010). Despite that, the two species can be distinguished by additional phenotypic evidence as listed in the diagnosis. Their divergence is small and *T. argos* and *T. brunoi* are clearly close relatives, an inference further strengthened by the proximity of their respective type localities, only *c*. 50 km distant in straight line, with many small tributaries between them (Fig. 13).

Geographical distribution: Trichomycterus argos is known only from the type material, collected in the Rio Casca, a tributary of Rio Doce Basin in the Serra do Brigadeiro State Park (Fig. 13).

Type material examined: MZUSP 106274, 3, 56.1–90.8 mm SL, 1 c&s 69.5 mm SL, paratypes, Brazil, state of Minas Gerais, Araponga Municipality, Parque Estadual da Serra do Brigadeiro, Córrego Serra Nova, headwaters of the Rio Casca, right bank tributary of Rio Doce at limit of Rio Doce and Rio Paraíba do Sul basins (20°43'19"S 42°28'43"W), col. P.S. Santos, 7 October 2001.

TRICHOMYCTERUS ASTROMYCTERUS REIS ET AL., 2019
(FIG. 14)

Trichomycterus astromycterus Reis, de Pinna & Pessali, 2019: 2, figs 1–8 [type locality: Rio do Peixe, tributary of Rio Doce Basin, 20°11'40.32"S, 42°51'8.47"W, Rio Doce Municipality, Minas Gerais, Brazil; holotype: MZUSP 124559, paratypes: MZUSP 123341 (1), MZUSP 123361 (13, 1 c&s), MZUSP 124760 (37, 3 c&s)]; Reis, 2018: 14 (morphology, relationships); ETYFish Project, 2020 (etymology); Reis *et al.*, 2020: 2 (diversity); Fernandez *et al.*, 2021: 15 (phylogenetic relationships).

Diagnosis: Autapomorphically diagnosed by the following characters, unique in Trichomycteridae: (1) distally expanded maxilla (Reis *et al.*, 2019: fig. 3) (vs. not expanded); (2) mesethmoid cornua thick and short, shorter than half width of premaxilla (vs. mesethmoid cornua slender and long, equal or longer than half width of premaxilla); and (3) long anterior process of the vomer (vs. short). Slightly asymmetrical caudal fin, with lower lobe longer than upper one further distinguishes the new species from all congeners (vs. with upper and lower lobes equal). In addition, it is distinguished from all congeners from south-eastern South America by the combination of the following traits: (1) eight or nine branched dorsal-fin rays (rarely six or seven) (vs. invariably seven); (2) seven to nine dorsal pterygiophores (vs. invariably eight); (3) narrow caudal peduncle (mean 9.3% vs. 10.1–15.1%); (4) short barbels, not surpassing anterior margin of eyes (vs. long barbels surpassing eyes); and (5) eyes dorsal
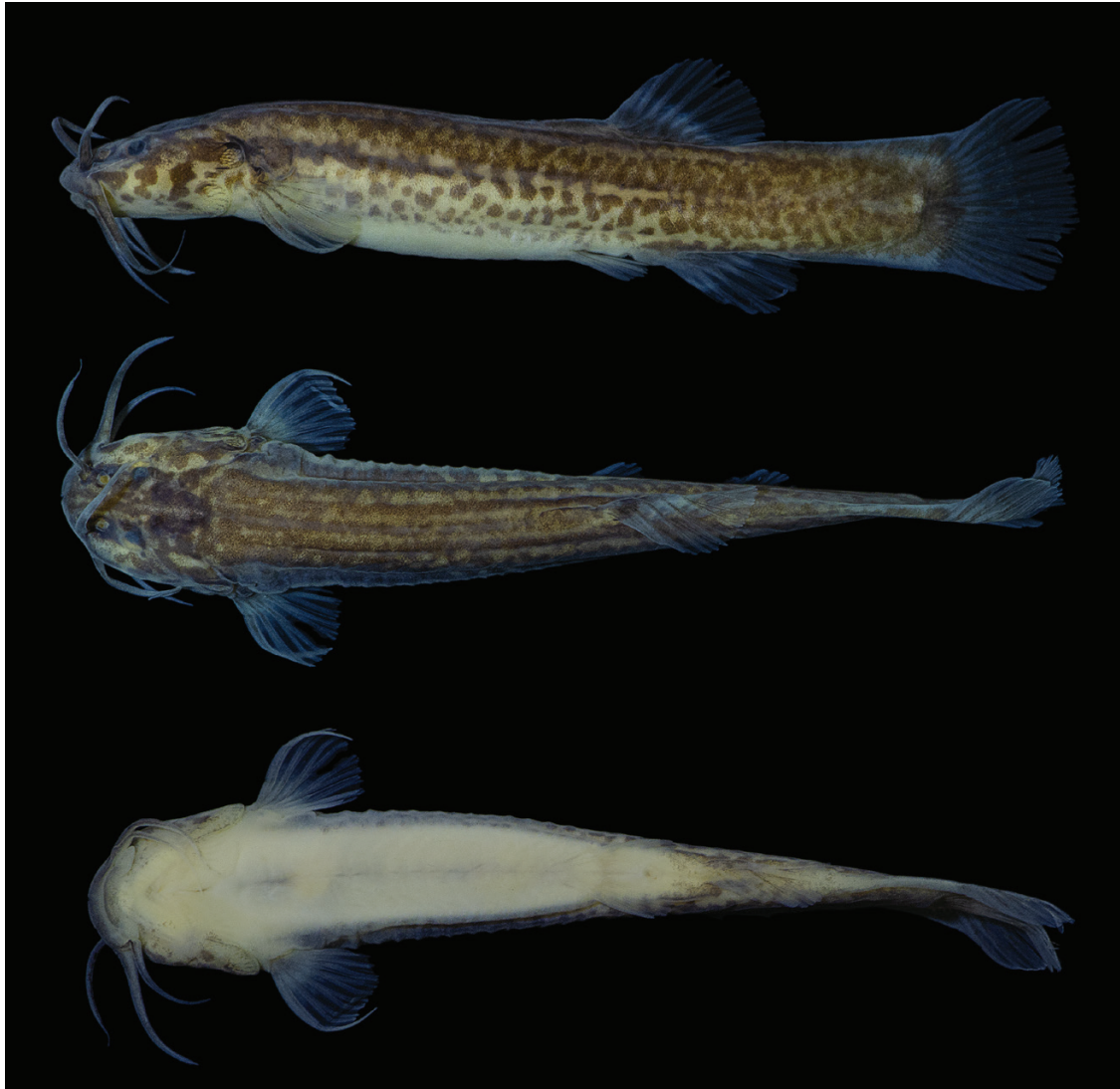
Figure 12. *Trichomycterus brunoi* (top: lateral; middle: dorsal; and bottom: ventral views), MBML 4308, 41.7 mm SL. Brazil, state of Espírito Santo, Iúna Municipality, Ribeirão do Brás Creek, Manhuaçu River.

and protruding (vs. more laterally located and not protruding). Further distinguished from all congeners from the Rio Doce Basin by highly discrepant numbers of dorsal (20–23) and ventral (9–13) proccurent caudal-fin rays (vs. less dissimilar numbers in the two series, 13–25 dorsally, 11–17 ventrally).

Description: Morphometric data for specimens examined is presented in Table 5. Body short and stout, trunk roughly round in cross-section near head, then slightly deeper than wide and abruptly compressed at caudal peduncle, tapering to caudal fin. Dorsal profile of body gently convex to dorsal-fin origin, then straight or slightly convex along caudal peduncle to caudal-fin origin. Ventral profile convex from gular region to vent, due partly to abdominal distension, then straight to anal-fin origin and straight or slightly concave along caudal peduncle to caudal-fin base. Caudal peduncle region markedly less deep than rest of body. Dorsal profile of caudal peduncle including vestigial fin fold or adipose fin, poorly defined and confluent with caudal fin.

Head longer than wide and depressed. Mouth inferior, located distant from anterior margin of snout. Upper jaw markedly longer than lower, with premaxillary dentition almost entirely exposed in ventral view. Upper lip broad, wide and fleshy in ventral view, its ventral surface covered with numerous large papillae. Each papilla formed by cluster of small villi. Lateral portion of upper lip continuous with base of rictal barbel. Lower lip small, approximately half as wide as upper one, median concavity slightly dividing it into
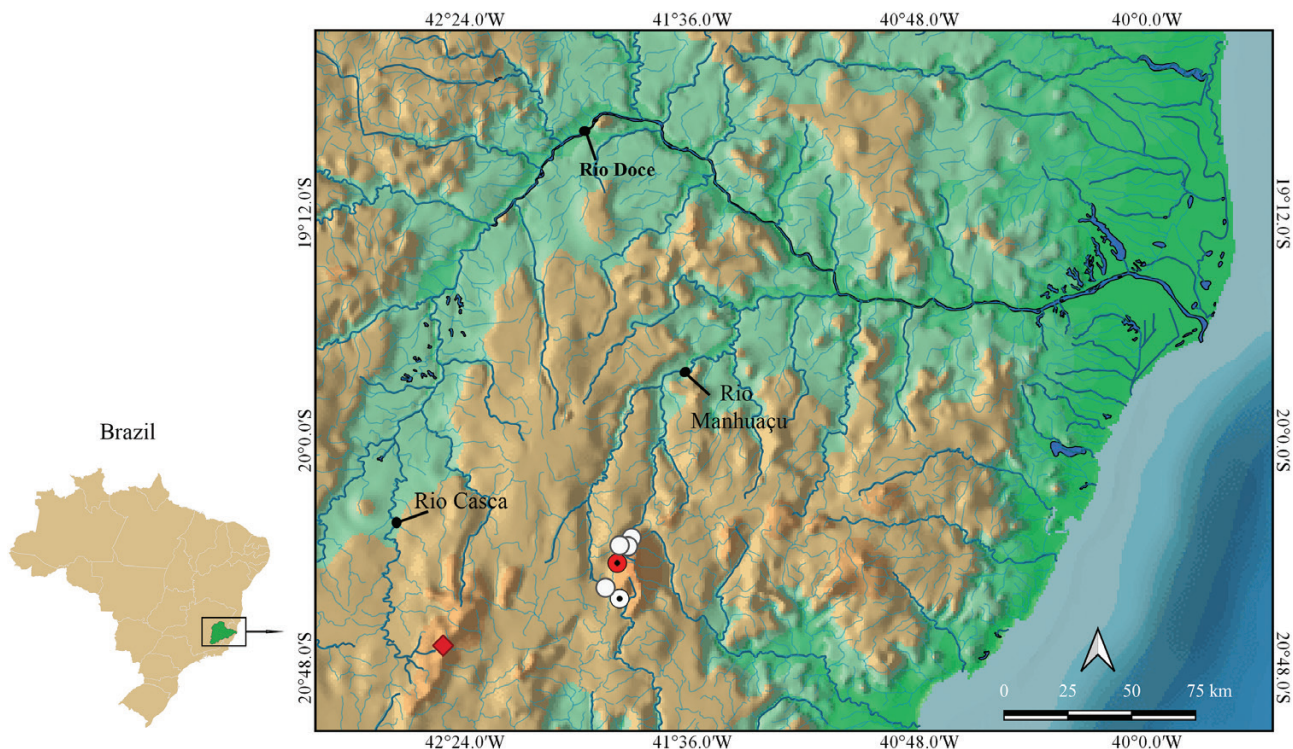
Figure 13. Geographical distribution of *T. argos* and *T. brunoi* in the Rio Doce Basin. Red diamond = type locality of *T. argos*; red dotted circle = holotype and paratype locality of *T. brunoi*; white dotted circle = paratype locality of *T. brunoi*; white circles = non-type localities of *T. brunoi*.

right and left portions. Lower lip with uniform coveling of tiny villi, velvet-like in aspect and not clustered into large papillae. Region between upper and lower lips with well-differentiated fleshy lobe, adpressed posteriorly to cheek musculature.

Dentary and premaxillary teeth similar to each other in shape and size. Dentary teeth approximately 45–55 in number, arranged in three irregular rows extending to base of coronoid process, with size of individual teeth increasing markedly towards symphysis and from posterior to anterior rows, with medialmost anterior tooth approximately seven times the length of lateralmost posterior tooth. In cleared and stained and CT-scanned paratypes, dentary teeth of first row mostly narrowly incisiform near symphysis, with remaining teeth conical (Reis *et al.*, 2019: fig. 7). Area of premaxillary teeth smaller than that of dentary, with 30–40 teeth arranged irregularly over entire ventral surface of premaxilla. In cleared and stained, and CT-scanned (in original description, Reis *et al.*, 2019) paratypes, premaxillary teeth near symphysis mostly narrowly incisiform, especially anteriorly, with remaining teeth conical. In considerably larger holotype, most jaw teeth incisiform.

Eyes large, protruding, positioned dorsally on head, without free orbital rim and covered with transparent skin. Eyes located slightly posterior to half of HL, closer to midline than to lateral border of head in dorsal view. Anterior naris surrounded by tube of integument directed anterolaterally, continuous posterolaterally with nasal barbel. Part of integument rim extending along posterior margin of barbel forming conspicuous flap for proximal 25% of barbel. Posterior naris slightly closer together than anterior ones, surrounded by tube of integument incomplete posteriorly. Maxillary barbel extremely wide at base and narrowing markedly towards fine tip, reaching slightly beyond middle of eye when completely extended. Rictal barbel inserted immediately ventral to maxillary barbel, but with base 1/3 as wide, its tip not reaching base of interopercular patch of odontodes when completely extended. Nasal barbel keel-like, originating on posterolateral region of anterior naris, reaching about 60% of distance between its base and anterior margin of eye. Interopercular patch of odontodes small in overall area, slightly larger than eye in lateral aspect, oval in shape and with well-developed odontodes, visible in ventral aspect of head but not conspicuously so. Interopercular patch of odontodes extending from vertical through posterior border of eye anteriorly to slightly to anterior to vertical through pectoral-fin base posteriorly. Odontodes arranged in two irregular series, with those

Figure 14. *Trichomycterus astromycterus* (top: lateral; middle: dorsal; and bottom: ventral views), MZUSP 123759, holotype, 51.5 mm SL. Brazil, Minas Gerais, Rio Doce Municipality, Rio do Peixe, tributary of Rio Piranga Drainage.

on mesial series much larger than those on lateral one; odontodes gradually larger posteriorly in both series, with those posteriorly on mesial row largest. Interopercular odontodes 23–24. Opercular patch of odontodes on dorsolateral surface of posterior part of head, anterodorsally to pectoral-fin base, roundish in shape and slightly smaller than eye in dorsal aspect of head. Opercular odontodes 11–16, each one sunk in individual slit of integument, progressively larger posteriorly, all with fine tips, with largest ones curved distally and claw-like. Entire patch surrounded by rim of integument.

Pectoral fin large (tip of first ray extending to middle of distance between occiput and pelvic-fin base), gently convex or sinusoidal in distal margin, its base immediately posterior and ventral to opercular patch of odontodes. Pectoral-fin rays I + 7 or I + 8 with counts asymmetrical in some specimens. First pectoral-fin ray (unbranched) longer than all others, prolonged as filament beyond fin margin. Other rays progressively shorter, their tips following continuous line along fin margin. Second ray sometimes longer than posterior ones. Pelvic fin with convex distal profile, its origin slightly posterior to middle of SL and anterior to

Table 5. Morphometric data of *T. astromycterus* based on holotype and part of paratype material (MZUSP 124559, 123341, 123361, 123760)

	Holotype	Range (*N* = 12)	Mean	SD
Standard length (mm)	52.0	11.1–52.0	35.7	-
% of standard length				
Anal-fin base	9.0	6.9–12.2	9.3	1.8
Body depth	15.4	13.1–16.7	14.8	1.5
Caudal peduncle depth	10.4	8.5–10.4	9.3	0.6
Dorsal-fin base	13.5	11.7–14.9	13.4	1.1
First pectoral-fin length	15.2	11.6–16.6	14.9	1.8
Head length	21.7	20.8–24.4	22.3	1.3
Preanal length	69.5	69.4–73.4	71.3	1.6
Predorsal length	58.5	56.6–60.7	58.7	1.6
Prepelvic length	51.9	51.5–69.3	55.6	6.1
% of head length				
Eye diameter	24.2	17.6–24.2	19.7	1.4
Interorbital width	24.7	20.2–24.7	22.1	1.7
Snout length	56.5	48.4–56.5	52.8	3.2
Mouth width	44.6	33.9–44.6	38.7	4.9

vertical through dorsal-fin origin, surpassing anal and urogenital openings by approximately half-fin length, but falling short of anal-fin origin also by half-fin length. Pelvic-fin rays I + 4, first ray (unbranched) shorter than others. Long and slender pelvic splint extending for almost half-length of first pelvic-fin ray. Dorsal fin long, its distal margin sinusoidal. Dorsal-fin origin closer to base of caudal-fin than to tip of snout. Dorsal-fin rays ii + II + 6 (1), ii + II + 7 (2), ii + II + 8 (2) or ii + II + 9 (2). Anal fin smaller and shorter than dorsal fin, its distal margin gently convex. Anal-fin origin slightly anterior to vertical through end of dorsal-fin base. Anal-fin rays i + II + 5 (6) or ii + II + 5 (1). Caudal fin bilobed with round corners, with lower lobe longer than upper one and 6 + 7 principal rays. Caudal-fin procurrent rays 20–23 dorsally and 9–13 ventrally, plus one segmented non-principal ray ventrally in some specimens. Adipose fin absent or modified into low integument fold extending between end of dorsal fin and caudal-fin origin. Vertebrae 32(2), 33(3), 34(1) or 35(1). First dorsal-fin pterygiophore immediately anterior to neural spine of 12th (3), 13th (2) or 14th (2) vertebra, first anal-fin pterygiophore immediately anterior to neural spine of 17th (3), 18th (2) or 19th (2) vertebra. Ribs 8 (2), 9 (4) or 10 (1). Branchiostegal rays 7. Dorsal-fin pterygiophores 7 (1), 8 (2) or 9 (4). Anal-fin pterygiophores 6 (7).

Cephalic lateral line canals with simple, non-dendritic tubes ending in single pores. Supraorbital canal mostly in frontal bone. Supraorbital pores invariably present: s1 mesial to nasal-barbel base and autopalatine, s3 elongate, mesial to posterior nostril and anterior to frontal and s6 single or closely set, posteromedial to eye and at midlength of frontal.

Infraorbital laterosensory canal incomplete, with four pores, i1 and i3 anteriorly and i10 and i11 posteriorly. Canal extending from sphenotic posteriorly to terminal pore located ventroposteriorly to eye. Infraorbital pores: i1 ventro-lateral to nasal-barbel base and autopalatine, i3 ventrolateral to posterior nostril and anterior to frontal, with its anterior border open, i10 and i11 posterior to eye, and anterolateral to anterior process of sphenotic. Otic canal without pores. Postotic pores po1 (anteromedial to opercular patch of odontodes and lateral to articulation between sphenotic-prootic-pterosphenoid and pterotic) and po2 (medial to opercular patch of odontodes and lateral to articulation between pterotic and posttemporo-supracleithrum). Lateral line of trunk anteriorly continuous with postotic canal and reduced to short, non-ossified tube in all four type specimens. Lateral line pores ll1, ll2 and ll3 dorsomedially to pectoral-fin base and posterior to posttemporo-supracleithrum.

Coloration in ethanol: Dorsum and sides of body with large roundish marks roughly arranged in rows, 12–15 laterally and 7–9 dorsally, progressively smaller and less aligned posteriorly. Narrow scattering of smaller spots ventral to large lateral ones, roughly following interface between myomeres and abdominal cavity and extending posteriorly onto ventral part of caudal peduncle. Conspicuous dark spot dorsal to base of pelvic fin. Abdominal region white.

Overall colour of head similar to, and slightly denser than, that of dorsum. Cheeks and snout with closely set, dark fields. Dorsal part of opercular patch of odontodes surrounded with dark field. Integument amidst opercular odontodes interspersed with dark

streaks, contrasting with white odontode slits. Region of head corresponding to skull roof almost continuously dark. Sensory pores on head white. Bases of nostrils extremely dark. Ventral surface of head white, except for sparse irregular melanophores close to angle of mouth and mentum. Dorsal surface of upper lip less dark than rest of head. Ventral part of upper lip and lower lip white or with sparse dark fields. Base of maxillary barbel darky pigmented dorsally, especially posteriorly. Dark fields extending onto basal third of dorsal surface of barbel, with remainder of barbel white on both sides. Rictal barbel mostly white, with few small elongate dark fields near base. Nasal barbel dark along nearly its entire length, on both sides. Base of pectoral fin with dense dark spots on dorsal surface, extending to half of fin as elongate fields along fin rays. Ventral surface of pectoral fin lacking dark pigment. Dorsal and anal fins with heavy dark covering over basal third or half of individual rays, fading distally. Fin web lacking dark chromatophores. Pelvic fins white. Basal 2/3 of caudal-fin rays darkly dashed, with individual dashes vertically aligned and forming pattern of three or four vertical stripes on fin, progressively less pronounced distally. Margin of caudal fin white.

Colour pattern of smallest juvenile (smallest examined specimen 12 mm SL) differing from that of adults in having only six dark spots along midline and by lacking dark maculae on the dorsal part of body.

Remarks: Trichomycterus astromycterus is a remarkable species differing from all trichomycterines in a number of peculiar traits (cf. diagnosis above). Its external morphology superficially resembles species of *Microcambeva* (Microcambevinae, formerly Sarcoglanidinae), but investigation of its anatomy and *COI* leave no doubt that it is unrelated to those subgroups but to Trichomycterinae instead. Also, as pointed out in the original description (Reis *et al.*, 2019), *T. astromycterus* shares some morphological convergences with *Bullockia maldonadoi* (Eigenmann, 1920). The numerous and conspicuous autapomorphies of *T. astromycterus* distinguish it not just from all *Trichomycterus* in the Rio Doce Basin, but from all other congeners in eastern South America. Other peculiarities are not necessarily autapomorphic, but still stand out as highly unusual. For example, its variation in number of dorsal-fin pterygiophores (seven to nine, modally nine) is anomalous. Species of *Trichomycterus* otherwise have a constant number of eight such elements. We know of only one species having such numerous dorsal-fin pterygiophores, *T. santaeritae*, the holotype of which has 11 dorsal-fin pterygiophores (but more information is needed on that species for further comparisons; see remarks on *T. alternatus*

above). Such a high degree of phenotypic divergence might suggest that *T. astromycterus* represents a separate genus under traditional generic concepts in Trichomycteridae. Nevertheless, no morphological evidence was found that might place it outside of the phylogenetic range currently circumscribed to species of *Trichomycterus* (de Pinna, 1998; Wosiacki, 2002; Ochoa *et al.*, 2017, 2020). This placement is here corroborated by *COI* data, which place the species nested in *T. alternatus* (see remarks on *T. alternatus* above, and discussion below). *Trichomycterus astromycterus* is definitely a taxon requiring more study, especially because of its combination of pronounced phenotypic differentiation (which extends to the morphology of juveniles) associated with no significant *COI* divergence (see Discussion).

Material of *T. astromycterus* comes from two different habitats. At the Rio do Peixe locality, adult specimens were found among rocks in an extremely fast-running water sector. At the Rio Santo Antônio locality, specimens were collected deeply buried in sand banks, in sectors with moderate current. Juvenile specimens were only found in the Rio do Peixe locality (16 specimens, 12.0–20.9 mm SL). They were found buried in sand banks in the margin of the stream in quiet sectors. The smallest specimen examined of *T. astromycterus* differs from adults in coloration (see description above), longer pectoral fin, reaching origin of pelvic fin, presence of a prominent dorsal fin fold (which remains until 15 mm SL; Fig. 15) and cephalic laterosensory canals mostly open (except the symphysial canal of pore S6, which is already closed, ending in a single pore).

Geographical distribution: Trichomycterus astromycterus was collected in tributaries of the Upper and Middle Rio Doce Basin. All localities are near the main channel of the Rio Doce (Fig. 16).

Type material examined: Holotype: MZUSP 124559, 52 mm SL; Brazil, Minas Gerais, Rio Doce, Rio do Peixe River tributary of Piranga River (20°11'40.32"S 42°51'8.47"W); col. V.J.C. Reis, M. de Pinna, G. Ballen & G.F. de Pinna. Paratype: MZUSP 123341, 1, 46.1 mm SL; Brazil, Minas Gerais, Naque Municipality, Rio Santo Antônio River, tributary of Rio Doce Basin (19°14'0.76"S 42°19'26.52"W); col. T.C. Pessali & E.P. Estevam, 1 September 2017. MZUSP 123361, 13, 29.3–38.5 mm SL, 2 c&s, 34.3–35.7 mm SL; Brazil, Minas Gerais, Naque Municipality, Rio Santo Antônio, tributary of Rio Doce Basin (19°14'0.76"S 42°19'26.52"W); col. T.C. Pessali, E.P. Estevam & V.J.C. Reis, 25 October 2017. MZUSP 123760, 37, 11.1–51.7 mm SL, 2 c&s, 44.1–45.8 mm SL; collected with holotype.

Figure 15. Juvenile specimen of *T. astromycterus*, MZUSP 123760, paratype, 10.3 mm SL, Rio do Peixe, tributary of Rio Piranga Drainage, lateral view.
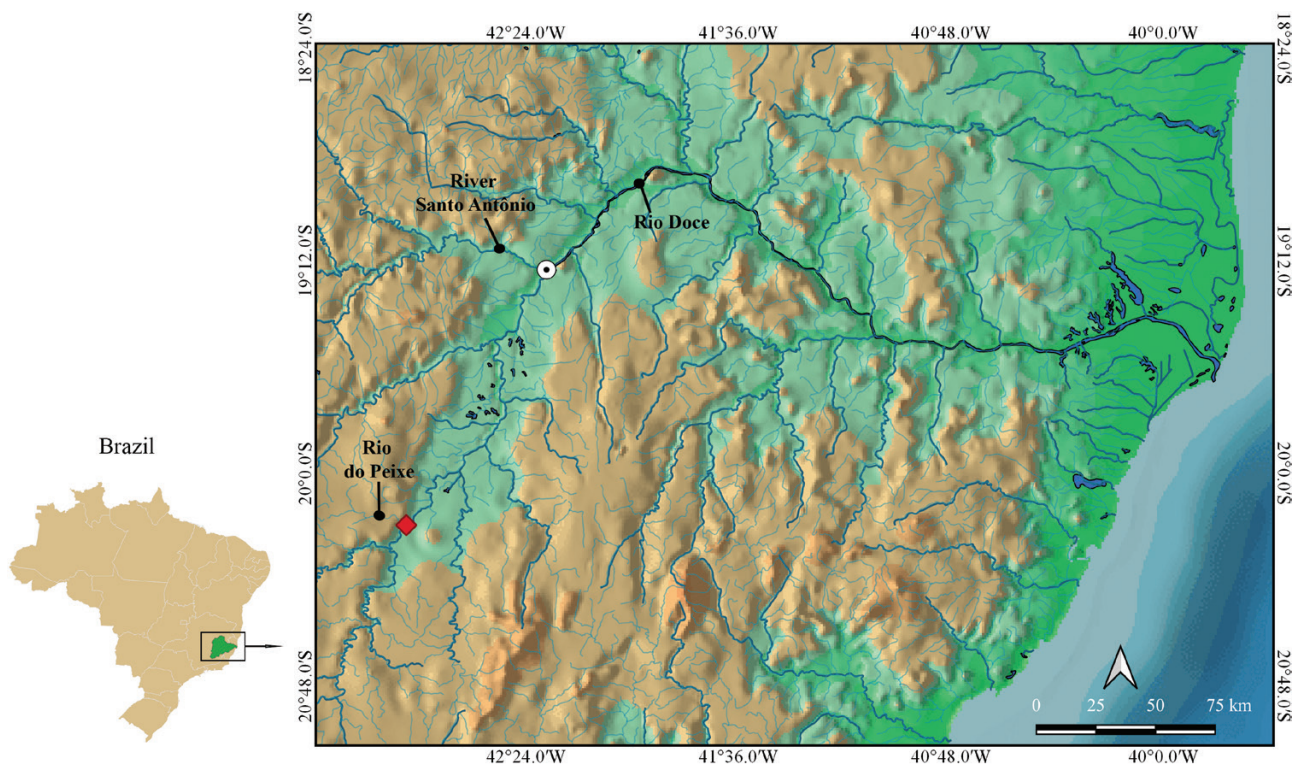
Figure 16. Geographical distribution of *T. astromycterus* in the Rio Doce Basin. Red diamond = holotype (MZUSP 124559) and paratype (MZUSP 123760); white dotted circle = paratypes (MZUSP 123341, 123361).

TRICHOMYCTERUS BARROCUS SP. NOV.

(FIG. 17)

Zoobank registration: urn:lsid:zoobank.org:act:2D2A53D8-7B5A-40BE-9373-D644C86DCEC4

Holotype: MBML 14092, 79.8 mm SL; Brazil, Espírito Santo, Afonso Cláudio, Boa Sorte River, Guandu River (20°10'57.00"S 41°4'50.00"W); col. L.M. Sarmento-Soares, R.F. Martins-Pinheiro, A.T. Aranda, R.L. Teixeira, M.M.C. Roldi & M.M. Lopes, 12 June 2009.

Paratypes: MBML 14093, 2, 54.9–79.8 mm SL, 1 c&s, 55.86 mm SL; Brazil, Espírito Santo, Afonso Cláudio, Boa Sorte River, Guandu River, (20°10'57.00"S

Figure 17. *Trichomycterus barrocus* sp. nov. (top: lateral; middle: dorsal; and bottom: ventral views). MBML 14092, holotype, 79.8 mm SL. Brazil, state of Espírito Santo, Afonso Cláudio Municipality, Boa Sorte River, tributary of Guandu River.

41°4'50.00"W); col. L.M. Sarmento-Soares, R.F. Martins-Pinheiro, A.T. Aranda, R.L. Teixeira, M.M.C. Roldi & M.M. Lopes, 12 June 2009. MZUSP 126763, 1, 66.7 mm SL, collected together with holotype.

Diagnosis: The combination of the following traits distinguishes *T. barrocus* from congeners: (1) colour pattern composed of dark maculae forming two thick longitudinal stripes (interrupted or continuous), one mid-dorsal and one mid-lateral; (2) barbels short, nasal barbel barely crossing the anterior border of eyes, maxillary and rictal barbels not reaching the interopercle (vs. long barbels surpassing posterior margin of eyes and reaching interopercle); (3) I + 7 pectoral-fin rays (vs. I + 5, I + 6 or I + 8); (4) two lateral line pores (vs. three or more). Among species of *Trichomycterus* in south-eastern South America, character 1 distinguishes *T. barrocus* from all congeners except some colour morphs of *T. alternatus*, *T. caipora*, *T.* aff. *caipora*, *T. giganteus*, *T. itatiayae* Miranda

Ribeiro 1906, *T. nigroauratus* Barbosa & Costa, 2008 and *T. reinhardti* (Eigenmann, 1917); character 2 distinguishes *T. barrocus* from all congeners except some morphs of *T. alternatus*, *T. astromycterus*, *T. caipora* and *T.* aff. *caipora*; character 3 from the entire *T. brasiliensis* and *T. reinhardti* species complex (Barbosa & Costa, 2010; Costa, 2021; Costa & Katz, 2021), plus *T. trefauti* (all with I + 6 or fewer) and from *T. astromycterus*, *T. giganteus*, *T. immaculatus*, *T. lauryi*, *T. nigricans*, *T. pradensis* and *T. tantalus* (all with I + 8 or more); character 4 distinguishes *T. barrocus* from *T. astromycterus*, *T. caipora*, *T.* aff. *caipora*, *T. ipatinga*, *T. nigricans*, *T. tantalus* and *T. vinnulus*. Among congeners in the Rio Doce Basin, *T. barrocus* is most similar to *T. alternatus* and *T.* aff. *caipora*. The species is further distinguished from *T. alternatus* by the absence of a large fenestra between the orbitosphenoid and the frontal (vs. presence), deeper body (9.0–13.9% SL vs. 18.3–13.8%), shorter pre-anal length (49–69% SL vs. 63.8–82.9%)

Table 6. Morphometric data of *T. barrocus* based on holotype and paratype material (MBML 14092, 14093, MZUSP 126763)

	Holotype	Range (*N* = 3)	Mean	SD
Standard length (mm)	78.9	55.9–78.9	71.2	-
% of standard length				
Anal-fin base	6.7	4.9–9.3	6.9	2.2
Body depth	11.6	9.0–13.9	11.5	2.4
Caudal peduncle depth	11.3	10.1–11.3	10.7	0.6
Dorsal-fin base	7.7	7.4–10.1	8.4	1.5
First pectoral-fin length	12.6	8.7–14.3	11.9	2.9
Head length	19.2	18.7–19.2	19.0	0.3
Preanal length	61.7	49.0–69.0	59.9	10.1
Predorsal length	54.8	41.2–60.7	52.2	10.0
Prepelvic length	47.2	41.9–52.5	47.2	5.3
% of head length				
Eye diameter	15.3	14.8–17.5	15.9	1.4
Interorbital width	28.4	25.0–28.4	26.7	1.7
Snout length	47.0	46.4–49.4	47.6	1.6
Mouth width	31.5	21.4–39.1	30.7	8.9

and shorter prepelvic length (41.9–52.5% SL vs. 52.8–70.9%). It is further distinguished from *T.* aff. *caipora* by the larger eye (14.8–17.5% SL vs. 12.2–14.4%) and by having seven branchiostegal rays (vs. six).

Description: Morphometric data is presented in Table 6. Body long and almost straight, trunk roughly round in cross-section near head, then slightly deeper than wide and gently compressed to caudal peduncle, tapering to caudal fin. Dorsal profile of body gently convex to dorsal-fin origin, then straight or slightly concave along caudal peduncle to caudal-fin origin. Ventral profile convex from gular region to vent, due partly to abdominal distension, then straight or slightly concave along anal-fin origin to caudal-fin base. Caudal peduncle long and less deep than body at end of anal-fin base.

Head approximately 1/5 of SL, pentagonal, longer than wide and depressed. Mouth subterminal. Upper jaw slightly longer than lower jaw. Upper lip wider than lower lip and laterally continuous with base of maxillary barbel. Lower lip small, approximately 2/3 width of upper one, partly divided into right and left portions by with median concavity. Lower lip with uniform covering of tiny villi, resulting in velvet-like surface and not clustered into large papillae. Region between upper and lower lips with slender fleshy lobe.

Dentary and premaxillary teeth similar to each other in shape. Dentary teeth conical, arranged in four irregular rows, first row with 12 teeth, extending from base to slightly up of coronoid process, with size of individual teeth increasing markedly towards symphysis and from posterior to anterior rows. Total area of premaxillary teeth slightly smaller than that of dentary, with teeth arranged irregularly in four rows, first row with approximately 13 teeth, over entire ventral surface of premaxilla. Premaxillary teeth conical.

Eye medium sized, slightly protruding, positioned dorsally on head, without free orbital rim and covered with transparent skin. Eye located on anterior half of HL, closer to lateral border of head than to midline in dorsal view. Anterior naris surrounded by tube of integument directed anterolaterally, continuous posterolaterally with nasal barbel. Posterior naris closer to anterior naris than to eyes, surrounded by tube of integument incomplete posteriorly. Maxillary barbel narrowing markedly towards fine tip, barely reaching vertical through posterior border of eye. Rictal barbel inserted immediately ventral to maxillary barbel, its tip reaching until vertically posterior border of eye, not reaching the interopercle. Nasal barbel originating on posterolateral region of anterior naris, minimally reaching posterior margin of eye, but not interopercle. Interopercular patch of odontodes large, compared to head length, oval in shape and with well-developed odontodes, prominent in ventral aspect of head. Interopercular patch of odontodes extending from vertical through ventroposterior border of eye to ventroanterior to opercular patch of odontodes. Odontodes arranged in two or three irregular series, with those on mesial series much longer than those on lateral one; odontodes gradually larger posteriorly in both series, with those posteriorly on mesial row largest. Interopercular odontodes 38–49. Opercular patch of odontodes on dorsolateral surface of posterior part of head, positioned anterodorsally to pectoral-fin base, roundish in shape and larger than eye in dorsal

aspect of head. Opercular odontodes 15–25, sunk in individual slits of integument, progressively larger posteriorly, all with fine tips, with largest ones curved distally and claw-like. Entire patch surrounded by rim of integument.

Pectoral fin, with its base immediately posterior and ventral to opercular patch of odontodes. Pectoral-fin rays I + 7. First pectoral-fin ray (unbranched) longest, prolonged as filament beyond fin margin. Other rays progressively shorter, their tips following continuous line along fin margin. Pelvic fin with convex distal profile, its origin slightly posterior to middle of SL and anterior to vertical through dorsal-fin origin, slightly covering anal and urogenital openings in adults. Base of pelvic fins positioned close to each other. Pelvic-fin rays I + 4. Anterior processes of basipterygium girdle short and thin. Dorsal fin long, its distal margin sinusoidal. Dorsal-fin origin closer to base of caudal fin than to tip of snout. Dorsal-fin rays ii + II + 6 (1) or iii + II + 7 (2). Anal fin slightly smaller than dorsal fin, its distal margin gently convex. Anal-fin origin posterior to vertical through end of dorsal-fin base. Anal-fin rays ii + I + 7 (1) or iii + II + 5 (2). Caudal fin subtruncated, with 6 + 7 principal rays. Adipose fin absent or modified into low integument fold extending between end of dorsal fin and caudal-fin origin. Post-Weberian vertebrae 36 (3) or 37 (1). First dorsal-fin pterygiophore immediately anterior to neural spine of 16th (1), 17th (1) or 18th (1) vertebra, first anal-fin pterygiophore immediately anterior to neural spine of 21st (2) or 22nd (1) vertebra. Caudal-fin procurrent rays plus one segmented non-principal ray dorsally and ventrally. Procurrent caudal-fin rays, 15–17 dorsally and 12–13 ventrally, beginning anteriorly at 31st (1), 32nd (1) or 33rd (1) vertebrae. Ribs 11 (1), 12 (1) or 13 (1). Branchiostegal rays 7 (3). Dorsal-fin pterygiophores 7 (1) or 8 (2). Anal-fin pterygiophores 6 (3).

Cephalic lateral line canals with simple, non-dendritic tubes ending in single pores. Supraorbital canal mostly in frontal bone. Supraorbital pores invariably present: s1 mesial to nasal-barbel base and autopalatine, s3 mesial to posterior nostril and anterior to frontal, paired s6 close to each other, posteromedial to eye and at midlength of frontal. Infraorbital laterosensory canal incomplete with four pores, i1 and i3 anteriorly and i10 and i11 posteriorly. Canal extending from sphenotic posteriorly to terminal pore located ventroposteriorly to eye. Infraorbital pore i1 located ventrolateral to nasal-barbel base and autopalatine, i3 ventrolateral to posterior nostril and anterior to frontal, i10 and i11 posterior to eye. Otic canal without pores. Postotic pores po1, anteromedial to opercular patch of odontodes, and po2, mesial to opercular patch of odontodes. Lateral line of trunk anteriorly continuous with postotic canal and reduced to short tube. Lateral line pores ll1 and ll2 dorsomedial to pectoral-fin base.

Coloration in ethanol: Body with two partially unfused rows of dark maculae. First row forming broad stripe along mid-dorsum of trunk from posterior margin of head to caudal fin, merged with amorphous dark maculae resembling drops of dark ink on a white background. Second row formed by large and round dark maculae along lateral midline from end of opercle to base of caudal fin, forming broad continuous stripe in some specimens. Small round or irregular dark maculae ventral to second row, from middle of body to caudal fin. Ventral part of the body with no dark pigmentation. Head with partly amalgamated brownish chromatophores. Tip of snout (from anterior naris to tip of upper lip), cheeks (to ventral margin of orbits) and region ventroposterior to eye (excluding portion anterior to opercle) with little or no dark pigment. Integument of opercular patch of odontodes darkly pigmented. Interopercular patch of odontodes with no pigmentation. Pectoral, pelvic, dorsal and anal fins with brownish spots mainly along their bases. Caudal fin with vertical dark stripe across base and spots amongst rays.

Etymology: The epithet is a Latinized adjective from Portuguese *barroco*, originally designating a pearl of irregular shape, here referring to the the baroque-style beauty of this species.

Remarks: Trichomycterus barrocus is a distinctive and readily diagnosable species, endemic to the Lower Rio Doce Basin. Some meristic values in this species are variable (number of post-Weberian vertebrae, position of first dorsal and ventral pterygiophores relative to vertebral column, number of ribs and anal-fin rays; cf. Description above). Despite such variation observed in only three specimens available for osteological examination, they fall in the range of variation seen in species of *Trichomycterus* represented by more abundant material. Because other diagnostic characters do not vary significantly, it seems likely that the type material represents a single species. The highly distinctive colour pattern of *T. barrocus* distinguishes it from all congeners. The dorsal colour pattern, in particular, has no parallel in the genus. The mid-lateral colour pattern vaguely resembles some species such as *T. reinhardti* (Eigenmann, 1917), some colour morphs of *T. alternatus*, *T. itatiayae* Miranda Ribeiro, 1906, *T. giganteus*, *T. nigroauratus* Barbosa & Costa, 2008 and some colour morphs of *T.* aff. *caipora*. However, in addition to the diagnostic characters listed above, in all of those the colour pattern is immediately distinguishable from that of *T. barrocus*. No material suitable for sequence analysis is currently available of the species.

Geographical distribution: Trichomycterus barrocus is endemic to the Lower Rio Doce Basin, at the Boa Sorte River, a tributary of Rio Guandu ([Fig. 18](#)).
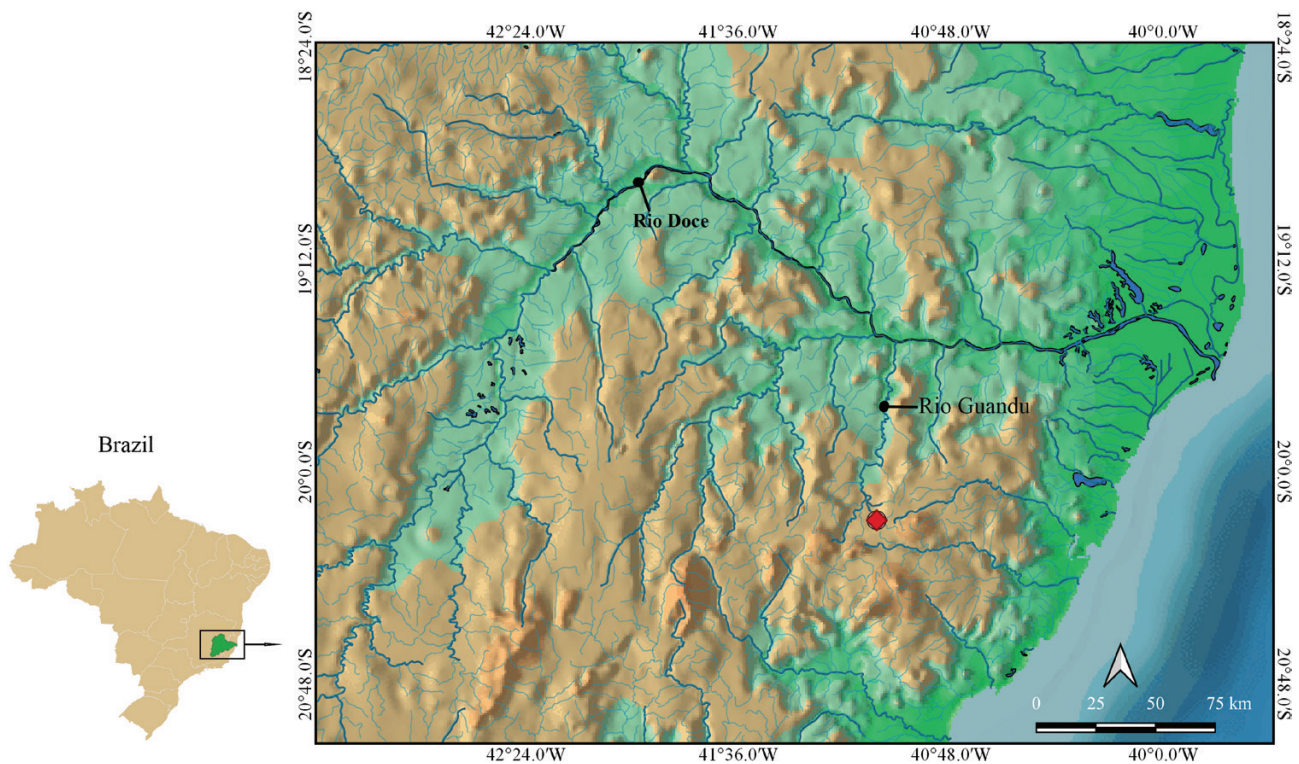
Figure 18. Geographical distribution of *T. barrocus* sp. nov. in the Rio Doce Basin. Red diamond = holotype (MBML 14092) and paratype (MBML 14093, MZUSP 126763).

TRICHOMYCTERUS BRUCUTU SP. NOV.

(FIG. 19)

Zoobank registration: urn:lsid:zoobank.
org:act:0E3EC319-DA7C-4D01-BE1F-C704D3347A2C

Holotype: MZUSP 87834, 103 mm SL; Brazil, state of Minas Gerais, Santo Antônio de Itambé, Lajeado Creek, tributary of Rio Mãe d'Água (18°30'0.00"S 43°17'60.00"W); col. A. Carvalho Filho, 30 August 2004.

Paratypes: MZUSP 126757, 2, 24.6–71.8 mm SL; collected with holotype. MNRJ 48472, 1, 120.6 mm SL; Brazil, state of Minas Gerais, Conceição do Mato Dentro Municipality: unamed creek, tributary of left margim of Ribeirão Santo Antônio or Cruzeiro at headwater region (18°46'46"S 43°33'21"W); col. S.A. Santos, M.R. Britto & D.F. Moraes, 30 July 2016.

Diagnosis: The combination of the following traits distinguishes *T. brucutu* from congeners: (1) body depth 19.0–19.9% SL (vs. 18.3% or lower); (2) long and deep dorsal and ventral integument folds from end of dorsal and anal fins to base of caudal-fin, with elongate procurrent rays (vs. dorsal and ventral integument folds beginning at middle of caudal peduncle length);

(3) colour pattern consisting of tiny spots, round to vermiculate, homogeneously distributed over entire body; and (4) pectoral-fin rays I + 7 (vs. I + 5, I + 6 or I + 8). Among congeners in south-eastern South America, character 1 and 2 distinguish *T. brucutu* from all congeners; character 3 from all congeners except *T. laury* and species in the *T. brasiliensis* species complex; character 4 from the *T. brasiliensis* and *T. reinhardti* species complex (Barbosa & Costa, 2010; Costa, 2021; Costa & Katz, 2021), plus *T. trefauti* (all preceding with I + 6 or fewer) and from *T. astromycterus*, *T. giganteus*, *T. immaculatus*, *T. lauryi*, *T. nigricans*, *T. pradensis* and *T. tantalus* (with I + 8 or higher). Among congeners in the Rio Doce Basin, *T. brucutu* is most similar to *T. argos* and *T. brunoi* and it can be distinguished from those two species, in addition to characters mentioned above, by the pelvic-fin bases spaced out (vs. closely set).

Description: Morphometric data for specimens examined is presented in Table 7. Body long and almost totally straight, trunk roughly round in cross-section near head, then slightly deeper than wide and gently compressed to caudal peduncle, tapering to caudal fin. Dorsal profile of body gently convex to dorsal-fin origin, then straight or slightly concave along caudal peduncle to caudal-fin origin. Ventral profile convex from gular

Figure 19. *Trichomycterus brucutu* sp. nov. (top: lateral; middle: dorsal; and bottom: ventral views)., MZUSP 87834, holotype, 103 mm SL. Brazil, state of Minas Gerais, Santo Antônio de Itambé Municipality, Lajeado Creek, tributary of Mãe D'água River.

region to vent, due partly to abdominal distension, then straight or slightly concave along anal-fin origin to caudal-fin base. Caudal peduncle long, wide and as deep as body at beginning of anal-fin base, with a long and wide dorsal and ventral integumentary folds from end of dorsal and anal fin to caudal fin, with long proccurent rays.

Head approximately 1/6 of SL, pentagonal, longer than wide and depressed. Mouth subterminal. Upper jaw slightly longer than lower jaw. Upper lip wider

Table 7. Morphometric data of *T. brucutu* based on holotype and paratype material (MZUSP 87834, MZUSP 126757, MNRJ 48472)

	Holotype	Range (*N* = 3)	Mean	SD
Standard length (mm)	103.3	71.8–120.3	98.5	-
% of standard length				
Anal-fin base	8.9	7.4–8.9	8.3	0.8
Body depth	19.9	15.3–19.9	18.1	2.4
Caudal peduncle depth	14.8	14.8–16.1	15.3	0.7
Dorsal-fin base	10.8	10.8–11.2	11.0	0.2
First pectoral-fin length	11.2	11.2–17.7	14.2	3.3
Head length	16.2	16.2–20.2	17.9	2.1
Preanal length	70.3	70.3–72.4	71.6	1.1
Predorsal length	58.1	58.1–64.6	61.5	3.3
Prepelvic length	58.0	56.7–58.0	57.4	0.7
% of head length				
Eye diameter	18.8	18.5–18.8	16.4	3.9
Interorbital width	30.3	30.0–31.4	30.4	0.9
Snout length	52.6	50.0–59.3	54.0	4.6
Mouth width	40.7	36.3–42.6	39.9	3.3

than lower lip and laterally continuous with base of maxillary barbel. Lower lip small, approximately 2/3 width of upper one, partly divided into right and left portions by median concavity. Lower lip with uniform covering of tiny villi, resulting in velvet-like surface and not clustered into large papillae. Region between upper and lower lips with slender fleshy lobe.

Dentary and premaxillary teeth similar to each other in shape. Dentary teeth conical, arranged in four irregular rows extending from base to slightly up of coronoid process, size of individual teeth increasing markedly towards symphysis and from posterior to anterior rows. Total area of premaxillary teeth slightly smaller than that of dentary, with teeth arranged irregularly in four rows over entire ventral surface of premaxilla. Premaxillary teeth conical.

Eye small sized, protruding, positioned dorsally on head, without free orbital rim and covered with transparent skin. Eye located on anterior half of HL, closer to lateral border of head than to the midline in dorsal view. Extensor tentaculi and dilatator operculi hypertrophied, creating crest-like elevation dorsal to eyes. Anterior naris surrounded by tube of integument directed anterolaterally, continuous posterolaterally with nasal barbel. Posterior naris closer to anterior naris than to eyes, surrounded by tube of integument incomplete posteriorly. Maxillary barbel narrowing markedly towards fine tip, reaching the base of pectoral fin. Rictal barbel inserted immediately ventral to maxillary barbel, its tip reaching lateroposterior border of interopercle. Nasal barbel originating on posterolateral region of anterior naris, reaching anterior border of opercle. Interopercular patch of odontodes oval in shape and with well-developed odontodes,

prominent in ventral aspect of head. Interopercular patch of odontodes extending from vertical through posteroventral border of eye to anteroventral of opercular patch of odontodes. Interopercular odontodes arranged in two or three irregular series, with those on mesial series much longer than those on lateral one; odontodes gradually larger posteriorly in both series, with those posteriorly on mesial row largest. Interopercular odontodes 37–47. Opercular patch of odontodes on dorsolateral surface of posterior part of head, positioned anterodorsally to pectoral-fin base, roundish in shape in dorsal aspect and with same size as eye diameter. Opercular odontodes 18–21, sunk in individual slits of integument, progressively larger posteriorly, all with fine tips, with largest ones curved distally and claw-like. Entire patch surrounded by rim of integument.

Pectoral fin with its base immediately posterior and ventral to opercular patch of odontodes. Pectoral-fin rays I + 7. First pectoral-fin ray (unbranched) longer, prolonged as filament beyond fin margin. Other rays progressively shorter, their tips following continuous line along fin margin. Pelvic-fin with convex distal profile, its origin slightly posterior to middle of SL and anterior to vertical through dorsal-fin origin, touching the anterior border of anal and urogenital openings in adults, but not beyond. Bases of pelvic fins separated by one eye diameter. Pelvic-fin rays I + 4, first ray. Dorsal fin long, its distal margin sinusoidal. Dorsal-fin origin closer to base of caudal-fin than to tip of snout. Dorsal-fin rays ii + II + 7 (2). Anal fin slightly smaller than dorsal fin, its distal margin gently convex. Anal-fin origin posterior to vertical through end of dorsal-fin base. Anal-fin rays ii + II + 5 (2). Caudal fin subtruncate

with 6 + 7 principal rays. Adipose fin, if present, incorporated or modified into deep integumentary fold extending between end of dorsal fin and caudal-fin origin. Post-Weberian vertebrae 37 (2) and 38 (1). First dorsal-fin pterygiophore immediately anterior to neural spine of 17th (2) and 18th (1) vertebrae, first anal-fin pterygiophore immediately anterior to neural spine of 21st (2) and 22nd (1) vertebrae. Caudal fin procurrent rays plus one segmented non-principal ray dorsally and ventrally. Procurrent caudal-fin rays, 24–25 (2) dorsally and 14–17 (2) ventrally, beginning anteriorly at 28th (2) vertebra. Ribs 12 (2) or 13 (1). Branchiostegal rays 8 (3). Dorsal-fin pterygiophores 8. Anal-fin pterygiophores 6.

Cephalic lateral line canals with simple, non-dendritic tubes ending in single pores. Supraorbital canal mostly in frontal bone. Supraorbital pores invariably present: s1 mesial to nasal-barbel base and autopalatine, s3 mesial to posterior nostril and anterior to frontal, paired s6, closer to mesial line than to eyes, posteromedial to eye and at midlength of frontal. Infraorbital latero-sensory canal incomplete, with four pores, i1 and i3 anteriorly and i10 and i11 posteriorly. Canal extending from sphenotic posteriorly to terminal pore located ventroposteriorly to eye. Infraorbital pore i1 located ventrolateral to nasal-barbel base and autopalatine, i3 ventrolateral to posterior nostril and anterior to frontal, i10 and i11 posterior to eye. Otic canal without pores. Postotic pores po1, anteromedial to opercular patch of odontodes, and po2, mesial to opercular patch of odontodes. Lateral line of trunk anteriorly continuous with postotic canal and reduced to short tube. Lateral line pores ll1, and ll2 dorsomedial to pectoral-fin base.

Coloration in ethanol: Dark chromatophores distributed on inner and outer skin layers throughout entire body. Margin of integumentary fold of opercular patch of odontodes darkly pigmented. Interopercular patch of odontodes white (no pigmentation). Base of nasal barbels surrounded with concentration of dark pigment, extending posteriorly as an elongate dark field to anterior margin of eyes. Tiny brownish round to amoeboid maculae shortly spaced covering entire body, except ventral part. Individual maculae rarely fusing to each other. Head darkest on region corresponding to neurocranium, outlined by brain pigment seen by transparency. Area of levator operculi and adductor operculi muscles on the cheeks with few chromatophores. Tiny round dark spots laterally on head, mainly anterolaterally to opercle. Spots limited to base of fins, with rays outlined in dark.

Etymology: The word *brucutu* is Brazilian Portuguese slang for rustic, rough or brute, in allusion to the thick deep body and caudal peduncle of this species.

The name is used for the Brazilian version of the main character of American cartoon character Alley Oop and it is also the name of the second largest iron cave in Brazil, located in the state of Minas Gerais, in the drainage area of the Rio Doce. It is a noun in apposition.

Remarks: Trichomycterus brucutu has a remarkably deep body when adult. A small specimen (24.7 mm SL) has been found, but was not deep-bodied to the same degree and thus the character is only useful to diagnose adult specimens. A second conspicuous diagnostic character for *T. brucutu* is the length and depth of dorsal and ventral integumentary folds on the caudal peduncle. Such traits accentuate the depth of the caudal peduncle and makes it externally even (in depth) from the level of dorsal- and anal-fin ends to slightly beyond the caudal-fin base. Such a condition is only shared by *Cambeva crassicaudata* (Wosiacki & de Pinna 2008) and *Cambeva stawiarski* (Miranda Ribeiro 1968) among the *Trichomycterus* lineage (*sensu* Ochoa *et al.*, 2020). In all other species with deep caudal peduncles (e.g. *T. brasiliensis*), the posterior part of caudal peduncle flares towards its fusion with the caudal fin. Material of the species suitable for sequence analysis is not currently available.

Geographical distribution: Trichomycterus brucutu is endemic to Lajeado Creek, in the headwaters of Rio Santo Antônio, a tributary of the Middle Rio Doce Basin (Fig. 20).

TRICHOMYCTERUS BRUNOI BARBOSA & COSTA, 2010
(FIG. 12)

Trichomycterus brunoi Barbosa & Costa, 2010: 97, figs 1, 3 [type locality: Brazil: state of Minas Gerais: Alto Caparaó Municipality: lateral channel of Rio Caparaó, Rio Itabapoana Basin, Alto Caparaó, 20°25'54"S 41°51'57"W, elevation 1047 m; holotype: UFRJ 6030, paratypes: UFRJ 5649 (11), 5650 (2), 5658 (5, c&s); Sarmento-Soares *et al.*, 2011: 262 (citation, diagnosis); Barbosa & Costa, 2012: 159 (citation, relationships); Barbosa & Azevedo-Santos, 2012: 358 (citation, diagnosis); Barbosa, 2013: 274 (citation, relationships); García-Melo *et al.*, 2016: 237 (citation, relationships); Barbosa & Katz, 2016: 262 (citation, relationships).

Diagnosis: The combination of the following traits distinguishes *T. brunoi* from congeners: (1) pectoral-fin rays I + 6 (vs. I + 5, I + 7 or I + 8); (2) colour pattern composed of stripes, vermiculations or reticulations; (3) eight branchiostegal rays (vs. either fewer or more); and (4) minute foramen for ramus lateralis accessorius
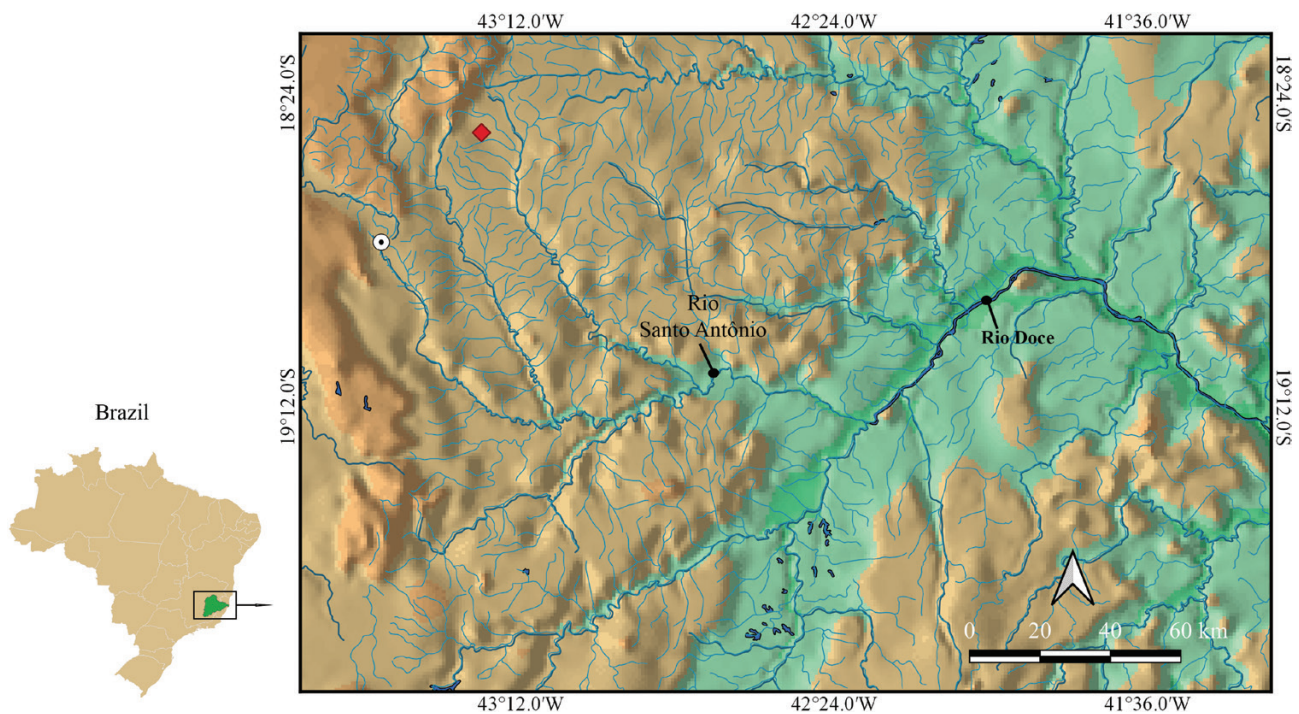
Figure 20. Geographical distribution of *T. brucutu* sp. nov. in the Rio Doce Basin. Red diamond = holotype (MZUSP 87834) and paratype (MZUSP 126757); White dotted circle = paratype (MNRJ 48472).

facialis nerve on parietosupraoccipital, visible in dorsal view (vs. foramen large, well visible in dorsal view). Among congeners in south-eastern South America, character 1 distinguishes *T. brunoi* from all congeners except *T. pirabitira*, *T. itatiayae*, *T. trefauti*, those in the *T. reinhardti* species complex (Costa & Katz, 2021), except from *T. humboldti*, *T. pauciradiatus*, *T. piratymbara* and *T. sainthilairei* and those in the *T. brasiliensis* species complex (Barbosa & Costa, 2010; Costa, 2021); character 2 from all congeners except for those in the *T. brasiliensis* species complex, plus *T. lauryi* and *T. pirabitira*; character 3 from all congeners except for *T. argos*, *T. brucutu*, *T. giganteus*, *T. ipatinga*, *T. itatiayae*, *T. mimosensis*, *T. nigroauratus,* *T. pirabitira* and *Trichomycterus potschi* Barbosa & Costa, 2003; character 4 from *T. argos*. Among congeners in the Rio Doce Basin, *T. brunoi* is most similar to *T. argos*. In addition to characters above, *T. brunoi* can be further distinguished from *T. argos* by the shorter snout (28–41.2% SL vs. 41.9–45.9% SL), by the shorter prepelvic length (41.4–58.5% SL vs. 59.5–60.6% SL) and by the fewer interopercular odontodes (26–31 vs. 39–40).

Description: Morphometric data for specimens examined is presented in Table 8. Body long and almost straight, trunk roughly round in cross-section near head, then slightly deeper than wide and gently compressed to caudal peduncle, tapering to caudal fin. Dorsal profile of body gently convex to dorsal-fin origin, then straight or slightly concave along caudal peduncle to caudal-fin origin. Ventral profile convex from gular region to vent, due partly to abdominal distension, then straight or slightly concave along anal-fin origin to caudal-fin base. Caudal peduncle as deep as body at end of anal-fin base.

Head approximately 1/5 to 1/4 of SL, pentagonal, longer than wide and depressed, with a long snout. Mouth subterminal. Upper jaw slightly longer than lower jaw. Upper lip wider than lower lip and laterally continuous with base of maxillary barbel. Lower lip small, approximately 2/3 width of upper one, partly divided into right and left portions by median concavity. Lower lip with uniform covering of tiny villi, resulting in velvet-like surface and not clustered into large papillae. Region between upper and lower lips with slender fleshy lobe.

Dentary and premaxillary teeth similar to each other in shape. Dentary teeth conical, arranged in four irregular rows, first row with 12 teeth, extending from base to slightly up of coronoid process, with size of individual teeth increasing markedly towards symphysis and from posterior to anterior rows. Total area of premaxillary teeth slightly smaller than that of dentary, with teeth arranged irregularly in four rows, first row with approximately 13 teeth, over entire ventral surface of premaxilla. Premaxillary teeth conical.

Table 8. Morphometric data of *T. brunoi* based on non-type material (MBML 4304, 4308, 4337)

	Range (*N* = 6)	Mean	SD
Standard length (mm)	29.7–85.8	47.7	-
% of standard length			
Anal-fin base	7.1–11.9	8.5	2.3
Body depth	10.5–15.3	12.7	2.3
Caudal peduncle depth	10.0–15.1	13.3	1.8
Dorsal-fin base	7.8–12.7	10.5	2.2
First pectoral-fin length	8.1–14.7	11.3	2.8
Head length	17.8–23.2	20.5	1.7
Preanal length	49.4–71.8	60.9	10.9
Predorsal length	46.3–68.8	56.9	11.5
Prepelvic length	41.4–58.5	50.1	9.5
% of head length			
Eye diameter	10.8–15.4	13.4	1.9
Interorbital width	20.0–27.7	26.1	2.9
Snout length	28.0–41.2	39.5	4.9
Mouth width	24.8–42.5	35.0	8.6

Eye small, protruding, positioned dorsally on head, without free orbital rim and covered with transparent skin. Eye located on anterior half of HL, closer to lateral border of head than to the midline in dorsal view. Anterior naris surrounded by tube of integument directed anterolaterally, continuous posterolaterally with nasal barbel. Posterior naris closer to anterior naris than to eyes, surrounded by tube of integument incomplete posteriorly. Maxillary barbel tubular narrowing markedly towards fine tip, reaching until half of pectoral-fin length. Rictal barbel inserted immediately ventral to maxillary barbel, its tip reaching gill opening. Nasal barbel originating on posterolateral region of anterior naris, reaching until posterior region of the opercle, not surpassing it. Interopercular patch of odontodes small compared to head length, oval in shape and with well-developed odontodes, prominent in ventral aspect of head. Interopercular patch of odontodes extending from vertical through ventroposterior border of eye to ventroanterior to opercle. Odontodes arranged in two or three irregular series, with those on mesial series much longer than those on lateral one; odontodes gradually larger posteriorly in both series, with those posteriorly on mesial row largest. Interopercular odontodes 26–31. Opercular patch of odontodes on dorsolateral surface of posterior part of head, positioned an interodorsally to pectoral-fin base, roundish in shape slightly smaller than eye in dorsal aspect of head. Opercular odontodes 13–16, sunk in individual slits of integument, progressively larger posteriorly, all with fine tips, with largest ones curved distally and claw-like. Entire patch surrounded by fleshy fold rim of integument.

Pectoral fin with its base immediately posterior and ventral to opercular patch of odontodes. Pectoral-fin rays I + 6. First pectoral-fin ray (unbranched) longest, prolonged as filament beyond fin margin. Other rays progressively shorter, their tips following continuous line along fin margin. Pelvic fin with convex distal profile, its origin slightly posterior to middle of SL and anterior to vertical through dorsal-fin origin, slightly surpassing anal and urogenital openings in adults. Pelvic-fin rays I + 4. Dorsal fin long, its distal margin sinusoidal. Dorsal-fin origin closer to base of caudal fin than to tip of snout. Dorsal-fin rays ii + II + 7 (3). Anal fin slightly smaller than dorsal fin, its distal margin gently convex. Anal-fin origin posterior to vertical through end of dorsal-fin base. Anal-fin rays ii + II + 5 (1) or iii + II + 5 (1). Caudal fin rounded in shape with 6 + 7 principal rays. Adipose fin absent or modified into low integumentary fold extending between end of dorsal fin and caudal-fin origin. Post-Weberian vertebrae 36 (1) or 38 (2). First dorsal-fin pterygiophore immediately anterior to neural spine of 18th (3) vertebra, first anal-fin pterygiophore immediately anterior to neural spine of 21st (3) vertebra. Caudal-fin procurrent rays plus one segmented non-principal ray dorsally and ventrally. Procurrent caudal-fin rays, 16 dorsally and 13 ventrally, beginning anteriorly at 32nd (1) vertebrae. Ribs 12 (2) or 13 (1). Branchiostegal rays 8. Dorsal-fin pterygiophores 8. Anal-fin pterygiophores 6.

Cephalic lateral line canals with simple non-dendritic tubes ending in single pores. Supraorbital canal mostly in frontal bone. Supraorbital pores invariably present: s1 mesial to nasal-barbel base and autopalatine, s3 mesial to posterior nostril and anterior to frontal, s6 paired and close to each other, posteromedial to eye and at midlength of frontal. Infraorbital laterosensory canal incomplete with four pores, i1 and i3 anteriorly and i10 and i11 posteriorly, extending from sphenotic posteriorly to terminal pore located ventroposteriorly

to eye. Infraorbital pore i1 located ventro-lateral to nasal-barbel base and autopalatine, i3 ventrolateral to posterior nostril and anterior to frontal, i10 and i11 posterior to eye. Otic canal without pores. Postotic pores po1, anteromedial to opercular patch of odontodes, and po2, mesial to opercular patch of odontodes. Lateral line of trunk anteriorly continuous with postotic canal and reduced to short tube. Lateral line pores ll1 and ll2 dorsomedial to pectoral-fin base.

Coloration in ethanol: Dark chromatophores agglutinating into round to vermiculate maculae. Individual maculae eye-sized or smaller, randomly distributed on body, except ventrally, from head to base of middle caudal-fin rays. Anteriorlly at midline of body, maculae sometimes roughly organized in line, coalescing into broken stripes. Maculae roundish and widely spaced-out ventral to lateral midline. Dorsal to lateral midline, maculae more numerous and predominantly vermiculate, often coalescent. Ventral part of body lacking dark pigmentation. Dark spots on bases of fins excluding pelvics.

Remarks: Trichomycterus brunoi belongs to the *T. brasiliensis* species complex (Barbosa & Costa, 2010), comprising *T. brasiliensis, Trichomycterus claudiae* Barbosa & Costa, 2010, *T. fuliginosus, Trichomycterus macrotrichopterus* Barbosa & Costa, 2010, *Trichomycterus maracaya* Bockmann & Sazima, 2004, *Trichomycterus mariamole* Barbosa & Costa, 2010, *Trichomycterus mimonha* Costa, 1992, *Trichomycterus mirissumba* Costa, 1992, *Trichomycterus novalimensis* Barbosa & Costa, 2010, *T. potschi, Trichomycterus rubiginosus* Barbosa & Costa, 2010, *Trichomycterus vermiculatus* (Eigenmann, 1917) and *T. argos* (herein included in the group; see Remarks for *T. argos*). Its placement in that assemblage is supported by the presence of I + 6 pectoral-fin rays, a colour pattern consisting of small dark maculae, usually horizontally distended, randomly distributed on flanks forming a vermiculated pattern, a slender posterior tip of the posterior ceratohyal and pelvic-fin bases closely-set (Barbosa & Costa, 2003; Bockmann & Sazima, 2004; Barbosa & Costa, 2010). Results from multilocus analyses and ultraconserved elements (Ochoa *et al.*, 2017, 2020; Katz *et al.*, 2018) have shown that species belonging to the *T. brasiliensis* species complex form a monophyletic group, but an analysis including all of its putative species has not yet been done.

The type locality of *T. brunoi* is in the Upper Rio Itabapoana, near the divide with the headwaters of the Rio Manhuaçu (tributary to Rio Doce; Fig. 13) and other specimens were collected in the latter. The species most similar to *T. brunoi* in the Rio Doce Basin is *Trichomycterus argos*, described from the Rio Casca,

a tributary of the Upper Rio Doce in the Serra do Brigadeiro State Park.

Barbosa & Costa (2010) distinguished *T. brunoi* from all species of the *T. brasiliensis* species complex, except *T. fuliginosus*, by the unique morphology of the metapterygoid, which has a distinct posterior process directed towards the anterior tip of the hyomandibula. However, the same posterior process of the metapterygoid is herein recorded also in *T. claudiae, T. mariamole, T. novalimensis, T. rubiginosus* and *T. brasiliensis*. In *T. claudiae*, there is an intermediate condition with a small posterior process on the metapterygoid, directed towards the anterior tip of the hyomandibula (Fig. 21; modified from Barbosa & Costa, 2010). The condition of this character varies considerably, with wide overlap among species in the *T. brasiliensis* species complex and does not seem to clearly diagnose *T. brunoi*.

Geographical distribution: Trichomycterus brunoi was described from the Itabapoana Basin in the Caparaó State Park and is also present in the Rio Doce at Rio Manhuaçu (Fig. 13).

Additional material: MBML 4304, 4, 29.6–55.1 mm SL; Brazil, Espírito Santo, Iúna; Rio Claro River, Manhuaçu River (20°22'22.00"S 41°49'40.90"W); col. L.M. Sarmento-Soares, M.R. Britto, V.C. Espindola, F.M.R.S. Pupo, R.F.M. Pinheiro and M.M.C. Roldi, 9 September 2011. MBML 4307, 1, 32.5 mm SL; Brazil, Espírito Santo, Iúna; Rio Claro River, Manhuaçu River (20°22'24.20"S 41°49'39.70"W); col. L.M. Sarmento-Soares, M.R. Britto, V.C. Espindola, F.M.R.S. Pupo, R.F.M. Pinheiro and M.M.C. Roldi, 9 September 2011. MBML 4308, 2, 30.2–41.7 mm SL, 1 c&s, 31.93 mm SL; Brazil, Espírito Santo, Iúna; Ribeirão do Brás Creek, Manhuaçu River (20°20'33.90"S 41°48'55.60"W); col. L.M. Sarmento-Soares, M.R. Britto, V.C. Espindola, F.M.R.S. Pupo, R.F.M. Pinheiro and M.M.C. Roldi, 10 September 2011. MNRJ 22401, 2, 33.6–75.0 mm SL; Brazil, Minas Gerais, Caparaó; Grumarim Creek, tributary of the Capim Roxo River (20°30'48"S 42°1'19" W); col. A.T. Aranda, F.A.G. Melo & F.P. Silva, 7 August 2001.

TRICHOMYCTERUS AFF. *CAIPORA* LIMA, LAZZAROTTO & COSTA, 2008
(FIG. 22)

Diagnosis: The combination of the following traits distinguishes this species from congeners: (1) short nasal, maxillary and rictal barbels, not reaching eyes (vs. barbels reaching or surpassing eyes); (2) marbled colour pattern formed by large round maculae blurred by dark chromatophores over entire body; (3) three lateral-line pores (vs. two); (4) interopercular odontodes
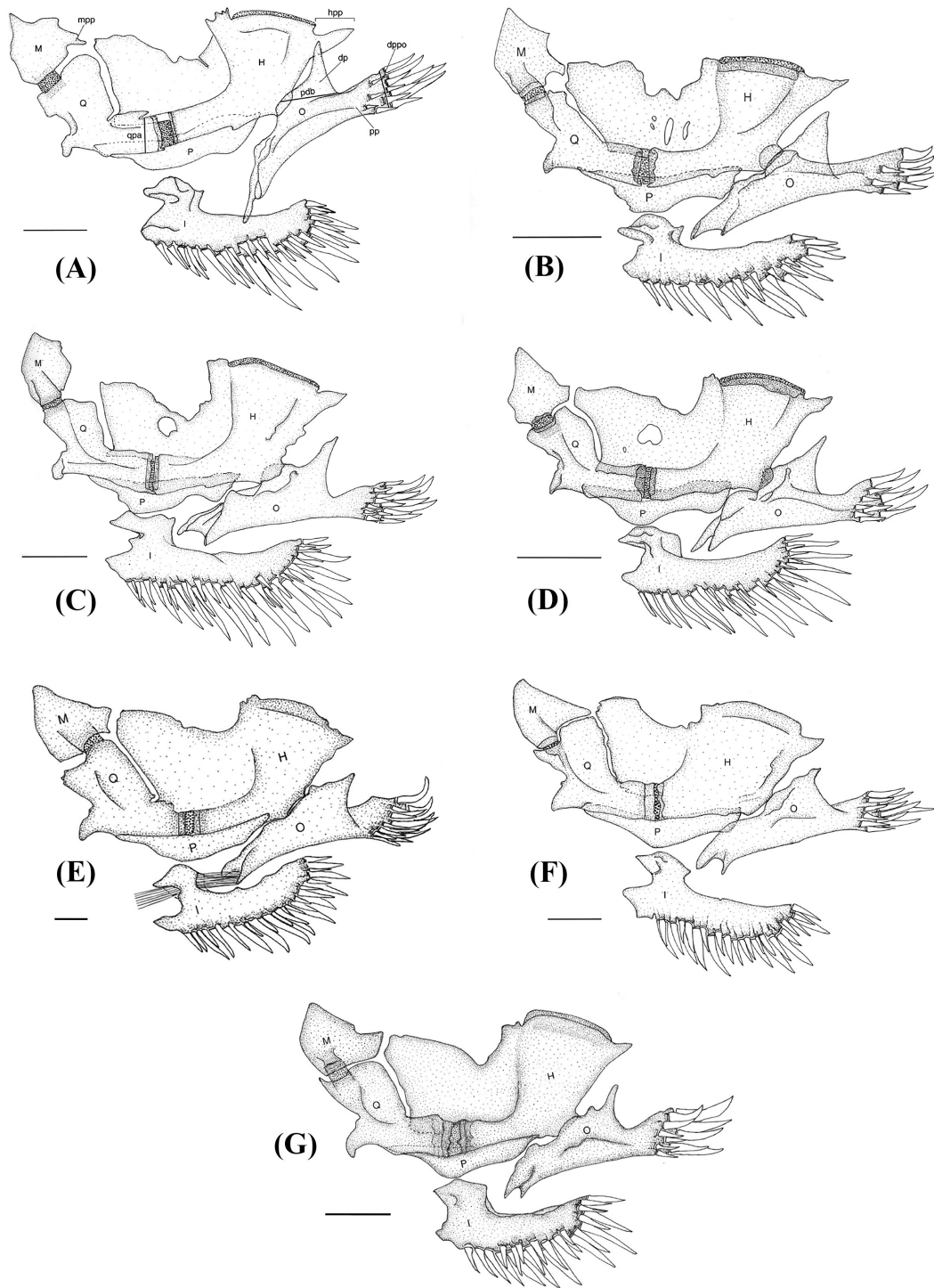
Figure 21. A, *Trichomycterus brunoi* (UFRJ5658); B, *T. fuliginosus* (MN18177); C, *T. claudiae* (UFRJ5685); D, *T. mariamole* (UFRJ5400); E, *T. novalimensis* (MZUSP37145); F, *T. rubiginosus* (MZUSP34168); G, *T. brasiliensis* (UFRJ4834). Left jaw suspensorium and opercular series, lateral view. Abbreviations: H, hyomandibula; I, interopercle; M, meta pterygoid; O, opercle; P, preopercle; Q, quadrate; dp, dorsal process of opercle; dppo, depth of posterior process of opercle; hpp, hyomandibula posterior projection; mpp, posterior projection of metapterygoid; pdb, base of dorsal process of opercle; pp, posterior process of opercle; qpa, posterior articulation of quadrate. Scale bar 1 mm. Modified illustrations of figures 1, 4, 5, 6, 7, 8 and 10 from Barbosa & Costa (2010) reproduced with permission from copyright holder.

© 2022 The Linnean Society of London, *Zoological Journal of the Linnean Society*, 2023, **197**, 344–441

Figure 22. *Trichomycterus* aff. *caipora*, MZUSP 73162, 78.3 mm SL, Brazil, state of Minas Gerais, Conceição do Mato Dentro Municipality, Rio do Peixe River, tributary of Santo Antônio River.

47–63 (vs. fewer); and (5) pectoral-fin rays I + 7 (vs. I + 5, I + 6 or I + 8). Among congeners in south-eastern South America, character 1 distinguishes *T.* aff. *caipora* from all congeners except for some morphs of *T. alternatus*, *T. astromycterus*, *T. barrocus* and *T. lauryi*; character 2 from all congeners except for *T. barrocus*; character 3 from all congeners except for *T. astromycterus*, *T. ipatinga*, *T. nigricans*, *T. tantalus* and *T. vinnulus*; character 4 from all congeners except for *T. barrocus*, *T. caipora*, *T. melanopygius*, *T. lauryi* and *T. tantalus*; and character 5 from species in the *T. brasiliensis* and *T. reinhardti* species complexes (Barbosa & Costa, 2010; Costa, 2021; Costa & Katz, 2021), plus *T. trefauti* (all preceding with I + 6 or fewer), and from *T. astromycterus*, *T. caipora*, *T. giganteus*, *T. immaculatus*, *T. lauryi*, *T. nigricans* and *T. tantalus* (the last seven species with I + 8 or more). Among congeners in the Rio Doce Basin, *T.* aff. *caipora* is most similar to *T. barrocus*. In addition to the characters above, *T.* aff. *caipora* is further distinguished from *T. barrocus*

by the smaller eye, 12.2–14.4% HL (vs. 14.8–17.5%) and by having six branchiostegal rays (vs. seven).

Description: Morphometric data for specimens examined is presented in Table 9. Body long and almost straight, trunk roughly round in cross-section near head, then slightly deeper than wide and gently compressed to caudal peduncle, tapering to caudal fin. Dorsal profile of body gently convex to dorsal-fin origin, then straight or slightly concave along caudal peduncle to caudal-fin origin. Ventral profile convex from gular region to vent, due partly to abdominal distension, then straight or slightly concave along anal-fin origin to caudal-fin base. Caudal peduncle slightly as deep as body at end of anal-fin base.

Head approximately one-fifth of SL, pentagonal, longer than wide and depressed. Mouth subterminal. Upper jaw slightly longer than lower. Upper lip wider than lower lip and laterally continuous with base of maxillary barbel. Lower lip small, approximately 2/3

Table 9. Morphometric data of *T.* aff. *caipora* based on non-type material (MZUSP 73162, 80309, 123340)

	Range (*N* = 4)	Mean	SD
Standard length (mm)	78.3–92.8	87.5	-
% of standard length			
Anal-fin base	6.6–9.7	9.0	0.6
Body depth	12.6–17.8	16.6	0.9
Caudal peduncle depth	8.9–15.4	12.7	1.8
Dorsal-fin base	8.2–11.5	11.1	0.5
First pectoral-fin length	10.3–13.2	12.7	0.5
Head length	13.6–20.9	19.1	1.5
Preanal length	56.1–72.1	71.7	0.3
Predorsal length	47.9–63.7	62.3	1.4
Prepelvic length	41.4–55.4	54.1	1.2
% of head length			
Eye diameter	12.2–14.4	13.3	0.9
Interorbital width	23.5–28.0	25.7	1.9
Snout length	46.2–52.7	49.6	2.8
Mouth width	31.7–38.1	34.8	2.7

width of upper one, partly divided into right and left portions by median concavity. Lower lip with uniform covering of tiny villi, resulting in velvet-like surface and not clustered into large papillae. Region between upper and lower lips with slender fleshy lobe. Dentary teeth conical. Total area of premaxillary teeth slightly smaller than that of dentary. Premaxillary teeth conical.

Eye medium sized, one-seventh of head length, protruding, positioned dorsally on head, without free orbital rim and covered with transparent skin. Eye located on anterior half of HL, closer to lateral border of head than to the midline in dorsal view. Anterior naris surrounded by tube of integument directed anterolaterally, continuous posterolaterally with nasal barbel. Posterior naris closer to anterior naris than to eyes, surrounded by tube of integument incomplete posteriorly. Maxillary barbel short, wide at base, narrowing markedly towards fine tip, reaching anteromesial margin of interopercle. Rictal barbel short, inserted immediately ventral to maxillary barbel, its tip goes until the most anteromesial portion of interopercle. Nasal barbel short and wide at base, originating on posterolateral region of anterior naris, its tip reaching slightly beyond eye. Interopercular patch of odontodes large compared to head length, oval in shape and with well-developed odontodes, prominent in ventral aspect of head. Interopercular patch of odontodes extending from vertical through ventroposterior border of eye to ventroanterior to opercle patch of odontodes. Odontodes arranged in three to four irregular series, with those on mesial series much longer than those on lateral one; odontodes gradually larger posteriorly in both

series, with those posteriorly on mesial row largest. Interopercular odontodes 47–63. Opercular patch of odontodes on dorsolateral surface of posterior part of head, positioned anterodorsally to pectoral-fin base, roundish in shape and larger than eye in dorsal aspect of head. Opercular odontodes 24–28, sunk in individual slits of integument, progressively larger posteriorly, all with fine tips, with largest ones curved distally and claw-like. Entire patch surrounded by fleshy fold rim of integument.

Pectoral fin with its base immediately posterior and ventral to opercular patch of odontodes. Pectoral-fin rays I + 7. First pectoral-fin ray (unbranched) longer, prolonged as filament beyond fin margin. Other rays progressively less longer, their tips following continuous line along fin margin. Pelvic fin with convex distal margin, its origin slightly posterior to middle of SL and anterior to vertical through dorsal-fin origin. Pelvic-fin bases close to each other, their tips touching but not covering anal and urogenital openings. Pelvic-fin rays I + 4. Dorsal fin long, its distal margin sinusoidal. Dorsal-fin origin closer to base of caudal fin than to tip of snout. Dorsal-fin rays iii + II + 7 (1). Anal fin slightly smaller than dorsal fin, its distal margin gently convex. Anal-fin origin posterior to vertical through end of dorsal-fin base. Anal-fin rays iii + II + 5 (1). Caudal fin round shape, with 6 + 7 principal rays. Adipose fin absent or modified into low integumentary fold extending between end of dorsal fin and caudal-fin origin. Post-Weberian vertebrae 37 (1). First dorsal-fin pterygiophore immediately anterior to neural spine of 18th (1) vertebra, first anal-fin pterygiophore immediately anterior to neural spine of 22nd (1) vertebra. Caudal-fin procurrent rays plus one segmented non-principal ray dorsally and

ventrally. Procurrent caudal-fin rays, 12 (1) dorsally and 11 (1) ventrally, beginning anteriorly at 33rd (1) vertebrae. Ribs 13 (1). Branchiostegal rays 6 (1). Dorsal-fin pterygiophores 8. Anal-fin pterygiophores 6.

Cephalic lateral line canals with simple, non-dendritic tubes ending in single pores. Supraorbital canal mostly in frontal bone. Supraorbital pores invariably present: s1 mesial to nasal-barbel base and autopalatine, s3 mesial to posterior nostril and anterior to frontal, and single or paired s6 posteromedial to eye and at midlength of frontal. Infraorbital laterosensory canal incomplete with four pores, i1 and i3 anteriorly and i10 and i11 posteriorly. Canal extending from sphenotic posteriorly to terminal pore located ventroposteriorly to eye. Infraorbital pore i1 located ventrolaterally to nasal-barbel base and autopalatine, i3 ventrolateral to posterior nostril and anterior to frontal, i10 and i11 posterior to eye. Otic canal without pores. Postotic pores po1, anteromedial to opercular patch of odontodes, and po2, mesial to opercular patch of odontodes. Lateral line of trunk anteriorly continuous with postotic canal and reduced to short tube. Lateral line pores ll1, ll2 and ll3 dorsomedial to pectoral-fin base.

Coloration in ethanol: Dark chromatophores distributed on inner and outer skin layers. Chromatophores on inner skin layer forming large roundish to ameboid blotches, larger than eye diameter, longitudinally aligned and partly coalescent, forming longitudinal stripes along body. Outer skin layer of pigmentation masking underlying pigmentation. Dorsum with two rows of dark blotches from head to caudal fin, extending bilaterally alongside dorsal midline on dorsum. Between lateral line of dorsum and the lateral midline, unpigmented area formed by lack of dark pigment on inner layer, creating lightly-coloured band from dorsal margin of opercle to base of upper caudal-fin rays. Lateral midline with broad dark stripe from dorsal margin of opercle to base of middle caudal-fin rays, mixing with adjacent maculae from middle caudal peduncle to base of caudal fin. Ventral to lateral midline, chromatophores organized in dusky blotches, sometimes forming round maculae. All fins heavily darkly-pigmented, except for margins, creating effect of distal white band. Ventral part of body lacking dark pigment. Head darkest on region corresponding to neurocranium, outlined by brain pigment seen by transparency. Light teardrop-shaped area extending from posterior margin of eye to base of opercular patch of odontodes, corresponding to levator operculi muscle. Base of nasal barbels surrounded with concentration of dark pigment, extending posteriorly as elongate dark field to anterior margin of eyes. Distal margin of integumentary fold of opercular patch of odontodes darkly pigmented. Interopercular patch of odontodes white.

Remarks: Trichomycterus aff. *caipora* is a large-sized *Trichomycterus* species when compared to its congeners from south-eastern Brazil. Although superficially similar to *T. caipora* from the Macabu River Basin, the form herein reported from the Rio Doce differs substantially in *COI* sequence distance. Our phylogenetic analysis indicates that the two forms are not even closely related, with the form from the Rio Doce internested in the Doce clade, as sister group to *T. tantalus* and in a subclade including also *T. ipatinga* and *T. melanopygius*. *Trichomycterus caipora* from Macabu River, in turn, is closely related to *T. nigricans* and at multiple levels to many other species in that basin. Some phenotypic differences also exist between the two forms which agree with the observed sequence differentiation, such as the number of pectoral-fin rays, number of sensory pores in the lateral line and number of post-Weberian vertebrae. The Rio Doce form is clearly a different, yet undescribed species. Because we have but a single sequence sample of *T*. aff. *caipora*, its phyletic status could not be determined at this time. We refer to it as *T*. aff. *caipora* simply because of superficial similarity to that species, but it remains unnamed. The taxon is currently under more detailed study by S. Santos and collaborators.

Geographical distribution: Trichomycterus aff. *caipora* occurs in the headwaters of the Rio Santo Antônio, Rio Suaçuí Grande and Rio Caratinga (Fig. 23). It has not yet been recorded from the main channel of the Rio Doce. The geographical distribution of *T. caipora* is the Rio Macabu Basin, Lagoa Feia System (historically connected with the Rio Paraíba do Sul).

Material examined: All from Brazil, state of Minas Gerais. MZUSP 73162, 78.3 mm SL; Conceição do Mato Dentro Municipality, Rio do Peixe River, tributary of Santo Antônio River (19°12'1.83"S 43°8'32.41"W); col. F. Di Dario & S. Kakinami, 14 January 2001; MZUSP 80309, 2, 82.6–92.4 mm SL; Suaçuí Grande River, Rio Doce Basin (18°29'48.86"S 42°19'53.66"W); col. C.B.M. Alves, 16 March 2001. MZUSP 123340, 1, 92.8 mm SL; Iapú Municipality, Caratinga River, Rio Doce Basin (19°28'36.41"S 42°7'44.44"W); col. T. Pessali, 8 October 2015.

TRICHOMYCTERUS ILLUVIES SP. NOV.
(FIG. 24)

Zoobank registration: urn:lsid:zoobank. org:act:734919BD-6C8A-4AA5-B2A4-B1EFE8F83059

Holotype: MZUSP 112750, 45 mm SL; Brazil, state of Minas Gerais, Ferros, Rio Santo Antônio (tributary of Rio Doce) at bridge in town of Ferros (19°13'34.50"S
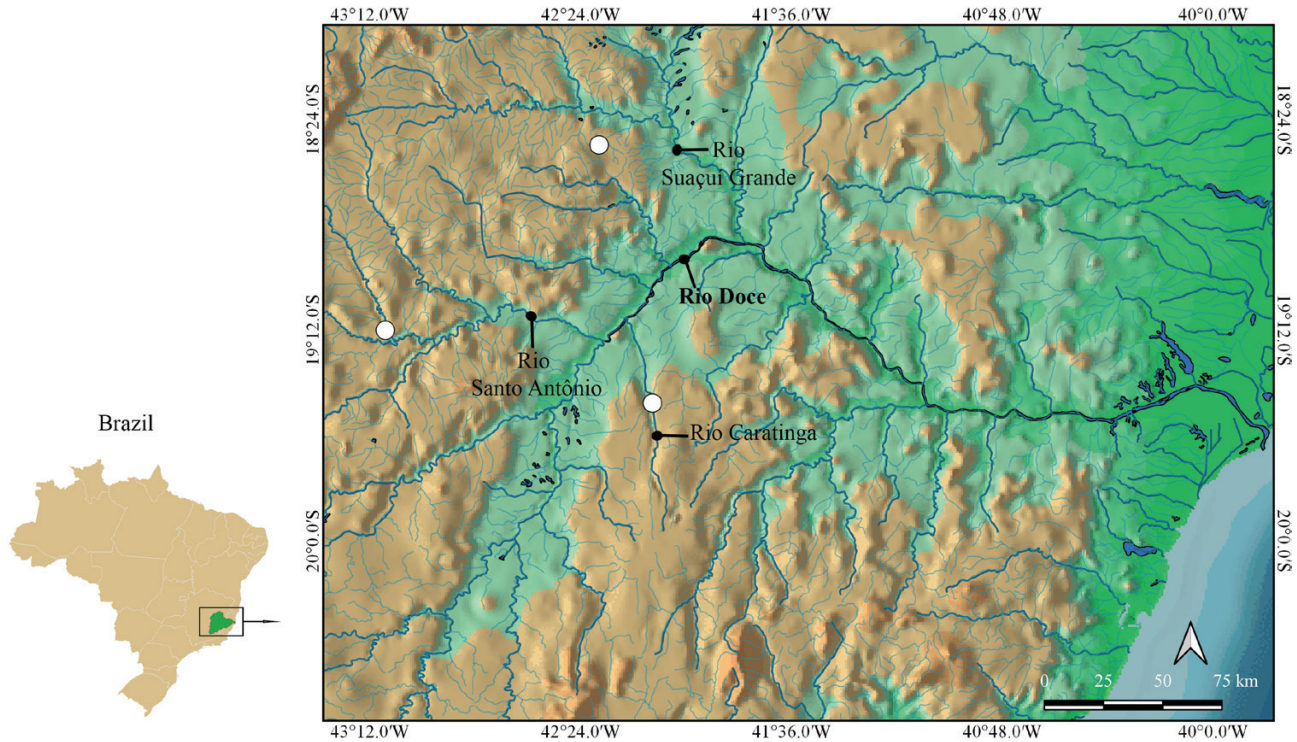
Figure 23. Geographical distribution of *Trichomycterus* aff. *caipora* in the Rio Doce Basin.

43°1'9.50''W); col. O.T. Oyakawa & T.F. Teixeira, 16 August 2012.

Paratypes: All from Brazil, state of Minas Gerais. MZUSP 126758, 10, 32.2–43.7 mm SL, 2c&s, 31.9, 40.8 mm SL; collected with holotype; MZUSP 110720, 1, 37.6 mm SL; Bom Jesus do Galho; Ribeirão Sacramento Creek, tributary of Rio Doce Basin (19°47'50.00''S 42°18'9.00''W); col. A. Netto-Ferreira & R. Pádua, 3 August 2010.

Diagnosis: The combination of the following traits distinguishes *T. illuvies* from congeners: (1) colour pattern consisting of a broad dark stripe running along mid-lateral line of body from immediately posterior to opercle to base of caudal fin; (2) pectoral-fin rays I + 7 (vs. I + 5, I + 6 or I + 8); (3) two lateral-line pores (vs. three); (4) first dorsal- and anal-fin pterygiophores positioned anteriorly to 18th and 23rd vertebrae, respectively; (5) six branchiostegal rays (vs. seven or more). Among congeners in south-eastern South America, character 1 distinguishes *T. illuvies* from all congeners except for *T. giganteus*, *T. itatiayae*, *T. nigroauratus* and the *T. reinhardti* species complex (Costa & Katz, 2021); character 2 from the *T. brasiliensis* and *T. reinhardti* species complexes (Barbosa & Costa, 2010; Costa, 2021; Costa & Katz, 2021), plus *T. trefauti* (all preceding with I + 6 or fewer pectoral-fin rays) and from *T. astromycterus*,

T. caipora, *T. giganteus*, *T. immaculatus*, *T. lauryi*, *T. nigricans*, *T. pradensis* and *T. tantalus* (with I + 8 or more); character 3 from *T. alternatus*, *T. astromycterus*, *T.* aff. *caipora*, *T. ipatinga*, *T. tantalus* and *T. vinnulus*; character 4 from all congeners except *T. maculosus* Barbosa & Costa, 2010, *T. melanopygius*, *T. nigricans*, *T. quintus* Costa, 2020; character 5 from all congeners except for *T. alternatus*, *T. astromycterus*, *T.* aff. *caipora* and *T. immaculatus*. Among congeners in the Rio Doce Basin, *T. illuvies* is most similar to *T. alternatus*. In addition to the characters above, *T. illuvies* can be further distinguished from *T. alternatus* by the absence of a large fenestra between the orbitosphenoid and the frontal (vs. presence), by the caudal-fin procurrent rays beginning anteriorly at 34th vertebrae (vs. 28th to 32nd vertebrae) and by the more numerous opercular odontodes (18–24 vs. 12–16).

Description: Morphometric data for specimens examined is presented in Table 10. Body long and almost straight, trunk roughly round in cross-section near head, then slightly deeper than wide and softly compressed to caudal peduncle, tapering to caudal fin. Dorsal profile of body gently convex to dorsal-fin origin, then straight or slightly concave along caudal peduncle to caudal-fin origin. Ventral profile convex from gular region to vent, due partly to abdominal distension, then straight or slightly concave along

Figure 24. *Trichomycterus illuvies* sp. nov. (top: lateral; middle: dorsal; and bottom: ventral views). MZUSP 112750, holotype, 45 mm SL; Brazil, Minas Gerais, Ferros Municipality, Rio Santo Antônio Drainage, at bridge in town of Ferros.

anal-fin origin to caudal-fin base. Caudal peduncle as deep as body at end of anal-fin base.

Head approximately one-fifth of SL, pentagonal, longer than wide and depressed. Mouth sub-terminal. Upper jaw slightly longer than lower. Upper lip wider than lower lip, and laterally continuous with base of maxillary barbel. Lower lip small, approximately 2/3 width of upper one, partly divided into right and left portions by median concavity. Lower lip with uniform covering of tiny villi, resulting in velvet-like surface and not clustered into large papillae. Region between upper and lower lips with slender fleshy lobe.

Dentary and premaxillary teeth similar to each other in shape. Dentary teeth conical, arranged in four irregular rows extending from symphysis to slightly up into coronoid process, with size of individual teeth increasing markedly towards symphysis and from posterior to anterior rows. Total area of premaxillary teeth slightly smaller than that of dentary teeth, with

conical teeth arranged irregularly in four rows over entire ventral surface of premaxilla.

Eye medium sized, protruding, positioned dorsally on head, without free orbital rim and covered with transparent skin. Eye located on anterior half of HL, closer to lateral border of head than to the midline in dorsal view. Anterior naris surrounded by tube of integument directed anterolaterally, continuous posterolaterally with nasal barbel. Posterior naris closer to anterior naris than to eyes, surrounded by tube of integument incomplete posteriorly. Maxillary barbel narrowing markedly towards fine tip, reaching lateroposterior border of interopercle. Rictal barbel inserted immediately ventral to maxillary barbel, its tip reaching anterolateral margin of interopercle. Nasal barbel originating on posterolateral region of anterior naris, its tip surpassing eye, but not reaching anterior margin of opercle. Interopercular patch of odontodes small compared to head length, oval in shape and with well-developed odontodes, prominent in ventral aspect

Table 10. Morphometric data of *T. illuvies* based on holotype and part of paratype material (MZUSP 112750, 126758, 110720)

	Holotype	Range (*N* = 11)	Mean	SD
Standard length (mm)	45.0	32.2–45.0	39.6	-
% of standard length				
Anal-fin base	9.0	4.4–9.0	7.8	1.7
Body depth	16.4	13.9–17.2	15.7	1.2
Caudal peduncle depth	13.9	11.1–13.9	12.6	1.1
Dorsal-fin base	12.3	9.8–12.3	10.5	0.9
First pectoral-fin length	13.5	13.0–15.8	14.6	1.1
Head length	22.6	18.9–22.6	20.7	1.2
Preanal length	71.2	70.7–73.0	71.5	0.9
Predorsal length	62.9	61.6–65.9	63.7	1.5
Prepelvic length	53.5	51.9–55.2	54.1	1.1
% of head length				
Eye diameter	16.0	13.1–20.0	17.5	2.3
Interorbital width	24.7	24.7–30.1	26.4	1.9
Snout length	38.8	38.8–52.6	45.7	4.0
Mouth width	30.2	27.9–34.1	30.5	2.2

of head. Interopercular patch of odontodes extending from vertical through ventroposterior border of eye to ventroanterior to opercle patch of odontodes. Odontodes arranged in two or three irregular series, with those on mesial series much longer than those on lateral one; odontodes gradually larger posteriorly in both series, with those posteriorly on mesial row largest. Interopercular odontodes 30–44. Opercular patch of odontodes on dorsolateral surface of posterior part of head, positioned anterodorsally to pectoral-fin base, roundish to oval in shape in dorsal aspect of head and with same size as eye diameter. Opercular odontodes 18–24, sunk in individual slits of integument, progressively larger posteriorly, all with fine tips, with largest ones curved distally and claw-like. Entire patch surrounded by fleshy fold rim of integument.

Pectoral fin with its base immediately posterior and ventral to opercular patch of odontodes. Pectoral-fin rays I + 7 or rarely I + 8. First pectoral-fin ray (unbranched) longest, prolonged as short filament beyond fin margin. Other rays progressively less long, their tips following continuous line along fin margin. Pelvic fin with convex distal margin, its origin slightly posterior to middle of SL and anterior to vertical through dorsal-fin origin, its tip variably reaching anywhere between anterior and posterior margins of urogenital opening. Bases of pelvic fins close to each other. Pelvic-fin rays I + 4. Dorsal fin long, its distal margin sinusoidal. Dorsal-fin origin closer to base of caudal fin than to tip of snout. Dorsal-fin rays iii + II + 7 (3). Anal fin slightly smaller than dorsal fin, its distal margin gently convex. Anal-fin origin

posterior to vertical through end of dorsal-fin base. Anal-fin rays iii + II + 5 (3). Caudal fin round, with 6 + 7 principal rays. Adipose fin absent or modified into low integumentary fold extending between end of dorsal fin and caudal-fin origin. Post-Weberian vertebrae, 37 (2) or 38 (1). First dorsal-fin pterygiophore immediately anterior to neural spine of 18th (3) vertebra, first anal-fin pterygiophore immediately anterior to neural spine of 23rd (3) vertebra. Caudal-fin procurrent rays plus one segmented non-principal ray dorsally and ventrally. Procurrent caudal-fin rays, 12–14 (3) dorsally and 11–13 (3) ventrally, beginning anteriorly at 34th (2) vertebra. Ribs 13 (3). Branchiostegal rays 6 (3). Dorsal-fin pterygiophores 8. Anal-fin pterygiophores 6.

Cephalic lateral line canals with simple, non-dendritic tubes ending in single pores. Supraorbital canal mostly in frontal bone. Supraorbital pores invariably present: s1 mesial to nasal-barbel base and autopalatine, s3 mesial to posterior nostril and anterior to frontal, single or paired s6, closer to mesial line than to eyes, posteromedial to eye and at midlength of frontal. Infraorbital latero-sensory canal incomplete with four pores, i1 and i3 anteriorly and i10 and i11 posteriorly. This canal extending from sphenotic posteriorly to terminal pore located ventroposteriorly to eye. Infraorbital pore i1 located ventrolateral to nasal-barbel base and autopalatine, i3 ventrolateral to posterior nostril and anterior to frontal, i10 and i11 posterior to eye. Otic canal without pores. Postotic pores po1, anteromedial to opercular patch of odontodes, and po2, mesial to opercular patch of odontodes. Lateral line of trunk anteriorly continuous with postotic canal and reduced to short tube. Lateral line pores ll1 and ll2 dorsomedial to pectoral-fin base.

Coloration in ethanol: Dark chromatophores distributed into inner and outer skin layers. Those on inner skin layer forming broad dark stripes or faded maculae responsible for main colour features of body. Basic arrangement composed of two stripes and one row of maculae. First stripe along mid-dorsal line from occiput to base of caudal fin. Row of maculae ventrolateral to that first stripe, extending from base of head through upper part of flanks, dorsal portion of caudal peduncle and upper part of caudal-fin base. In some specimens, row fusing with the first stripe. Second stripe running along mid-lateral line, from immediately posterior to opercle to middle of caudal-fin base. In some specimens, second short row ventral to main one, extending from mid-length of abdomen through ventral margin of caudal peduncle to base of caudal-fin. Dorsal stripes and rows disrupted by fusions (mostly along anterior part of body). Second stripe never fusing with first one. Head darkest on region corresponding to neurocranium, outlined by brain pigment seen by transparency. Unpigmented circular area extending from posterior margin of eye to base of opercular patch of odontodes. Base of nasal barbels surrounded with concentration of dark pigment, extending posteriorly as elongate dark field to anterior margin of eyes. Margin of integumentary fold of opercular patch of odontodes darkly pigmented. Interopercular patch of odontodes white. Ventral side of the body lacking dark pigment. Fins with small brownish spots randomly distributed on fin rays. Caudal fin with vertical dark stripe crossing bases of principal rays.

Remarks: Although *T. illuvies* seems to be part of the *T. alternatus* metaspecies due to its general morphology and colour pattern of some specimens, it differs from the latter in many traits as listed in the diagnosis. One of those is the the absence of a large fenestra between the orbitosphenoid and frontal bones, a conspicuous feature of the skull in *T. alternatus* (cf. Reis *et al.*, 2019: fig. 5C) and its close relatives such as *T. immaculatus* and *T. melanopygius* and its exospecies (see Remarks on *T. alternatus*), such as *T. astromycterus* and *T. vinnulus* relative to *T. alternatus*. Currently there is no DNA sample of *T. illuvies*.

Etymology: The name is derived from Latin *illuvies*, meaning filth, dirt or flood, alluding to the environmental mayhem caused by the mining company Samarco SA on the Rio Doce. This is a long-term reminder of the catastrophe suffered by that hydrographic basin.

Geographical distribution: Trichomycterus illuvies is found in two drainages belonging to Rio Doce Basin, the Santo Antônio River (holotype locality) and Ribeirão Sacramento (paratype locality) (Fig. 25). The two localities are separated by 97.9 km in straight line and the species is expected to occur in some of the intervening areas.

TRICHOMYCTERUS IMMACULATUS (EIGENMANN & EIGENMANN, 1889)
### (FIGS 8–9, 26)

Pygidium immaculatum Eigenmann & Eigenmann, 1889: 52 (syntypes from Juiz de Fora, Parahybuna River; São Matheos River; Juiz de Fora, Paraíba do Sul River; Goiás, Brazil; syntypes: MCZ 8266, 8300, 8302, 8305, 8307; lectotype herein designated as MCZ 8302, from Rio São Matheus); Gosline, 1945: 60 (date of authorship mistakenly cited as Eigenmann, 1918).

Trichomycterus immaculatum; Burgess, 1989: 322 (list).

Trichomycterus immaculatus; Caramaschi & Caramaschi, 1991: 1 (diagnosis); Bizerril, 1994: 623 (list); Costa & Bockmann, 1994: 717 (comparative material); Braga, 2004: 35 (anatomy); Triques & Vono, 2004: 82 (list, relationships); Bockmann & Sazima, 2004: 71 (comparisons); Bockmann *et al.*, 2004: 227 (comparisons); Lima & Costa, 2004: 3 (comparisons); Fernandez & Vari, 2004: 881 (comparative material); Diogo *et al.*, 2004: 264 (comparative material); Sarmento-Soares *et al.*, 2005: 209 (comparisons); Wosiacki & Oyakawa, 2005: 471 (comparisons); Wosiacki, 2005: 52 (comparisons); Diogo, 2006: 17 (comparative material); Ingenito & Buckup, 2007: 1177 (biogeography); Ferraris 2007: 419 (check list); Lima *et al.*, 2008: 316 (comparisons); Barbosa & Costa, 2010: 121 (comparisons); Pereira *et al.*, 2010: 5 (barcoding); Roldi *et al.*, 2011: 2 (comparisons); Sarmento-Soares *et al.*, 2011: 262 (comparisons); Ferrer & Malabarba, 2011: 66 (comparative material); DoNascimiento *et al.*, 2014a: 709 (comparisons); García-Melo *et al.*, 2016: 237 (comparisons); Ochoa *et al.*, 2017: 75 (relationships); Sales *et al.*, 2018: 3 (citation); Katz *et al.*, 2018: 559 (comparative material); Reis *et al.*, 2019: 12 (citation); Reis & de Pinna, 2019: 118 (comparisons); Donin *et al.*, 2020: 1 (comparisons); Costa *et al.*, 2020a: 1 (relationships); Costa *et al.*, 2020b: 1 (relationships); Reis *et al.*, 2020: 1 (relationships); DoNascimiento & Prada-Pedreros, 2020: 981 (comparative material); Ochoa *et al.*, 2020: 3 (relationships); Fernandez *et al.*, 2021 (relationships).

Trichomycterus pradensis Sarmento-Soares *et al.*, 2005 (Jucuruçu, Rio Jucuruçu, 2 km before the city of Jucuruçu on road Itamaraju-Jucuruçu, middle of Rio Jucuruçu Basin, 16°50'10"S, 40°08'40"W, Bahia, Brazil); Ferraris, 2007: 422 (comparisons); Barbosa & Costa, 2011: 308 (comparisons); Schaefer & Férnandez, 2009: 518 (comparisons); DoNascimiento *et al.*, 2014a: 709 (comparisons); García-Melo *et al.*, 2016: 237 (comparisons); Ochoa *et al.*, 2017: 75
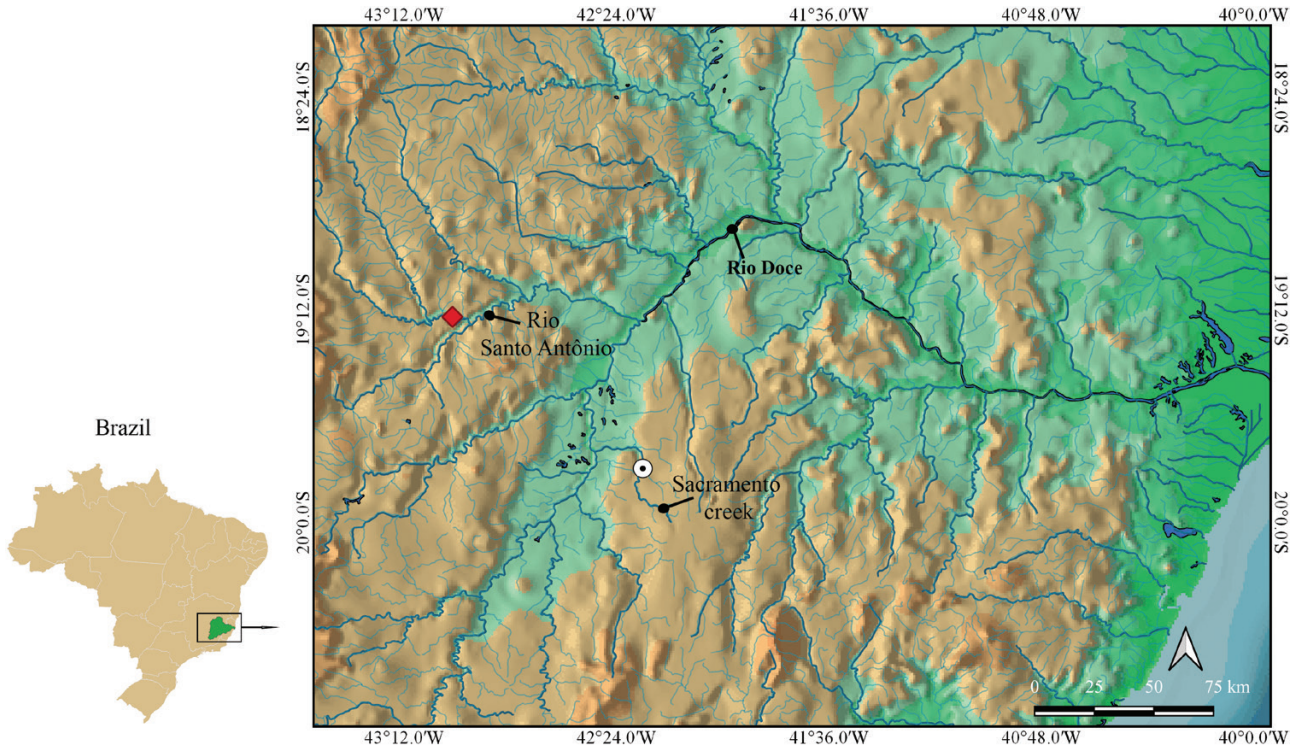
Figure 25. Geographical distribution of *T. illuvies* sp. nov. in the Rio Doce Basin. Red diamond = holotype MZUSP 112750 and paratype (MZUSP 126758); white dotted circle = paratype (MZUSP 110720).

Figure 26. *Trichomycterus immaculatus* (top: lateral; bottom: dorsal views). MCZ 8302, lectotype, 121.4 mm SL; Brazil, Espírito Santo, São Mateus Municipality, Rio São Mateus Drainage.

(comparisons); Volpi, 2017 (molecular data; comparisons); Sales *et al.*, 2018: 6 (citation); Katz *et al.*, 2018: 559 (comparative material); Donin *et al.*, 2020: 9 (comparisons); Ochoa *et al.*, 2020: 3 (relationships); Costa *et al.*, 2020b: 2912 (relationships); Costa *et al.*, 2020a: 6 (comparisons); DoNascimiento & Prada-Pedreros, 2020: 978 (comparisons); Reis *et al.*, 2020: 1 (relationships).

Trichomycterus inmaculatus; Fernández *et al.*, 2015: 11 (misspelling).

Diagnosis: The combination of the following traits distinguishes *T. immaculatus* from congeners: (1) most common colour pattern uniform greyish to nearly black over entire body, with less frequent colour variants with round dark maculae randomly distributed on dorsum; caudal fin dusky in adults or with slender dark horizontal stripe from base to tip of fin in some juveniles; (2) pectoral-fin rays I + 8 (vs. I + 5, I + 6 or I + 7); and (3) two lateral-line pores (vs. three or more). Among congeners in south-eastern South America, character 1 distinguishes *T. immaculatus* from all congeners (although the plain colour pattern is present also in *T. jacupiranga*, *T. melanopygius*, *T. nigricans*, *T. tantalus* and *T. trefauti*, the variable colour pattern including round dark maculae randomly distributed on dorsum distinguishes *T. immaculatus* from all latter); character 2 distinguishes *T. immaculatus* from all congeners except for *T. astromycterus*, *T. caipora*, *T. giganteus*, *T. immaculatus*, *T. lauryi*, *T. nigricans* and *T. tantalus*; character 3 distinguishes *T. immaculatus* from *T. astromycterus*, *T.* aff. *caipora*, *T. nigricans*, *T. ipatinga*, *T. tantalus* and *T. vinnulus*. Among congeners in the Rio Doce Basin, *T. immaculatus* is most similar to *T. melanopygius* and *T. tantalus*. It can be distinguished from those two species, in addition to characters aforementioned, from *T. melanopygius* by the fewer post-Weberian vertebrae (36–37 vs. 38–40) and by a dusky caudal fin in adults (vs. a well delimited horizontal dark stripe in the middle of caudal fin); and from *T. tantalus* by fewer opercular odontodes (15–25 vs. 25 to 33) and a truncated caudal fin (vs. forked).

Description: Morphometric data for specimens examined is presented in Table 11. Body long and nearly straight, trunk roughly round in cross-section near head, then slightly deeper than wide and gently compressed to caudal peduncle, tapering to caudal fin. Dorsal profile of body gently convex to dorsal-fin origin, then straight or slightly concave along caudal peduncle to caudal-fin origin. Ventral profile convex from gular region to vent, due partly to abdominal distension, then straight or slightly concave along anal-fin origin to caudal-fin base. Caudal peduncle varying from nearly as deep as body at the beginning of dorsal-fin base to as deep as body at the end of anal-fin base.

Head length approximately one-fifth of SL, roughly pentagonal, longer than wide and depressed. Mouth subterminal. Upper jaw slightly longer than lower. Upper lip wider than lower one and laterally continuous with base of maxillary barbel. Lower lip small, approximately 2/3 width of upper one, partly divided into right and left portions by median concavity. Lower lip with uniform covering of tiny villi, not clustered into large papillae, resulting in velvet-like surface. Region between upper and lower lips with slender fleshy lobe.

Dentary and premaxillary teeth similar to each other in shape and size. Dentary teeth conical, arranged in four irregular rows, first row with 9–12 teeth extending from symphysis to slightly up of coronoid process, with size of individual teeth increasing markedly towards symphysis and from posterior to anterior rows. Total area of premaxillary teeth smaller than that of the dentary, with conical teeth arranged irregularly in four rows, first row with 10–16 teeth over entire ventral surface of premaxilla.

Eye medium sized, slightly protruding, positioned dorsally on head, without free orbital rim and covered with transparent skin. Eye located on anterior half of HL, closer to lateral border of head than to the midline in dorsal view. Anterior naris surrounded by tube of integument directed anterolaterally, continuous posterolaterally with nasal barbel. Posterior naris closer to anterior naris than to eye, surrounded by tube of integument incomplete posteriorly. Length of all barbels variable. Maxillary barbel narrowing markedly towards fine tip, variably reaching from middle of interopercle to the base of pectoral fin. Rictal barbel inserted immediately ventral to maxillary barbel, its tip reaching from anterolateral to posterolateral border of interopercle. Nasal barbel originating on posterolateral region of anterior naris, reaching anywhere from middle of eye to anterior border of opercle. Interopercular patch of odontodes large compared to head length, oval in shape and with well-developed odontodes, prominent in ventral aspect of head. Interopercular patch of odontodes extending from vertical through posterior border of eye to anterior margin of opercle patch of odontodes. Interopercular odontodes arranged in two or three irregular series, with those on mesial series much longer than those on lateral one; odontodes gradually larger posteriorly in both series, with those posteriorly on mesial row largest. Interopercular odontodes 37–59. Opercular patch of odontodes on dorsolateral surface of posterior part of head, positioned anterodorsally to pectoral-fin base, roundish in shape and larger than eye in dorsal aspect of head. Opercular odontodes 15–25, sunk in individual slits of integument, progressively larger posteriorly, all with fine tips, with largest ones curved distally and claw-like. Entire patch surrounded by well-differentiated fleshy fold rim of integument.

Pectoral fin with its base immediately posterior and ventral to opercular patch of odontodes. Pectoral-fin rays invariably I + 8. First pectoral-fin ray, unbranched, longer and prolonged as filament beyond fin margin.

Table 11. Morphometric data of *T. immaculatus* based on type and non-type material. A, lectotype MCZ 8302 from Rio São Mateus; B, paralectotypes (*T. paquequerensis*) from Rio Paraíba do Sul Basin MCZ 8266, 8300, 8305, 8307; C, paralectotype (*Trichomycterus* sp.) from Tocantins-Araguaia Drainage MCZ 8296; D, non-type material from Rio Doce Basin MZUSP 123348, 123353, 126408, 123357, 123335; E, type material of *T. pradensis* (synonym of *T. immaculatus*) MNRJ 28490, 28485, 28488, 28484

	A				C	D			E		
	Lectotype	Range (N = 7)	Mean	SD	Paralecto-type	Range (N = 19)	Mean	SD	Range (N = 12)	Mean	SD
Standard length (mm)	121.4	116.2–165.0	123.2	-	51.6	42.8–104.2	69.0	-	39.9–109.7	71.2	-
% of standard length											
Anal-fin base	7.2	5.8–9.7	7.5	1.1	6.2	6.9–9.8	8.2	0.7	7.8–9.3	8.6	0.4
Body depth	14.1	15.8–17.9	16.9	0.8	12.0	11.6–17.0	14.3	1.4	13.5–16.4	15.3	0.9
Caudal peduncle depth	11.3	13.2–14.9	14.0	0.5	9.2	10.6–14.1	12.0	0.9	10.8–13.4	12.4	0.8
Dorsal-fin base	9.2	9.4–11.0	10.0	0.6	8.7	9.9–12.4	11.2	0.8	8.3–12.6	11.0	1.2
First pectoral-fin length	13.8	10.4–16.1	13.4	1.6	11.5	11.0–15.1	13.4	1.1	12.1–15.9	14.3	1.1
Head length	15.7	17.5–19.3	18.5	0.6	17.6	17.0–21.1	19.6	1.0	18.4–20.8	19.6	0.7
Preanal length	77.6	74.5–82.1	77.8	2.2	74.0	55.9–76.0	73.2	1.4	55.9–75.8	71.2	5.1
Predorsal length	65.7	61.5–67.7	64.8	2.1	60.0	60.2–64.6	62.4	1.1	59.2–65.9	62.4	1.8
Prepelvic length	55.9	60.6–63.3	61.5	1.0	53.9	52.0–58.0	55.1	1.7	50.8–57.9	54.2	1.9
% of head length											
Eye diameter	15.8	12.3–15.8	13.9	0.9	17.9	14.0–19.7	17.1	1.7	13.8–21.4	18.0	2.3
Interorbital width	31.1	26.8–34.8	30.7	2.8	24.1	19.5–26.7	23.5	2.0	21.1–27.4	24.0	1.8
Snout length	49.4	43.4–48.8	46.5	1.9	43.0	39.8–50.4	46.5	2.8	44.4–50.9	47.8	1.8
Mouth width	48.9	34.8–43.8	40.2	2.9	43.0	27.2–37.0	32.3	2.4	26.1–40.7	33.2	4.3

Other rays progressively less longer, their tips following continuous line along fin margin. Pelvic fin with convex distal profile, its origin slightly posterior to middle of SL and anterior to vertical through dorsal-fin origin, its length varying from not reaching to reaching (but never entirely covering) anal and urogenital openings in adults. Base of pelvic fins positioned close to each other. Pelvic-fin rays I + 4, first ray unbranched. Dorsal fin long, its distal margin sinusoidal. Dorsal-fin origin closer to base of caudal fin than to tip of snout. Dorsal-fin rays iii + II + 7 (12), iii + III + 6 (1) or iv + II + 7 (2). Anal fin slightly smaller than dorsal fin, its distal margin gently convex. Anal-fin origin posterior to vertical through end of dorsal-fin base. Anal-fin rays ii + II + 5 (2) or iii + II + 5 (13). Caudal fin from subtruncate to gently concave or emarginate, with 6 + 7 (14) or 5 + 7 (1) principal rays. Adipose fin absent or modified into low integumentary fold extending between end of dorsal fin and caudal-fin origin. Post-Weberian vertebrae 34 (2), 35 (5) or 36 (8). First dorsal-fin pterygiophore immediately anterior to neural spine of 16th (9) or 17th (6) vertebra, first anal-fin pterygiophore immediately anterior to neural spine of 20th (1), 21st (9) or 22nd (4) vertebra. Procurrent caudal-fin rays, 13–17 dorsally and 12–14 ventrally, beginning anteriorly at 31st or 32nd vertebrae plus one posterior segmented non-principal ray in each lobe. Ribs 10 (5), 11 (9) or 12 (1). Branchiostegal rays 6 (1) or 7 (14). Dorsal-fin pterygiophores 8. Anal-fin pterygiophores 6.

Cephalic lateral line canals with simple, non-dendritic tubes ending in single pores. Supraorbital canal mostly in frontal bone. Supraorbital pores invariably present: s1 mesial to nasal-barbel base and autopalatine, s3 mesial to posterior nostril and anterior to frontal, s6 single or, more commonly, paired, posteromedial to eye and at midlength of frontal. Infraorbital latero-sensory canal incomplete with four pores, i1 and i3 anteriorly and i10 and i11 posteriorly. Canal extending from sphenotic posteriorly to terminal pore located ventroposteriorly to eye. Infraorbital pore i1 located ventrolateral to nasal-barbel base and autopalatine, i3 ventrolateral to posterior nostril and anterior to frontal, i10 and i11 posterior to eye. Otic canal without pores. Postotic pores po1, anteromedial to opercular patch of odontodes, and po2, mesial to opercular patch of odontodes. Lateral line of trunk anteriorly continuous with postotic canal and reduced to short tube, with one lateral line bone partially ossified in some specimens. Lateral line pores ll1 and ll2 dorsomedial to pectoral-fin base.

Coloration in ethanol: Trichomycterus immaculatus is variable in pigmentation pattern, with two extreme colour morphs bridged by intermediate conditions (Figs 8–9). At one extreme, entire body covered with uniform scattering of dark chromatophores in inner and outer integument layers, not forming maculae or spots.

Specimens with this colour pattern usually with dusky caudal fin with transparent margin. At other extreme, chromatophores usually uniformly distributed on inner skin layer. On outer layer, chromatophores darker and coalescing to form round maculae, as large as or larger than, eye diameter. Maculae covering dorsum to the mid-lateral line, completely absent ventral to that limit. Maculae randomly distributed in adults, but in young specimens, maculae more evident and arranged in rows along midline of body, from dorsoposteriorly to opercle to base of caudal-fin resulting in pattern similar to that of *T. alternatus*. Fins mostly transparent, except for caudal dusky in adults and, in some juveniles, dark stripe from base of caudal-fin to its tip. Specimens intermediate between two extreme colour morphs with faint maculae, only slightly darker than background colour and restricted to dorsum, never extending ventrally beyond lateral midline. Colour pattern of head, caudal fin and ventral part of body not correlated with spotted or plain morphs. Head lacking maculae or blotches, with area corresponding to neurocranium darker than rest of head. Integument surrounding opercular odontodes darkly pigmented. Interopercular patch of odontodes white. Cheeks less darkly pigmented than rest of head. Caudal fin ranging from uniformly dusky with hyaline margins to darkly pigmented along middle caudal-fin rays, forming dark longitudinal stripe in young specimens. Stripe gradually less evident in larger specimens, due to fading or masking by additional caudal-fin pigmentation. Ventral part of body without dark pigmentation.

Remarks: Trichomycterus immaculatus stands out, along with *T. alternatus*, as one of the most complex taxonomic cases in this paper and requires a comparatively detailed discussion. A number of factors contribute to such situation, such as a non-monospecific series of syntypes, a substantial degree of intraspecific variation, the existence of synonyms, and pseudocryptic species (in sympatry). Below we address each of those points in sequence.

Trichomycterus immaculatus was described on the basis of 14 syntypes from three different basins, mostly collected in association with the Thayer Expedition to Brazil (1865–1866): Rio Paraíba do Sul (MCZ 8300, 10 ex.; MCZ 8305, 1 ex.; MCZ 8307, 1 ex.), Rio São Mateus (an isolated coastal basin north of the Rio Doce; MCZ 8302, 1 ex.) and an unspecified locality in the state of Goiás, probably in the Rio Tocantins-Araguaia system (MCZ 8298, 1 ex.). Localities and dates of Thayer Expedition collections follow Higuchi (1996). The latter lot contains a single small specimen which differs in key characteristics from all remaining syntypes. It has I + 7 pectoral-fin rays (vs. I + 8 in remaining syntypes), body depth 12% SL (vs. 14–17.9%); caudal

peduncle depth 9.2% SL (vs. 11.3–14.9%) and paired S6 cephalic laterosensory pore (vs. single). Its specific identity cannot be determined at this point because of broader uncertainties in *Trichomycterus* taxonomy, the resolution of which extrapolate the scope of the present study. It is certain however that this specimen from Goiás is not conspecific with remaining syntypes and, given morphological differences, is not closely related to them. Syntypes from Rio Paraíba do Sul differ from the one from Rio São Mateus in number of interopercular odontodes (59 vs. 66–75) and in some body proportions such as the head length (15.7% SL vs. 17.5–19.3%), body depth (14.1% SL vs. 15.8–17.9%) and position of pelvic fin (55.9% SL vs. 60.6–63.3%). Recent molecular analyses have repeatedly indicated that forms referrable to *T. immaculatus* from the Rio Doce and Rio Paraíba do Sul are not conspecific and not closely related (Ochoa *et al.*, 2020; Costa *et al.*, 2020b). The problem has been impervious to proper resolution so far because of incomplete representation from the Rio Doce and Rio São Mateus. Herein we have included samples of *T. immaculatus* and possibly related forms from all relevant sites, including Eigenmann's locality in the Rio São Mateus (S127 and S146 on Fig. 1), and Rio Doce (S142 on Fig. 1) and from localities in the Paraíba do Sul (S194 to S196 on Fig. 1). The resulting picture makes it clear that the form in the Rio Doce is a single species throughout the basin, also occurring, with little differentiation, in adjacent basins to the north (Rio Jucuruçu, Rio Peruípe, Rio Itanhaém, Rio Itaúnas and Rio São Mateus). On the other hand, large genetic and phylogenetic distances between *T. immaculatus*-like taxa from the Doce and the one from the Paraíba do Sul, as found in previous studies (Katz *et al.*, 2018; Costa *et al.*, 2020b), are unabiguously corroborated, strongly supporting their separate specific status.

The biological situation of the entities involved is therefore clear in terms of general patterns in major basins. However, the nomenclatural problem is aggravated because the type series includes syntypes from both the São Mateus (a costal basin near the lower Rio Doce Basin) and Rio Paraíba do Sul, in addition to the distantly-related one from Goiás. This renders the applicability of available names unstable, even more so because there are potential synonyms in both basins. In order to avoid taxonomic uncertainties and to stabilize the associated nomenclature, it is necessary to designate a lectotype. We discard the Goiás specimen from consideration because it belongs to a taxon markedly distinct from all other syntypes, not matching the concept of *T. immaculatus* in virtually the entire literature (including the original description of the species). Its small size and outlying provenance relative to other syntypes also make it inadequate as a name-bearer. Among remaining syntypes, the

specimen from the Rio São Mateus is well preserved and allows observation of all characters mentioned in the original description. Additionally, a non-type specimen from the Rio Doce was also subsequently chosen to illustrate the species in Eigenmann (1918: pl. 52), further demonstrating that the authors considered the taxon in the Rio Doce as conforming to their conception of *T. immaculatus*. Therefore, we herein designate specimen MCZ 8302 (Fig. 26) as the lectotype of *T. immaculatus*. The specimen was collected in the Rio São Mateus, an isolated coastal basin near the Rio Doce in the state of Espírito Santo. Our decision has nomenclatural ramifications because it implies that *T. pradensis* is a synonym of *T. immaculatus* and that the taxon from Rio Paraíba do Sul must bear the next available name [in this case *Trichomycterus paquequerensis* (Miranda Ribeiro, 1943); see below]. Our decision is based on the state of knowledge of the taxon in the Rio Doce and adjacent basins, represented in this study by hundreds of specimens and 33 molecular samples from throughout its geographic distribution. This database constitutes a solid basis on which to associate the name *T. immaculatus* with a well-delimited entity, both taxonomically and geographically. The taxon in the Rio Paraíba do Sul is not as well known and is represented by comparatively limited samples from few localities in this and other studies. An alternative decision to designate the name *T. immaculatus* to the Paraíba do Sul taxon runs the risk of once again perpetuating nomenclatural instability. As further corollary of lectotype designation, the type locality of *T. immaculatus* is now restricted to the Rio São Mateus, state of Espírito Santo, Brazil. With that act, the name *T. immaculatus* now applies to the taxon occurring in the Rio Doce and adjacent basins, but not to the form in the Rio Paraíba do Sul. Also, the remaining 13 syntypes, MCZ 8298, MCZ 8300, MCZ 8305 and MCZ 8307 are now paralectotypes.

With the issue of type determination resolved, it is possible to proceed to other problems about the taxonomic situation of *T. immaculatus*. The first of which is the status of potentially closely related nominal forms. *Trichomycterus pradensis* was described from three adjacent but independent basins in southern Bahia and northern Minas Gerais, Brazil: Jucuruçu (locality of the holotype), Peruípe and Itanhém. The three basins are sequentially north of the Rio Doce. The original description (Sarmento-Soares *et al.*, 2005) states that *T. pradensis* is distinguished from all congeners by a combination of three characters: closely-set S6 pores, a small patch of robust opercular odontodes (with 8 to 10 odontodes) and eight branched pectoral-fin rays. Examination of the holotype and 52 paratypes of *T. pradensis*, along with other data obtained for the present paper, shows that those traits need reevaluation. First, the number and spacing

between S6 pores is variable in the type series, a situation similar to that in several other species of *Trichomycterus* from the Rio Doce. Second, the number of opercular odontodes actually varies between 13 and 25 in the type series of *T. pradensis*, with no specimens in the 8–10 range. Finally, eight branched pectoral-fin rays can be found in other *Trichomycterus* species (e.g. *T. immaculatus*, *T. tantalus* and in some rare cases in *T. astromycterus* also in the Rio Doce Basin). The combination of all three characteristics (considering the corrected values for opercular odontode number) is matched in *T. immaculatus*, and we could not find additional distinguishing traits once all evidence is taken into consideration. The spotted colour pattern of the holotype of *T. pradensis* (cf. Sarmento *et al.*, 2005: fig. 1) might superficially seem to distinguish it from the uniform-coloured *T. immaculatus*. However, the colour pattern varies in the entire range between those two extremes in the type series of *T. pradensis* (as mentioned in the original description; Sarmento-Soares *et al.*, 2005: 296) (Fig. 8), with such variation seen also in *T. immaculatus* (Fig. 9). This variation may even be seasonal or environmentally induced, considering that a uniformly-coloured specimen from the Rio Doce reportedly changed to a spotted pattern in the course of 2 months in aquarium conditions (Costa *et al.*, 2020a). Careful examination of specimens referable to both *T. pradensis* and *T. immaculatus*, including type material of the two species and data from both internal and external anatomy, fails to reveal any other possibly diagnostic phenotypic characteristics. The same conclusion is reflected in DNA sequences, with little genetic barcoding divergence (1.2%) between specimens referable to *T. pradensis* (including topotypic material) and forms referable to *T. immaculatus* from throughout the Rio Doce and the Rio São Mateus. Finally, results of our phylogenetic analysis place samples of *T. pradensis* from the type locality in a clade including remaining specimens from the Rio Doce and adjacent basins, with divergence values insufficient to demontrate species differentiation (an observation previously made by Volpi, 2017). With both phenotypic and molecular evidence failing to demonstrate species-level divergence between forms referable to *T. pradensis* and *T. immaculatus*, plus the determination of the lectotype of the latter, the former species is proposed as a junior synonym of the latter.

Our analyses have shown that sequences of *T. immaculatus* from the Rio Doce are highly divergent from those of the Paraíba do Sul, fitting in widely disjunct branches of the phylogenetic tree obtained (Fig. 1). This indicates that the populations identified as *T. immaculatus* from those two basins are actually two different species, cryptic or semi-cryptic. Because the lectotype is from the Rio São Mateus and demonstrably conspecific with the form

in the Rio Doce, then the species in the Rio Paraíba do Sul must bear another name. Costa *et al.* (2020a) has recently demonstrated that *T. paquequerensis* (Miranda Ribeiro, 1943) is conspecific with the form then known as *T. immaculatus* in the Rio Paraíba do Sul. Their conclusion is based on both molecular and morphological data, and on recently collected topotypes of *T. paquequerensis*. Such conclusions led Costa *et al.* (2020a) to propose the latter species as a junior synonym of *T. immaculatus*. The biological situation is correctly inferred and we concur with their conclusion. However, with the determination of the lectotype situation implemented here, the name *T. immaculatus* no longer applies to the Rio Paraíba do Sul form. Therefore, it follows that *T. paquequerensis* is the oldest available name and the valid name for the species in the Rio Paraíba do Sul previously identified as *T. immaculatus*. This scenario solves the apparent conundrum of *T. immaculatus* coming out as two separate (and phylogenetically disjunct) terminals in the trees of Katz *et al.* (2018) and Costa *et al.* (2020b) (identified as *T. immaculatus* and *T.* cf. *immaculatus* in the former and as *T. immaculatus* and *T.* 'immaculatus' in the latter), a result corroborated here. The pairs of homonimous species each refer to the Rio Doce on the one hand and the Rio Paraíba do Sul on the other. In both papers, the sequences of *T. immaculatus* from the Rio Doce were originally from Ochoa *et al.* (2017), collected in the middle course of the basin and well within the sampling coverage of the present analysis. Although the situation seems clear nomenclaturally and biologically on the basis of sequence data, the morphological differentiation between the two species is subtle. We have found that among specimens examined for this study, *T. immaculatus* differs from the Paraíba do Sul taxon (*T. paquequerensis*) only by the fewer interopercular odontodes (37–59 vs. 66–75 in adult specimens) and by a shorter prepelvic length (50.9–58.0% SL vs. 60.6–63.3%). The holotype of *T. paquequerensis* is small (34 mm SL) and in poor preservation condition (Fig. 27), but a count of 40 and 43 interopercular odontodes (on each side) can still be determined. The number of odontodes in species of *Trichomycterus* increases with growth, so that similar-sized specimens should be used for meaningful comparisons. Specimens 35–50 mm SL of *T. immaculatus* (*sensu stricto*) have 30–36 interopercular odontodes, therefore confirming that the species still has fewer odontodes than *T. paquequerensis* at those sizes, although the difference is expectedly less pronounced than in large specimens. Such differences still await confirmation on additional specimens of *T. paquequerensis*.

Two species are particularly prone to confusion with *T. immaculatus* in the Rio Doce, namely *T. melanopygius*

and *T. tantalus*. *Trichomycterus melanopygius* is the species most similar to *T. immaculatus*, especially due to its homogeneous greyish colour pattern and to the presence of a dark horizontal stripe along the middle caudal-fin rays, visible in all specimens of the former and in small specimens (rarely adults) of the latter (in large specimens the trait is usually concealed by additional pigmentation). The two species look so similar in external aspect that they may easily be mistaken in superficial examination and have in fact been mixed together in museum collections. They have been proposed as pseudocryptic species (Reis *et al.*, 2020), which means that despite such similarities they can be readily distinguished by examination of details (given here in their respective diagnoses). This conclusion is corroborated by their highly significant *COI* genetic distance of 3.9% (cf. molecular results, Table 2).

Trichomycterus tantalus (described below) is another species that is similar to *T. immaculatus*, although not to the same degree as *T. melanopygius*. Most specimens of *T. tantalus* are different from *T. immaculatus* in colour pattern, because of an abrupt fading of dark coloration ventral to the lateral midline. However, such difference is not absolute, and some specimens are within the range of colour patterns seen in *T. immaculatus* (Fig. 6A), but the two species are still easily distinguishable on the basis of several other traits, including an evident concave or forked caudal fin and a hypertrophied opercular patch of odontodes in *T. tantalus* (vs. a truncate caudal fin and regular-sized opercle in *T. immaculatus*), among other characters described in more detail in their diagnoses. Their species-level differentiation is also corroborated by a barcoding divergence of 3.8% (Table 2).

Geographical distribution: Trichomycterus immaculatus is widely distributed in the entire Rio Doce and adjacent basins (Rios Jucuruçu, Peruípe and Itanhaém, Itaúnas and São Mateus) (Fig. 28). As defined here, *T. immaculatus* does not occur in the Rio Paraíba do Sul Drainage (see Remarks above). The species has a broad range of habitats, including both the main channel of large rivers (such as that of the Rio Doce) and smaller tributaries and headwaters (also observed in the Rio Doce Basin). In this regard, it differs from similar-looking relatives, *T. melanopygius* and *T. tantalus*, the former being restricted to small tributaries and headwaters and the latter occurring exclusively in main channels.

Type material examined (*localities and respective dates of Thayer Expedition material follow Higuchi, 1996*): type material of *Pygidium immaculatum*; lectotype (designated herein): MCZ 8302, 1, 121.4 mm SL; Sao Matheos (state of Espírito Santo, Rio São Mateus at
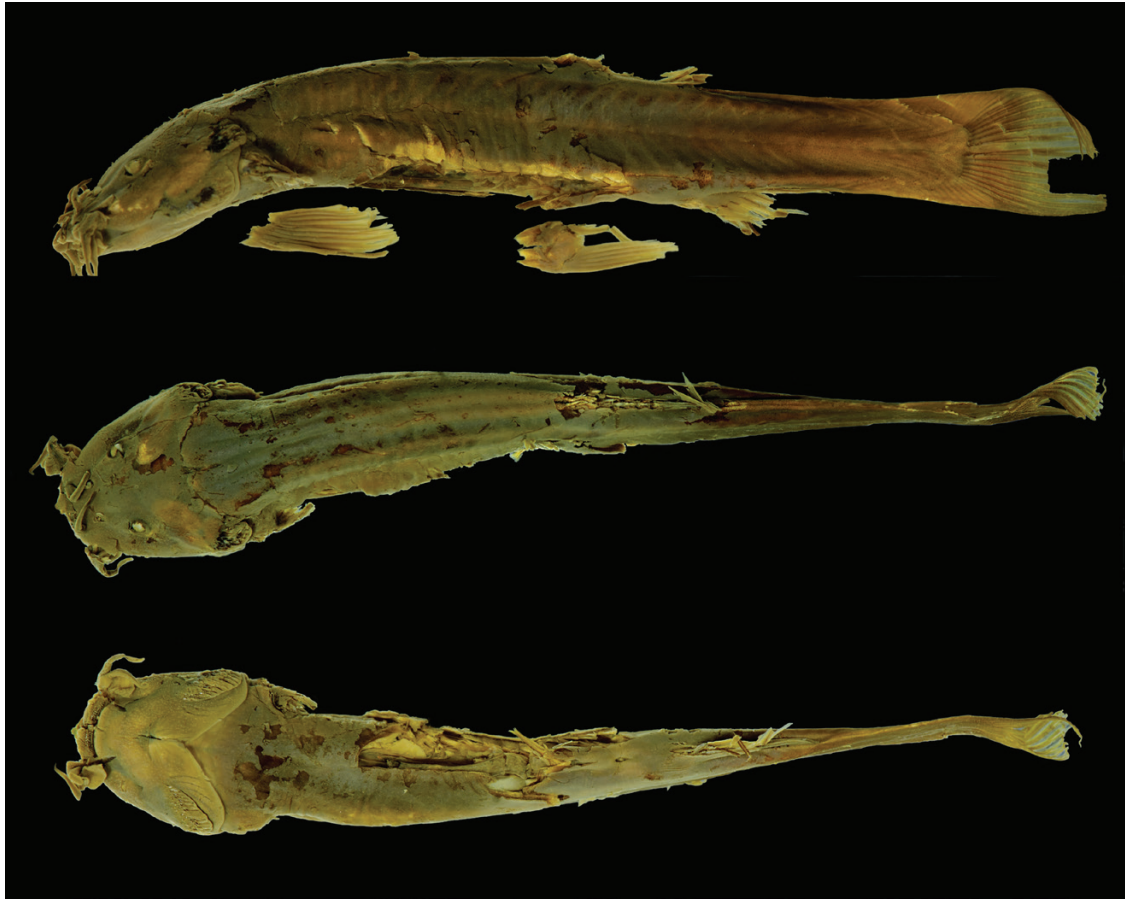
Figure 27. *Trichomycterus paquequerensis* (top: lateral; middle: dorsal; and bottom: ventral views). MNRJ 1159, holotype, 34 mm SL; Brazil, state of Rio de Janeiro, Paquequer Grande River.

São Mateus); col. C.F. Hartt & E. Copeland in Thayer Expedition to Brazil, November-December 1865. Paralectotypes: MCZ 8300, 5, paralectotypes, 123.2–165.0 mm SL; Juiz de Fora, Parahybuna (state of Minas Gerais, Rio Paraibuna at Juiz de Fora); col. H.W. Halfeld, 1854. MCZ 8305, 1, paralectotype, 117.6 mm SL; Juiz de Fora and Parahyba (state of Minas Gerais, Juiz de Fora and environs in the Paraiba Valley); col. L. Agassiz & J. Whitaker, in Thayer Expedition to Brazil, 21–27 June 1865. MCZ 8307, 1, paralectotype, 116.2 mm SL; same data as MCZ 8305. MCZ 8296, 1, paralectotype, 51.6 mm SL, Goyaz (state of Goiás or Tocantins, probably somewhere in the Tocantins-Araguaia Basin); col. Senhor Honorio (A.H. Ferreira), 1867. Type material of *Trichomycterus pradensis*; MNRJ 28484, 09, paratypes, 39.4–109.0 mm SL; Jucuruçu, Rio Jucuruçu. MNRJ 28485, 5, paratypes, 40.0–66.5 mm SL; Bahia, riacho a 500 m do ponto anterior, bacia do Rio Peruípe; MNRJ 28488, 7, paratypes, 49.1–99.0 mm SL; Palmópolis, Rio Dois de Abril, bacia do Rio Jucuruçu. MNRJ 28490, 9, paratypes, 46.7–74.1 mm SL; Itanhém, Córrego Água Fria, Rio Itanhém.

Additional material studied: All following from Brazil, state of Minas Gerais; MZUSP 58479, 29, 47.5–115.2 mm SL; Joanésia; Guacho Creek, tributary of Santo Antônio River Basin (19° 7'37.86"S 42°39'48.93"W); col. F.A. Bockmann & P.M.C. Araujo, 5 October 1997. MZUSP 69333, 1, 63 mm SL; Coroaci, Suaçuí Pequeno River (18°36'45.93"S 42°16'52.91"W); col. A.M. Zanata, 28 April 2001. MZUSP 69359, 1, 77.8 mm SL; Coroaci; Suaçuí Pequeno River (18°37'20.29"S 42°16'16.34"W); col. A.M. Zanata, 29 April 2001. MZUSP 69367, 1, 83.5 mm SL; Coroaci, Suaçuí Pequeno River (18°41'38.00"S 42°12'50.00"W); col. A.M. Zanata, 29 April 2001. MZUSP 75034, 2, 67 mm SL; Sarduá Tronqueiras River, tributary of Suaçuí River Basin (18°46'44.29"S 42°23'41.00"W); col. F. Di Dario & B. Di Dario, 8 December 2001. MZUSP 75059, 8, 78.6–48.8 mm SL; Coroaci, Suaçuí River Basin (18°36'45.57"S 42°16'18.73"W); col. F. Di Dario & B. Di Dario, 6 December 2001. MZUSP 81028, 9, 133.8–55.8 mm SL; Manhuaçu, Manhuaçu River (20°15'24.00"S 42°7'2.00"W); col. Carlos B.M. Alves, 23 April 2002. MZUSP 81029, 6, 59–114 mm SL;
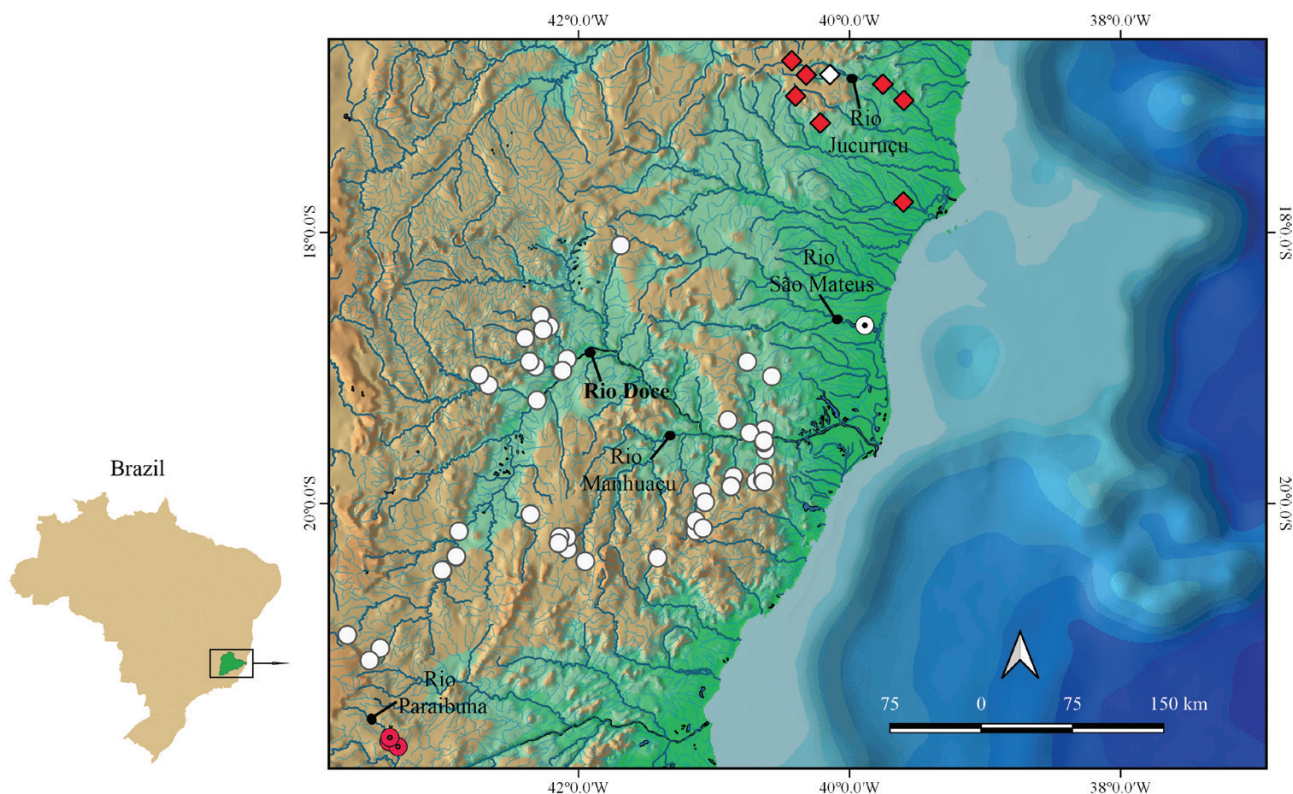
Figure 28. Geographical distribution of *T. immaculatus*. White dotted circle = lectotype (MCZ 8302); red dotted circles = paralectotypes (MCZ 8300, 8305, 8307); white diamond = holotype of *T. pradensis* (MNRJ 28483); red diamonds = paratypes of *T. pradensis* (MNRJ 28484, 28485, 28486, 28487, 28488, 28489, 28490, 28491, AUM, 42733, 42734, AMNH 3236101, ANSP 180783, FLMNH 148993); white circles = additional Rio Doce localities.

Manhuaçu, Manhuaçu River (20°15'24.00"S 42°7'2.00"W); col. Carlos B.M. Alves, 22 April 2002. MZUSP 81032, 8, 37.1–79.7 mm SL; São Luiz, Manhuaçu River (20°20'12.00"S 42°4'48.00"W); col. Carlos B.M. Alves, 21 April 2002. MZUSP 94488, 2, 65.9–82.3 mm SL; Alto Rio Doce, Xopotó River, Piranga River Basin (21°4'4.00"S 43°27'50.00"W); col. Oyakawa, Baena e Loeb, 11 July 2007. MZUSP 123334, 45, 38.5–85.3 mm SL; Bom Jesus do Manhuaçu, Manhuaçu River (20°17'34.24"S 42°8'50.88"W); col. T. Pessali, 7 September 2015. MZUSP 123335, 10, 45.3–55.9 mm SL; Bom Jesus do Manhuaçu, Manhuaçu River, Rio Doce Basin (20°17'34.24"S 42°8'50.88"W); col. T. Pessali, 22 April 2015. MZUSP 123336, 22, 53.1–105.3 mm SL; Realeza, Manhuaçu River, Rio Doce Basin (20°14'49.13"S 42°5'2.18"W); col. T. Pessali, 21 April 2015. MZUSP 123337, 92, 52.2–98.3 mm SL; Realeza, Manhuaçu River, tributary of Rio Doce Basin (20°14'49.13"S 42°8'26.17"W); col. T. Pessali, 8 September 2015. MZUSP 123342, 1, 67.5 mm SL; Naque, main channel of Rio Doce River (19°14'19.42"S 42°18'22.65"W); col. T. Pessali, 19 July 2017. MZUSP 123344, 7, 45.6–84.6 mm SL; Açucena, Corrente Grande River, Rio Doce Basin (18°57'9.86"S 42°21'38.20"W);

col. T. Pessali, 31 July 2017. MZUSP 123345, 123, 48.4–112.9 mm SL; Baguari, main channel of Rio Doce River (19°1'3.06"S 42°7'16.31"W); col. T. Pessali, 12 December 2016. MZUSP 123347, 12, 39.2–77.7 mm SL; Açucena, Corrente Grande River, Rio Doce Basin (18°57'9.86"S 42°21'38.20"W); col. T. Pessali, 31 May 2017. MZUSP 123348, 83, 50.2–111.4 mm SL; Baguari, main channel of Rio Doce River (19°1'27.83"S 42°7'34.40"W); col. T. Pessali, 20 December 2016. MZUSP 123349, 74, 43.7–76.7 mm SL, Itambacuri, Suaçui Grande River, tributary of Rio Doce Basin (18°5'42.17"S 41°41'22.16"W); col. T. Pessali, 9 September 2015. MZSUP 123352, 4, 40–67.3 mm SL; Açucena, Corrente Grande River, Rio Doce Basin (18°57'9.86"S 42°21'38.20"W); col. T. Pessali, 31 May 2017. MZUSP 123353, 23, 40.3–70.3 mm SL; Baguari, São Mateus Creek, tributary of Corrente Grande River (18°59'24.54"S 42°18'57.98"W); col. T. Pessali & V. Reis, 17 November 2017. MZUSP 123354, 1, 43.7 mm SL; Açucena, São Mateus Creek, tributary of Corrente Grande River (18°59'24.54"S 42°18'57.98"W); col. T. Pessali, August 2013. MZUSP 123356, 15, 46.9–79.4 mm SL; Açucena, São Mateus Creek, tributary of Corrente Grande River (18°57'10.39"S 42°21'39.81"W);

col. T. Pessali, 2 September 2017. MZUSP 123357, 3, 69.3–80.2 mm SL; Baguari, Suaçui Pequeno, tributary of Rio Doce Basin (18°56'2.50"S 42°5'2.18"W); col. T. Pessali & V. Reis, 16 November 2017. MZUSP 123367, 1, 51.8 mm SL; Bom Jesus do Manhuaçu, Manhuaçu River, Rio Doce Basin (20°17'34.24"S 42°8'50.88"W); col. T. Pessali, 27 April 2015. MZUSP 123368, 18, 45.6–85.7 mm SL; Baguari, main channel of Rio Doce River (19°1'14.68"S 42°7'6.81"W); col. T. Pessali, 13 December 2016. MZUSP 123370, 8, 44.5–56.0 mm SL; Itambacuri, Suaçui Grande River, Rio Doce Basin (18°5'42.17"S 41°41'22.16"W); col. T. Pessali, 9 September 2015; Minas Gerais MZUSP 126408, 1, 91 mm SL, Rio Doce Municipality, Rio Doce Basin, Córrego dos Borges, stream flowing into left bank of Risoleta Neves Reservoir, (20°12'21.63"S 42°52'56.24"W); col. V.J.C. Reis, M.C.C. de Pinna, G.F. de Pinna & G. Ballen, 24 June 2018. LBP 1019, 2, 68.8–114.9 mm SL; between Capela Nova and Caranaíba, Piranga River, tributary of Rio Doce Basin (20°58'10.26"S 43°42'19.86"W); col. J.C. Oliveira, A.L. Alves & L.R. Sato, 13 October 2001. MZUFV 3335, 3, 109.4–118.3 mm SL; Guaraciaba, UHE Brecha, Piranga River, Rio Doce Basin (20°29'42.01"S 43°0'15.59"W); col. J.A. Dergam & Tottola, 23 March 2003. MZUFV 3348, 2, 100.7–105.5 mm SL; Ponte Nova, UHE Brito, Rio Piranga River (20°23'22.43"S 42°54'9.23"W); col. J.A. Dergam & M.R. Tottola, 24 March 2003. MZUFV 3378, 3, 82.5–99.7 mm SL; Guaraciaba, UHE Brecha, Piranga River, Rio Doce Basin (20°29'34.47"S 43°0'24.18"W); col. J.A. Dergam & M.R. Tottola, 10 April 2003. MZUFV 3393, 10, 9.0–110.5 mm SL; Ponte Nova, UHE Brito, Rio Piranga River (20°23'42.38"S 42°54'9.36"W); col. J.A. Dergam & M.R. Tottola, 12 April 2003. MNRJ 22453, 6, 41.8–81.3 mm SL; Manhuaçu, Rio Doce, tributary of Rio Manhuaçu, São Luiz Stream; col. P.A. Buckup, A.T. Aranda, F.A.G. Melo, 8 August 2001. MNRJ 37629, 3, 67.4–129.7 mm SL; Baixo Guandu, Mutum Preto River, locality between a village located at the KM14 and Alto Mutum; col. M. Britto, F. Pupo, L. Sarmento-Soares, 1 August 2010. Brazil, state of Espírito Santo: MZUSP 41738, 2, 48.4–71.6 mm SL; Ibatiba; São João River Basin (20°23'60.00"S 41°25'0.00"W); col. C.A.S. Lucena & P.V. Azevedo, 6 September 1989. MBML 55, 1, 49.7 mm SL; Colatina, Santa Maria do Rio Doce Basin (19°36'14.00"S 40°37'13.00"W); col. R.L. Teixeira & J.A.P. Scheneider, 29 August 1996. MBML 438, 12, 34.2–53.2 mm SL; Santa Teresa, Rúdio Waterfall, Santa Maria do Rio Doce Basin (19°50'11.00"S 40°41'27.00"W); col. R.L. Teixeira, 30 June 2000. MBML 636, 3, 70.0–100.5 mm SL; Itaguaçu, Fazenda Coser, Santa Joana Basin (19°48'6.00"S 40°51'20.00"W); col. R.L.Teixeira & P.S.Miller, 8 September 2000. MBML 648, 5, 66.2–85.3 mm SL; Itarana, Jatibocas Stream, Santa Joana Basin (19°52'26.00"S 40°52'31.00"W); col. R.L.Teixeira & P.S.Miller, 19 April 2001. MBML 672, 2,

66.6–74.8 mm SL; Itaguaçu, Fazenda Coser, Santa Joana Basin (19°48'6.00"S 40°51'20.00"W); col. R.L.Teixeira & P.S. Miller, 21 May 2001. MBML 695, 24, 44.4–104.6 mm SL; Itarana, Jatibocas Stream, Santa Joana Basin (19°52'26.00"S 40°52'31.00"W); col. R.L. Teixeira & P.S. Miller, 10 August 2000. MBML 701, 13, 36.5–71.9 mm SL; Itarana, Santa Joana Basin (19°52'26.00"S 40°52'31.00"W); col. R.L. Teixeira & P.S. Miller, 19 August 2000. MBML 753, 10, 62.1–117.5 mm SL; Itarama, Jatiboca Stream, Santa Joana Basin (19°52'26.00"S 40°52'31.00"W); col. R.L. Teixeira & P.S. Miller, 18 October 2000. MBML 765, 1, 94.7 mm SL; Itarana, Santa Joana River (19°52'26.00"S 40°52'31.00"W); col. R.L. Teixeira & P.S. Miller, 8 February 2002. MBML 788, 1, 79.6 mm SL; Itarana, Jatibocas Stream, Santa Joana Basin (19°52'26.00"S 40°52'31.00"W); col. R.L. Teixeira, 12 October 2000. MBML 805, 4, 71.6–93.1 mm SL; Itarana, Jatibocas Stream, Santa Joana Basin (19°52'26.00"S 40°52'31.00"W); col. R.L. Teixeira & P.S. Miller, 21 June 2001. MBML 807, 7, 65.5–80.5 mm SL; Itarana, Jatibocas Stream, Santa Joana Basin (19°52'26.00"S 40°52'31.00"W); col. R.L. Teixeira & P.S. Miller, 8 February 2001. MBML 999, 4, 40.4–51.1 mm SL; Itarana, Santa Joana River, tributary of Rio Doce Basin (19°52'26.00"S 40°52'31.00"W); col. R.L. Teixeira & P.C.M. Mili, 21 June 2001. MBML 1014, 1, 43.8 mm SL; Itarana, Limoeiro Creek, Santa Joana River (19°52'26.00"S 40°52'31.00"W); col. R.L. Teixeira, 19 April 2001. MBML 1357, 3, 43.4–66.4 mm SL; Colatina, Cachoeira do Oito Waterfall, Pancas River Basin (19°27'21.00"S 40°37'29.00"W); col. R.L. Teixeira & G.I. Almeida, 8 December 2005. MBML 1395, 1, 57.7 mm SL; Colatina, Santa Maria do Rio Doce Basin (19°32'55.00"S 40°38'7.00"W); col. R.L. Teixeira & Borlute, 11 October 2005. MBML 2243, 1, 71.7 mm SL; Laranja da Terra e Serra Pelada, Timbuva Stream, Gandu River Basin (19°54'55.00"S 41°5'18.00"W); col. L.M. Sarmento-Soares, R.F. Martins-Pinheiro, A.T. Aranda, R.L. Teixeira, M.M.C. Roldi & M.M. Lopes, 12 June 2009. MBML 2274, 3, 50.2–118.9 mm SL; Laranja da Terra, Lagoa Stream, Gandu River Basin (19°59'26.00"S 41°3'55.00"W); col. L.M. Sarmento-Soares, R.F. Martins-Pinheiro, A.T. Aranda, R.L. Teixeira, M.M.C. Roldi & M.M. Lopes, 12 June 2009. MBML 2290, 11, 27.6–85.6 mm SL; Afonso Cláudio, Rio do Cobre River, tributary of Guandu Basin (20°9'19.00"S 41°8'31.00"W); L.M. Sarmento-Soares, R.F. Martins-Pinheiro, A.T. Aranda, R.L. Teixeira, M.M.C. Roldi & M.M. Lopes, 14 June 2009. MBML 2295, 2, 34.7–38.2 mm SL; Afonso Claudio Rio do Peixe River, Gandu River Basin (20°7'39.00"S 41°8'9.00"W); col. A.T. Aranda, R.F. Martins-Pinheiro, R.L. Teixeira & M.M.C. Roldi, 14 June 2009. MBML 2304, 18, 34.2–58.1 mm SL; Afonso Cláudio, Rio da Cobra River, tributary of Guandu River (20°12'4.00"S 41°8'7.00"W); col. A.T.

Aranda, R.F. Martins-Pinheiro, R.L. Teixeira & M.M.C. Roldi, 14 June 2009. MBML 2312, 13, 33.1–76.5 mm SL; Afonso Cláudio, Rio da Cobra River, Guandu Basin (20°10'57.00"S 41°4'50.00"W); col. A.T. Aranda, R.F. Martins-Pinheiro, R.L. Teixeira & M.M.C. Roldi, 14 June 2009. MBML 2974, 10, 50.9–99.2 mm SL; Colatina, Santa Maria do Rio Doce Basin (19°32'21.00"S 40°37'50.00"W); col. R.L. Teixeira & E.C. Perrone, 6 November 1988. MBML 3465, 4, 53.1–103.5 mm SL; Baixo Gandu, Mutum Preto River, Mutum Preto River (19°23'7.00"S 40°53'52.00"W); col. L.M. Sarmento-Soares, R.F. Martins-Pinheiro, M.R. Britto & F.M.R.S. Pupo, 1 October 2010. MBML 3571, 9, 31.2–61.5 mm SL; Águia Branca, Águas Claras Stream, São José River (18°57'17.00"S 40°45'19.00"W); col. L.M. Sarmento-Soares, R.F. Martins-Pinheiro, M.R. Britto & F.M.R.S. Pupo, 5 October 2010. MBML 3878, 1, 47 mm SL; Colatina, São João Pequeno River (19°28'45.00"S 40°44'15.00"W); col. M.M. Martinelli, 27 September 2010. MBML 4274, 3, 32.3–42.1 mm SL; Águia Branca, Braço Azul River, São José Basin (19°3'44.00"S 40°34'21.00"W); col. J.L. Helmer, 12 August 2011. MBML 4385, 1, 49.35 mm SL; Santa Teresa, Santa Maria do Rio Doce River (19°46'21.10"S 40°38'2.70"W); col. R.B. Soares, J. Gurtler & V.R. Bada, 24 September 2011. MBML 4431, 1, 39.91 mm SL; Santa Teresa, Santa Maria do Rio Doce River (19°46'21.10"S 40°38'2.70"W); col. R.B. Soares, J. Gurtler & V.R. Bada, 24 September 2011. MBML 6139, 1, 66.2 mm SL; Santa Teresa, Cinco de Novembro River, Santa Maria do Rio Doce Basin (19°49'42.90"S 40°38'18.40"W); col. C.J. Cunha, J.P. Silva & R.B. Soares, 20 August 2012. MBML 6153, 8, 23.7–84.4 mm SL; Santa Teresa, Cinco de Novembro River, Santa Maria do Rio Doce River (19°50'26.00"S 40°37'47.30"W); col. C.J. Cunha, J.P. Silva & R.B. Soares, 20 August 2012.

TRICHOMYCTERUS IPATINGA SP. NOV.
(FIGS 7, 29)

Zoobank registration: urn:lsid:zoobank.org:act:BE65375F-FE39-4F4D-BD8D-1FC7EB4002BB

Holotype: MZUSP 112279, 67.6 mm SL; Brazil, state of Minas Gerais, Conceição do Mato Dentro, Meloso Creek, tributary Rio Santo Antônio (19°4'35.98"S 43°20'28.84"W); col. M.V. Loeb, 12 January 2011.

Paratypes: All from Brazil, state of Minas Gerais. MZUSP 87814, 11, 39.2–103.5 mm SL, 2 c&s, 102.5–114.9 mm SL; Serro, creek tributary of Rio Doce Basin (18°34'50.11"S 43°23'31.49"W); col. A. Carvalho Filho; 27 August 2004. MZUSP 104682, 4, 31.3–46.1 mm SL; Conceição do Mato Dentro, Axupé Creek (19°06'41"S

43°16'02"W), col. I Fichberg & M.V. Loeb, 22 March 2009. MZUSP 104699, 6, 25.2–52.6 mm SL; Conceição do Mato Dentro, São João Creek, tributary of Santo Antônio River (19°02'29"S 43°20'34"W), col. I. Fichberg & M.V. Loeb, 19 March 2009. MZUSP 104700, 2, 42.8–45.0 mm SL; Conceição do Mato Dentro, creek on the road between Conceição do Mato Dentro and Meloso District (19°2'58.00"S 43°21'45.00"W), col. I. Fichberg & M.V. Loeb, 18 March 2009. MZUSP 104701, 10, 26.4–39.7 mm SL; Conceição do Mato Dentro, creek on the road that crosses the Meloso Municipality, Rio Doce Basin (19°04'33.0"S 43°20'26.0"W); col. I. Fichberg & M.V. Loeb, 21 March 2009. MZUSP 104702, 6, 27.0–78.9 mm SL, 1 c&s, 50.13 mm SL; Conceição do Mato Dentro, Faia Creek, tributary of São João River (19°01'19"S 49°20'39"W); col. I. Fichberg & M.V. Loeb, 19 March 2009. MZUSP 104706, 1, 52.3 mm SL; Conceição do Mato Dentro, Axupé Creek, Santo Antonio River (19°6'36.00"S 43°17'55.00"W); col. I. Fichberg & M.V. Loeb, 18 March 2009. MZUSP 109370, 2, 47.8–56.4 mm SL, 1 c&s, 56 mm SL; Brazil, Minas Gerais, Santa Barbara; Ribeirão Preto Creek, Piracicaba River (20°5'36.00"S 43°39'26.00"W); col. B.P. Maia, 31 July 2010. MZUSP 109385, 1, 100.5 mm SL; Santa Barbara; São João River, Piracicaba River (20°2'28.00"S 43°40'2.00"W); col. B. P. Maia, 31 July 2010. MZUSP 109393, 2, 50.1–112.6 mm SL; Brazil, Minas Gerais, Santa Barbara; Ribeirão Preto Creek, Piracicaba River (20°3'57.00"S 43°40'16.00"W); col. B.P. Maia, 31 July 2010. MZUSP 112237, 5, 26.5–31.6 mm SL; Conceição do Mato Dentro, Axupé Creek, Santo Antônio River (19°6'44.10"S 43°16'4.65"W), col. M.V. Loeb, 6 January 2011; MZUSP 112241, 2, 27.8–32.6 mm SL; Conceição do Mato Dentro, Axupé Creek, Santo Antônio River (19°6'44.47"S 43°16'44.68"W), col. M.V. Loeb, 6 January 2011; MZUSP 112253, 1, 25.7 mm SL; Conceição do Mato Dentro, Ponte Nova Creek, Santo Antônio River (18°59'24.67"S 43°23'1.62"W); col. M.V. Loeb, 10 January 2011; MZUSP 112260, 6, 29.7–58.4 mm SL; Conceição do Mato Dentro, Antonieta Creek, Santo Antônio River (19°0'42.07"S 43°22'20.42"W); col. M.V. Loeb, 10 January 2011; MZUSP 112270, 7, 28.8–63.9 mm SL, 3 c&s, 29.0–41.2 mm SL; Conceição do Mato Dentro, São João River, Santo Antônio River (19°2'30.77"S 43°20'34.02"W); col. M.V. Loeb, 11 January 2011; MZUSP 112271, 4, 39.3–103.8 mm SL, 1 c&s, 39.1 mm SL; Conceição do Mato Dentro, São João Creek, Santo Antônio River (19°1'21.73"S 43°20'38.60"W); col. M.V. Loeb, 11 January 2011. MZUSP 112277, 1, 94.7 mm SL; Conceição do Mato Dentro, São João Creek, Santo Antônio River (19°1'57.18"S 43°22'42.57"W); col. M.V. Loeb, 12 January 2011. All from state of Espírito Santo—MBML 4337, 4, 31–60.9 mm SL; Iúna, José Preto River in the National Park of Caparaó, Manhuaçu River (20°22'9.50"S 41°51'27.50"W); col. L.M. Sarmento-Soares, M.R. Britto, V.C. Espíndola, F.M.R.S. Pupo,

Figure 29. *Trichomycterus ipatinga* sp. nov. (top: lateral; middle: dorsal; and bottom: ventral views). MZUSP 112279, holotype, 67.6 mm SL; Brazil, state of Minas Gerais, Conceição do Mato Dentro Municipality, Meloso Creek, tributary of Rio Santo Antônio Drainage.

R.F.M. Pinheiro & M.M.C. Roldi, 10 September 2011. MBML 4340, 1, 73.7 mm SL; Iúna, Córrego Feio Creek, Manhuaçu Basin (20°22'9.40"S 41°51'28.70"W); col. L.M. Sarmento-Soares, M.R. Britto, V.C. Espíndola, F.M.R.S. Pupo, R.F.M. Pinheiro & M.M.C. Roldi, 10 September 2011. MBML 6223, 13, 30.1–95.4 mm SL; Afonso Cláudio, Rio Guandu (20°4'12.00"S 41°13'44.00"W); col. Researches from the BIOdiversES Project, 11 August 2012. MBML 6825, 1, 52.4 mm SL; Santa Teresa, Vinte Cinco de Julho River, Santa Maria do Rio Doce River (19°50'14.60"S 40°33'18.80"W); col. L.M. Sarmento-Soares, R.F. Martins Pinheiro, M.M.C. Roldi & R. Becalli, 5 May 2013. MBML 6844, 34, 40.7–100.5 mm SL; Santa Teresa, Vinte e Cinco de Julho River, tributary of Santa Maria do Rio Doce (19°50'20.70"S 40°34'4.30"W); col. L.M. Sarmento-Soares, R.F. Martins Pinheiro, M.M.C. Roldi & R. Becalli, 5 May 2013. MNRJ 52979, 1, 53.9 mm SL; came from MZUSP 112271. MNRJ 52980, 3, 30 - 34.5 mm SL; came from MZUSP 104701.

Diagnosis: The combination of the following traits distinguishes *T. ipatinga* from congeners: (1) body randomly covered by roundish maculae, either far larger or far smaller than eye, evenly and densely spaced; (2) horizontal dark stripe on the caudal fin extending from base to tip of middle rays (vs. absent); and (3) pectoral-fin rays I + 7 (I + 5, I + 6 or I + 8); (4) two or, rarely, three lateral line pores (vs. always three or more). Among congeners in south-eastern South America, character 1 distinguishes *T. ipatinga* from all species except for some colour morphs of *T. brasiliensis*, *T. lauryi* and *T. vinnulus*; character 2 from all except for *T. melanopygius*, young stages of *T. immaculatus*, *T. reinhardti* and *T. tantalus*; character 3 distinguishes *T. ipatinga* from all species in the *T. brasiliensis* and *T. reinhardti* species complex (Barbosa & Costa, 2010; Costa, 2021; Costa & Katz, 2021), plus *T. trefauti* (all preceding with I + 6 or fewer) and from *T. astromycterus*, *T. caipora*, *T. giganteus*,

T. immaculatus, *T. lauryi*, *T. nigricans* and *T. tantalus* (with I + 8 or more); character 4, when three lateral line pores are present, from all except *T. astromycterus*, *T.* aff. *caipora*, *T. nigricans* and *T. vinnulus*. Among congeners in the Rio Doce Basin, *T. ipatinga* is most similar to *T. vinnulus*. In addition to characters above, *T. ipatinga* can be further distinguished from *T. vinnulus* by more numerous premaxillary teeth (10–14 vs. 8); more numerous interopercular odontodes (25–38 vs. 25–26). The two species are separated by a barcoding distance of 3.8%.

Description: Morphometric data for specimens examined is presented in Table 12. Body long and almost straight, trunk roughly round in cross-section near head, then slightly deeper than wide and gently compressed to caudal peduncle, tapering to caudal fin. Dorsal profile of body gently convex to dorsal-fin origin, then straight or slightly concave along caudal peduncle to caudal-fin origin. Ventral profile convex from gular region to vent, due partly to abdominal distension, then straight or slightly concave along anal-fin origin to caudal-fin base. Caudal peduncle nearly as deep as body at end of anal-fin base.

Head approximately 1/6 to 1/5 of SL, pentagonal, longer than wide and depressed. Mouth subterminal. Upper jaw slightly longer than lower. Upper lip wider than lower lip, and laterally continuous with base of maxillary barbel. Lower lip small, approximately 2/3 width of upper one, partly divided into right and left portions by median concavity. Lower lip with uniform covering of tiny villi, resulting in velvet-like surface

and not clustered into large papillae. Region between upper and lower lips with slender fleshy lobe.

Dentary and premaxillary teeth similar to each other in shape. Dentary teeth conical, arranged in four irregular rows, first row with 10–14 teeth, extending from base to slightly up of coronoid process, with size of individual teeth increasing markedly towards symphysis and from posterior to anterior rows. Total area of premaxillary teeth slightly smaller than that of dentary, with teeth arranged irregularly in four rows, first row with approximately 11–14 teeth, over entire ventral surface of premaxilla. Premaxillary teeth conical.

Eye medium-sized, slightly protruding, positioned dorsally on head, without free orbital rim and covered with transparent skin. Eye located on anterior half of HL, closer to lateral border of head than to the midline in dorsal view. Anterior naris surrounded by tube of integument directed anterolaterally, continuous posterolaterally with nasal barbel. Posterior naris closer to anterior naris than to eyes, surrounded by tube of integument incomplete posteriorly. Maxillary barbel narrowing markedly towards fine tip, reaching from lateroposterior side of interopercle until base of pectoral fin. Rictal barbel inserted immediately ventral to maxillary barbel, its tip reaching from anterolateral to the middle of interopercle. Nasal barbel originating on posterolateral region of anterior naris, reaching from posterior border of eyes to anterior portion of opercle. Interopercular patch of odontodes large compared to head length, oval in shape and with well-developed odontodes, prominent in ventral aspect of head. Interopercular patch of odontodes extending

Table 12. Morphometric data of *T. ipatinga* based on holotype and part of paratype material (MZUSP 104702, 112237, 112260, 112270, 112271, 112277, 112279, MBML 4337, 6825)

	Holotype	Range (*N* = 15)	Mean	SD
Standard length (mm)	67.2	31.7–99.6	59.3	-
% of standard length				
Anal-fin base	8.4	7.6–10.2	8.5	0.7
Body depth	16.8	12.0–17.4	15.3	1.4
Caudal peduncle depth	13.3	10.5–14.5	13.1	1.2
Dorsal-fin base	11.2	8.9–11.5	10.8	0.6
First pectoral-fin length	17.4	14.6–18.4	16.2	1.1
Head length	18.0	16.0–21.3	19.1	1.6
Preanal length	69.7	65.8–73.9	70.4	2.1
Predorsal length	61.7	59.7–65.6	62.2	1.7
Prepelvic length	55.5	51.3–58.4	54.9	1.9
% of head length				
Eye diameter	15.3	12.8–17.1	15.3	1.3
Interorbital width	28.4	22.0–33.2	28.6	2.9
Snout length	48.7	46.5–54.9	50.5	2.3
Mouth width	35.3	27.6–39.6	34.7	2.7

from vertical through ventroposterior border of eye to ventroanterior to opercular patch of odontodes. Interopercular odontodes arranged in two or three irregular series, with those on mesial series much longer than those on lateral one; odontodes gradually larger posteriorly in both series, with those posteriorly on mesial row largest. Interopercular odontodes 25–38. Opercular patch of odontodes on dorsolateral surface of posterior part of head, positioned anterodorsally to pectoral-fin base, roundish in shape and larger than eye in dorsal aspect of head. Opercular odontodes 13–18, sunk in individual slits of integument, progressively larger posteriorly, all with fine tips, with largest ones curved distally and claw-like. Entire patch surrounded by rim of integument.

Pectoral fin with its base immediately posterior and ventral to opercular patch of odontodes. Pectoral-fin rays I + 7. First pectoral-fin ray (unbranched) longer, prolonged as filament beyond fin margin. Other rays progressively less long, their tips following continuous line along fin margin. Pelvic fin with convex distal margin, its origin slightly posterior to middle of SL and anterior to vertical through dorsal-fin origin, anteriorly touching anal and urogenital openings in adults but never covering them. Bases of pelvic fins separated by less than eye diameter close to each other. Pelvic-fin rays I + 4, first ray unbranched. Anterior process of basipterygium long and laterally curved. Dorsal fin long, its distal profile sinusoidal. Dorsal-fin origin closer to base of caudal fin than to tip of snout. Dorsal-fin rays ii + II + 7 (2); iii + II + 7 (5). Anal fin slightly smaller than dorsal fin, its distal profile gently convex. Anal-fin origin posterior to vertical through end of dorsal-fin base. Anal-fin rays ii + II + 5 (2) or iii + II + 5 (5). Caudal fin rounded shape, with 6 + 7 principal rays. Adipose fin absent or modified into low integumentary fold extending between end of dorsal fin and caudal-fin origin. Post-Weberian vertebrae 37 (7). First dorsal-fin pterygiophore immediately anterior to neural spine of 17th (5) or 18th (2) vertebra, first anal-fin pterygiophore immediately anterior to neural spine of 21th (4) or 22th (3) vertebra. Caudal-fin procurrent rays plus one segmented non-principal ray dorsally and ventrally. Procurrent caudal-fin rays, 16–21 dorsally and 11–15 ventrally, beginning anteriorly at 32th (7) vertebrae. Pleural ribs 12 (5) or 13 (2). Branchiostegal rays 7 (1) or 8 (6). Dorsal-fin pterygiophores 8. Anal-fin pterygiophores 6.

Cephalic lateral line canals with simple, non-dendritic tubes ending in single pores. Supraorbital canal mostly in frontal bone. Supraorbital pores invariably present: s1 mesial to nasal-barbel base and autopalatine, s3 mesial to posterior nostril and anterior to frontal and paired s6 posteromedial to eye and at midlength of frontal. Infraorbital latero-sensory canal incomplete with four pores, i1 and i3 anteriorly

and i10 and i11 posteriorly. This canal extending from sphenotic posteriorly to terminal pore located ventroposteriorly to eye. Infraorbital pore i1 located ventro-lateral to nasal-barbel base and autopalatine, i3 ventrolateral to posterior nostril and anterior to frontal, i10 and i11 posterior to eye. Otic canal without pores. Postotic pores po1, anteromedial to opercular patch of odontodes, and po2, mesial to opercular patch of odontodes. Lateral line of trunk anteriorly continuous with postotic canal and reduced to short tube. Lateral line pores ll1 and ll2, in some specimens the ll3 is present dorsomedial to pectoral-fin base.

Coloration in ethanol: Body covered with small to large round to amoeboid dark maculae. Individual maculae rarely fusing with each other, varying bimodally in size and number, creating two extreme colour patterns ([Fig. 7](#)). At one extreme, maculae mostly twice eye diameter. At the other extreme, maculae smaller than eye diameter and more numerous. Head and base of all fins, except for caudal fin, following colour pattern of body. Caudal fin with dark stripe extending from the base of middle principal caudal-fin rays to nearly margin of fin, evident in young specimens and gradually fading or masked by additional caudal-fin pigmentation in larger individuals. Ventral part of body without dark pigmentation.

Etymology: The name honours Ipatinga, a city located in the state of Minas Gerais where the Piracicaba River joins the Rio Doce. It is a noun in apposition.

Remarks: Trichomycterus ipatinga varies in colour pattern, a situation common in species of the genus ([Arratia *et al.*, 1978](#); [Triques & Vono, 2004](#); [Castellanos-Morales, 2007](#); [Lima *et al.*, 2008](#); [Silva *et al.*, 2010](#); [Ferrer & Malabarba, 2013](#); [Buckup *et al.*, 2014](#); [Nascimento *et al.*, 2017](#)). The overall colour pattern of *T. ipatinga* may resemble the well-known *T. brasiliensis* or other species in the *T. brasiliensis* complex ([Barbosa & Costa, 2010](#)). However, the species is highly divergent from *T. brasiliensis* both in other morphological traits and in DNA sequences ([Table 2](#)). Contrastingly, *T. tantalus* and *T. melanopygius* (both outside of the *T. brasiliensis* complex) display low DNA barcoding divergence relative to *T. ipatinga*. Nevertheless, those two species are distinct phenotypically from each other and from *T. ipatinga* (cf. Remarks, *T. tantalus*). In the phylogenetic hypothesis, samples of *T. ipatinga* form a monophyletic group and are included in a clade with *T.* aff. *caipora*, *T. melanopygius* and *T. tantalus*, but its closest relative is unresolved.

Geographical distribution: Trichomycterus ipatinga is distributed in headwaters throughout the entire
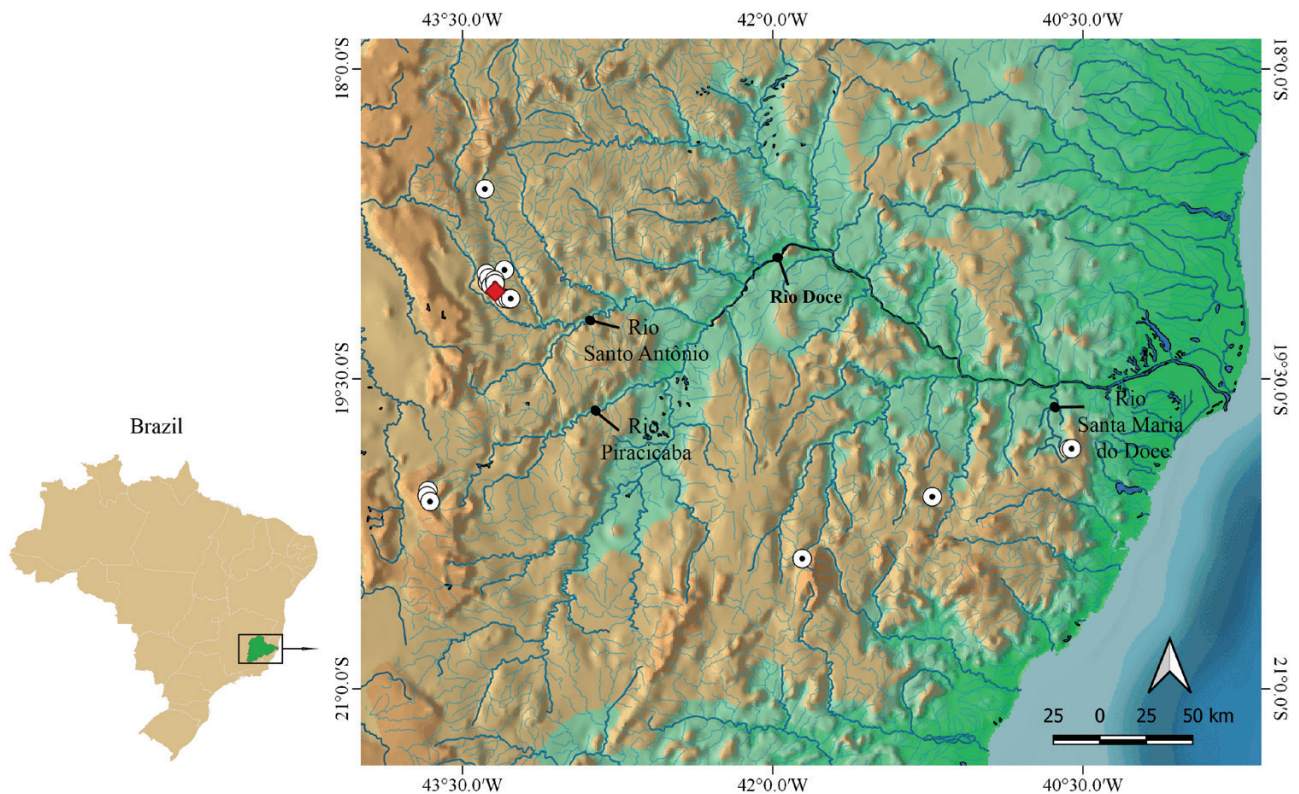
Figure 30. Geographical distribution of *Trichomycterus ipatinga* sp. nov. in the Rio Doce Basin. Red diamond = holotype (MZUSP 112279); white dotted circles = paratypes (MZUSP 87814, 104682, 104699, 104700, 104701, 104702, 104706, 109370, 109385, 109393, 112237, 112241, 112253, 112260, 112270, 112271, 112277, MBML 4337, 4340, 6223, 6825, 6844).

Rio Doce Basin ([Fig. 30](#)), but not in the main channel. The same phenomenon happens with *T. melanopygius* according to Reis *et al.* (2020). As with the latter species, such absence is not a result of the destruction of the main channel by the Samarco Dam rupture, because older collection records from the main channel also fail to reveal the species. Thus, the species distribution seems to be a result of habitat preferences, with the main channel serving as a dispersion corridor only.

TRICHOMYCTERUS MELANOPYGIUS REIS ET AL., 2020
(FIG. 31)

Trichomycterus melanopygius Reis, dos Santos, Britto, Volpi & de Pinna, 2020: 4, figs 1–3 [type locality: Brazil, state of Minas Gerais, Rio Doce Municipality, Rio Doce Basin, Córrego dos Borges, stream flowing into left bank of Risoleta Neves Reservoir, (20°12'21.63"S 42°52'56.24"W)]; col. V.J.C. Reis, M.C.C. de Pinna, G.F. de Pinna & G. Ballen, 24 June 2018.

Diagnosis: The combination of the following traits distinguishes *T. melanopygius* from its congeners: (1) the combination of invariably uniform body coloration with a horizontal dark stripe in the middle of caudal fin; (2) pectoral-fin rays I + 7 (vs. I + 5, I + 6 or I + 8); (3) post-Weberian vertebrae 38–40 (vs. fewer). Among congeners in south-eastern South America, character 1 distinguishes *T. melanopygius* from all species except young stages of *T. immaculatus*; character 2 distinguishes it from all species in the *T. brasiliensis* and *T. reinhardti* species complex (Barbosa & Costa, 2010; Costa, 2021; Costa & Katz, 2021), plus *T. trefauti* (with I + 6 or fewer) and from *T. astromycterus*, *T. caipora*, *T. giganteus*, *T. immaculatus*, *T. lauryi*, *T. nigricans* and *T. tantalus* (with I + 8 or more); character 3 distinguishes *T. melanopygius* from all congeners except for *T. candidus*, *T. claudiae*, *T. gasparinii* and *T. novalimensis*. Among congeners in the Rio Doce Basin, *T. melanopygius* is most similar to *T. immaculatus*. In addition to characters above, *T. melanopygius* can be further distinguished from *T. immaculatus* by a number of anatomical features: (1) hyomandibula narrow, with a deep concavity at middle of its dorsal margin (vs. hyomandibula wide, with a small and attenuated dorsal concavity; Reis *et al.*, 2020: fig. 4); (2) opercular patch of odontodes small, its height 10.3–14.3% HL (vs. 14.9–20%); (3) differently shaped urohyal, with a slender head and wide wings (vs. a wide head and slender wings) (Reis

Figure 31. *Trichomycterus melanopygius* (top: lateral; middle: dorsal; and bottom: ventral views). MZUSP 123762, holotype, 64.3 mm SL; Brazil, state of Minas Gerais, Rio Doce Basin, Córrego dos Borges.

et al., 2020: figs 5–6); (4) uncinate process of second epibranchial long and undivided (vs. short and forked; Reis *et al.*, 2020: fig. 7); and (5) third pharyngobranchial thin (vs. thick; Reis *et al.*, 2020: fig. 7). In addition to morphological distinctions, the barcoding distance between *T. melanopygius* and *T. immaculatus* is 3.8% (Table 2).

Description: Morphometric data for specimens examined is presented in Table 13. Body long and almost straight, trunk roughly round in cross-section near head, then slightly deeper than broad and gently compressed to caudal peduncle, tapering to caudal fin. Dorsal profile of body gently convex to dorsal-fin origin, then straight or slightly concave along caudal peduncle to caudal-fin origin. Ventral profile convex from gular region to vent, due partly to abdominal distension, then straight or slightly concave along anal-fin origin to caudal-fin base. Caudal peduncle as deep as body at beginning of anal-fin base.

Head approximately 1/4 of SL, pentagonal, longer than wide and depressed. Mouth subterminal. Upper jaw slightly longer than lower. Upper lip wider than lower lip and laterally continuous with base of maxillary barbel. Lower lip small, approximately 2/3 width of upper one, partly divided into right and left portions by with median concavity. Lower lip with uniform covering of tiny villi, resulting in velvet-like surface and not clustered into large papillae. Region between upper and lower lips with slender fleshy lobe.

Dentary and premaxillary teeth similar to each other in shape. Dentary teeth conical, 43–57 arranged in four irregular rows, first row with 10–13 teeth, extending from base to slightly above the coronoid process, with size of individual teeth increasing markedly towards symphysis and from posterior to anterior rows. Total area of premaxillary teeth slightly smaller than that of dentary, with 45–60 teeth arranged irregularly in four rows, first row with approximately 12–13 teeth, over entire ventral surface of premaxilla. Premaxillary teeth conical.

Eye medium-sized, protruding, positioned dorsally on head, without free orbital rim and covered with transparent skin. Eye located on anterior half of HL, closer to lateral border of head than to the midline in dorsal view. Anterior naris surrounded by tube of integument directed anterolaterally, continuous posterolaterally with nasal barbel. Posterior naris closer to anterior naris than to eyes,

Table 13. Morphometric data of *T. melanopygius* based on holotype and part of paratype material (MZUSP 94508, 94537, 110714, 110932, 110936, 112748, 123762, MNRJ 38472, 46933, 46926, 48462, 48469)

	Holotype	Range (*N* = 23)	Mean	SD
Standard length (mm)	64.3	28.3–100.7	50.4	-
% of standard length				
Anal-fin base	9.9	7.1–13.6	9.2	2.5
Body depth	14.2	11.7–17.1	14.2	1.4
Caudal peduncle depth	13.7	9.4–13.8	12.1	1.0
Dorsal-fin base	14.5	9.2–18.9	11.1	2.0
First pectoral-fin length	12.3	10.9–18.4	14.9	5.1
Head length	19.7	18.0–24.3	21.0	1.5
Preanal length	74.0	63.1–75.0	71.4	2.2
Predorsal length	64.7	53.1–68.3	64.o	2.8
Prepelvic length	57.9	51.2–59.7	58.8	2.1
% of head length				
Eye diameter	19.3	12.7–20.5	16.5	2.0
Interorbital width	26.3	18.9–27.0	23.0	2.5
Snout length	45.1	38.8–53.2	45.0	3.7
Mouth width	35.7	26.1–40.0	33.0	4.1
Length of opercle	19.3	16.8–21.9	19.5	1.4
Height of opercle	13.6	10.3–14.3	12.7	1.2

surrounded by tube of integument incomplete posteriorly. Maxillary barbel narrowing markedly towards fine tip, reaching from lateroposterior side of interopercle until base of pectoral fin. Rictal barbel inserted immediately ventral to maxillary barbel, its tip reaching from anterolateral to the middle of interopercle. Nasal barbel originating on posterolateral region of anterior naris, reaching from posterior border of eyes to anterior portion of opercle. Interopercular patch of odontodes large, oval in shape and with well-developed odontodes, prominent in ventral aspect of head. Interopercular patch of odontodes extending from vertical through ventroposterior border of eye to ventroanterior to opercle patch of odontodes. Interopercular odontodes arranged in two or three irregular series, with those on mesial series much longer than those on lateral one; odontodes gradually larger posteriorly in both series, with those posteriorly on mesial row largest. Interopercular odontodes 39–51. Opercular patch of odontodes on dorsolateral surface of posterior part of head, positioned anterodorsally to pectoral-fin base, roundish in shape and larger than eye in dorsal aspect of head. Opercular odontodes 18–23, sunk in individual slits of integument, progressively larger posteriorly, all with fine tips, with largest ones curved distally and claw-like. Entire patch surrounded by fleshy fold rim of integument.

Pectoral fin with its base immediately posterior and ventral to opercular patch of odontodes. Pectoral-fin rays I + 7 or rarely I + 8. First pectoral-fin ray (unbranched) longer, prolonged as filament beyond fin margin. Other rays progressively less longer, their tips following continuous line along fin margin. Pelvic fin with convex distal margin, its origin slightly posterior to middle of SL and anterior to vertical through dorsal-fin origin, covering anal and urogenital openings in adults. Base of pelvic fins positioned close to each other. Pelvic-fin rays I + 4, first ray unbranched. Anterior process of basipterygium short and thin. Dorsal fin long, its distal profile sinusoidal. Dorsal-fin origin closer to base of caudal fin than to tip of snout. Dorsal-fin rays iii + II + 7 (6) or iii + II + 6 (1), three unsegmented and unbranched rudimentary rays, two segmented and unbranched procurrent rays and six or seven branched and segmented rays. Anal fin slightly smaller than dorsal fin, its distal margin gently convex. Anal-fin origin posterior to vertical through end of dorsal-fin base. Anal-fin rays ii + II + 5 (2) or iii + II + 5 (5), two unsegmented and unbranched rudimentary rays, two segmented and unbranched procurrent rays and five branched and segmented rays. Caudal fin round to subtruncate, with 6 + 7 principal rays. Adipose fin absent or modified into low integumentary fold extending between end of dorsal fin and caudal-fin origin. Post-Weberian vertebrae 38 (5), 39 (2) or 40 (1). First dorsal-fin pterygiophore immediately anterior to neural spine of 18th (1), 19th (3) or 20th (1) vertebra, first anal-fin pterygiophore immediately anterior to haemal spine of 22th (7) or 23rd (2) vertebra. Caudal-fin procurrent rays plus one segmented non-principal ray dorsally and ventrally. Procurrent caudal-fin rays 17–22 (9) dorsally and 14–16 (9) ventrally, beginning anteriorly at 34th (1) or 35th (1) vertebrae. Ribs 12 (1), 13 (5) or 14 (2). Branchiostegal rays 7 (5) or 8 (2). Dorsal-fin pterygiophores 8. Anal-fin pterygiophores 6.

Cephalic lateral line canals with simple, non-dendritic tubes ending in single pores. Supraorbital canal mostly in frontal bone. Supraorbital pores invariably present: s1 mesial to nasal-barbel base and autopalatine, s3 mesial to posterior nostril and anterior to frontal and paired s6 posteromedial to eye and at midlength of frontal. Infraorbital laterosensory canal incomplete with four pores, i1 and i3 anteriorly and i10 and i11 posteriorly. Canal extending from sphenotic posteriorly to terminal pore located ventroposteriorly to eye. Infraorbital pore i1 located ventrolateral to nasal-barbel base and autopalatine, i3 ventro-lateral to posterior nostril and anterior to frontal, i10 and i11 posterior to eye. Otic canal without pores. Postotic pores po1, anteromedial to opercular patch of odontodes, and po2, mesial to opercular patch of odontodes. Lateral line of trunk anteriorly continuous with postotic canal and reduced to short tube. Lateral line pores ll1 and ll2 dorsomedial to pectoral-fin base.

Coloration in ethanol: Dorsal and lateral parts of body covered with uniform scattering of dark chromatophores on inner and outer layers of skin, not forming maculae or spots. Ventral part of body, from lower lip to anal-fin base, without pigment. Dorsal and anal fins darkly pigmented, but each with conspicuous unpigmented band longitudinally along their middle portion. Caudal fin with broad longitudinal dark stripe from base of middle caudal-fin rays nearly to margin of fin. Caudal stripe more evident in young specimens (a pattern similar to that in *T. ipatinga* and *T. tantalus*). Integument surrounding opercular odontodes darkly pigmented. Interopercular patch of odontodes without dark pigment. In life, *T. melanopygius* has the same basic coloration pattern, but with more vivid colours and less opaque integument and fins (Reis *et al.*, 2020: fig. 3). The body is a uniform brown colour, slightly darker on head. Pectoral-, dorsal- and caudal-fin rays are finely outlined in dark and the longitudinal caudal-fin stripe is conspicuously visible.

Remarks: Trichomycterus melanopygius is easily mistaken for *T. immaculatus*, due to some similarities such as the uniformly dark colour pattern (similar to the most common colour morph of the latter species) and the first pectoral-fin ray prolongued as a long filament. However, *T. melanopygius* is distinguished from *T. immaculatus* by several additional morphological and molecular features, such as I + 7 pectoral-fin rays, rarely I + 8 (vs. invariably I + 8 for *T. immaculatus*), 38–40 post-Weberian vertebrae (vs. 34 to 37 in *T. immaculatus*), by the more posteriorly positioned first dorsal-fin pterygiophore (anterior to neural spine 18–20 vs. 16 or 17 in *T. immaculatus*) and by the different shape of some bones, as presented in the original description

(Reis *et al.*, 2020). Additionally, *T. melanopygius* is well-differentiated by DNA barcoding, with 3.8% divergence from *T. immaculatus* (against 0.3% intraspecific divergence). Phylogenetically, the species is not closely related to *T. immaculatus*, instead forming a clade with *T.* aff. *caipora*, *T. ipatinga* and *T. tantalus*. Despite clear-cut morphological distinctiveness of the species, samples of *T. melanopygius* do not form a monophyletic group on the basis of *COI* data.

Geographical distribution: Trichomycterus melanopygius is distributed in tributaries throughout the Rio Doce Basin. It has so far not been recorded from the main channel (Fig. 32). This distribution pattern is similar to that of *T. ipatinga* (see later species for additional information).

Type material examined: all from Brazil, state of Minas Gerais, Rio Doce Basin. Holotype: MZUSP 123762, 64.0 mm SL, Córrego dos Borges, stream flowing into left bank of Risoleta Neves Reservoir. Paratypes: MNRJ 38472, 2, 34.2–38.7 mm SL; Catas Altas, Rio Conceição, tributary to Rio Piracicaba (20°0'20"S 43°30'28"W); col. M.R. Britto & J. Gomes, 28 November 2010; MNRJ 46933, 2, 51.9 (c&s), 59.1 mm SL; Conceição do Mato Dentro, Córrego Pica-Pau, tributary to Ribeirão Santo Antônio (also called Cruzeiro) (18°46'58"S 43°33'11"W); col. S.A. dos Santos, D.F. Moraes Jr. & M.R. Britto, 5 March 2016. MNRJ 46926, 5, 29.6–65.1 mm SL; Conceição do Mato Dentro, Ribeirão Santo Antônio (also called Cruzeiro), near confluence with Pica-Pau Creek (18°47'0"S 43°33'37"W); col. S.A. dos Santos, D.F. Moraes Jr. & M.R. Britto, 5 March 2016; MNRJ 48462, 5, 37.9–97.2 mm SL; Conceição do Mato Dentro, Santo Antônio Stream (also called Cruzeiro), near confluence with Pica-Pau Creek (18°47'0"S 43°33'37"W); col. S.A. dos Santos, D.F. Moraes Jr. & M.R. Britto, 30 July 2016; MNRJ 48469, 1, 95.0 mm SL; Conceição do Mato Dentro, Pica-Pau Creek, tributary of Santo Antônio Stream (also called Cruzeiro) (18°47'1"S 43°33'23"W); col. S.A. dos Santos, D.F. Moraes Jr. & M.R. Britto, 30 July 2016. MZUSP 94508, 1, 34.7 mm SL; Desterro de Melo, Ribeirão Xopotó, at bridge in town of Desterro de Melo (21°8'53"S 43°30'46"W); col. O.T. Oyakawa, E. Baena & M. Loeb, 10 July 2007; MZUSP 94537, 1, 41.1 mm SL; Desterro de Melo, Ribeirão Xopotó at entrance of town of Desterro de Melo (21°9'10.00"S 43°31'28.00"W); col. O.T. Oyakawa, E. Baena & M. Loeb, 10 July 2007; MZUSP 110714, 1, 69.1 mm SL; Itambé do Mato Dentro, Tanque River (19°25'28.00"S 43°12'1.00"W); col. A. de Castro & R. Pádua, 5 August 2010; MZUSP 110932, 2, 28.3–100.7 mm SL; Mariana, Rio Gualaxo do Sul (20°30'16.97"S 43°24'39.28"W); col. L.F. Salvador Jr. & L.A.C. Missiaggia, 5 July 2012. MZUSP 110936, 97.7 mm SL; Mariana, Gualaxo do Sul River (20°25'59.995"S 43°23'46.756"W); col. L.F. Salvador Jr. & L.A.C. Missiaggia, 5 June 2012.
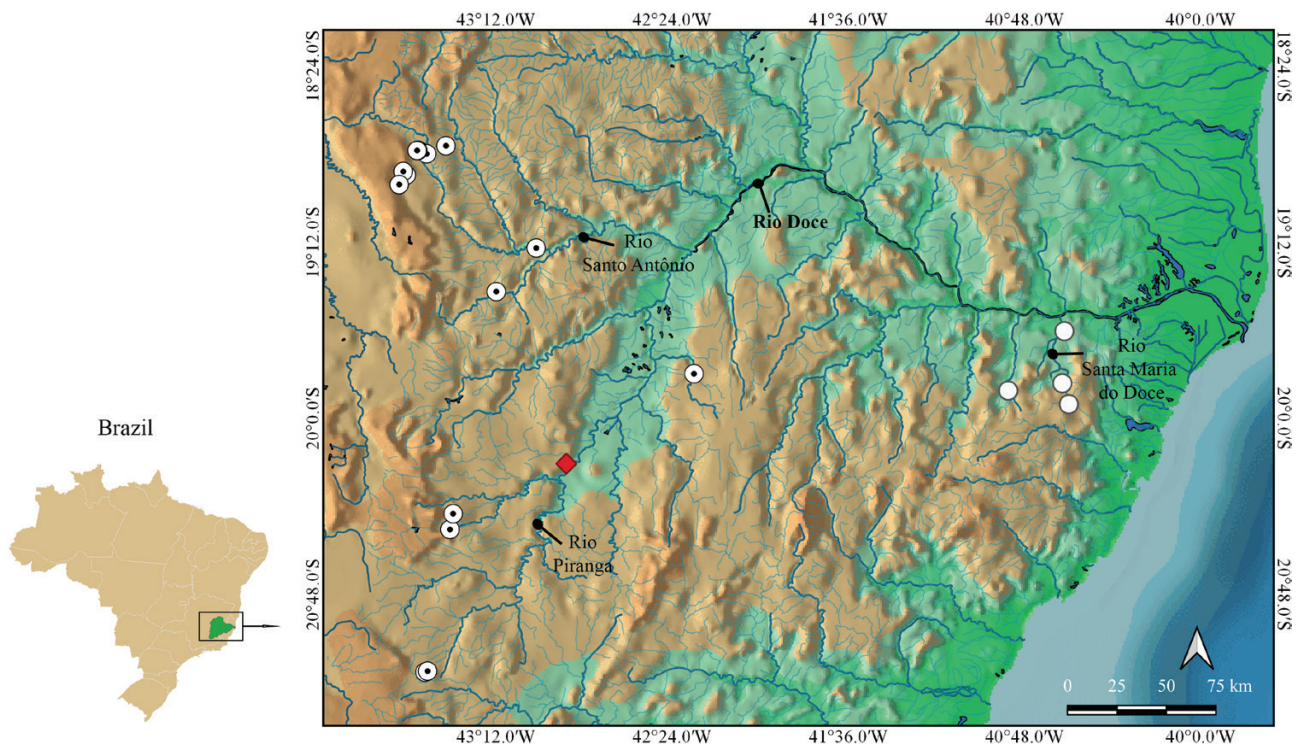
Figure 32. Geographical distribution of *T. melanopygius* in the Rio Doce Basin. Red diamond = holotype (MZUSP 123762); white dotted circles = paratypes (MNRJ 38472, 46933, 46926, 48462, 48469, 94508, 94537, 110714, 110932, 110936, 112748); white circles = non-type localities.

MZUSP 112748, 4, 37.2–49.2 mm SL, 2 c&s (42.8–49 mm SL); Ferros, Santo Antônio River, at bridge in downtown Ferros (19°13'34.5"S 43°1'9.5"W); col. O.T. Oyakawa & T.F. Teixeira, 16 August 2012.

Additional material studied: All from Brazil, Rio Doce Basin. MZUSP 121713, 6, 16.7–22.4 mm SL, 2 c&s, 17.5–17.8 mm SL; Coronel Fabriciano, cachoeira da Limeira, Rio Piracicaba, state of Minas Gerais (19°23'42.63"S 42°42'51.30"W); col. V.J.C. Reis, 22 March 2017. MBML 54, 2, 44.8–46.0 mm SL; Colatina, Santa Maria do Rio Doce River, state of Espírito Santo (19°36'14.00"S 40°37'13.00"W); col. R.L. Teixeira & J.A.P. Scheneider, 29 August 1996. MBML 701, 3, 36.5–71.9 mm SL; Itarana, Rio Santa Joana, state of Espírito Santo (19°52'26.00"S 40°52'31.00"W); col. R.L. Teixeira & P.S. Miller, 19 August 2000. MBML 1049, 1, 107.0 mm SL; Santa Teresa, Córrego Vinte e Cinco de Julho, Santa Maria do Rio Doce River, state of Espírito Santo (19°56'8.00"S 40°36'1.00"W); col. R.L. Teixeira, 19 March 2005. MBML 6151, 1, 65.3 mm SL; Santa Teresa, Cinco de Novembro Tiver (tributary to Santa Maria do Rio Doce River), next to road ES-080 to Santo Antônio do Canaã, state of Espírito Santo (19°50'26.00"S 40°37'47.30"W); col. C.J. Cunha, J.P. Silva & R.B. Soares, 20 August 2012. MNRJ 38505, 1, 42.4 mm SL; Catas Altas, Córrego do Frade (tributary of Ribeirão Caraça), state of Minas Gerais

(20°7'53"S 43°34'21"W); col. M.R. Britto & J. Gomes, 12 January 2010. MNRJ 42073, 2, 28.5–39.0 mm SL; Catas Altas, Córrego do Engenho (tributary of Ribeirão Caraça), state of Minas Gerais (20°2'9"S 43°29'28"W); col. M.R. Britto, D.F. Moraes Jr. & D. Almeida, 6 October 2013. MNRJ 45816, 1, 25.6 mm SL; Conceição do Mato Dentro, Rio Parauninha (tributary of Santo Antônio River), at Baú Village, state of Minas Gerais (18°56'16"S 43°38'30"W); col. S.A. dos Santos, D.F. Moraes Jr. & M.R. Britto, 2 March 2016. MNRJ 46854, 1, 24 mm SL; Congonhas do Norte, Rio Lambari (also called Cachoeira do Jacu) (left-hand tributary to Rio Parauninha), at Coqueiros Village, state of Minas Gerais (18°52'43"S 43°37'23"W); col. S.A. dos Santos, D.F. Moraes Jr. & M.R. Britto, 2 March 2016. MNRJ 46865, 1, 88.8 mm SL; Congonhas do Norte, Rio Lambari (also called Cachoeira do Jacu) (left-hand tributary to Rio Parauninha), at bridge at road Conceição do Mato Dentro-Congonhas do Norte, state of Minas Gerais (18°53'43"S 43°36'34"W); col. S.A. dos Santos, D.F. Moraes Jr. & M.R. Britto, 2 March 2016. MNRJ 47902, 1, 85.4 mm SL; Alvorada de Minas, Ribeirão das Pedras (right-hand tributary to Rio do Peixe), state of Minas Gerais (18°45'43"S 43°25'45"W); col. R.F. Miranda, A. Correia & M. Castro, 22 December 2015. MNRJ 48404, 1, 32 mm SL; Conceição do Mato Dentro, Rio Parauninha (right-hand tributay to Santo Antônio River), upstream of Candeias Village, state of

Minas Gerais (18°56'16"S 43°38'29"W); col. S.A. dos Santos, D.F. Moraes Jr. & M.R. Britto, 2 August 2016. MNRJ 48477, 1, 31.8 mm SL; Conceição do Mato Dentro, Ribeirão Santo Antônio do Norte (tributay to Santo Antônio River), upstream of Santo Antônio do Norte Village, state of Minas Gerais (18°47'54"S 43°31'0"W); col. S.A. dos Santos, D.F. Moraes Jr. & M.R. Britto, 30 July 2016.

TRICHOMYCTERUS REINHARDTI (EIGENMANN, 1917)

(FIG. 33)

Pygidium reinhardti Eigenmann, 1917: 699 [type locality: Rio Itabira at Burmier (probably Miguel Burnier, a district of the municipality of Ouro Preto), tributary of Rio das Velhas, Brazil; holotype (unique): FMNH 58081, ex CM 7078]; Eigenmann, 1918: 333 (redescription); Henn, 1928: 80 (type catalogue); Ibarra & Stewart, 1987: 73 (type catalogue); Ferraris, 2007: 422 (checklist).

Trichomycterus reinhardti Burgess, 1989: 323 (list); Fernández & Bichuette, 2002: 278 (comparison); de Pinna & Wosiacki in Reis *et al.*, 2003: 283 (checklist); Wosiacki & Garavello, 2004: 3 (list); Bockmann & Sazima, 2004 (colour comparison); Bockmann *et al.*, 2004: 227 (cited); Sato *et al.*, 2004 (cytogenetics); Alencar & Costa, 2006: 48 (diagnosis); Ferraris, 2007: 422 (checklist); Barbosa & Costa, 2010: 121 (comparison); Datovo *et al.*, 2012: 36 (comparative material); Katz *et al.*, 2013 (diagnosis); Donin *et al.*, 2020: 16 (comparison), Ochoa *et al.*, 2017 (relationships); Ochoa *et al.*, 2020 (relationships); Costa & Katz, 2021: 18 (phylogeny); Costa, 2021 (taxonomic discussion).

Diagnosis: The combination of the following traits distinguishes *T. reinhardti* from congeners: 1—broad mid-lateral dark stripe with notched edges extending from posterior margin of opercle to base of caudal fin; 2—reduced opercular armature, with 6–7 odontodes (vs. count more numerous); 3—pectoral-fin rays I + 5, (vs. I + 6, I + 7 or I + 8); 4—horizontal dark stripe along middle caudal-fin rays, more evident in juvenile specimens (vs. stripe absent); 5—pelvic-fin rays I + 4 (vs. I + 3); 6—ribs 14 (vs. 16–19). Among congeners in south-eastern South America, character 1 distinguishes *T. reinhardti* from all congeners except for *Trichomycterus anaisae* Costa & Katz, 2021, *Trichomycterus funebris* Costa & Katz, 2021, *T. humboldti* Costa & Katz, 2021, *Trichomycterus ingaiensis* Costa & Katz, 2021, *Trichomycterus luetkeni* Costa & Katz, 2021, *T. pauciradiatus* Alencar & Costa, 2006, *T. piratymbara* Katz *et al.*, 2013, *T. sainthilairei* Costa & Katz, 2021 and *Trichomycterus septemradiatus* Katz *et al.*, 2013; character 2 from all congeners; character 3 from all congeners except for *T. humboldti*, *T. sainthilairei*, *T. pauciradiatus* and *T. piratymbara*; character 4 from all congeners except for *T. immaculatus*, *T. ipatinga*, *T. melanopygius*, *T. reinhardti* species complex (Costa & Katz, 2021) and *T. tantalus*; character 5 from *T. humboldti* and *T. pauciradiatus*; character 6 from *T. piratymbara*, *T. funebris*, *T. ingaiensis* and *T. sainthilairei*.

Description: Morphometrics in Table 14. Body long and almost straight, trunk roughly round in cross-section near head, then slightly deeper than wide and
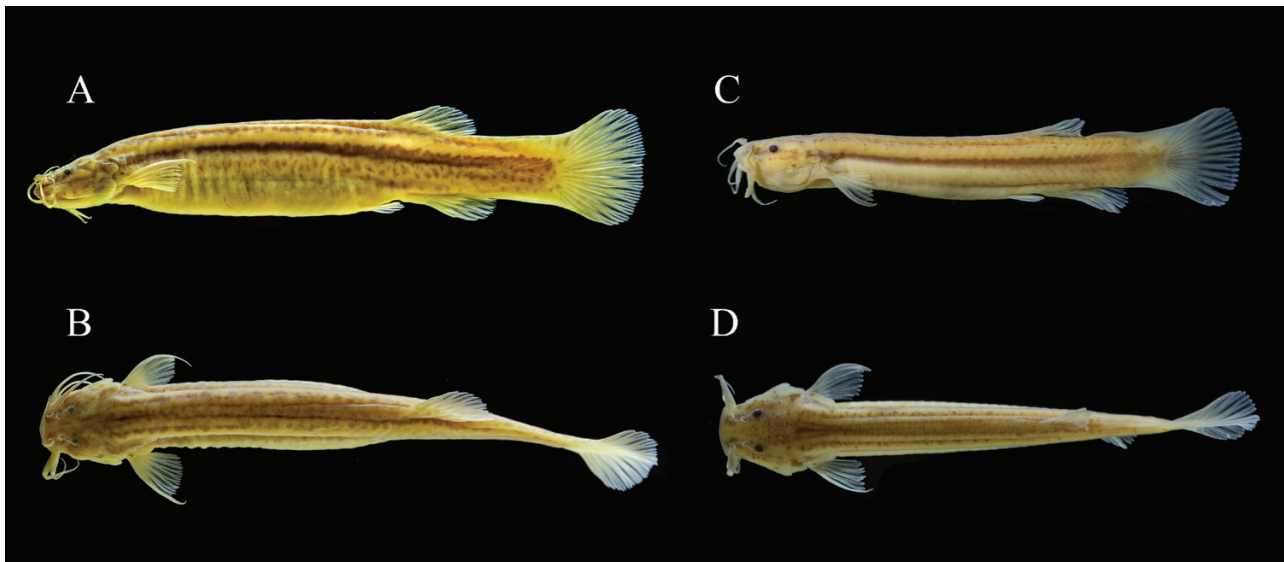
Figure 33. *Trichomycterus reinhardti* (A and C: lateral; B and D: dorsal views). MNRJ 21560, A-B, 60.4 mm SL; C-D, 28.5 mm SL; Brazil, Minas Gerais, south-east of the Ouro Preto-Ouro Branco Road, small stream in deep ravine, Rio Doce Basin.

Table 14. Morphometric data of *T. reinhardti* based on holotype (FMNH 58081) and non-type material from the Rio Doce (MNRJ 21560)

	Holotype	Range (N = 2)	Mean	SD
Standard length (mm)	53.1	28.5–60.4	47.3	-
% of standard length				
Anal-fin base	7.7	7.0–10.2	8.3	1.7
Body depth	13.9	14.o–16.7	14.9	1.6
Caudal peduncle depth	11.5	12.3–12.7	12.2	0.6
Dorsal-fin base	9.6	10.2–10.6	10.1	0.5
First pectoral-fin length	14.7	13.9–14.2	14.1	0.2
Head length	16.7	15.5–18.6	16.9	1.6
Preanal length	72.1	69.8–77.0	73.0	3.7
Predorsal length	68.8	64.9–68.4	67.4	2.12
Prepelvic length	61.5	62.5–63.1	62.4	0.8
% of head length				
Eye diameter	14.5	11.8–13.2	13.2	1.4
Interorbital width	30.0	26.7–30.2	29.0	2.0
Snout length	37.5	45.9–46.4	43.3	5.0
Mouth width	34.0	35.3–32.1	33.8	1.6

gently compressed towards caudal peduncle, tapering to caudal fin. Dorsal profile of body straight or gently convex to dorsal-fin origin, then straight or slightly concave along caudal peduncle to caudal-fin origin. Ventral profile convex from gular region to vent, due partly to abdominal distension, then straight or slightly concave along anal-fin origin to caudal-fin base. Caudal peduncle almost as deep as body at beginning of anal-fin base.

Head approximately 1/5 of SL, roughly pentagonal, slightly longer than wide and depressed. Mouth sub-terminal. Upper jaw slightly longer than lower one. Upper lip wider than lower lip, laterally continuous with base of maxillary barbel. Lower lip small, approximately 2/3 width of upper one, partly divided into right and left portions by median concavity. Lower lip with uniform covering of tiny villi, not clustered into large papillae, resulting in velvet-like surface. Region between upper and lower lips with slender fleshy lobe.

Dentary and premaxillary teeth similar to each other in shape. Dentary teeth conical, 27–30, arranged in three or four irregular rows, first row extending from base to slightly up of coronoid process, with size of individual teeth increasing markedly towards symphysis and from posterior to anterior rows. Premaxillary teeth conical, 26–27, arranged in three or four irregular rows over entire ventral surface of premaxilla. Total area of premaxillary teeth visually slightly smaller than that of dentary.

Eye slightly protruding, positioned dorsolaterally on head, without free orbital rim and covered with transparent skin. Eye located on anterior half of HL, closer to lateral border of head than to the midline in dorsal view. Anterior naris surrounded by tube of integument directed anterolaterally, continuous posterolaterally with nasal barbel. Posterior naris closer to anterior naris than to eyes, rimmed anteriorly by flap of integument. Maxillary barbel narrowing markedly towards fine tip, reaching pectoral-fin base. Rictal barbel inserted immediately ventral to maxillary barbel, its tip reaching margin of interopercular patch of odontodes. Nasal barbel originating on posterolateral region of anterior naris, reaching posterior portion of opercular patch of odontodes. Interopercular patch of odontodes medium to large compared to head length, oval in shape and with well-developed odontodes, prominent in ventral aspect of head. Interopercular patch of odontodes extending from vertical through posterior margin of eye to vertical through anterior margin of opercular patch of odontodes. Interopercular odontodes 19 or 20, arranged in three or four irregular series, with those on mesial series longer than those on lateral one; odontodes gradually larger posteriorly in all series, with those posterior on mesial row largest. Opercular patch of odontodes on dorsolateral surface of posterior part of head, positioned anterodorsally to pectoral-fin base, roundish in shape and larger than eye in dorsal aspect of head. Opercular odontodes 6–7, sunk in individual slits of integument, progressively larger posteriorly, all with fine tips, with largest ones curved distally and claw-like. Entire patch surrounded by rim of integument.

Pectoral fin with its base immediately posterior and ventral to opercular patch of odontodes. Pectoral-fin rays I + 5 (3). First pectoral-fin ray (unbranched) longer, prolonged as filament beyond fin margin, with variable length. Other rays progressively shorter,

their tips following continuous line along fin margin. Pelvic fin with convex distal profile, slightly covering anal and urogenital openings in adults, its origin slightly posterior to middle of SL and anterior to vertical through dorsal-fin origin. Bases of pelvic fins separated by one eye diameter. Pelvic-fin rays I + 4. Anterior processes of basipterygium long and thin. Dorsal fin long, its distal margin sinusoidal. Dorsal-fin origin closer to base of caudal-fin than to tip of snout. Dorsal-fin rays ii + II + 7(2). Anal fin slightly smaller than dorsal fin, its distal margin gently convex. Anal-fin origin posterior to vertical through end of dorsal-fin base. Anal-fin rays ii + II + 5(2). Caudal fin truncated with round edges, with 6 + 7 principal rays. Adipose fin absent or represented by low integument fold extending between end of dorsal fin and caudal-fin origin. Post-Weberian vertebrae, 37(1) and 38 (1). First dorsal-fin pterygiophore immediately anterior to neural spine of 20th (1), vertebra, first anal-fin pterygiophore immediately anterior to neural spine of 22nd (1) and 23rd (1) vertebra. Caudal-fin procurrent rays plus one segmented non-principal ray dorsally and ventrally. Procurrent caudal-fin rays, 20 - 21 dorsally and 13 - 15 ventrally, beginning anteriorly at vertebrae 31. Ribs 14 (1), 15 (1). Branchiostegal rays 8. Dorsal-fin pterygiophores 8. Anal-fin pterygiophores 6.

Cephalic lateral-line canals with simple non-dendritic tubes ending in single pores. Supraorbital canal mostly in frontal bone. Supraorbital pores invariably present: s1 mesial to nasal-barbel base and autopalatine, s3 mesial to posterior nostril and anterior to frontal, and paired s6 posteromedial to eye and at midlength of frontal. Infraorbital latero-sensory canal incomplete, with four pores, i1 and i3 anteriorly and i10 and i11 posteriorly, extending from sphenotic posteriorly to terminal pore located ventroposteriorly to eye. Infraorbital pore i1 located ventrolateral to nasal-barbel base and autopalatine, i3 ventrolateral to posterior nostril and anterior to frontal, i10 and i11 posterior to eye. Otic canal without pores. Postotic pores po1, anteromedial to opercular patch of odontodes, and po2, mesial to opercular patch of odontodes. Lateral line of trunk anteriorly continuous with postotic canal and reduced to short tube. Lateral line pores ll1 and ll2 dorsomedial to pectoral-fin base.

Coloration in ethanol: Trichomycterus reinhardti has a distinct colour pattern that changes only slightly during development. In adults, basic pigmentation consisting of broad dark mid-lateral stripe, covering nearly 1/3 of body depth in lateral view and extending from posterior border of opercle to base of caudal fin. Stripe with notched edges formed by small dark spots usually overlapping each other. Long area dorsal and ventral to mid-lateral stripe, forming trailing white bands highlighting latter. On dorsum, colour pattern ranging from broad dark mid-dorsal band consisting of tiny dark spots occupying almost entire dorsum to three rows of round small maculae longitudinally arranged along dorsum: mid-dorsal row along entire dorsum from occiput to dorsal edge of caudal peduncle (forming a broad cloudy band in some adults and all young specimens), two rows ventrolaterally on each side of mid-dorsal one, extending from base of head to base of caudal fin. In young specimens, latter row consisting of small dark spots, forming notched edge. Ventral to mid-lateral stripe, row of tiny dark spots, less conspicuous and shorter than dorsal ones, extending along posterior part of abdomen, through midlength of body to base of caudal fin. Ventral side of abdomen lacking dark pigment. Head darkest on region corresponding to neurocranium, outlined by brain pigment seen by transparency. Dark spots randomly distributed over entire head, except region of levator operculi muscle. Distal margin of integument fold of opercular patch of odontodes darkly pigmented. Interopercular patch of odontodes lacking dark pigment. Fin rays outlined in dark coloration. Pelvic fin slightly pigmented only in large adults (64.5–70.0 mm SL). Caudal fin with broad longitudinal dark stripe from base of middle caudal-fin rays to nearly margin of fin. Caudal stripe more evident in young specimens (a pattern similar to that in *T. immaculatus*, *T. ipatinga* and *T. tantalus*).

Remarks: Trichomycterus reinhardti was described from Miguel Burnier on the Rio Itabira, a tributary of the Rio das Velhas, São Francisco Basin, at Minas Gerais State, Brazil (Eigenmann, 1918). Until recently, representatives of the species were known only from the São Franscisco and Rio Grande (Rio Paraná Drainage) basins in Central Minas Gerais State. However, Katz *et al.* (2021) reported two specimens of *T. reinhardti* (MNRJ 21560) from a small stream in the Gualaxo do Sul River, a tributary of the Rio Doce, this being the first record of the species in the Rio Doce. As suggested by the authors, that population might have reached the Rio Doce by headwater capture, since its locality is close to the São Francisco Basin. The phenomenon is common and may explain the across-basin distribution of a number of other species in the Rio Doce (see Discussion).

Trichomycterus reinhardti is a particularly distinctive species, which until recently could not be confused with any other *Trichomycterus*. Starting with Alencar & Costa (2006), a number of species obviously close to *T. reinhardti* have been described in the past 15 years, such as *T. pauciradiatus*, *T. septemradiatus*, *T. piratymbara*, *T. anaisae*, *T. sainthilairei*, *T. luetkeni*, *T. funebris*, *T. humboldti* and *T. ingaiensis* (Alencar & Costa, 2006; Katz *et al.*, 2013; Costa & Katz, 2021). All these species are from adjacent localities covering a continuous area of Central Minas Gerais State, with some of them from the same tributary of the São Francisco

as the type locality of *T. reinhardti* (Rio das Velhas). Morphometric and meristic characters used to segregate these species usually overlap, so their identification is difficult without resorting to locality information. The specimens found in the Rio Doce were considered as *T. reinhardti* by Costa & Katz (2021). Examination of the same specimens and comparisons with the holotype made herein confirm that identification. The status of the nine *T. reinhardti*-like species described more recently still needs close scrutiny.

Geographic distribution: Trichomycterus reinhardti was described from the Rio Itabira, a tributary of Rio das Velhas, Minas Gerais and is also present in the Rio Doce on a stream tributary of the Gualaxo do Sul River, bordering the São Francisco Basin (Fig. 34).

Type material examined: holotype FMNH 58081, 53.1 mm SL; Miguel Burnier, state of Minas Gerais, Brazil, Rio Itabira, tributary of Rio das Velhas; col. J. Haseman, 14 May 1908.

Additional material studied: Brazil, state of Minas Gerais. MNRJ 21560, 2, 28.5–60.4 mm SL; south-east of the Ouro Preto-Ouro Branco road, small stream at deep ravine, Rio Doce Basin, 20°29'57"S 43°37'13"W; col. P.A. Buckup, A.T. Aranda, M.R.S. Melo, F.M. Costa & J.J. Vital, 22 November 2000. MZUSP 109431, 5, 44.2–68.3 mm SL, 1 c&s 55.8 mm SL; Ouro Preto, stream at the right border of Córrego das Almas, tributary of the Rio das Velhas, São Francisco Basin, 20°23'51"S 43°53'04"W; col. G. Padilha, 22 March 2011. MZUSP 109371, 3, 59.4–64.2 mm SL; Caeté, Maquiné Creek, tributary of Ribeirão da Prata, tributary of Rio das Velhas, São Francisco Basin, 20°01'39"S 43°41'57"W; col. B. Maia, August 2010. MZUSP 82366, 2, 49.3–50.4 mm SL; Barbacena, Sapateiro Creek; col. J.C. Oliveira, A.L. Alves, L.R. Sato, 12 October 2001. MZUSP 90850, 2, 43.3–59.3 mm SL; Belo Horizonte, Parque das Manguabeiras, stream tributary of Rio das Velhas, São Francisco Basin; col. C.B.M. Alves, July 2002.

TRICHOMYCTERUS TANTALUS SP. NOV. REIS, VIEIRA, DE PINNA
(FIGS 6, 35)

Zoobank registration: urn:lsid:zoobank. org:act:F805C7B2-84E0-4B9C-97D5-94A41A7D2731

Holotype: MZUSP 123369, 76 mm SL; Brazil, state of Minas Gerais, Baguari, main stream of Rio Doce Basin (19°1'33.62"S 42°7'29.12"W); col. V. J. C. Reis & T. Pessali, 12 November 2017.

Paratypes: All from Brazil, state of Minas Gerais. MZUFV 2565, 1, 154 mm SL; Raul Soares, Matipó River, downstream from UHE Emboque (20°7'25.71"S 42°23'6.07"W); col. J. Dergam, 27 August 1998. MZUSP 126759, 23, 68.4–80.2 mm SL, 2 (c&s) 64.6–80.3 mm SL; same data as holotype.

Diagnosis: The combination of a yellowish body colour with uniform dark colour concentrated on dorsum with a bifurcated caudal fin is unique to *T. tantalus* among all congeners. The combination of the following traits further distinguishes *T. tantalus* from congeners: (1) numerous opercular odontodes (25–33); (2) I + 8 pectoral-fin rays; (3) three lateral-line pores (vs. two); and (4) caudal fin bifurcated. Among congeners in south-eastern South America, character 1 distinguishes *T. tantalus* from all except for *T. barrocus*, *T. caipora*, *T.* aff. *caipora*, *T. immaculatus* and *T. lauryi*; character 2 from all except for *T. astromycterus*, *T. caipora*, *T. giganteus*, *T. immaculatus*, *T. lauryi*, *T. nigricans*; character 3 from all except *T. astromycterus*, *T.* aff. *caipora*, *T. ipatinga*, *T. nigricans* and *T. vinnulus*; and character 4 from all except for *T. astromycterus*. Among congeners in the Rio Doce Basin, *T. tantalus* is most similar to *T. immaculatus*. In addition to characters above, *T. tantalus* is further distinguished from *T. immaculatus* by the more numerous dentary teeth (13–15 vs. 9–12). The two species are separated by a barcoding distance of 3.8%.

Description: Morphometric data for specimens examined is presented in Table 15. Body long and almost straight, trunk roughly round in cross-section near head, then slightly deeper than broad and gently compressed to caudal peduncle, tapering to caudal fin. Dorsal profile of body gently convex to dorsal-fin origin, then straight or slightly concave along caudal peduncle to caudal-fin origin. Ventral profile convex from gular region to vent, due partly to abdominal distension, then straight or slightly concave along anal-fin origin to caudal-fin base. Caudal peduncle thin and abruptly expanding at base of caudal fin, caused by increase in length of dorsal and ventral procurrent caudal-fin rays.

Head approximately 1/5 of SL, pentagonal, slightly longer than wide and depressed. Mouth subterminal. Upper jaw longer than lower. Upper lip wider than lower lip and laterally continuous with base of maxillary barbel. Lower lip small, atrophied in many specimens from MZUSP 126759, approximately 1/2 width of upper one, partly divided into right and left portions by median concavity. Lower lip with uniform covering of tiny villi, resulting in velvet-like surface and not clustered into large papillae. Region between upper and lower lips with slender fleshy lobe.
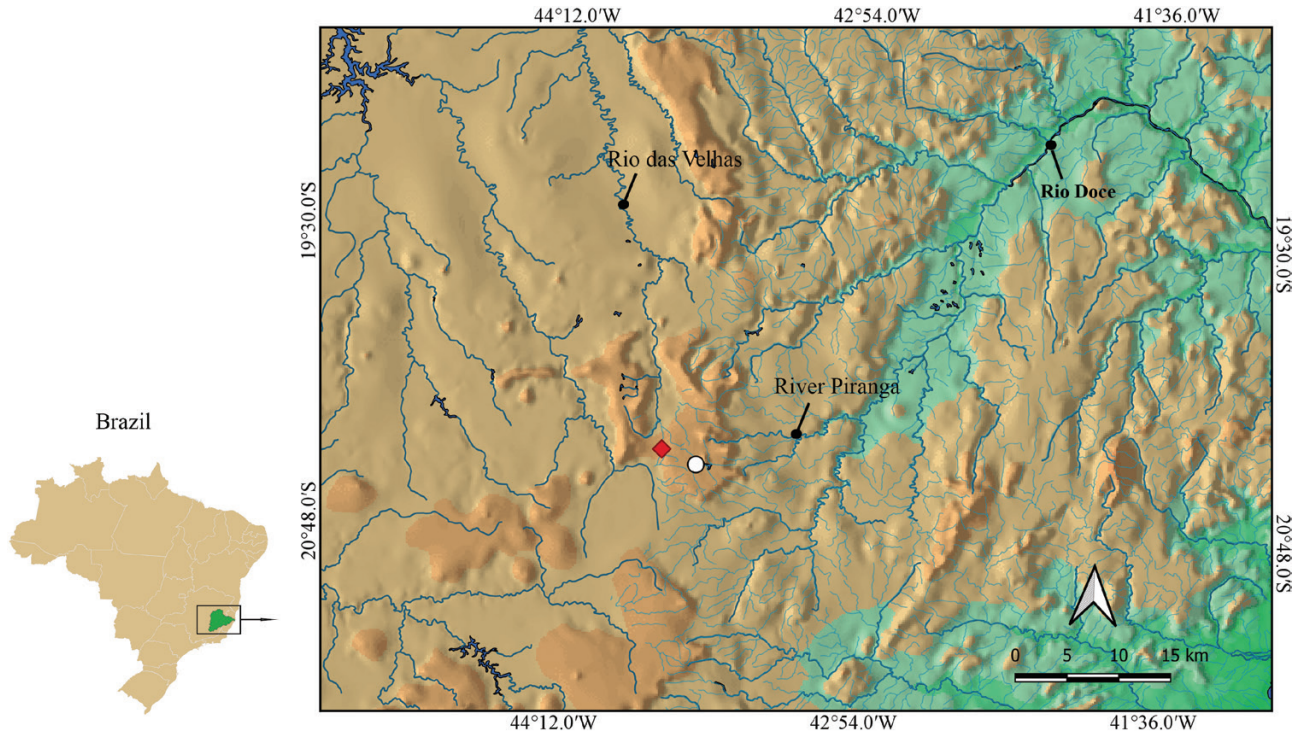
Figure 34. Geographical distribution of *T. reinhardti* in the Rio Doce Basin and in its type locality in the Rio São Francisco Basin. Red diamond = holotype (FMNH 58081); white circle = Rio Doce specimen (MNRJ 21560).

Dentary and premaxillary teeth similar to each other in shape. Dentary teeth conical, 67–75 arranged in four irregular rows, first row with 13–15 teeth, extending from base to slightly up of coronoid process, with size of individual teeth increasing markedly towards symphysis and from posterior to anterior rows. Total area of premaxillary teeth slightly smaller than that of dentary, with 67–70 conical teeth arranged in four irregular rows, first row with approximately 11–15 teeth, over entire ventral surface of premaxilla.

Eye medium-sized, slightly protruding, positioned latero-dorsally on head, without free orbital rim and covered with transparent skin. Eye located on anterior half of HL, closer to lateral border of head than to the midline in dorsal view. Anterior naris surrounded by tube of integument directed anterolaterally, continuous posterolaterally with nasal barbel. Posterior naris closer to anterior naris than to eyes, surrounded by tube of integument incomplete posteriorly. Maxillary barbel tubular narrowing markedly towards fine tip, reaching from anterior border of eyes until anteromesial border of interopercle. Rictal barbel inserted immediately ventral to maxillary barbel, its tip reaching from posterior border of posterior naris to posterior border of eyes, not touching the interopercle. Nasal barbel originating on posterolateral region of anterior naris, reaching from posterior border of posterior naris to slightly posterior to eyes. Interopercular patch of odontodes large compared to head length, oval in shape and with well-developed odontodes, prominent in ventral aspect of head. Interopercular patch of odontodes extending from vertical through ventroposterior border of eye to ventroanterior to opercle. Interopercular odontodes arranged in three or four irregular series, with those on mesial series much longer than those on lateral one; odontodes gradually larger posteriorly in both series, with those posteriorly on mesial row largest. Interopercular odontodes 40–52. Opercular patch of odontodes on dorsolateral surface of posterior part of head, positioned anterodorsally to pectoral-fin base, roundish in shape and large, 2 twice or more eye diameter in dorsal aspect of head. Opercular odontodes 25–33, sunk in individual slits of integument, progressively larger posteriorly, all with fine tips, with largest ones curved distally and claw-like. Entire patch surrounded by fleshy fold rim of integument.

Pectoral fin with its base posterior and ventral to opercular patch of odontodes. Pectoral-fin rays I + 8. First pectoral-fin ray (unbranched) longest and prolonged as filament beyond fin margin. Other rays progressively less long, their tips following continuous line along fin margin. Pelvic fin with convex distal margin, its origin slightly posterior to middle of SL and anterior to vertical through dorsal-fin origin, slightly

Figure 35. *Trichomycterus tantalus* sp. nov. (top: lateral; middle: dorsal; and bottom: ventral views). MZUSP 123369, holotype, 76 mm SL; Brazil, Minas Gerais, Baguari Municipality, main channel of Rio Doce Basin.

Table 15. Morphometric data of *T. tantalus* based on holotype and part of paratype material (MZUSP 123369,126759, MZUFV 2565)

	Holotype	Range (*N* = 10)	Mean	SD
Standard length (mm)	74.8	74.8–155.0	82.9	-
% of standard length				
Anal-fin base	8.7	7.2–8.7	8.0	0.4
Body depth	14.5	13.3–17.2	14.4	1.2
Caudal peduncle depth	10.7	9.4–12.5	10.5	0.9
Dorsal-fin base	8.9	8.9–12.1	10.1	0.9
First pectoral-fin length	12.7	12.2–15.0	13.6	0.9
Head length	20.9	19.8–22.1	20.8	0.8
Preanal length	71.0	69.1–73.4	71.5	1.5
Predorsal length	62.1	57.4–64.5	60.8	2.3
Prepelvic length	53.4	50.6–56.3	53.7	1.6
% of head length				
Eye diameter	16.9	13.4–17.1	15.2	1.2
Interorbital width	24.0	23.4–27.3	25.1	1.2
Snout length	45.8	43.0–51.4	45.4	2.3
Mouth width	30.4	30.4–42.8	34.0	3.5

covering anal and urogenital openings in adults. Bases of pelvic fins positioned close to each other. Pelvic-fin rays I + 4, first ray unbranched. Anterior process of basipterygium long, hook-like and laterally curved. Dorsal fin long, its distal margin sinusoidal. Dorsal-fin origin closer to base of caudal fin than to tip of snout. Dorsal-fin rays iii + II + 7 (1) or iv + II + 7 (1). Anal fin slightly smaller than dorsal fin, its distal margin gently convex. Anal-fin origin posterior to vertical through end of dorsal-fin base. Anal-fin rays iii + II + 5 or iv + II + 5. Caudal fin bifurcated, with 6 + 7 principal rays. Adipose fin absent or modified into low integumentary fold extending between end of dorsal fin and caudal-fin origin. Post-Weberian vertebrae 36 (2). First dorsal-fin pterygiophore immediately anterior to neural spine of 16th (1) or 17th (1) vertebra, first anal-fin pterygiophore immediately anterior to neural spine of 21st (1) or 22nd (1) vertebra. Caudal-fin procurrent rays plus one segmented non-principal ray dorsally and ventrally extending until 1/4 on caudal-fin rays. Procurrent caudal-fin rays, 16–17 dorsally and 13–14 ventrally, beginning anteriorly at 32nd vertebrae. Ribs 11 (1) or 12 (1). Branchiostegal rays 7 (2). Dorsal-fin pterygiophores 8. Anal-fin pterygiophores 6.

Cephalic lateral line canals with simple, non-dendritic tubes ending in single pores. Supraorbital canal mostly in frontal bone. Supraorbital pores invariably present: s1 mesial to nasal-barbel base and autopalatine, s3 mesial to posterior nostril and anterior to frontal, and single s6 posteromedial to eye and at midlength of frontal. Infraorbital latero-sensory canal incomplete with four pores, i1 and i3 anteriorly and i10 and i11 posteriorly. This canal extending from sphenotic posteriorly to terminal pore located ventroposteriorly to eye. Infraorbital pore i1 located ventrolateral to nasal-barbel base and autopalatine, i3 ventrolateral to posterior nostril and anterior to frontal, i10 and i11 posterior to eye. Otic canal without pores. Postotic pores po1, anteromedial to opercular patch of odontodes and po2, mesial to opercular patch of odontodes. Lateral line of trunk anteriorly continuous with postotic canal and reduced to short tube. Lateral line pores ll1, ll2 and ll3 present dorsomedial to pectoral-fin base.

Coloration in ethanol: Yellowish body with dark chromatophores homogeneously distributed not forming maculae. Dark pigmentation varying interspecifically from body totally darkly pigmented, except to ventral region (rare), to dark covering uniformly distributed dorsally from head to posterior end of caudal peduncle, laterally reaching mid-lateral line and abruptly ending ventral to that. Head darkest on region corresponding to neurocranium, outlined by brain pigment. Cheeks less heavily pigmented than neurocranium over area of dilatactor perculi muscle. Base of nasal barbels surrounded with concentration of dark pigment, extending posteriorly as elongate dark field to anterior margin of eyes. Distal margin of integument fold of opercular patch of odontodes darkly pigmented. Interopercular patch of odontodes white. Ventral side of the body lacking dark pigment. Base of pectoral and dorsal fins darkly pigmented. Caudal fin with broad longitudinal dark stripe from base of middle caudal-fin rays to nearly margin of fin.

Etymology: From the Ancient Greek mythological figure Τάνταλος (Tantalos), who was eternally tormented in the underworld, the word '*tantalus*' going on to refer to acts of torment in Latin and other languages. The name is chosen for the hypertrophied opercular patch of odontodes in this species, the largest among species of *Trichomycterus* in the Rio Doce Basin.

Remarks: Trichomycterus tantalus is a distinctive species, not only in the Rio Doce, but across the south-eastern Brazilian region. This is a rheophilic species, found so far only in the main channel of the Rio Doce and the main channel of the Rio Matipó. In both cases, specimens were collected near hydropower plants during fish transposition activities. The species has obvious rheophilic characters such as a bifurcated caudal fin (Lujan & Conway, 2015; Zanata *et al.*, 2020). Its extremely tough, resilient integument is also suggestive of an adaptation to withstand attrition among boulders in strong currents. Numerous specimens of *T. tantalus* display severe head abnormalities, such as deformed and asymmetrical metapterygoids, quadrate and autopalatines, bent mesethmoid and other deformities in anterior cranial bones. These abnormalities are perhaps caused by repeated trauma and subsequent healing in their turbulent habitat, where specimens supposedly collide often with rocks, causing osseous damage and growth aberrations. Interestingly, other species collected syntopically with *T. tantalus*, such as *T. immaculatus*, do not show such skeletal alterations.

Although it differs markedly morphologically from congeners in the Rio Doce Basin, *T. tantalus* differs relatively little in barcoding data from *T. ipatinga* (1.8%) and *T. melanopygius* (1.5%). Such low genetic distances among morphologically distinct species is a common phenomenon among Neotropical freshwater fishes (see Discussion below and Perdices *et al.*, 2002, 2005; Montoya-Burgos, 2003; Hubert *et al.*, 2007; Ornelas-Gacia *et al.*, 2008; Costa-Silva *et al.*, 2015). In the phylogenetic hypothesis (Fig. 1), all samples referable to *T. tantalus* cluster in a clade. The species is included in a group with *T.* aff. *caipora*, *T. ipatinga* and *T. melanopygius*, but its sister group is unresolved. Also, despite a normal degree of intraspecific morphological variation, *T. tantalus* displays low intraspecific DNA barcoding divergence (> 0.2%). The recently described

Trichomycterus largoperculatus Costa & Katz, 1922 (Zoosyst. Evol. 98, 13–21) from the Rio Paraíba do Sul, is probably closely related to *T. tantalus*. The two species share a caudal fin bilobed with pointed corners, nine pectoral-fin rays, a single s6 pore, and a vertical dark band across the base of the caudal fin. They differ in the number of lateral-line pores (two in *T. largoperculatus* and three in *T. tantalus*); and in the number opercular and interopercular odontodes respectively (48–62, 92–100 in *T. largoperculatus*, vs. 25–33, 40–52 in *T. tantalus*).

Geographical distribution: Trichomycterus tantalus occurs in the middle sectors of the main channel of the Rio Doce and in the main channel of the Matipó River (Fig. 36).

TRICHOMYCTERUS VINNULUS SP. NOV.

(Fig. 10, 37)

*Zoobank registration:* urn:lsid:zoobank. org:act:68036FCA-384B-4449-8FBA-626C38B445E1

Holotype: MZUSP 123750, 54.0 mm SL; Brazil, state of Minas Gerais, Rio Doce Municipality, Córrego dos Borges Creek running into left margin of the reservoir and the Rio do Peixe River, Risoleta Neves Hydroelectric Dam (20°12'21.63"S 42°52'56.24"W); col. V. J.C. Reis, M. de Pinna, G. Ballen, G. F. de Pinna, 24 June 2018.

Paratypes: MZUSP 126760, 43, 28.8–60.7 mm SL; same data as holotype; MZUSP 123757, 7, 32.3–59.3 mm SL; Rio Doce Municipality, Rio do Peixe, Rio Piranga Basin (left-margin tributary of Rio Doce, downstream from the Risoleta Neves reservoir) (20°11'40.32"S 42°51'8.47"W); col. V.J.C. Reis, M. de Pinna, G. Ballen, G.F. de Pinna, 24 June 2018.

Diagnosis: The combination of the following traits distinguishes *T. vinnulus* from other *Trichomycterus* species: (1) numerous round dark maculae randomly distributed throughout body; (2) pectoral fin rays I + 7 (vs. I + 5, I + 6 or I + 8); and (3) three lateral-line pores (vs. two). Among congeners in south-eastern South America, character 1 distinguishes *T. vinnulus* from all except some colour morphs of *T. brasiliensis*, *T. ipatinga* and *T. laury*; character 2 distinguishes *T. vinnulus* from all species in the *T. brasiliensis* and *T. reinhardti* species complexes (Barbosa & Costa, 2010; Costa, 2021; Costa & Katz, 2021), plus *T. trefauti* (with I + 6 or fewer) and from *T. astromycterus*, *T. caipora*, *T. giganteus*, *T. immaculatus*, *T. lauryi*,
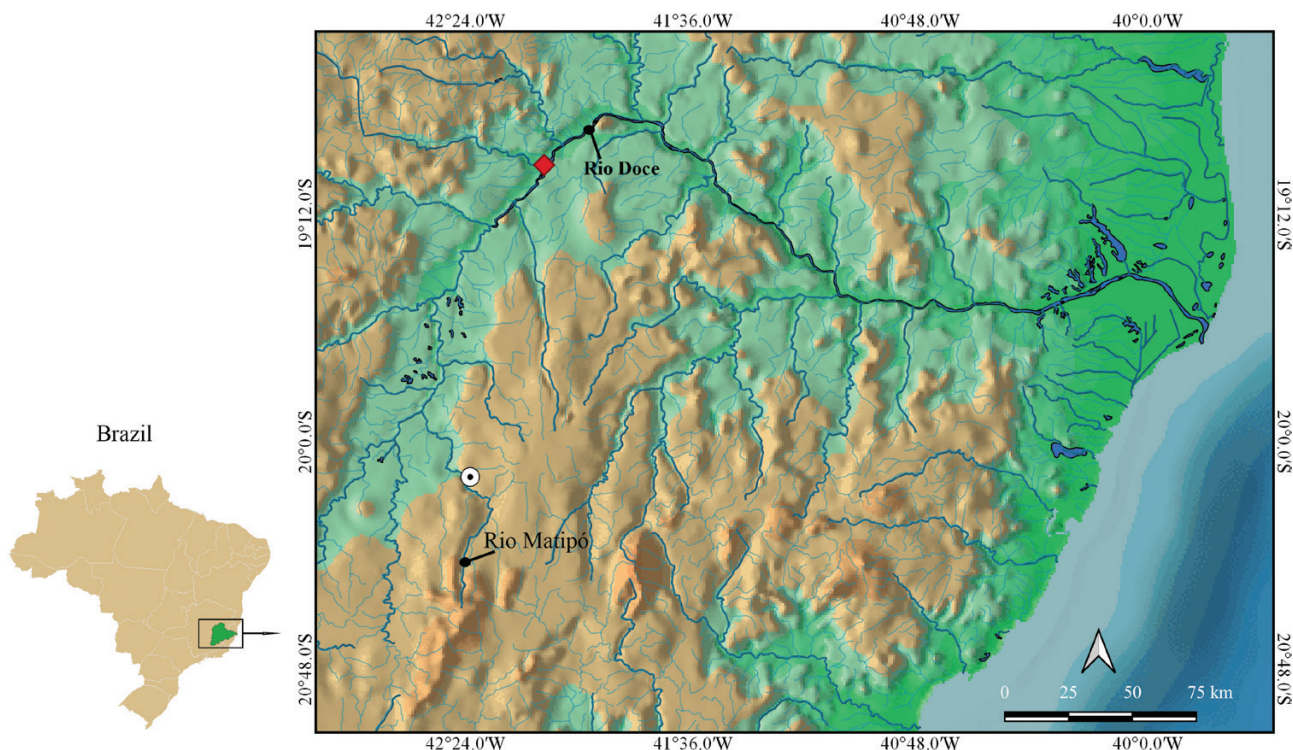
Figure 36. Geographical distribution of *T. tantalus* sp. nov. in the Rio Doce Basin. Red diamond = holotype (MZUSP 123369) and paratypes (MZUSP 126759); white dotted circle = paratype (MZUFV 2565).

Figure 37. *Trichomycterus vinnulus* sp. nov. (top: lateral; middle: dorsal; and bottom: ventral views). MZUSP 123750, holotype, 54 mm SL; Brazil, state of Minas Gerais, Rio Doce Municipality, Córrego dos Borges, tributary of Rio Doce Basin.

T. nigricans and *T. tantalus* (with I + 8 or more); character 3 from all except *T. astromycterus*, *T.* aff. *caipora*, *T. ipatinga*, *T. nigricans* and *T. tantalus*. Among congeners in the Rio Doce Basin, *T. vinnulus* is most similar to *T. ipatinga* and *T. alternatus*. In addition to the characters above, *T. vinnulus* can be further distinguished from *T. ipatinga* by having fewer premaxillary teeth on first row (8 vs. 10–14); and by number of interopercular odontodes (25–26 vs. 25–38). *Trichomycterus vinnulus* can be further distinguished from *T. alternatus* by number of lateral line pores (3 vs. 2); colour pattern consisting of numerous round maculae randomly distributed through the body (vs. round maculae anteroposteriorly distributed in four rows in each side of body).

Description: Morphometric data for specimens examined is presented in Table 16. Body long and almost straight in lateral aspect, trunk roughly round in cross-section near head, then slightly deeper than broad and gently compressed to caudal peduncle, tapering to caudal fin. Dorsal profile of body gently convex to dorsal-fin origin, then straight or slightly concave along caudal peduncle to caudal-fin origin. Ventral profile convex from gular region to vent, due partly to abdominal distension, then straight or slightly concave along anal-fin origin to caudal-fin base. Caudal peduncle long, as deep as body and slightly expanding at caudal-fin base.

Head approximately 1/5 of SL, pentagonal, slightly longer than wide and depressed. Mouth subterminal.

Table 16. Morphometric data of *T. vinnulus* based on holotype and part of paratype material (MZUSP 123750, 123757, 126760)

	Holotype	Range (*N* = 10)	Mean	SD
Standard length (mm)	55.8	21.21–61.00	49.7	-
% of standard length				
Anal-fin base	8.0	6.6–9.5	7.7	0.9
Body depth	11.9	11.5–14.6	13.1	1.0
Caudal peduncle depth	10.2	10.1–12.0	10.9	0.7
Dorsal-fin base	10.8	8.7–12.2	10.8	1.1
First pectoral-fin length	14.3	10.5–15.2	12.9	1.5
Head length	19.3	18.3–21.2	19.6	1.0
Preanal length	69.1	69.1–73.5	71.7	1.5
Predorsal length	62.9	60.0–63.5	62.3	1.2
Prepelvic length	51.6	51.5–55.1	52.5	1.2
% of head length				
Eye diameter	22.1	18.6–22.9	21.2	1.4
Interorbital width	21.8	21.0–25.5	23.4	1.6
Snout length	55.3	50.1–58.9	53.8	2.6
Mouth width	35.5	30.4–40.5	35.9	3.0

Upper jaw longer than lower. Upper lip wider than lower lip and laterally continuous with base of maxillary barbel. Lower lip small, approximately 2/3 width of upper one, partly divided into right and left portions by median concavity. Lower lip with uniform covering of tiny villi, resulting in velvet-like surface and not clustered into large papillae. Region between upper and lower lips with slender fleshy lobe.

Dentary and premaxillary teeth similar to each other in shape. Dentary teeth conical, 35–46 arranged in four irregular rows, first row with 9–11 teeth, extending from base to slightly up of coronoid process, with size of individual teeth increasing markedly towards symphysis and from posterior to anterior rows. Total area of premaxillary teeth slightly smaller than that of dentary, with 36–40 teeth arranged irregularly in four rows, first row with approximately 9–13 teeth, over entire ventral surface of premaxilla. Premaxillary teeth conical.

Eye large sized, slightly protruding, positioned laterodorsally on head, without free orbital rim and covered with transparent skin. Eye located on anterior half of HL, closer to lateral border of head than to the midline in dorsal view. Anterior naris surrounded by tube of integument directed anterolaterally, continuous posterolaterally with nasal barbel. Posterior naris closer to anterior naris than to eyes, surrounded by tube of integument incomplete posteriorly. Maxillary barbel narrowing markedly towards fine tip, reaching base of pectoral fin. Rictal barbel inserted immediately ventral to maxillary barbel, its tip reaching from posterior border of posterior naris to anteromesial border of interopercle. Nasal barbel originating on posterolateral region of anterior naris, reaching posterior margin of eyes or slightly beyond, never reaching opercular patch of odontodes. Interopercular patch of odontodes small compared to head length, oval in shape and with well-developed odontodes, prominent in ventral aspect of head. Interopercular patch of odontodes extending from vertical through ventroposterior border of eye to ventroanterior to opercle. Interopercular odontodes arranged in three irregular series, with those on mesial series much longer than those on lateral one; odontodes gradually larger posteriorly in both series, with those posteriorly on mesial row largest. Interopercular odontodes 25–26. Opercular patch of odontodes on dorsolateral surface of posterior part of head, positioned anterodorsally to pectoral-fin base, roundish in shape and small, smaller than eye diameter in dorsal aspect of head. Opercular odontodes 11–14, sunk in individual slits of integument, progressively larger posteriorly, all with fine tips, with largest ones curved distally and claw-like. Entire patch surrounded by rim of integument.

Pectoral fin with its base ventroposterior to opercular patch of odontodes. Pectoral-fin rays I + 7. First pectoral-fin ray (unbranched) slightly longer than remaining in rays, prolonged as filament beyond fin margin. Other rays progressively less long, their tips following continuous line along fin margin. Pelvic fin with convex distal profile, its origin slightly posterior to middle of SL and anterior to vertical through dorsal-fin origin, covering anal and urogenital openings in adults. Base of pelvic fins separated from each other by one eye diameter. Pelvic-fin rays I + 4. Anterior

process of basipterygium long, hook-like and laterally curved. Dorsal fin long, its distal margin sinusoidal. Dorsal-fin origin closer to base of caudal fin than to tip of snout. Dorsal-fin rays iii + II + 7 or iv + II + 7. Anal fin slightly smaller than dorsal fin, its distal margin gently convex. Anal-fin origin posterior to vertical through end of dorsal-fin base. Anal-fin rays ii + II + 5 or iii + II + 5. Caudal fin subtruncate, with 6 + 7 principal rays. Adipose fin absent or modified into low integument fold extending between end of dorsal fin and caudal-fin origin. Post-Weberian vertebrae 36 (1) or 37 (1). First dorsal-fin pterygiophore immediately anterior to neural spine of 16th (1) or 17th (1) vertebra, first anal-fin pterygiophore immediately anterior to neural spine of 20th (1) or 21st (1) vertebra. Caudal-fin procurrent rays plus one segmented non-principal ray dorsally and ventrally extending until ¼ on caudal-fin rays. Procurrent caudal-fin rays, 19–21 dorsally and 12 or 13 ventrally, beginning anteriorly at 32nd vertebrae. Ribs 9 (1) or 12 (2). Branchiostegal rays 7 (3). Dorsal-fin pterygiophores 8. Anal-fin pterygiophores 6.

Cephalic lateral line canals with simple, non-dendritic tubes ending in single pores. Supraorbital canal mostly in frontal bone. Supraorbital pores invariably present: s1 mesial to nasal-barbel base and autopalatine, s3 mesial to posterior nostril and anterior to frontal, paired s6 posteromedial to eye and at midlength of frontal. Infraorbital laterosensory canal incomplete with four pores, i1 and i3 anteriorly and i10 and i11 posteriorly. Canal extending from sphenotic posteriorly to terminal pore located ventroposteriorly to eye. Infraorbital pore i1 located ventrolateral to nasal-barbel base and autopalatine, i3 ventrolateral to posterior nostril and anterior to frontal, i10 and i11 posterior to eye. Otic canal without pores. Postotic pores po1, anteromedial to opercular patch of odontodes, and po2, mesial to opercular patch of odontodes. Lateral line of trunk anteriorly continuous with postotic canal and reduced to short tube. Lateral line pores ll1, ll2 and ll3 present dorsomedial to pectoral-fin base.

Coloration in ethanol: Trichomycetus vinnulus has a wide range of colour patterns between two extreme morphs. One colour morph consists of round dark maculae organized in four longitudinal rows. The size, shape and number of maculae vary among specimens, with bigger, round and less numerous (minimum 11 in the mid-line) maculae in young specimens. First row along mid-dorsal line from occiput, through entire dorsum, into dorsal edge of caudal peduncle and to base of caudal fin. Second row ventrolateral to that, extending from base of head through upper part of flanks, dorsal portion of caudal peduncle, to base of caudal fin. Third row running along mid-lateral line,

from immediately posterior to opercle to base of caudal fin. Fourth and ventralmost row shorter, extending from anterior region of abdomen through ventral margin of caudal peduncle to base of caudal fin. Fourth row usually composed of unaligned maculae. Rows mostly independent, rarely fusing. Another colour morph, common in adults, has the entire body (except for ventral region), covered with dark amorphous maculae, smaller than eye diameter. Head entirely covered by small dark spots or with dark blotches probably resulting from fusion of smaller maculae. Head darkest on region corresponding to neurocranium, outlined by brain pigment. Cheeks over protractor uencan muscle region less heavily pigmented than uencanem. Base of nasal barbels surrounded with concentration of dark pigment, extending posteriorly as elongate dark field to anterior margin of eyes. Distal margin of integumentary fold of opercular patch of odontodes darkly pigmented. Interopercular patch of odontodes white. Ventral side of the body lacking dark pigment. Fin rays covered with small dark spots.

Etymology: From the Latin adjective *vinnulus*, delightful, often used to refer to wine.

Remarks: Trichomycterus vinnulus is a distinctive and readily diagnosable species. However, DNA barcoding shows relatively low divergence relative to its sympatric species *T. alternatus*, 1.9% and *T. astromycterus*, 2% (Table 2). Barcoding divergence values found among *T. vinnulus*, *T. alternatus* and *T. astromycterus* are low when compared with other divergence values for *Trichomycterus* reported here and in previous works (Pereira *et al.*, 2013; Sales *et al.*, 2018). However, Ward *et al.* (2009) estimated that specimens with 2% barcoding divergence have a > 95% probability to belong to different species. Low genetic distance among morphologically distinct Neotropical freshwater fish species can be explained by many factors, including recent speciation, mitochondrial introgression due to hybridization and also incomplete lineage sorting (Montoya-Burgos, 2003; Hubert *et al.*, 2007; Perdices *et al.*, 2002, 2005; Ornelas-Gacia *et al.*, 2008; Costa-Silva *et al.*, 2015).

Trichomycterus vinnulus co-inhabits the same creek and was collected in the same microhabitat with *T. alternatus* and *T. astromycterus*. Therefore, the possibility of mitochondrial introgression by hybridization is plausible. Similar situations were reported in various other fish groups, for example *Mobula alfredi* (Krefft, 1868) vs. *Mobula birostris* (Walbaum, 1792) (Kashiwagi *et al.*, 2012) and *Rineloricaria langei* Ingenito *et al.* 2008 vs. *Rineloricaria kronei* (Miranda Ribeiro, 1911) (Costa-Silva *et al.*, 2015). In the present case, analyses using
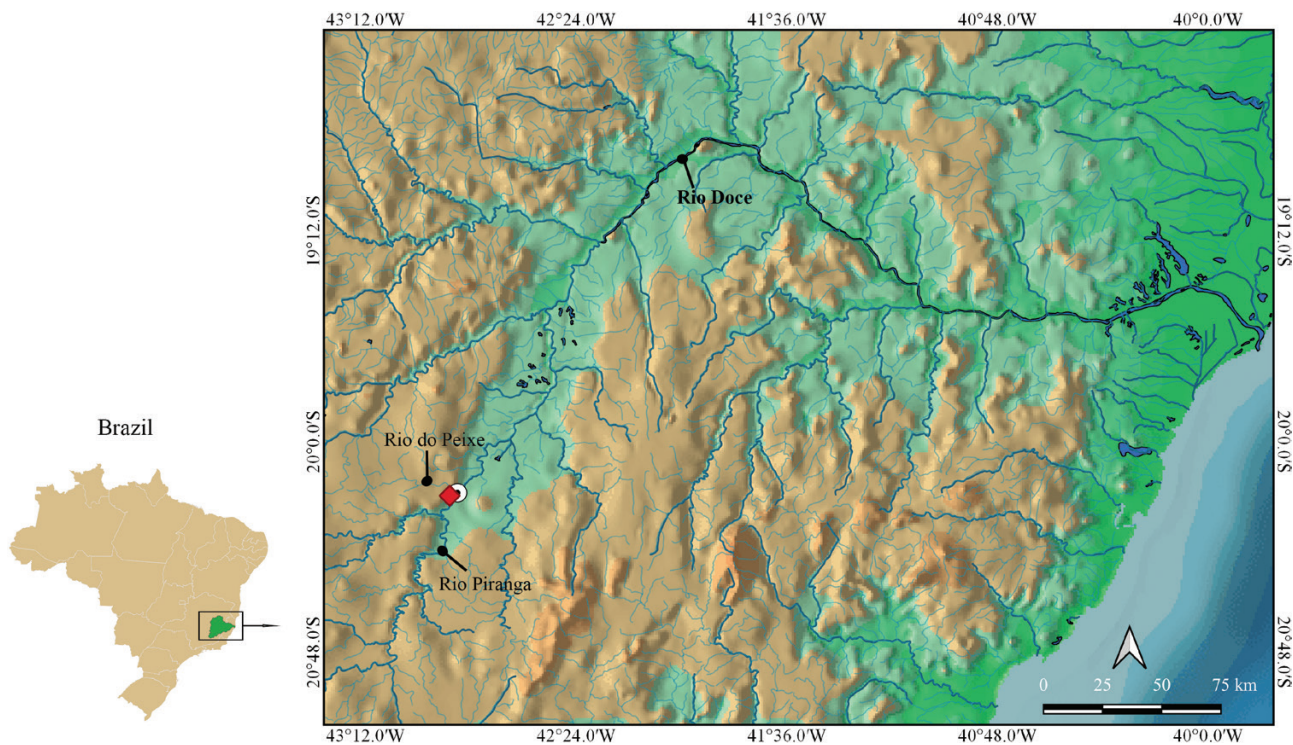
Figure 38. Geographical distribution of *T. vinnulus* sp. nov. in the Rio Doce Basin. Red diamond = holotype (MZUSP 123750) and paratypes (MZUSP 126760); white dotted circle = paratype (MZUSP 123757).

<div style="border:1px solid">

KEY TO SPECIES OF *TRICHOMYCTERUS* IN THE RIO DOCE BASIN

This key is provided as an identification aid to the numerous taxonomic changes presented herein. It is eminently practical, referring mostly to external traits readily observable in preserved specimens. The key should be followed from beginning to end each time, because some doublets are repeated in more than one level of the hierarchy. Thus, strings of traits should not be seen as diagnoses of endpoint taxa (for that, see Diagnoses for each individual species). Because of the extreme variability of observable traits, *T. alternatus* is keyed out twice.

1a. Pectoral-fin rays I + 6 or fewer; colour pattern formed by irregular roundish maculae and vermiculations randomly distributed over most of body or stripes over most of body. 2

1b. Pectoral-fin rays I + 7 or I + 8; colour pattern uniform or formed by round maculae (randomly distributed or arranged in rows) or stripes over most of body. 4

2a. Pectoral-fin rays I + 5; colour pattern consisting of broad dark mid-lateral stripe, covering nearly 1/3 of body depth in lateral view and extending from posterior border of opercle to base of caudal-fin. ....*Trichomycterus reinhardti*

2b. Pectoral-fin rays I + 6; colour pattern formed by irregular roundish maculae and vermiculations randomly distributed over most of body. 3

3a. Interopercular odontodes 26–31; snout length 28.0–41.2% HL. ....*Trichomycterus brunoi*

3b. Interopercular odontodes 39–40; snout length 41.9–45.9% HL................................*Trichomycterus argos*

4a. Colour pattern uniform or with round maculae equivalent in size to eye or larger, randomly distributed; caudal fin with dark horizontal band along middle rays, extending to margin of fin. 5

4b. Colour pattern with round maculae usually smaller than eye (randomly distributed or arranged in rows) or longitudinal stripes; caudal fin without horizontal dark band. 8

5a. Pectoral-fin rays I + 7; maximum of eight branchiostegal rays; ribs 13. 6

5b. Pectoral-fin rays I + 8; maximum of seven branchiostegal rays; ribs 12 or fewer. 7

6a. Colour pattern with round dark maculae mostly larger than eye, randomly distributed on body; post-Weberian vertebrae 37; interopercular odontodes 25–38. .... *Trichomycterus ipatinga*

</div>

6b. Colour pattern uniform; post-Weberian vertebrae 38–40; interopercular odontodes 39–51. ....*Trichomycterus melanopygius*

7a. Colour pattern uniform or with dark round spots randomly distributed on body; opercular odontodes 15–25; caudal fin emarginate or truncate; two lateral-line pores; integument thin, easy to tear apart (integument resistance usual for species of *Trichomycterus*). ....*Trichomycterus immaculatus*

7b. Colour pattern invariably uniform; opercular odontodes 25–33; caudal fin forked; three lateral-line pores; integument thick, extremely resistant to tearing .... *Trichomycterus tantalus*

8a. Nasal barbel not reaching posterior margin of eye. 9

8b. Nasal barbel reaching beyond posterior margin of eye. 12

9a. Interopercular odontodes 38–63; maculae along mid-lateral line of body usually fused, creating wide continuous stripe extending between posterior margin of opercle and base of middle caudal-fin rays. 10

9b. Interopercular odontodes 25–35; rounded maculae unfused (rarely fused along region between posterior margin of opercle and vertical through base of dorsal fin) forming discontinuous line along mid-lateral line of body. 11

10a. Three lateral-line pores; six branchiostegal rays; eye diameter 12.2–14.4% HL; colour pattern darkly marbled. ....*Trichomycterus* aff. *caipora*

10b. Two lateral-line pores; seven branchiostegal rays; eye diameter 14.8–17.5% HL; colour pattern not marbled, with discontinued stripes on mid-line of body. ....*Trichomycterus barrocus*

11a. Three lateral-line pores; caudal fin slightly to deeply bilobed, with lower lobe longer than upper one; eyes protruding, positioned dorsally on head; maxilla distally expanded; I + 8 or I + 9 dorsal-fin rays. ....*Trichomycterus astromycterus*

11b. Two lateral-line pores; caudal fin round to emarginate; eyes not protruding and positioned dorsolaterally on head; I + 7 dorsal-fin rays. ....*Trichomycterus alternatus*

12a. Mid-lateral line of body with dark stripe or row of round maculae extending from posterior margin of opercle to base of caudal fin. 13

12b. Mid-lateral line of body lacking stripe or series of round maculae; body covered with round maculae eye-sized or smaller and randomly distributed. 14

13a. First dorsal-fin pterygiophore immediately anterior to neural spine of 18th vertebra; first anal-fin pterygiophore immediately anterior to neural spine of 23rd vertebrae; procurrent caudal-fin rays beginning anteriorly at 34th vertebrae. ....*Trichomycterus illuvies*

13b. First dorsal-fin pterygiophore immediately anterior to neural spine of 15th to 17th vertebrae; first anal-fin pterygiophore immediately anterior to neural spine of 19th to 21st vertebrae; procurrent caudal-fin rays beginning anteriorly at 28th to 32nd vertebrae. ....*Trichomycterus alternatus*

14a. Three lateral-line pores; pelvic fin covering urogenital opening; seven branchiostegal rays. ....*Trichomycterus vinnulus*

14b. Two lateral-line pores; pelvic-fin rays not covering urogenital opening; eight branchiostegal rays. ....*Trichomycterus brucutu*

nuclear DNA markers would be necessary to determine the reasons for low barcode divergence in association with pronounced phenotypic divergence among *T. vinnulus*, *T. alternatus* and *T. astromycterus*. However, *T. vinnulus* differs from its congeners by phenotypic divergence as large as, or larger than, normally seen among other *Trichomycterus* species in the *T. alternatus* clade and even in the whole genus.

Geographical distribution: Trichomycterus vinnulus is known from two localities in the Upper Rio Doce Basin near the Risoleta Neves hydropower reservoir: an unnamed creek on the left margin of the reservoir and the Rio do Peixe, left tributary of Rio Doce, downstream from the Risoleta Neves hydropower reservoir (Fig. 38).

DISCUSSION

COI DIVERGENCE AS A PROXY FOR TAXONOMIC DELIMITATION

Although degree of similarity in *COI* sequence data has severe limitations as a general systematic method, it may be useful as an identification tool in other areas that require specimen identification. Among species from the Rio Doce with both morphological and molecular data available, four of them display differentiation in the two sources of data, namely *T. tantalus*, *T. immaculatus*, *T. ipatinga* and *T.* aff. *caipora*. While degree of *COI* divergence is not always pronounced, patterns of similarity agree with those based on morphological delimitation. Such cases are straightforward and

simply indicate that differentiation in those lineages is expressed at both levels. A remarkable exception involves *T. alternatus* and its closest relatives. For example, *T. astromycterus* is one of the best-characterized species morphologically, with a large array of distinguishing characteristics from various body systems (in both internal and external anatomy), some of which are unique and probably autapomorphic. Corroborating its condition as a separate lineage, there are no morphologically intermediate specimens between *T. astromycterus* and *T. alternatus*. Further, juvenile specimens as small as 12 mm SL of the two species are readily distinguishable. However, such pronounced phenotypic divergence is not at all reflected in *COI* sequences. Samples of *T. astromycterus* are nested in the Bayesian tree in a large clade composed of *T. alternatus* representatives (Fig. 1). Without morphological information, this species is virtually impossible to diagnose by *COI* alone. Tangled in the *T. alternatus* complex is *T. vinnulus*, another species also well-differentiated morphologically yet similar in *COI* sequences. Still another case happens with *T. melanopygius*, where available samples do not even form a monophyletic group. The phenomenon of lineage differentiation without equivalent mitochondrial divergence is common in fishes, both Neotropical and elsewhere (Perdices *et al.*, 2002, 2005; Montoya-Burgos, 2003; Hubert *et al.*, 2007; Ornelas-Gacia *et al.*, 2008; Pereira *et al.*, 2010, 2013; Carvalho *et al.*, 2011; Costa-Silva *et al.*, 2015), and this is usually attributable to three causes: recently-split lineages, mitochondrial introgression and incomplete lineage sorting. At present, it is not possible to determine which of the causes are responsible for the cases reported here. However, the fact that both *T. astromycterus* and *T. vinnulus* are sympatric with *T. alternatus* is suggestive that mitochondrial introgression may be a relevant factor. This is not the case with *T. melanopygius* and other species in its clade (*T. melanopygius*, *T. ipatinga*, *T. tantalus* and *T.* aff. *caipora*), with which it is entirely allopatric. Of course, introgression and recent divergence are not mutually exclusive and the two factors may be concurrent. Resolution of this issue requires further research and additional data from nuclear markers or cytogenetic analyses.

The opposite situation happens when species with pronounced *COI* divergence show little or no morphological differentiation. Again, this has been abundantly reported in several nominal species of Neotropical fishes such as *Piabina argentea* Reinhardt, 1867 (Pereira *et al.*, 2011), *Hoplias malabaricus* (Bloch, 1794) (Marques *et al.*, 2013), *Rineloricaria* Bleeker, 1862 (Costa-Silva *et al.*, 2015) and *Curimatopsis* Steindachner, 1876 (Melo *et al.*, 2016). This phenomenon is the most commonly-reported result from barcoding studies and is usually interpreted as indicative of hidden diversity in the form of cryptic species. Although common in fishes in general, this is a much rarer phenomenon among *Trichomycterus* from the Rio Doce and we have identified only two cases mentioned above in the *T. alternatus* complex: *Trichomycterus* sp. 1 and *Trichomycterus* sp. 2.

Degree of barcode differentiation cannot be translated into a single cut-off value for species delimitation. Initial proposals of barcoding taxonomy expected a uniform divergence rate as a general standard for specific differentiation (Hebert *et al.*, 2003; Ward, 2009). Later, researchers quickly demonstrated that those initial expectations were unrealistic and that taxonomic differentiation reflective of specific distinctiveness varies widely among different groups of organisms (DeSalle *et al.*, 2005; Pereira *et al.*, 2013; Costa-Silva *et al.*, 2015; Sales *et al.*, 2018) and even in closely related clades (Carvalho *et al.*, 2015; Costa-Silva *et al.*, 2015; Sales *et al.*, 2018). However, beyond questions of congruence or incongruence, the most interesting situations are those where separate types of data are reciprocally illuminating. Cases such as those of *T. astromycterus*, *T. vinnulus*, *T. melanopygius* and *T. ipatinga* on the one hand, and the populations of *T. alternatus* from Rio Cubatão, its closest relatives from adjacent basins, and the specimen from Rio Doce at Baguari (Fig. 1; S148MRD) on the other hand, show that no single type of data can be taken as prima facie evidence of taxonomic differentiation. In the former two cases, *COI* differentiation alone would be utterly incapable to detect the existence of those two well-differentiated and readily diagnosable species morphologically. In the latter, morphological data have as yet failed to reflect pronounced barcoding divergence, most likely reflective of yet unrecognized taxonomic distinctiveness.

Sampling and taxonomic density are decisive factors for phylogenetic accuracy and for the resolution of taxonomic questions. Classical taxonomic studies attempt to scan as many individuals as possible across the geographic range of a putative species to chart in detail the variation within a species and to separate it from other species. Ideally, all specimens of the target species available in museum collections should be examined, since one or a few individuals most of the time do not represent the entire range of morphological variation for a given species, especially for those with broad distributions and high levels of variation. Of course, in practice limitations exist and several taxa have been, and continue to be, justifiably described on the basis of few or even single specimens, because they are the only ones available.

The need for adequate sampling of individuals applies to both morphological and molecular data. Especially in higher-level questions, the impact of taxonomic representation in molecular markers has been known for a long time (e.g. Heath *et al.*, 2008).

The issue is equally relevant—perhaps even more so—in questions addressing species composition and taxonomic problems. In the latter case, a more proper term would be sampling density, because research dealing with species boundaries rely heavily not only on nominal species representation, but also on multiple samples from each of them. The numerous samples representing some of the species in this study may seem excessive. However, this is necessary because species boundaries at the beginning of the study were just conjectures based on a limited array of phenotypic characteristics guiding traditional identifications. Sampling density allows the necessary conditions for existing phylogenetic patterns to emerge with the detail needed in order to resolve both the biological situation and the associated taxonomic questions. The denser the sampling, the clearer the emerging picture.

The cases of *T. immaculatus* and *T. alternatus* are again exemplary. The former species was represented by 33 a priori samples, including those formerly assignable to *T. pradensis*. In the phylogenetic scheme, all those samples came together in a clade neatly supporting traditional concepts of the taxon in the Rio Doce and some neighbouring basins. So, preconditions for the species to reveal itself as non-cohesive were there, but were not realized. This result, in the face of dense sampling, only strenghthens the resulting hypothesis that *T. immaculatus* is a well-defined biological entity. At the other extreme, *T. alternatus* was represented by a set of 87 samples, made larger still by the addition of samples from potentially different but similar species (*T. caudofasciatus*, *T. florensis*). In this case, the ample representation permitted a complex scenario to unfold. *Trichomycterus alternatus* proved to be a complex metaspecies containing several mini clusters, some containing full exospecies. The apparent oversampling was instrumental in properly resolving the nomenclatural situation of several of those supposedly closely-related species. Echoing previous studies (Funk & Omland, 2003; Mutanen *et al.*, 2016), the present case demonstrates that sampling and taxonomic density are necessary preconditions for a more comprehensive resolution of phylogenetic and taxonomic situations.

DIVERSITY OF *TRICHOMYCTERUS* IN THE RIO DOCE BASIN

Most of the species of *Trichomycterus* recorded for the Rio Doce are narrowly endemic in distribution, with some of them known from a single locality, e.g. *T. argos*, *T. barrocus*, *T. brunoi*, *T. brucutu* and *T. vinnulus*. Of course, some of those may in part be simply a result of collection gaps, because sampling in the Rio Doce is still far from satisfactory. While the latter factor is always a possibility, existing collections are sufficient to reveal a number of species distributed in several far-ranging localities, such as *T. astromycterus*, *T. tantalus*, *T. illuvies* and *T.* aff. *caipora*, as well as a few which are truly widely distributed throughout the Rio Doce Basin like *T. alternatus*, *T. immaculatus*, *T. ipatinga* and *T. melanopygius*. The great diversity and often narrow geographical distribution of species of *Trichomycterus* in south-eastern Brazil supports past proposals of pronounced endemism in the genus (Eigenmann, 1918; Tchernavin, 1944; Costa, 1992; de Pinna, 1992a; Bizerril, 1994; Barbosa & Costa, 2003). Species of the genus tend to inhabit headwaters, a fact that in itself correlates with high levels of isolation and endemism. However, some species of *Trichomycterus* are reported to migrate up and down watercourses and even undergo mass migrations (Dahl, 1960; de Pinna, 1998; Miranda-Chumacero *et al.*, 2015). In the present case, this seems to be the explanation for the broad distribution of some species, such as *T. immaculatus*, which is regularly collected both in the lower courses of streams and in the main channel of the Rio Doce, indicating that individuals of the species are capable of living and moving throughout a large gradient of river conditions as part of their life cycle. *Trichomycterus immaculatus* has been reported to form massive congregations suggestive of some sort of migratory behaviour (along with *T. tantalus* in smaller numbers), in the fish transposition system of the Baguari Hydroeletric Plant, at the main channel of the Rio Doce (T. Pessali, pers. comm.; Fig. 39). The lack of significant morphological or genetic divergence among populations (cf. Table 2) strongly agrees with such a high-vagility scenario.

The situation with *Trichomycterus alternatus* is more complex. Within the Rio Doce, *T. alternatus* has a distribution as wide as that of *T. immaculatus*. However, an important additional difference exists between the two species. There is far more genetic divergence and structuring in *T. alternatus* than in *T. immaculatus* (cf. Table 2; Fig. 1). Preliminary evidence suggests that *T. alternatus* has reduced vagility potential when compared to *T. immaculatus*. Records of *T. alternatus* from the main channel are rare, and there have been no reports of mass migrations so far. The species has an apparent preference for headwaters and thus is more prone to form small isolated populations. This probably explains its greater degree of genetic structuring when compared to *T. immaculatus*. On the other hand, *T. alternatus* occurs in several major basins to the south of the Rio Doce, where *T. immaculatus*, as defined here, has not been recorded.

In this case, the explanation seems to involve factors additional to simply the vagility of the species. Geological processes are possibly an important factor in the trans-basin distribution of *Trichomycterus alternatus*. According to Cherem *et al.* (2012), the

Figure 39. Mass concentration of *Trichomycterus* (*T. immaculatus*, *T. tantalus* sp. nov. and *Trichomycterus* sp. 1) in the fish transposition system at the Baguari Hydroelectric Plant, main channel of Middle Rio Doce. Photo by Tiago Pessali.

São Geraldo steps (an escarpment dividing the Rio Doce from the Paraíba do Sul) have been constantly denudated by geological process and weathering in an inland direction. As a result, the Paraíba do Sul is abducting 15.68 m/Myr from the Rio Doce, a process that has resulted in stream capture events from the Rio Doce into the Paraíba do Sul (Cherem *et al.*, 2012: figs 3, 4). Such processes are general and have also been reported in other parts of the world such as the Drakenberg escarpment in southern Africa (Fleming *et al.*, 1999), the Namibia escarpment in south-western Africa (Bierman & Caffee, 2001), the Great Escarpment in south-eastern Australia (Heimsath *et al.*, 2001, 2006), the Blue Ridge escarpment in eastern North America (Sullivan *et al.*, 2007) and the Sri Lankan escarpment in Asia (Vanacker *et al.*, 2007). In such a scenario, *T. alternatus* might have dispersed into the Paraíba do Sul from the Rio Doce, and from there onto other basins further south. This scenario agrees with the phylogenetic structure of *T. alternatus* and related taxa, where non-Doce components are internested in both the Doce clade and the *T. alternatus* clade. Although the details and chronology of such an event are yet unknown and certainly need further study, it is at least a plausible preliminary explanation for the observed distribution of *T. alternatus*. The wide distribution of *T. alternatus* in the Rio Doce and its pronounced

preference for headwaters are preconditions that may have positively influenced its dispersal into the Paraíba do Sul and then other basins via stream capture caused by denudation phenomena described above.

The same basin-abducting phenomenon between the Rio Paraíba do Sul and Rio Doce occurs also between the latter and the Rio São Francisco. The Rio Doce is invading 8.77 m/Myr into the São Francisco Basin (Cherem *et al.*, 2012) with presumably associated stream-capture events (Cherem *et al.*, 2012: figs 3, 4). Only a few species of *Trichomycterus* are so far reported to co-occur in those two basins such as *T. reinhardti* (Ferraris, 2007; Sales *et al.*, 2018; Costa & Katz, 2021), but *T. argos* and *T. brunoi* in the Rio Doce seem to be close relatives of *T. brasiliensis* from the São Francisco (Lezama *et al.*, 2012). This is possibly a result of biotic dispersal from the São Francisco into the Rio Doce by the denudation process, in this case with subsequent phenotypic divergence. This is a topic for further investigation once more specimens and data on *T. argos*, *T. brunoi* and other species of the *T. brasiliensis* clade become available.

The phylogenetic scheme presented here shows a large monophyletic group of *Trichomycterus* in the Rio Doce (the Doce clade mentioned earlier), comprising *T. alternatus*, *T. astromycterus*, *T.* aff.

caipora, *T. immaculatus*, *T. ipatinga*, *T. melanopygius*, *T. tantalus* and *T. vinnulus*. Although DNA data of *T. reinhardti* reported in the Rio Doce are not available, results of Costa and Katz (2021) plus our present phylogeny show that this species is not part of the Doce clade. *Trichomycterus reinhardti* was reported in a headwater stream from the Rio Doce Drainage at the Serra do Espinhaço, close to the water divide with the Rio São Francisco. Thus, its presence in the Rio Doce is probably due to headwater capture, a phenomenon likely explained by the same denudation process shown above. Other Rio Doce species such as *T. argos*, *T. barrocus*, *T. brucutu*, *T. brunoi* and *T. illuvies* are not available for sequence analysis at this time and their phylogenetic position is still unresolved.

The existence of one major clade comprising the bulk of *Trichomycterus* diversity in the Rio Doce, along with the relatively distal position of that clade in the phylogeny of the genus suggests that the basin was colonized from nearby basins. In that scenario, *T. alternatus*, as seen above, is a lineage which subsequently undertook the opposite route, spreading more recently from the Rio Doce to other basins.

TAXONOMIC SITUATION IN *TRICHOMYCTERUS*

Trichomycterus is a hyperdiverse, non-monophyletic taxon (de Pinna, 1989, 1998; Wosiacki, 2002; Ochoa *et al.*, 2017, 2020; Fernandez *et al.*, 2021). Recently, some nomenclatural suggestions were made, which partly help and partly aggravate its long-standing problems. The genus has been restricted to a clade composed of south-eastern Brazilian trichomycterines exclusive of *Cambeva* and *Scleronema* by Katz *et al.* (2018). While this move makes *Trichomycterus* a monophyletic group of some 65 species, it leaves more than 135 species without generic allocation. Also, Fernández *et al.* (2021) proposed to transfer *Eremophilus mutisii* Humboldt, 1805, type species of *Eremophilus*, into *Trichomycterus*. Such a move in effect synonymizes *Trichomycterus* and *Eremophilus*. However, *Eremophilus* Humboldt, 1805 has nomenclatural priority over *Trichomycterus* Valenciennes, 1832, which thus would result in the—apparently inadvertent—generic change of nearly 200 species into *Eremophilus*. Because such a large-scale consequence was neither foreseen nor dealt with in that proposal, we do not follow the move of *Eremophius mutisii* into *Trichomycterus*. While both Fernández *et al.* (2021) and Costa *et al.* (2020b) provide interesting original information on poorly known taxa, the nomenclatural proposals therein need to be re-evaluated in a wider context.

Generic delimitation issues aside, the taxonomic history of species described in *Trichomycterus* is complex at a basic level, with many cases of synonymy and heterogeneous descriptive methodologies (Eigenmann, 1918; Tchernavin, 1944; Baskin, 1973; de Pinna, 1989; Wosiacki, 2002; Barbosa, 2004; Bockmann & Sazima, 2004; DoNascimiento & Prada-Pedreros, 2020). Of the 14 species herein recognized to occur in the Rio Doce, only seven were previously described. Of those, *T. immaculatus* and *T. alternatus* are particularly illustrative cases to demonstrate the ill effects of poor taxonomic standards.

Although published by the same author, Eigenmann's descriptions of *T. immaculatus* and *T. alternatus* adopted different methodologies. Their subsequent redescriptions (Eigenmann, 1918) still follow a third set of parameters. While the multiplicity of descriptive standards is in itself undesirable, the real problem is the lack of methodological objectivity. Often it is unclear how simple data such as fin-ray counts and proportional measurements were taken. This makes meaningful comparisons impossible in subsequent works. Such difficulties were reported and harshly criticized by Tchernavin (1944) and reiterated many decades later by Reis & de Pinna (2019). Despite such warnings, the same caveats still plague the taxonomy of *Trichomycterus* to the present date.

As discussed above (see remarks on *T. immaculatus*), the lack of unified taxonomic standards allied with the use of taxonomically unsound characters can lead to errors in species identification and redundant species descriptions. Again, a particularly illustrative example is seen in *T. alternatus*. This species is widely distributed in the Rio Doce and adjacent basins. In the course of more than 100 years since its description, several species closely resembling *T. alternatus* have been described from the Rio Doce and other adjacent basins. Some of those have already been synonymized under *T. alternatus*, such as *T. travassosi* (Miranda Ribeiro, 1949), *T. auroguttatus* and *T. longibarbatus*, but those three junior synonyms are probably just the tip of the iceberg. Other species such as *T. caudofasciatus*, *T. gasparinii*, *T. jequitinhonhae*, *T. landinga*, *T. mimosensis*, *T. nigroauratus* and *T. puriventris* are all obviously part of the *T. alternatus* gestalt as presented in Reis & de Pinna (2019). They still await a careful evaluation of their distinctiveness from *T. alternatus* on the basis of realistic estimates of geographic and intraspecific variation and resort to information from type material.

A final species which deserves mention is *Trichomycterus goeldii* Boulenger, 1896, from a tributary of the Paraíba do Sul Basin. The taxon was described with a brief diagnosis and no illustration. The identity of that species is still nebulous and resolution of its status awaits additional material from the type locality and further study. The species was nominally

included as a terminal in Vilardo *et al.* (2020), but with no comments on its identity or other details, so it is still uncertain whether the sample actually represents the species. Among species of *Trichomycterus* from the Rio Doce, *T. alternatus* is superficially most similar to *T. goeldii*, based on examination of specimens from the type locality. Despite the paucity of data on the latter, preliminary observations suggest that *T. goeldii* is a taxon distinct from *T. alternatus*. Resolution of the taxonomic status of *T. goeldii*, its geographical distribution, relationships, etc. will be the subject of a separate contribution (in collaboration with S. Santos and M. Britto).

CONCLUSION

The Rio Doce Basin has a rich assemblage of *Trichomycterus* species which is just beginning to be revealed. Our investigation based on extensive museum material searches and new collections shows the existence of at least 14 species in the basin, six of which are newly described here. The iteration of morphological and DNA sequence data permits the delimitation of that diversity, despite extreme heterogeneity of data, with some species known from a few specimens available for morphology only, and others represented by abundant material of both kinds of data. Taxonomic representation and sampling density are of utmost importance in solving problems related to the circumscription of species-level taxa. Examination and analysis of large numbers of specimens are important for both morphological and sequence data, for different yet equally relevant reasons, allowing the discovery of new taxa and the delimitation of species which would be otherwise intractable. One of them is *T. immaculatus*, here restricted to the taxon occurring in the Rio Doce and satellite basins. The morphologically similar (and often equally named) form from the Rio Paraíba do Sul is a different species, probably bearing the name *T. paquequerensis*. *Trichomycterus alternatus* is another complex taxon, in this case a metaspecies because some of its internal lineages have differentiated into full species (exospecies, as denominated here). *COI* data indicate that a large assemblage of *Trichomycterus* in the Rio Doce Drainage forms an unexpected monophyletic group (called the Doce clade), including *T. alternatus*, *T. astromycterus*, *T.* aff. *caipora*, *T. immaculatus*, *T. ipatinga*, *T. melanopygius*, *T. tantalus* and *T. vinnulus*. Of those, the only one distributed beyond the Rio Doce and immediately neighbouring basins is *T. alternatus*. Other species such as *T. argos*, *T. barrocus*, *T. brucutu*, *T. brunoi*, *T. reinhardti* (from the Rio Doce) and *T. illuvies* are yet unavailable as DNA material and their position cannot be resolved at this time. Morphological and molecular data presented herein and from Costa (2021), provides evidence that three of these (*T. argos*, *T. brunoi* and *T. reinhardti*) have their closest relatives outside of the Rio Doce region. Phylogenetic structure indicates that the Doce-clade probably had its common ancestor dispersing into the Rio Doce from surrounding basins. Subsequent to that event and ensuing diversification, a sublineage of *T. alternatus* seemingly took the opposite route, colonizing other basins to the south via stream capture caused by denudation processes.

COMPARATIVE MATERIAL EXAMINED

Bullockia maldonadoi (Eigenmann, 1920): MZUSP 88527, 25, 27.6–47.7 mm SL; MZUSP 107499, 3 c&s, 23.4–51.4 mm SL. *Hatcheria macraei* (Girard, 1855): MZUSP 35687, 7, 37.5–68.3 mm SL; MZUSP 25657 1 c&s, 83.8 mm SL. *Cambeva zonata* (Eigenmann, 1918): FMNH 58573 (holotype of *Pygidium zonatum*), 52.3 mm SL; FMNH 58572 (paratypes of *Pygidium zonatum*), 1, 50.7 mm SL; FMNH 58574 (paratypes of *Pygidium zonatum*), 2, 42.8–46.9 mm SL; MZUSP 83139, 8, 28.4–53.4 mm SL, 2 c&s, 35.3–41.2 mm SL; MZUSP 123175, 10, 35.9–56.3 mm SL. *Trichomycterus anaisae* Costa & Katz, 2021: MZUSP 37146 (paratype), 7, 35.0–51.5 mm SL. *Trichomycterus areolatus* Valenciennes, 1846: MZUSP 88531, 17, 27–76.2 mm SL, 2 c&s, 51.6–63.6 mm SL. *Trichomycterus auroguttatus* Costa, 1992: MZUSP 43341 (holotype), 51.5 mm SL; MZUSP 43342 (paratypes), 3, 34.2–47.7 mm SL, 1 c&s, 35.3 mm SL. *Trichomycterus bahianus* Costa, 1992: MZUSP 43340 (holotype), 65.8 mm SL; MZUSP 38636 (paratypes), 8, 14.4–88.6 mm SL. *Trichomycterus brasiliensis* Lütken, 1874: MZUFV 3527, 5, 90.3–112.1 mm SL; MZUSP 109379, 2, 36.8–49.2 mm SL; MZUSP 109433, 2, 26.0–80.6 mm SL; MNRJ 789, 2, 89–105.9 mm SL; *Trichomycterus albinotatus* Costa, 1992: MZUSP 42312 (holotype), 46.8 mm SL; MZUSP 42315 (paratypes), 3, 35.0–40.9 mm SL; MZUSP 87829 2 c&s, 40.3–46.7 mm SL. *Trichomycterus longibarbatus* Costa, 1992: MZUSP 43339 (holotype), 57.8 mm SL; MZUSP 23812 (paratypes), 15, 23.3–47.8 mm SL, 2 c&s, 36.1–41.4 mm SL. *Trichomycterus goeldii* Boulenger, 1896: MNRJ 51640, 11, 65.8–76.6 mm SL; MNRJ 51651, 4, 42.7–63.0 mm SL; MNRJ 956, 7, 37.8–79.7 mm SL. *Trichomycterus funebris* Costa & Katz, 2021: MZUSP 94511 (paratype), 17, 30.6–70.1 mm SL. *Trichomycterus humboldti* Costa & Katz, 2021: MZUSP 23769, 5, 25.1–33.1 mm SL. *Trichomycterus luetkeni* Costa & Katz, 2021: MZUSP 37169 (paratype), 1, 64 mm SL. *Trichomycterus novalimensis* Barbosa & Costa, 2010: MZUSP 114034, 27, 27.9–123.4 mm SL. *Trichomycterus nigricans* Valenciennes, 1832: MNRJ 17805, 1, 82.1 mm SL. *Trichomycterus paquequerensis* (Miranda Ribeiro, 1943): MNRJ 1159 (holotype), 34.7 mm SL; MZUSP 53756, 1, 36.7 mm SL; MZUSP 125283, 6, 31.9–71.0 mm

SL; UFJF 0338, 2, 46.9–90.7 mm SL; UFJF 0333, 3, 74.6–89.9 mm SL, 1 c&s 79.9 mm SL; UFJF 0505, 2, 35.8–56.4 mm SL; UFJF 1448, 2, 59.1–61.5 mm SL; UFJF 0941, 5, 84.3–160.6 mm SL, 2 c&s 84.5–87.8 mm SL; MNRJ 44073, 19, 28.6–98.31 mm SL; MNRJ 46427, 1, 106.1 mm SL; MNRJ 22611, 1, 57.4 mm SL; MNRJ 28737, 3, 59.1–85.4 mm SL; MNRJ 38220, 1, 96.2 mm SL; MNRJ 38235, 2, 67.4–82.3 mm SL; MNRJ 38250, 1, 46.6 mm SL; MNRJ 39345, 1, 102 mm SL; MNRJ 41174, 2, 118.5–162.0 mm SL; MNRJ 44009, 2, 64.4–85.5 mm SL; MNRJ 46124, 1, 84.1 mm SL. *Trichomycterus pantherinus* Alencar & Costa, 2004, MNRJ 41920, 6, 42.8–50.1 mm SL. *Trichomycterus pradensis* Sarmento-Soares, Martins-Pinheiro, Aranda & Chamon, 2005: MNRJ 28483 (holotype), 63.3 mm SL; MNRJ 28487 (paratypes), 8, 43.6–65.9 mm SL; MNRJ 28488 (paratype), 4, 52.7–76.7 mm SL. *Trichomycterus pauciradiatus* Alencar & Costa, 2006: MNRJ17059, 1, 44.1 mm SL. *Trichomycterus piratymbara* Katz *et al.*, 2013: MNRJ 31877, 7, 21.2–60.4 mm SL. *Trichomycterus sainthilairei* Costa & Katz, 2021: MZUSP 87188 (paratype), 15, 28.3–51.9 mm SL; MNRJ 28660 (paratype), 33, 33–56 mm SL. *Trichomycterus trefauti* Wosiacki, 2004: MZUSP 79911 (holotype), 49.5 mm SL; MZUSP 36966 (paratype), 5, 36.6–54.2 mm SL. *Scleronema operculatum* Eigenmann, 1917: FMNH 58080 (holotype), 1, 63.5 mm SL. *Scleronema angustirostris* (Devincenzi, 1942): MZUSP 81017, 1, 39.6 mm SL. *Scleronema* sp.: MZUSP 101361, 1, 25.7 mm SL. *Ituglanis proops* (Miranda Ribeiro, 1908): MZUSP 69688, 55, 26.1–39.0 mm SL. *Silvinichthys mendozensis* (Arratia, Chang G., Menu-Marque & Rojas M., 1978): MZUSP 75189, 1, 44.8 mm SL; MZUSP 75189, 1 c&s, 44.9 mm SL. *Rhizosomicthys totae* (Miles, 1942): MCZ 35744 (paratype), 1, 121.8 mm SL. *Eremophilus mutisii* Humboldt, 1805: MCZ 35805, 1, 142.1 mm SL.

ACKNOWLEDGEMENTS

REFERENCES

Ackery PR, **Vane-Wright RI. 1984**. *Milkweed butterflies*. New York: Cornell University Press.

Adriaens D, **Baskin JN**, **Coppens H. 2010**. Evolutionary morphology of trichomycterid catfishes: about handing on and digging. In: Nelson JS, Schultze HP, Wilson MVH, eds. *Origin and phylogenetic interrelationships of teleosts*. Munich: Verlag Dr. Friedrich Pfeil, 337–362.

Alencar AR, **Costa WJEM. 2004**. Description of two new species of the catfish genus *Trichomycterus* from southeastern Brazil (Siluriformes: Trichomycteridae). *Zootaxa* **744**: 1–8.

Archibald JD. 1994. Metataxon concepts and assessing possible ancestry using phylogenetic systematics. *Systematic Biology* **43**: 27–40.

Arratia G, **Chang A**, **Menu-Marque S**, **Rojas G. 1978**. About *Bullockia* gen. nov., *Trichomycterus mendozensis* n. sp. and revision of the family *Trichomycteridae* (Pisces, Siluriformes). *Studies on Neotropical Fauna and Environment* **13**: 157–194.

Avise JC, **Walker D. 1999**. Species realities and numbers in sexual vertebrates: perspectives from an asexually transmitted genome. *Proceedings of the National Academy of Science of the USA* **96**: 992–995.

Avise JC, **Walker D**, **Glenn CJ. 1998**. Speciation durations and Pleistocene effects on vertebrate phylogeography. *Proceedings of the Royal Society of London. Series B: Biological Sciences* **265**: 1707–1712.

Barbosa MAS. 2004. *Revisão Sistemática do gênero Trichomycterus Valenciennes do Sudeste do Brasil (Siluriformes: Loricarioidea: Trichomycteridae)*. Unpublished D. Phil. Thesis, Universidade Federal do Rio de Janeiro.

Barbosa MA. 2013. Description of two new species of the catfish genus *Trichomycterus* (Teleostei: Siluriformes: Trichomycteridae) from the coastal river basins, southeastern Brazil. *Vertebrate Zoology* **63**: 269–275.

Barbosa MA, **Costa WJEM. 2003**. *Trichomycterus potschi* (Siluriformes: Loricarioidei): a new trichomycterid catfish from coastal streams of southeastern Brazil. *Ichthyological Exploration of Freshwaters* **14**: 281–287.

Barbosa MA, **Costa WJEM. 2010**. Seven new species of the catfish genus *Trichomycterus* (Teleostei: Siluriformes:

Trichomycteridae) from southeastern Brazil and redescription of *T. brasiliensis*. *Ichthyological Exploration of Freshwaters* 21: 97–122.

Barbosa MA, **Costa WJEM. 2011**. Description of a new species of the catfish genus *Trichomycterus* (Teleostei: Siluriformes: Trichomycteridae) from the Rio de Contas basin, northeastern Brazil. *Vertebrate Zoology* 61: 307–312.

Barbosa MA, **Costa WJEM. 2012**. *Trichomycterus puriventris* (Teleostei: Siluriformes: Trichomycteridae), a new species of catfish from the rio Paraíba do Sul basin, southeastern Brazil. *Vertebrate Zoology* 62: 155–160.

Barbosa MA, **Katz AM. 2016**. A new species of the catfish genus *Trichomycterus* (Teleostei: Siluriformes: Trichomycteridae) from the Paranaíba basin, Central Brazil. *Vertebrate Zoology* 66: 261–265.

Barros LC, **Santos U**, **Zanuncio JC**, **Dergam JA. 2012**. *Plagioscion squamosissimus* (Sciaenidae) and *Parachromis managuensis* (Cichlidae): a threat to native fishes of the Doce River in Minas Gerais, Brazil. *PloS One* 7: e39138.

Baskin JN. 1973. *Structure and relationships of the Trichomycteridae*. Unpublished D. Phil. Thesis, City University of New York.

Bierman PR, **Caffee M. 2001**. Slow rates of rock surface erosion and sediment production across the Namib Desert and escarpment, southern Africa. *American Journal of Science* 301: 326–358.

Bizerril CRSF. 1994. Descrição de uma nova espécie de *Trichomycterus* (Siluroidei, Trichomycteridae) do Estado de Santa Catarina, com uma sinopse da composição da família Trichomycteridae no leste brasileiro. *Arquivos de Biologia e Tecnologia* 37: 617–628.

Bockmann FA, **Casatti L**, **de Pinna MCC. 2004**. A new species of trichomycterid catfish from the Rio Paranapanema basin, southeastern Brazil (Teleostei: Siluriformes), with comments on the phylogeny of the family. *Ichthyological Exploration of Freshwaters* 15: 225–242.

Bockmann FA, **Sazima I. 2004**. *Trichomycterus maracaya*, a new catfish from the Upper Rio Paraná, southeastern Brazil (Siluriformes: Trichomycteridae), with notes on the *T. brasiliensis* species complex. *Neotropical Ichthyology* 2: 61–74.

Braga FMS. 2004. Habitat, distribuição e aspectos adaptativos de peixes da microbacia do ribeirão Grande, Estado de São Paulo, Brasil. Acta Scientiarum. *Biological Sciences* 26: 31–36.

Buckup PA. 1992. Redescription of *Characidium fasciatum*, type species of the Characidiinae (Teleostei, Characiformes). *Copeia* 4: 1066–1073.

Buckup PA, **Brito MR**, **Souza-Lima R**, **Pascoli JC**, **Villa-Verde L**, **Ferraro GA**, **Salgado FLK**, **Gomes JR. 2014**. *Guia de identificação das espécies de peixes da bacia do rio das pedras município de Rio Claro, RJ*. Rio de Janeiro: The Nature Conservancy.

Burgess WE. 1989. *An atlas of freshwater and marine catfishes. A preliminary survey of the Siluriformes*. Neptune City: T.F.H. Publications.

Caramaschi EP, **Caramaschi U. 1991**. Taxonomic status of the trichomycterid catfish *Trichomycterus itatiayae*. *Copeia* 222–224.

Cardoso YP, **Montoya-Burgos JI. 2009**. Unexpected diversity in the catfish *Pseudancistrus brevispinis* reveals dispersal routes in a Neotropical center of endemism: the Guyanas Region. *Molecular Ecology* 18: 947–964.

Carvalho CC, **Oliveira DAA**, **Pompeu PS**, **Leal CG**, **Olivera C**, **Hanner R. 2011**. Deep barcode divergence in Brazilian freshwater fishes: the case of the São Francisco River basin. *Mitochondrial DNA* 22: 80–86.

Carvalho PH, **Lima MQ**, **Zawadzki CH**, **Oliveira C**, **Pinna M. 2015**. Phylogeographic patterns in suckermouth catfish *Hypostomus ancistroides* (Loricariidae): dispersion, vicariance and species complexity across a Neotropical biogeographic region. *Mitochondrial DNA* 27: 3590–3596.

Castellanos-Morales CA. 2007. *Trichomycterus santanderensis*: a new species of troglomorphic catfish (Siluriformes, Trichomycteridae) from Colombia. *Zootaxa* 1541: 49–55.

Cherem LFS, **Varajão CAC**, **Braucher R**, **Bourlé D**, **Salgado AAR**, **Varajão AC. 2012**. Long-term evolution of denudational escarpments in southeastern Brazil. *Geomorphology* 173–174: 118–127.

Chiachio MC, **Oliveira C**, **Montoya-Burgos JI. 2008**. Molecular systematics and historical biogeography of the armored Neotropical catfishes Hypoptopomatinae and Neoplecostominae (Siluriformes: Loricariidae). *Molecular Phylogenetics and Evolution* 49: 606–617.

Chu J-H, **Lin Y-S**, **Wu H-Y. 2007**. Evolution and dispersal of three closely related macaque species, *Macaca mulatta*, *M. cyclopis*, and *M. fuscata*, in the eastern Asia. *Molecular Phylogenetics and Evolution* 43: 418–429.

CONCEA. **2013**. *Conselho Nacional de Controle de Experimentação Animal. Diretriz Brasileira para o cuidado e a utilização de animais para fins científicos e didáticos–DBCA*. Brasília: Distrito Federal.

Costa WJEM. 1992. Description de huit uencane espèces du genre *Trichomycterus* (Siluriformes: Trichomycteridae), du Brésil oriental. *Revue Française d'Aquariologie et Herpetologie* 18: 101–110.

Costa WJEM. 2021. Comparative osteology, phylogeny and classification of the eastern South American catfish genus *Trichomycterus* (Siluriformes: Trichomycteridae). *Taxonomy* 1: 160–191.

Costa WJEM, **Bockmann FA. 1994**. Un nouveau genre neotropical de la famille des *Trichomycteridae* (Siluriformes: Loricarioidei). *Revue Française d'Aquariologie et Herpétologie* 20: 43–46.

Costa WJEM, **Katz AM. 2021**. Integrative taxonomy supports high species diversity of south-eastern Brazilian mountain catfishes of the *T. reinhardti* group (Siluriformes: Trichomycteridae). *Systematics and Biodiversity* 19: 601–621.

Costa WJEM, **Katz AM**, **Mattos JL**, **Amorim PF**, **Mesquita BO**, **Vilardo PJ**, **Barbosa MA. 2020a**. Historical review and redescription of three poorly known species of the catfish genus *Trichomycterus* from south-eastern Brazil (Siluriformes: Trichomycteridae). *Journal of Natural History* 53: 47–48.

Costa WJEM, **Mattos JL**, **Amorim PF**, **Vilardo PJ**, **Katz AM. 2020b**. Relationships of a new species support

multiple origin of melanism in *Trichomycterus* from the Atlantic Forest of south-eastern Brazil (Siluriformes: Trichomycteridae). *Zoologischer Anzeiger* **288**: 74–83.

Costa-Silva GJ, **Rodriguez MS**, **Roxo FF**, **Foresti F**, **Oliveira C. 2015**. Using different methods to access the difficult task of delimiting species in a complex Neotropical hyperdiverse group. *PloS One* **10**: e0135075.

Craig JM, **Kim LY**, **Tagliacollo VA**, **Albert JS. 2019**. Phylogenetic revision of Gymnotidae (Teleostei: Gymnotiformes), with descriptions of six subgenera. *PLoS ONE* **14**: e0224599.

Dagosta FCP, **de Pinna M. 2017**. Biogeography of Amazonian fishes: deconstructing river basins as biogeographic units. *Neotropical Ichthyology* **15**: e170034.

Dahl G. 1960. Nematognathous fishes collected during the Macarena Expedition 1959. *Novedades Colombianas* **1**: 302–317.

Datovo A, **Bockmann FA. 2010**. Dorsolateral head muscles of the catfish families Nematogenyidae and Trichomycteridae (Siluriformes: Loricarioidei): Comparative anatomy and phylogenetic analysis. *Neotropical Ichthyology* **8**: 193–246.

Dergam JAS, **Ferreira FF**, **Machado FP. 2017**. *Primeiro levantamento de ictiofauna da bacia do rio Doce após o rompimento da uenca de rejeito da Samarco, em Mariana-MG*. Viçosa: Universidade Federal de Viçosa.

DeSalle R, **Egan MG**, **Siddall M. 2005**. The unholy trinity: taxonomy, species delimitation and DNA barcoding. *Philosophical Transactions of the Royal Society B: Biological Sciences* **360**: 1905–1916.

Diogo R, **Chardon M**, **Vandewalle P. 2004**. Osteology and myology of the cephalic region and pectoral girdle of *Batrochoglanis raninus*, with a discussion on the synapomorphies and phylogenetic relationships of the Pseudopimelodinae and Pimelodidae (Teleostei: Siluriformes). *Animal Biology* **54**: 261–280.

Diogo R, **Chardon M**, **Vandewalle P. 2006**. Osteology and myology of the cephalic region and pectoral girdle of *Cetopsis coecutiens* Spix & Agassiz, 1829, comparison with other cetopsids, and comments on the synapomorphies and phylogenetic position of the Cetopsidae (Teleostei : Siluriformes). *Belgian Journal of Zoology* **136**: 3–13.

DoNascimiento C, **Prada-Pedreros S. 2020**. A new troglomorphic species of *Trichomycterus* (Siluriformes: Trichomycteridae) from northeastern Colombia, with proposal of a new *Trichomycterus* (Siluriformes: Trichomycteridae) from northeastern Colombia, with proposal of a new *Trichomycterus* subclade and remarks on some nominal species from Colombia. *Journal of Fish Biology* **96**: 968–985.

DoNascimiento C, **Prada-Pedreros S**, **Guerrero-Kommritz J. 2014a**. *Trichomycterus venulosus* (Steindachner, 1915), a junior synonym of *Eremophilus mutisii* Humboldt, 1805 (Siluriformes: Trichomycteridae) and not an extinct species. *Neotropical Ichthyology* **12**: 707–715.

DoNascimiento C, **Prada-Pedreros S**, **Guerrero-Kommritz J. 2014b**. A new catfish species of the genus *Trichomycterus* (Siluriformes: Trichomycteridae) from the Río Orinoco versant of Páramo de Cruz Verde, eastern Cordillera of Colombia. *Neotropical Ichthyology* **12**: 717–728.

Donin LM, **Ferrer J**, **Carvalho TP. 2020**. Taxonomical study of *Trichomycterus* (Siluriformes: Trichomycteridae) from the Ribeira de Iguape River basin reveals a new species recorded in the early 20th century. *Journal of Fish Biology* **96**: 886–904.

Donoghue MJ. 1985. A critique of the biological species concept and recommendations for a phylogenetic alternative. *Bryologist* **88**: 172–181.

Edgar RC. 2004. Muscle: a multiple sequence alignment method with reduced time and space complexity. *BMC Bioinformatics* **5**: 1–19.

Eigenmann CH. 1918. The Pygidiidae, a family of South American catfishes. *Memoirs of the Carnegie Museum* **7**: 259–398.

Evans BJ, **Gansauge M-T**, **Tocheri MW**, **Schillaci MA**, **Sutikna T**, **Saptomo EW**, **Klegarth A**, **Tosi AJ**, **Melnick DJ**, **Meyer M. 2020**. Mitogenomics of macaques (*Macaca*) across Wallace's Line in the context of modern human dispersals. *Journal of Human Evolution* **146**: 102852.

Fernández L, **Vari R. 2004**. New species of *Trichomycterus* from Midelevation localities of Northwestern Argentina (Siluriformes: Trichomycteridae). *Copeia* **4**: 876–882.

Fernandez L, **Arroyave J**, **Schaefer SA. 2021**. Emerging patterns in phylogenetic studies of trichomycterid catfishes (Teleostei, Siluriformes) and the contribution of Andean diversity. *Zoologica Scripta* **50**: 318–336.

Ferraris CJ Jr. **2007**. Checklist of catfishes, recent and fossil (Osteichthyes: Siluriformes), and catalogue of siluriform primary types. *Zootaxa* **1418**: 1–628.

Ferrer J, **Malabarba L. 2011**. A new *Trichomycterus* lacking pelvic fins and pelvic girdle with a very restricted range in Southern Brazil (Siluriformes: Trichomycteridae). *Zootaxa* **2912**: 59–67.

Ferrer J, **Malabarba LR. 2013**. Taxonomic review of the genus *Trichomycterus* Valenciennes (Siluriformes: Trichomycteridae) from the laguna dos Patos system, southern Brazil. *Neotropical Ichthyology* **11**: 217–246.

Fleming A, **Summerfield MA**, **Stone JOH**, **Fifield LK**, **Cresswell LG. 1999**. Denudation rates for the southern Drakensberg escarpment, SE Africa, derived from *in-situ* produced cosmogenic 36Cl: initial results. *Journal of the Geological Society* **156**: 209–212.

Fricke R, **Eschmeyer WN**, **Fong JD. 2021**. *Species of fishes by family: Trichomycteridae*. Available at: https://researcharchive.calacademy.org/research/ichthyology/catalog/fishcatmain.asp.

Fooden J. 1980. Classification and distribution of living macaques (*Macaca* Lacepede 1799). In: Lindburg DG, ed. *The macaques: studies in ecology, behavior and evolution*. New York: Van Nostrand Reinhold, 1–9.

Funk DJ, **Omland KE. 2003**. Species-level paraphyly and polyphyly: frequency, causes, and consequences, with insights from animal mitochondrial DNA. *Annual Review of Ecology and Systematics* **34**: 397–423.

García-Melo LJ, **Villa-Navarro FA**, **DoNascimiento C. 2016**. A new species of *Trichomycterus* (Siluriformes: Trichomycteridae) from the Upper Río Magdalena basin, Colombia. *Zootaxa* **4117**: 226–240.

Heath TA, **Hedtke SM**, **Hillis DM. 2008**. Taxon sampling and the accuracy of phylogenetic analyses. *Journal of Systematics and Evolution* **46**: 239–257.

Hebert PD, **Cywinska A**, **Ball SL**, **deWaard JR. 2003**. Biological identifications through DNA barcodes. *Proceedings of the Royal Society of London. Series B: Biological Sciences* **270**: 313–321.

Heimsath AM, **Chappell J**, **Dietrich WE**, **Nishiizumi K**, **Finkel RC. 2001**. Late Quaternary erosion in southeastern Australia: a field example using cosmogenic nuclides. *Quaternary International* **83–85**: 169–185.

Heimsath AM, **Chappell J**, **Finkel RC**, **Fifield K**, **Alimanovic A. 2006**. Escarpment erosion and landscape evolution in southeastern Australia. *GSA Special Papers* **398**: 173–190.

Henn AW. 1928. List of types of fishes in the collection of the Carnegie Museum on September 1, 1928. *Annals of the Carnegie Museum* **19**: 51–99.

Higuchi H. 1996. *An updated list of ichthyological collecting stations of the Thayer Expedition to Brazil (1865–1866)*. Available at: https://hwpi.harvard.edu/files/mcz/files/higuchi_1996_thayer_formated_prelim.pdf. Accessed 17 December 2021.

Hoelzer GA, **Meinick DJ. 1994**. Patterns of speciation and limits to phylogenetic resolution. *Trends in Ecology & Evolution* **9**: 104–107.

Hubert N, **Duponchelle F**, **Nuñez J**, **Garcia-Davila C**, **Paugy D**, **Renno JF. 2007**. Phylogeography of the piranha genera *Serrasalmus* and *Pygocentrus*: implications for the diversification of the Neotropical ichthyofauna. *Molecular Ecology* **16**: 2115–2136.

Hubert N, **Hanner R**, **Holm E**, **Mandrak NE**, **Taylor E**, **Burridge M**, **Watkinson D**, **Dumont P**, **Curry A**, **Bentzen P**, **Zhang J**, **April J**, **Bernatchez L. 2008**. Identifying Canadian freshwater fishes through DNA barcodes. *PloS One* **3**: e2490.

Huelsenbeck J, **Ronquist F. 2001**. MRBAYES: Bayesian inference of phylogenetic trees. *Bioinformatics Applications Note* **17**: 754–755.

Ibarra M, **Stewart DJ. 1987**. Catalogue of type specimens of recent fishes in Field Museum of Natural History. *Fieldiana Zoology (New Series)* **35**: 1–112.

Ingenito LFS, **Buckup PA. 2007**. The Serra da Mantiqueira, south-eastern Brazil, as a biogeographical barrier for fishes. *Journal of Biogeography* **34**: 1173–1182.

Johnson GD, **Patterson C. 1993**. Percomorph phylogeny: a survey of acanthomorphs and a new proposal. *Bulletin of Marine Science* **52**: 554–626.

Kashiwagi T, **Marshall AD**, **Bennett MB**, **Ovenden JR. 2012**. The genetic signature of recent speciation in manta rays (*Manta alfredi* and *M. birostris*). *Molecular Phylogenetics and Evolution* **64**: 212–218.

Katz AM, **Barbosa MA**, **Mattos JLO**, **Costa WJEM. 2018**. Multigene analysis of the catfish genus *Trichomycterus* and description of a new South American trichomycterine genus (Siluriformes, Trichomycteridae). *Zoosystematics and Evolution* **94**: 557–566.

Kimura M. 1980. A simple method for estimating evolutionary rate of base substitutions through comparative studies of nucleotide sequences. *Journal of Molecular Evolution* **16**: 111–120.

Krieger J, **Fuerst PA. 2002**. Evidence for a slowed rate of molecular evolution in the order Acipenseriformes. *Molecular Biology and Evolution* **19**: 891–897.

Kumar S, **Stecher G**, **Li M**, **Knyaz C**, **Tamura K. 2018**. MEGA X: molecular evolutionary genetics analysis across computing platforms. *Molecular Biology and Evolution* **35**: 1547–1549.

Lezama AQ, **Triques ML**, **Santos PS. 2012**. *Trichomycterus argos* (Teleostei: Siluriformes: Trichomycteridae), a new species from the Doce River Basin, eastern Brazil. *Zootaxa* **3352**: 60–68.

Lima SMQ. 2008. *Filogeografia e sistemática molecular de dois bagres das bacias costeiras da Serra do Mar,* Trichomycterus zonatus *(Eigenmann, 1983) e* Trichogenes longipinnis *Britski & Ortega, 1983 (Siluriformes: Trichomycteridae)*. Unpublished D. Phil. Thesis, Universidade Federal do Rio de Janeiro.

Lima SMQ, **Berbel-Filho WM**, **Vilasboa A**, **Lazoski C**, **Volpi TA**, **Lazzarotto H**, **Russo CAM**, **Tatarenkov A**, **Avise JC**, **Solé-Cava AM. 2021**. Rio de Janeiro and other palaeodrainages evidenced by the genetic structure of an Atlantic Forest catfish. *Journal of Biogeography* **48**: 1475–1488.

Lima SMQ, **Costa WJEM. 2004**. *Trichomycterus giganteus* (Siluriformes: Loricarioidea: Trichomycteridae): a new catfish from the Rio Guandu basin, southeastern Brazil. *Zootaxa* **761**: 1–6.

Lima SMQ, **Lazzarotto H**, **Costa WJEM. 2008**. A new species of *Trichomycterus* (Siluriformes: Trichomycteridae) from Iagoa Feia Drainage, southeastern Brazil. *Neotropical Ichthyology* **6**: 315–322.

Lundberg JG. 1982. The comparative anatomy of the toothless blindcat, *Trogloglanis pattersoni* Eigenmann, with a phylogenetic analysis of the ictalurid catfishes. *Miscellaneous Publications, Museum of Zoology, University of Michigan* **163**: 1–85.

Lujan NK, **Conway KW. 2015**. Life in the fast lane: a review of rheophily in freshwater fishes. In: Riesch R, Tobler M, Plath M, eds. *Extremophile fishes: ecology, evolution, and physiology of teleosts in extreme environments*. Cham: Springer International Publishing, 107–136.

Mabragaña E, **Astarloa JMD**, **Hanner R**, **Zhang J**, **Castro MG. 2011**. DNA barcoding identifies uenca ne fishes from marine and brackish waters. *PloS One* **6**: e28655.

Marques D, **Santos F**, **Silva S. 2013**. Cytogenetic and DNA barcoding reveals high divergence within the trahira, *Hoplias malabaricus* (Characiformes: Erythrinidae) from the lower Amazon River. *Neotropical Ichthyology* **11**: 459–466.

Martin AP, **Bermingham E. 2000**. Regional endemism and cryptic species revealed by molecular and morphological analysis of a widespread species of Neotropical catfish. *Proceedings of the Royal Society of London. Series B: Biological Sciences* **1448**: 1135–1141.

Mayr E. 1969. *Principles of systematic zoology*. New York: McGraw-Hill.

Melo BF, **Ochoa LE**, **Vari RP**, **Oliveira C. 2016**. Cryptic species in the Neotropical fish genus *Curimatopsis* (Teleostei, Characiformes). *Zoologica Scripta* **45**: 650–658.

Miquelarena AM, **Fernández LA. 2000**. Presencia de *Trichomycterus davisi* (Haseman, 1911) en la uenca del Alto Paraná misionero (Siluriformes: Trichomycteridae). *Revista de Ictiología* **8**: 41–45.

Miranda-Chumacero G, **Alvarez G**, **Luna V**, **Wallace RB**, **Painter L. 2015**. First observations on annual massive upstream migration of juvenile catfish *Trichomycterus* in an Amazonian River. *Environmental Biology of Fishes* **98**: 1913–1926.

Montoya-Burgos JI. 2003. Historical biogeography of the catfish genus *Hypostomus* (Siluriformes: Loricariidae), with implications on the diversification of Neotropical ichthyofauna. *Molecular Ecology* **12**: 1855–1867.

Mutanen M, **Kivela SM**, **Vos RA**, **Doorenweerd C**, **Ratnasingham S**, **Hausmann A**, **Huemer P**, **Dinca V**, **Van Nieukerken EJ**, **Lopez-Vaamonde C**, **Vila R**, **Aarvik L**, **Decaens T**, **Efetov KA**, **Herbet PDN**, **Johnsen A**, **Karsholt O**, **Pentinsaari M**, **Rougerie R**, **Segerer A**, **Tarmann G**, **Zahiri R**, **Godfray CJ. 2016**. Species-level para- and polyphyly in DNA barcode gene trees: strong operational bias in European Lepidoptera. *Systematic Biology* **65**: 1024–1040.

Nascimento CHR, **Frantine-Silva W**, **Souza-Shibatta L**, **Sofia SH**, **Ferrer J**, **Shibatta OA. 2017**. Intrapopulational variation in color pattern of *Trichomycterus davisi* (Haseman, 1911) (Siluriformes: Trichomycteridae) corroborated by morphometrics and molecular analysis. *Zootaxa* **4290**: 503–518.

Nelson GJ, **Platnick NI. 1981**. *Systematics and biogeography: cladistics and vicariance*. New York: Columbia University Press.

Nixon KC, **Wheeler QD. 1990**. An amplification of the phylogenetic species concept. *Cladistics* **6**: 211–223.

Ochoa LE, **Datovo A**, **DoNascimiento C**, **Roxo FF**, **Sabaj MH**, **Chang J**, **Melo FB**, **Silva GC**, **Foresti F**, **Alfaro M**, **Oliveira C. 2020**. Phylogenomic analysis of trichomycterid catfishes (Teleostei: Siluriformes) inferred from ultraconserved elements. *Scientific Reports* **10**: 2697.

Ochoa LE, **Silva GSC**, **Costa e Silva GJ**, **Oliveira C**, **Datovo A. 2017**. New species of *Trichomycterus* (Siluriformes: Trichomycteridae) lacking pelvic fins from Paranapanema basin, southeastern Brazil. *Zootaxa* **4319**: 550–560.

Ornelas-Garcia CP, **Dominguez-Dominguez O**, **Doadrio I. 2008**. Evolutionary history of the fish genus *Astyanax* Baird & Girard (1854) (Actynopterigii, Characidae) in Mesoamerica reveals multiple morphological homoplasies. *BMC Evolutionary Biology* **8**: 1–17.

Pastana MNL, **Bockmann FA**, **Datovo A. 2019**. The cephalic lateral-line system of Characiformes (Teleostei: Ostariophysi): anatomy and phylogenetic implications. *Zoological Journal of the Linnean Society* **20**: 1–46.

Perdices A, **Birmingham E**, **Montilla A**, **Doadrio I. 2002**. Evolutionary history of the genus *Rhamdia* (Teleostei: Pimelodidae) in Central America. *Molecular Phylogenetics and Evolution* **25**: 172–189.

Perdices A, **Doadrio I**, **Bermingham E. 2005**. Evolutionary history of the synbranchid eels (Teleostei: Synbranchidae) in Central America and the Caribbean islands inferred from their molecular phylogeny. *Molecular Phylogenetics and Evolution* **37**: 460–473.

Pereira LH, **Maia GM**, **Hanner R**, **Foresti F**, **Oliveira C. 2010**. DNA barcodes discriminate freshwater fishes from the Paraíba do Sul River Basin, São Paulo, Brazil. *Mitochondrial DNA* **22**: 71–79.

Pereira LH, **Maia GM**, **Hanner R**, **Foresti F**, **Oliveira C. 2011**. DNA barcoding reveals hidden diversity in the Neotropical freshwater fish *Piabina argentea* (Characiformes: Characidae) from the Upper Paraná Basin of Brazil. *Mitochondrial DNA* **22**: 87–96.

Pereira LH, **Maia GM**, **Hanner R**, **Foresti F**, **Oliveira C. 2013**. Can DNA barcoding accurately discriminate megadiverse Neotropical freshwater fish fauna? *BMC Genetics* **14**: 1–14.

de Pinna MCC. 1989. A new sarcoglanidine catfish, phylogeny of its subfamily, and an appraisal of the phyletic status of the Trichomycterinae. *American Museum Novitates* **2950**: 1–39.

de Pinna MCC. 1992a. *Trichomycterus castroi*, a new species of trichomycterid catfish from the Rio Iguaçu of southeastern Brazil (Teleostei: Siluriformes). *Ichthyological Exploration of Freshwaters* **3**: 89–95.

de Pinna MCC. 1992b. A new subfamily of Trichomycteridae (Teleostei, Siluriformes), lower loricarioid relationships and a discussion on the impact of additional taxa for phylogenetic analysis. *Zoological Journal of the Linnean Society* **106**: 175–229.

de Pinna MCC. 1998. Phylogenetic relationships of Neotropical Siluriformes (Teleostei: Ostariophysi): historical overview and synthesis of hypotheses. In: Malabarba LR, Reis RE, Vari RP, Lucena ZM, Lucena CAS, eds. *Phylogeny and classification of Neotropical fishes*. Porto Alegre: Edipucrs, 279–330.

de Pinna MCC. 1999. Species concepts and phylogenetics. *Reviews in Fish Biology and Fisheries* **9**: 353–373.

de Pinna MCC, **Keith P. 2019**. *Mastiglanis durantoni* from French Guyana, a second species in the genus (Siluriformes: Heptapteridae), with a CT scan survey of phylogenetically-relevant characters. *Cybium: Revue Internationale d'Ichtyologie* **43**: 125–135.

de Pinna MCC, **Wosiacki W. 2003**. Trichomycteridae. In: Reis RE, Kullander SO, Ferraris CJ, eds. *Check list of the freshwater fishes of South and Central America*. Porto Alegre: Edipucrs.

de Queiroz K, **Donoghue MJ. 1988**. Phylogenetic systematics and the species problem. *Cladistics* **4**: 317–338.

de Queiroz LJ, **Cardoso Y**, **Jacot-des-Combes C**, **Bahechar IA**, **Lucena CA**, **Rapp Py-Daniel L**, **Sarmento-Soares LM**, **Nylinder S**, **Oliveira C**, **Parente TE**, **Torrente-Vilara G**, **Covain R**, **Buckup P**, **Montoya-Burgos JI. 2020**. Evolutionary units delimitation and continental multilocus phylogeny of the hyperdiverse catfish genus *Hypostomus*. *Molecular Phylogenetics and Evolution* **145**: 106711.

Reis RE, **Kullander SO**, **Ferraris CJ** Jr. **2003**. *Check list of the freshwater fishes of South and Central America*. Porto Alegre: Edipucrs.

Reis VJC, **de Pinna MCC. 2019**. The type specimens of *Trichomycterus alternatus* (Eigenmann, 1917) and *Trichomycterus zonatus* (Eigenmann, 1918), with elements for future revisionary work (Teleostei: Siluriformes: Trichomycteridae). *Zootaxa* **4585**: 100–120.

Reis VJC, **de Pinna MCC**, **Pessali TC. 2019**. A new species of *Trichomycterus* Valenciennes 1832 (Trichomycteridae: Siluriformes) from the Rio Doce Drainage with remarkable similarities with *Bullockia* and a CT-scan survey. *Journal of Fish Biology* **95**: 918–931.

Reis VJC, **dos Santos SA**, **Britto MR**, **Volpi TA**, **de Pinna MCC. 2020**. Iterative taxonomy reveals a new species of *Trichomycterus* Valenciennes 1832 (Siluriformes, Trichomycteridae) widespread in Rio Doce Basin: a pseudocryptic of *T. immaculatus*. *Journal of Fish Biology* **97**: 1607–1623.

Rieppel O. 2000. *Sauropterygia I. Handbuch der Paläoherpetologie*. Munich: Verlag Dr. Friedrich Pfeil.

Roldi MMC, **Sarmento-Soares LM**, **Pinheiro RFM**, **Lopes MM. 2011**. Os *Trichomycterus* das drenagens fluviais no Espírito Santo, Sudeste do Brasil (Siluriformes: Trichomycteridae). *Boletim Sociedade Brasiliera de Ictiologia* **103**: 1–3.

Rubinoff D, **Cameron S**, **Will K. 2006**. A genomic perspective on the shortcomings of mitochondrial DNA for '"barcoding"' identification. *Journal of Heredity* **97**: 581–594.

Saccone C, **DeCarla G**, **Gissi C**, **Pesole G**, **Reynes A. 1999**. Evolutionary genomics in the Metazoa: the mitochondrial DNA as a model system. *Gene* **238**: 195–210.

Sales SM, **Salvador GN**, **Pessali TC**, **Carvalho DC. 2018**. Hidden diversity hampers conservation efforts in a highly impacted Neotropical river system. *Frontiers in Genetics* **9**: 1–11.

Santos JF. 2012. *Revisão taxonômica do gênero* Trichomycterus *Valenciennes, 1832 (Siluriformes: Trichomycteridae) no sitema da laguna dos Patos*. Unpublished Master's Thesis, Universidade Federal do Rio Grande do Sul.

Sarmento-Soares LM, **Zanata AM**, **Martins-Pinheiro RF. 2011**. *Trichomycterus payaya*, new catfish (Siluriformes: Trichomycteridae) from headwaters of rio Itapicuru, Bahia, Brazil. *Neotropical Ichthyology* **9**: 261–271.

Sarmento-Soares LM, **Martins-Pinheiro RF**, **Aranda AT**, **Chamon CC. 2005**. *Trichomycterus pradensis*, a new catfish from southern Bahia coastal rivers, northeastern Brazil (Siluriformes: Trichomycteridae). *Ichthyological Explorations of Freshwaters* **16**: 289–302.

Sato LR, **Oliveira C**, **Foresti F. 2004**. Karyotype description of five species of *Trichomycterus* (Teleostei: Siluriformes: Trichomycteridae). *Genetics and Molecular Biology* **27**: 45–50.

Shum P, **Moore L**, **Pampoulie C**, **Di Muri C**, **Vandamme S**, **Mariani S. 2017**. Harnessing mtDNA variation to resolve ambiguity in 'Redfish' sold in Europe. *PeerJ* **2**: 1–18.

da Silva AM, **Belei F**, **Giongo P**, **Sampaio WMS. 2013**. Estado da conservação da ictiofauna do Rio Guandu, afluente do baixo Rio Doce, Espírito Santo, sudeste do Brasil. *Evolução e Conservação da Biodiversidade* **4**: 8–13.

Silva CCF, **Matta LSF**, **Hilsdorf AWS**, **Langeani F**, **Marceniuk AP. 2010**. Color pattern variation in *Trichomycterus iheringi* (Eigenmann, 1917) (Siluriformes: Trichomycteridae) from Rio Itatinga and Rio Claro, São Paulo, Brasil. *Neotropical Ichthyology* **8**: 49–56.

Sullivan C, **Bierman P**, **Reusser L**, **Pavich M**, **Larsen J**, **Finkel R. 2007**. *Erosion and landscape evolution of the Blue Ridge escarpment, southern Appalachian Mountains. Earth Surface Processes and Landforms*. Unpublished Master Dissertation, University of Vermont.

Taylor R, **Van Dyke CC. 1985**. Revised procedures for staining and clearing small fishes and other vertebrates for bone and cartilage study. *Cybium* **9**: 107–119.

Tchernavin VV. 1944. A revision of some Trichomycterinae based on material in the British Museum (Natural History). *Proceedings of the Zoological Society of London* **114**: 234–275.

Triques ML, **Vono V. 2004**. Three new species of *Trichomycterus* (Teleostei: Siluriformes: Trichomycteridae) from the Rio Jequitinhonha Basin, Minas Gerais, Brazil. *Ichthyological Exploration of Freshwaters* **15**: 161–172.

Vanacker V, **von Blanckenburg F**, **Hewaeasam T. 2007**. Constraining landscape development of the Sri Lankan Escarpment with cosmogenic nuclides in river sediment. *Earth and Planetary Science Letters* **253**: 402–414.

Vieira F. 2010. Distribuição, impactos ambientais e conservação da fauna de peixes da bacia do Rio Doce. *MG-Biota* **2**: 5–22.

Vilardo P, **Katz AM**, **Costa WJEM. 2020**. Relationships and description of a new species of *Trichomycterus* (Siluriformes: Trichomycteridae) from the Rio Paraíba do Sul basin, southeastern Brazil. *Zoological Studies* **59**: 1–12.

Vinas J, **Tudela S. 2009**. A validated methodology for genetic identification of tuna species (genus *Thunnus*). *PloS One* **4**: e7606.

Volpi TA. 2017. *Filogeografia de* Trichomycterus *(Siluriformes: Trichomycteridae) na Mata Atlântica*. Unpublished D. Phil. Thesis, Universidade Federal do Espírito Santo.

Ward RD. 2009. DNA barcode divergence within species and genera of birds and fishes. *Molecular Ecology Resources* **9**: 1077–1085.

Ward RD, **Hanner R**, **Hebert PDN. 2009**. The campaign to DNA barcode all fishes, FISH-BOL. *Journal of Fish Biology* **74**: 329–356.

Ward RD, **Zemlak TS**, **Innes BH**, **Last PR**, **Hebert PD. 2005**. DNA barcoding Australia's fish species. *Philosophical Transactions of the Royal Society B: Biological Sciences* **360**: 1847–1857.

Weitzman SH. 1974. Osteology and evolutionary relationships of the Sternoptychidae, with a new classification of stomiatoid families. *Bulletin of the American Museum of Natural History* **153**: 327–478.

Wosiacki WB. 2002. *Estudo das relações filogenéticas de Trichomycterinae (Teleostei, Siluriformes, Trichomycteridae) com uma proposta de classificação*. Unpublished D. Phil. Thesis, Universidade de São Paulo.

Wosiacki WB. 2005. A new species of *Trichomycterus* (Siluriformes: Trichomycteridae) from south Brazil and redescription of *T. iheringi* (Eigenmann). *Zootaxa* **1040**: 49–64.

Wosiacki WB, **Garavello JC. 2004**. Five new species of *Trichomycterus* from the Rio Iguaçu (Rio Paraná

Basin), southern Brazil (Siluriformes: Trichomycteridae). *Ichthyological Exploration of Freshwaters* **15**: 1–16.

Wosiacki WB, **Oyakawa OT. 2005**. Two new species of the catfish genus *Trichomycterus* (Siluriformes: Trichomycteridae) from the rio Ribeira de Iguape Basin, Southeastern Brazil. *Neotropical Ichthyology* **3**: 465–472.

Yang L, **Kong H**, **Huang JP**, **Kang M. 2019**. Different species or genetically divergent populations? Integrative species delimitation of the *Primulina hochiensis* complex from isolated karst habitats. *Molecular Phylogenetics and Evolution* **132**: 219–231.

Xia X. 2013. DAMBE5: a comprehensive software package for data analysis in molecular biology and evolution. *Molecular Phylogenetics and Evolution* **30**: 1720–1728.

Xia X, **Lemey P. 2009**. Assessing substitution saturation with DAMBE. In: Lemey P, Salemi M, Vandamme AM, eds. *The phylogenetic handbook: a practical approach to DNA and protein phylogeny*, *2nd edn*. Cambridge: Cambridge University Press, 615–663.

Xia X, **Xie Z**, **Salemi M**, **Chen L**, **Wang Y. 2003**. An index of substitution saturation and its application. *Molecular Phylogenetics and Evolution* **26**: 1–7.

Zanata AM, **Ohara WM**, **Oyakawa OT**, **Dagosta FC. 2020**. A new rheophilic South American darter (Crenuchidae: *Characidium*) from the Rio Juruena Basin, Brazil, with comments on morphological adaptations to life in fast-flowing waters. *Journal of Fish Biology* **97**: 1343–1353.

SUPPORTING INFORMATION

Additional Supporting Information may be found in the online version of this article at the publisher's web-site:

Appendix S1. Terminal taxa obtained from GenBank for barcoding and phylogenetic analyses, and respective GenBank accession numbers.
Appendix S2. New sequences of terminal taxa for barcoding and phylogenetic analyses and respective GenBank accession numbers.